The University Of Sheffield.

Central Biomarkers of Painful Diabetic Peripheral Neuropathy

Dr Gordon Sloan, MBChB

PhD Thesis

Department of Infection, Immunity and Cardiovascular Disease

University of Sheffield

2021

Acknowledgements

I am grateful to Professor Solomon Tesfaye, Dr Dinesh Selvarajah and Professor Iain Wilkinson for giving me the opportunity to join their research group. All three have provided excellent supervision and mentorship throughout my PhD research. I look forward to continuing to work under the guidance of Solomon and Dinesh, but am saddened that Iain will not see the finished thesis; I hope he would have been proud of it.

My thanks also go to Dr Sharon Caunt who has frequently provided guidance and expertise. It has been a real pleasure sharing an office with her.

I greatly appreciate the time and support of all the other members of the research group - Dr Adriana Anton, Dr Kevin Teh, Dr Leanne Hunt, Dr Marni Greig, Dr Shillo Pallai and Navone Thompson.

The Academic Unit of Radiology MR staff, particularly Julia Bigley, ensured the imaging aspects of the study were performed accurately and efficiently. Professor Praveen Anand and his research group at Imperial College helped me with the analysis of the skin biopsy samples. I am appreciative of their hard work and professionalism.

I am especially grateful to the participants in the study who gave their time and underwent tests which may have caused discomfort. I would particularly like to thank those who live with diabetic neuropathy. This patient group is a huge inspiration to me. I hope my work contributes to a greater understanding and better treatment for those with this condition.

Finally, many thanks to my family for their patience and support during this research.

Abstract

Painful-diabetic sensorimotor peripheral neuropathy (Painful-DPSN) is a common chronic complication of diabetes mellitus. Unfortunately, the condition is poorly understood and is inadequately treated. The studies included within this thesis aimed to improve our understanding of the mechanisms underlying the condition and its treatment, with a particular focus upon the central nervous system.

Cross-sectional multi-modal imaging studies were performed to determine the cerebral structural and functional alterations in the brain in DSPN. In the largest cerebral imaging in DSPN, volumetric analysis showed group differences in cortical thickness at the primary somatosensory, primary motor and the insular cortices. There was greater reduction in cortical thickness in painless- compared with painful-DSPN at the primary somatosensory and insular cortices; however, at the primary motor cortex the reduction in cortical thickness was similar for both DSPN groups compared to the non-neuropathy groups. The cortical thickness correlated with age, as well as measures of neuropathy severity. Moreover, in sub-group analysis of painful-DSPN participants there was a significant reduction in anterior cingulate cortical thickness in the irritable nociceptor compared with the non-irritable nociceptor phenotype.

Proton and 31-phosphorus magnetic resonance spectroscopy (1H- and 31P-MRS, respectively) neurometabolites were then investigated to determine cerebral neuronal function in the primary somatosensory cortex and thalamus in participants with type 2 diabetes mellitus (T2DM) and DSPN. This study demonstrated reduced NAA:Cho, indicating neuronal dysfunction, in the dominant hemisphere thalamus in painless-DSPN compared to painful-DSPN and HV. The NAA:Cho in painful-DSPN was comparable with HV at this region.

Additionally, the NAA:Cho at the dominant thalamus correlated with body mass index, blood glucose taken just before the magnetic resonance imaging (MRI) and peroneal motor nerve conduction velocity. Also, were no group differences in any neurometabolites at the somatosensory cortex. These results suggest that there is preservation of neuronal function in the thalamus in painful-DSPN, perhaps as a result of persisting painful neuronal signalling, essential for the perception of pain.

Using 31P-MRS at the somatosensory cortex, the phosphocreatine to ATP ratio (PCr:ATP) a marker of energy usage, was numerically the lowest in painful-DSPN, reaching significance compared with HV and painless-DSPN. The PCr:ATP ratio correlated with a number of measures of neuropathic pain and was lower in participants with a higher Numeric Rating Scale (NRS) pain score during MRI, indicating that there is higher energy usage with higher levels of pain. The pattern of thalamic 31P-MRS metabolite ratios was different in the thalamus, with markers of mitochondrial function, the inorganic phosphate (Pi) to PCr ratio (Pi:PCr) and Pi:ATP, being numerically the highest in painless-DSPN and reaching significance versus HV and painful-DSPN. These ratios correlated more with metabolic measures, rather than neuropathy/neuropathic pain measures. There were also correlations seen with 31P and 1H neurometabolites, indicating a correlation with neuronal function and cerebral energetics. In this first ever study using 31P-MRS in clinical DSPN, these results suggest differing bioenergetic processes occurring in the thalamus and the somatosensory cortex. Mitochondrial dysfunction predominated at the thalamus, with preservation of function in painful-DSPN probably due to persisting neuronal impulses. At the somatosensory cortex, however, there was a diabetes effect upon this region with evidence of reduced energy usage in painless-DSPN.

Two pre-post neuroimaging studies were undertaken in participants undergoing the OPTION-DM trial, a neuropathic pain treatment randomised controlled trial to determine the most efficacious pathway for the management of painful-DSPN. Cerebral images were taken at the end of a treatment pathway within the study when participants were optimally treated for their neuropathic pain, and again one-week later after medication had been withdrawn. There were no significant differences in neurotransmitter levels; although, methodological limitations may have contributed to the negative findings in the study. However, resting state function MRI analysis showed a significant increase in functional connectivity between the left thalamus and somatosensory cortex and left thalamus and insular cortex after withdrawal of neuropathic pain medications. The change in thalamic to somatosensory cortical functional connectivity also correlated with severity of baseline pain numeric rating and baseline total neuropathic pain symptom inventory scores. This study therefore further highlights the importance of the function of the thalamus as a pivotal pain processing centre in painful-DSPN. Moreover, functional connectivity of the thalamus to other regions of the brain may act as biomarkers of pain in clinical trials. However, future validation is required in prospective studies.

The final study in this thesis performed thigh skin biopsies in four well characterized groups with the aim to determine whether neuronal or vascular markers in the skin differentiate painful- and painless-DSPN. The study demonstrated there was a significant increase in the vascular marker von Willebrand Factor (vWF) in painful-DSPN compared with all other groups. This confirms the findings of a previous study within the research group when biopsies were taken at the ankle. Further mechanistic studies are necessary to determine

the cause of the elevated vWF in the skin of patients with painful-DSPN; however, vWF may act as a peripheral marker of painful-DSPN in the future.

Overall, these studies highlight key mechanisms of cerebral involvement in painless- and painful-DSPN. Further mechanistic studies, particularly prospective with longitudinal imaging are necessary to determine the underlying mechanisms of neuroplasticity in DSPN.

Overview of Studies

Title	Aims	Design	Results	Conclusions
Chapter 3 **Cerebral morphometric alterations in painless- and painful-DSPN**	To determine cerebral morphological alterations in DSPN (painless, painful and IR- and NIR-phenotypes) and their relationship to clinical/ neurophysiological measures.	Case controlled cross-sectional volumetric brain imaging study.	Reduced S1/M1 cortical thickness in painless- and painful-DSPN, which related to neurophysiological measures. Reduced ACC cortical thickness in the IR-painful-DSPN phenotype.	DSPN leads to structural alterations in brain regions involved in somatosensory/ motor function. Neuroplasticity at the ACC may play a role determining clinical phenotypes in painful-DSPN.
Chapter 4 **Cerebral Magnetic Resonance Spectroscopy alterations in DSPN: Neuronal function in painful- and painless-DSPN**	To assess proton metabolite ratios, as measures of neuronal function, in the S1 cortices and thalami in patients with T2DM and DSPN.	Case controlled cross-sectional 1H-MRS brain imaging study.	Reduced dominant hemisphere thalamic NAA:Cho in painless-DSPN compared with painful-DSPN and HV, with lesser reductions in no-DSPN. NAA:Cho correlated with BMI and glucose. No group difference in S1 1H metabolite ratios.	Diabetes leads to neuronal dysfunction in the thalamus especially in painless-DSPN, but not in painful-DSPN. This suggests a preservation of neuronal function which may be due to persisting neuronal impulses due to neuropathic pain.
Chapter 5 **Cerebral Magnetic Resonance Spectroscopy alterations in DSPN: Cerebral bioenergetics in painful- and painless-DSPN**	To assess 31-phosphorus metabolite ratios, as measures of cerebral bioenergetics/ mitochondrial dysfunction, of the S1 cortices and thalami in patients with DSPN.	Case controlled cross-sectional 31P-MRS brain imaging study.	S1 cortex: PCr:ATP was lowest in painful-DSPN and significantly higher in painless-DSPN. PCr:ATP related to measures of neuropathic pain. Thalami: Pi:PCr and Pi:ATP were highest in painless-DSPN and correlated with HbA1c and duration of diabetes. NAA:Cho and Pi:PCr correlated.	Mitochondrial dysfunction at the level of the thalamus may be the cause of neuronal dysfunction in painless-DSPN and to some extent in no-DSPN, whilst there is retained mitochondrial and neuronal function in painful-DSPN. At the S1 cortex, there is increased cortical energy metabolism in painful-DSPN, which may act as a

				marker of neuropathic pain in diabetes.
<u>Chapter 6</u> **The impact of optimised neuropathic pain treatment on the magnetic resonance imaging correlates of painful-DSPN 1: Neurotransmitters**	To determine whether GABA/Glx levels change when painful-DSPN patients are optimally treated for painful symptoms compared to after treatment is withdrawn.	Pre-post 1H-MRS brain imaging study.	GABA and Glx levels in the ACC were not different after withdrawal of treatment. Glx levels correlated with pain severity when patients were off neuropathic pain treatments.	ACC GABA and Glx are unsuitable biomarkers of painful-DSPN in clinical trials.
<u>Chapter 7</u> **The impact of optimised neuropathic pain treatment on the magnetic resonance imaging correlates of painful-DSPN 2: Functional connectivity**	To determine whether there are differences in cerebral neuronal functional connectivity in patients with painful-DSPN on neuropathic pain treatments and after these had been discontinued.	Pre-post rs-fMRI brain imaging study.	Functional connectivity rose between the left thalamus and S1 cortex and the left thalamus and insular cortex after treatment withdrawal. ΔS1-Thalamic connectivity correlated with measures of pain and was higher in participants with High compared to Low Baseline Pain groups.	Functional connectivity of the thalamus, S1 and insular cortex are shown to be key components of the cerebral mechanisms of painful-DSPN. These rs-fMRI measures may act as pain biomarkers in clinical trials.
<u>Chapter 8</u> **Peripheral vascular markers of painful-DSPN: A Pilot Study**	To determine if there are any differences in peripheral vascular markers at the thigh in participants with painful- and painless-DSPN compared with controls.	Case controlled cross-sectional skin biopsy study.	IENFD was not different between painful- and painless-DSPN. vWF stained dermal vessels were higher in painful-DSPN compared to all other groups and correlated with clinical and neurophysiological measures, including the severity of neuropathic pain.	PGP 9.5 IENFD does not discriminate between painful- and painless-DSPN. The raised vWF in thigh skin of painful-DSPN suggests altered microvascular function associated with neuropathic pain and if replicated in a larger study may act as a diagnostic predictor of painful-DSPN.

Author's Declaration

My contribution to the Chapters were as follows:

1. Creating the concept and design of each of the studies in concert with Professor Solomon Tesfaye, Dr Dinesh Selvarajah and Professor Iain Wilkinson
2. Recruitment of all study participants for Chapters 4, 5, 6, 7 and 8 and recruitment of approximately one fifth of the study participants for Chapter 3.
3. Co-ordination of study visits for all study participants I recruited
4. Consenting, clinical and neuropathy assessments for all participants I recruited
5. Providing support to departmental radiographers for placement of MRS voxels during neuroimaging studies
6. Collecting and fixing skin biopsies
7. All magnetic resonance spectroscopy scan analysis
8. Statistical analysis of all clinical, biochemical, neurophysiological and MR data
9. Writing the thesis

Contribution from others included:

1. Professor Iain Wilkinson and Dr Adriana Anton designed the magnetic resonance imaging (MRI) protocols
2. Resting State Functional MRI and cerebral anatomical data analysed by Dr Kevin Teh
3. Skin biopsies analysed by Department of Neurology, Imperial College London under supervision of Professor Praveen Anand
4. Editing and proofing of the thesis by Professor Solomon Tesfaye and Dr Dinesh Selvarajah

Articles published contributing to this thesis:

Review articles

Sloan G, Shillo P, Selvarajah D, Wu J, Wilkinson ID, Tracey I, Anand P, Tesfaye S. A new look at painful diabetic neuropathy. **Diabetes Research and Clinical Practice**. 2018; 144: 177-191. DOI: 10.1016/j.diabres.2018.08.020.

Shillo P*, Sloan G*, Greig M, Hunt L, Selvarajah D, Elliott J, Gandhi R, Wilkinson ID, Tesfaye S. Painful and Painless Diabetic Neuropathies: What Is the Difference? **Current Diabetes Reports**. 2019;19(6):32. DOI: 10.1007/s11892-019-1150-5 (*joint first authors)

Alam U, Sloan G, Tesfaye S. Treating Pain in Diabetic Neuropathy: Current and Developmental Drugs. **Drugs**. 2020; DOI: 10.1007/s40265-020-01259-2.

Yang H*, Sloan G*, Yingchun Y, Wang S, Duan B, Tesfaye S, Gao L. New perspective in Diabetic neuropathy: From the periphery to the brain, a call for early detection and precision medicine. **Frontiers in Endocrinology**. 2020; DOI: 10.3389/fendo.2019.00929

Tesfaye S, Sloan G. Diabetic Polyneuropathy - Advances in Diagnosis and Intervention Strategies. **Eur Endocrinol.** 2020; 16: 15-20. DOI: 10.17925/EE.2020.16.1.15.

Sloan G, Selvarajah D, Tesfaye S. Pathogenesis, diagnosis and clinical management of diabetic sensorimotor neuropathy. **Nature Reviews Endocrinology**. 2021; 17: 400-420. DOI:10.1038/s41574-021-00496-z

Sloan G, Alam U, Selvarajah D, Tesfaye S. The Treatment of Painful Diabetic Neuropathy. **Current Diabetes Reviews**. 2021; 17. DOI: 10.2174/1573399817666210707112413.

Original articles

Wilkinson ID, Teh K, Heiberg-Gibbons F, Awadh M, Kelsall A, Shillo P, Sloan G, Tesfaye S, Selvarajah D. Determinants of Treatment Response in Painful Diabetic Peripheral Neuropathy: A Combined Deep Sensory Phenotyping and Multimodal Brain MRI Study. **Diabetes**. 2020; 69: 1804-1814. DOI: 10.2337/db20-0029

Heiberg-Gibbons F, Awadh M, Kelsall A, Shillo P, Sloan G, Tesfaye S, Selvarajah D. Somatosensory network functional connectivity differentiates clinical pain phenotypes in diabetic neuropathy. **Diabetologia**. 2021; 64: 1412-1421. DOI: 10.1007/s00125-021-05416-4

Abstracts presented at international conferences

Sloan G, Anton A, Selvarajah D, Tesfaye, Wilkinson ID. 129-OR. Oral presentation at the 80th Scientific Sessions of the American Diabetes Association: Abnormal Mitochondrial Activity in Pain Processing Regions of the Brain in Painful Diabetic Peripheral Neuropathy. **Diabetes.** 2020; 69 (Supplement 1) https://doi.org/10.2337/db20-129-OR

Sloan G, Selvarajah D, Teh K, Shillo R, Wilkinson ID, Tesfaye S. 210-OR. Oral presentation at the 81st Scientific Sessions of the American Diabetes Association: Cerebral Morphometric Alterations in Painless and Painful Diabetic Peripheral Neuropathy. **Diabetes**. 2021; 70 (Supplement 1) https://doi.org/10.2337/db21-210-OR

Sloan G, Selvarajah D, Teh K, Wilkinson ID, Tesfaye S. OR-29. Oral presentation at the 31st Annual Meeting of the Diabetes Neuropathy Study Group of the EASD 2021. INCREASED

FUNCTIONAL CONNECTIVITY OF THE THALAMUS TO THE PRIMARY SOMATOSENSORY CORTEX AND INSULAR CORTEX FOLLOWING TREATMENT WITHDRAWAL: A POTENTIAL BIOMARKER OF PAINFUL-DPN.

Table of Contents

Index of Figures

Index of Tables

List of abbreviations

1H-MRS	Proton Magnetic Resonance Spectroscopy
31P-MRS	31-Phosphorus Magnetic Resonance Spectroscopy
ACC	Anterior Cingulate Cortex
ACR	Albumin to creatinine ratio
ADA	American Diabetes Association
AMARES	Accurate, Robust, and Efficient Spectral fitting
AMPA	α-amino-3-hydroxy-5-methyl-4-isoxazolepropionic acid
ANOVA	Analysis of variance
ATP	Adenosine tri-phosphate
AFT	Autonomic Function Testing
BMI	Body mass index
BOLD	Blood oxygen level-dependent
CAN	Cardiac Autonomic Neuropathy
CDT	Cold detection threshold
CMAP	Compound muscle action potential
CPT	Cold pain threshold
Cho	Choline
Cr	Creatine
DFNS	German Research Network on Neuropathic Pain
DM	Diabetes Mellitus
DMA	Dynamic mechanical allodynia
DN4	Doleur Neuropathique en 4 Questions
DSPN	Diabetic sensorimotor polyneuropathy
ESC	Electrochemical skin conductance

fMRI	Functional magnetic resonance imaging
GABA	γ-aminobutyric acid
Glx	Glutamine and glutamate
HADS	Hospital Anxiety and Depression Scale
HbA1c	Glycated Haemoglobin
HLSVD	Hankel Lanczos Squares Singular Values Decomposition
HPT	Heat pain threshold
HSMN	Hereditary sensory motor neuropathy
HV	Healthy volunteer
IASP	International Association for the Study of Pain
Kv	Potassium channel
IENFD	Intra-epidermal nerve fibre density
IR	Irritable nociceptor
ISIS	Image Selected In Vivo Spectroscopy
M1	Primary motor cortex
MDT	Mechanical detection threshold
MPS	Mechanical pain sensitivity
MPT	Mechanical pain threshold
MMSE	Mini-mental state examination
MNDL	Motor nerve distal latency
MRI	Magnetic resonance imaging
MRS	Magnetic Resonance Spectroscopy
mTCNS	Modified Toronto clinical neuropathy score
NAA	N-acetylaspartate
Nav	Sodium Channel
NCS	Nerve Conduction Studies
NCV	Nerve conduction velocity

NeuPSIG	Neuropathic Pain Special Interest Group
NIR	Non-irritable nociceptor
NIS	Neuropathy Impairment Score
NIS-LL	Neuropathy Impairment Score of the Lower Limb
NIS-LL+7	Neuropathy Impairment Score of the Lower Limb plus 7 tests
NMDA	N-methyl-D-aspartate
NRS	Numeric Rating Scale
No-DSPN	Diabetes without DSPN
OPTION-DM	Optimal Pathway for TreatIng neuropathic paiN in Diabetes Mellitus trial
Painful-DSPN	Painful diabetic sensorimotor polyneuropathy
PCr	Phosphocreatine
PGP 9.5	Protein Gene Product 9.5
Pi	Inorganic phosphate
ppm	Parts per million
PPT	Pressure pain thresholds
PRESS	Point Resolved Spectroscopy
QST	Quantitative Sensory Testing
ROI	Region of interest
ROS	Reactive oxygen species
Rs-fMRI	Resting State Functional magnetic resonance imaging
S1	Primary somatosensory cortex
SFN	Small fibre neuropathy
SNAP	Sensory nerve action potential
T	Tesla

TCNS	Toronto Clinical Neuropathy Score
T1DM	Type 1 Diabetes Mellitus
T2DM	Type 2 Diabetes Mellitus
TE	Echo time
TR	Repetition time
TRPA1	Transient receptor potential cation channel subfamily A member 1
TRPM8	Transient receptor potential cation channel subfamily M member 8
TRPV1	Transient receptor potential cation subfamily V member 1
TSL	Thermal sensory limen
VAS	Visual analogue scale
VGCC	Voltage-gated calcium channel
VGSC	Voltage-gated sodium channel
VDT	Vibration Detection Threshold
WDT	Warm detection thresholds
WUR	Wind-up ratio

1. Introduction

1. 1 Diabetes Mellitus

Diabetes mellitus (DM) is a common group of disorders characterised by chronic hyperglycaemia and metabolic dysfunction. Type 1 diabetes (T1DM) is associated with absolute insulin deficiency because of autoimmune destruction of pancreatic beta-cells. In type 2 diabetes (T2DM), hyperglycaemia develops secondary to insufficient insulin production due to insulin resistance.

There is currently a worldwide pandemic of diabetes mellitus. The International Diabetes Foundation estimated that 463 million people were diagnosed with diabetes in 2019, giving a worldwide prevalence of 9.3%, and this is forecasted to rise to 10.9% by 2045 (Saeedi et al., 2019). Diabetes and its chronic complications are associated with enormous healthcare costs, the estimated global direct health expenditure was 760 billion USD in 2019 (Williams et al., 2020).

1.2 Complications of Diabetes Mellitus

There are many complications attributable to diabetes which are broadly categorised as acute or chronic. The most common acute complications are related to severe hyperglycaemia or hypoglycaemia, the latter generally occurring due to diabetes

treatments. Chronic complications are typically classified as either macrovascular or microvascular, both of which may cast a heavy burden on patients' lives and are independently associated with an increased risk of death (Mohammedi et al., 2017). Macrovascular disorders associated with diabetes include myocardial infarction, peripheral vascular disease and cerebrovascular accidents. The microvascular complications are diabetic retinopathy, nephropathy and neuropathy. Diabetic retinopathy affects up to 100 million people globally and is a common cause of visual impairment and blindness (Leasher et al., 2016, Corcóstegui et al., 2017). Whereas diabetic nephropathy is a leading cause of end stage renal disease and even the presence of milder forms of the condition confers an elevated mortality risk (Matsushita et al., 2010, Ilyas et al., 2017). There is a considerable overlap in the underlying aetiopathogenesis for all three microvascular, and the macrovascular, complications, but the rest of the introduction will focus on neuropathy (Brownlee, 2001, Forbes and Cooper, 2013).

1.3 Diabetic Neuropathy

1.3.1 Classification of diabetic neuropathies

The diabetic neuropathies are heterogenous in their pathophysiology, neurological deficits, clinical features and treatment, with a classification shown in Table 1.1. The diffuse neuropathies affecting the peripheral and autonomic nervous system are the most common, with diabetic sensorimotor polyneuropathy (DSPN) the most prevalent. Indeed, the term 'diabetic neuropathy' is often used to refer to DSPN only. Diabetic autonomic

neuropathy may affect any organ within the body, with cardiac autonomic neuropathy (CAN) the most common. CAN may present with orthostatic hypotension or exercise intolerance, but is often subclinical, requiring cardiac autonomic functions tests (AFT) to make the diagnosis. Mononeuropathies may be due to microvasculitis induced ischaemic injury or nerve entrapment. Radiculoplexus neuropathies have a common pathophysiology and may involve the lower or upper limb or cause truncal radiculopathy.

Generalized symmetrical polyneuropathies

Diabetic sensorimotor polyneuropathy

- Mixed sensorimotor neuropathy
- Predominantly large-fibre neuropathy
- Predominantly small-fibre neuropathy
- Pure small-fibre neuropathy

Acute painful–distal sensorimotor polyneuropathies

- Treatment-induced neuropathy of diabetes mellitus
- Hyperglycaemia-induced neuropathy

Autonomic neuropathy

- Cardiovascular autonomic neuropathy
  - Reduced heart rate variability
  - Resting tachycardia
  - Orthostatic hypotension
  - Exercise intolerance
  - Silent myocardial ischaemia
  - Sudden cardiac death
- Gastrointestinal autonomic neuropathy
  - Oesophageal dysmotility
  - Gastroparesis
  - Diabetic diarrhoea
  - Constipation
  - Faecal incontinence
- Urogenital
  - Neurogenic bladder
  - Sexual dysfunction (erectile and female sexual dysfunction; retrograde ejaculation)
- Sudomotor dysfunction
  - Peripheral anhidrosis
  - Hyperhidrosis
  - Gustatory sweating

Metabolic (that is, hypoglycaemia unawareness)

Pupillary dysfunction

Focal or multifocal neuropathies

Mononeuropathy

- Mononeuropathies
  - Cranial nerve (for example, oculomotor nerve palsy or facial nerve palsy)
  - Peripheral nerve (for example, peroneal nerve palsy)

Mononeuritis multiplex

Radiculoplexus neuropathy

- Radiculopathy
  - Thoracic
  - Abdominal
  - Thoraco–abdominal
- Radiculoplexopathy
  - Lumbosacral radiculoplexopathy
  - Cervical radiculoplexopathy

Entrapment neuropathies

- For example, carpal tunnel syndrome, ulnar neuropathy

Table 1.1. Classification of Diabetic Neuropathies, reproduced from Sloan et al. (Sloan et al., 2021).

1.3.2 Definition of DSPN, painful-DSPN and small fibre neuropathy

The Toronto Diabetic Neuropathy Expert Group convened in 2009 and developed definitions and diagnostic criteria for DSPN and painful-DSPN, shown in Table 1.2 (Tesfaye et al., 2010). These definitions are still widely used. Another more simple definition for clinical practice was suggested by the 2017 American Diabetes Association (ADA) position statement, 'the presence of symptoms and/or signs of peripheral nerve dysfunction in people with diabetes after the exclusion of other causes' (Pop-Busui et al., 2017).

Neuropathic pain has been defined by the International Association for the Study of Pain (IASP) as 'pain caused by a lesion or disease of the somatosensory nervous system' (IASP, 2012). The 2009 Toronto Diabetic Neuropathy Expert Group definition adapts the 2008 definition proposed by IASP, Table 1.2 (Treede et al., 2008).

Small fibre neuropathy (SFN) refers to selective damage to thinly myelinated Aδ and unmyelinated C fibres (Lauria and Lombardi, 2012). These fibres are responsible for transmission of nociception. A definition for SFN currently does not exist, but the diagnostic criteria proposed by the Toronto Diabetic Neuropathy Expert Group is included in Table 1.2 (Tesfaye et al., 2010).

Definition of typical diabetic length dependent sensorimotor polyneuropathy (DSPN)	Symmetrical, length dependent sensorimotor polyneuropathy attributable to metabolic and microvessel alterations as a result of chronic hyperglycaemia exposure (diabetes) and cardiovascular risk covariates
Definition of peripheral neuropathic pain in diabetes	Pain arising as a direct consequence of abnormalities in the peripheral somatosensory system in people with diabetes
Diagnostic criteria of small fibre neuropathy	1. Possible: the presence of length dependent symptoms and/or clinical signs of small fibre damage 2. Probable: the presence of length-dependent symptoms, clinical signs of small fibre damage, and normal NCS 3. Definite: the presence of length-dependent symptoms, clinical signs of small fibre damage, normal NCS and altered IENFD at the ankle or abnormal QST thermal thresholds at the foot

Table 1.2. The definition of DSPN and painful-DSPN and diagnostic criteria of small fibre neuropathy. The grading of small fibre neuropathy, rather than the definition, is provided as a definition of small fibre neuropathy is currently unavailable (Tesfaye et al., 2010). IENFD, Intra epidermal nerve fibre density; NCS, Nerve conduction studies; QST, Quantitative Sensory Testing.

1.3.3 Epidemiology of DSPN

The exact prevalence of DSPN is unknown (Ziegler et al., 2014). This uncertainty exists predominantly because of the methodological discrepancies in the epidemiological literature studying the disorder. The reported prevalence differs depending on the diagnostic criteria used, the population under investigation and the type of diabetes. The influential study, 'The Rochester Diabetic Neuropathy Study' found 60% of those with diabetes to suffer from a neuropathic disorder of some description including DSPN, other diabetic neuropathies and neuropathy unrelated to diabetes (Dyck et al., 1993). When less sensitive measures of DSPN are used, such as questionnaire based assessments without clinical examination or neurophysiological measures, the prevalence may be as low as 11-13% in T1DM (Jeyam et al., 2020, Mizokami-Stout et al., 2020) or 13-18% in T2DM

(Andersen et al., 2018, Christensen et al., 2020, Gylfadottir et al., 2020). However, when neurophysiological measures, such as nerve conduction studies (NCS), are performed the prevalence rises to 42%-54% (Dyck et al., 1993, Partanen et al., 1995, Martin et al., 2014).

1.3.4 Risk factors for DSPN

Advancing age, duration of diabetes and elevated glycated haemoglobin (HbA1c) levels are the most well-known risk factors for the development and progression of DSPN, shown in Figure 1.1 (Maser et al., 1989, Young et al., 1993, Tesfaye et al., 1996, Adler et al., 1997, Tesfaye et al., 2005, Ziegler et al., 2014). In addition, risk factors commonly associated with cardiovascular disease are also related to DSPN, including: hypertension, obesity, dyslipidaemia, smoking and an increase waist/hip ratio (Tesfaye et al., 2005, Jaiswal et al., 2017, Andersen et al., 2018, Jeyam et al., 2020, Mizokami-Stout et al., 2020). Preliminary evidence has also implicated certain genetic polymorphisms which may pre-dispose patients to DSPN, such as variants in the angiotensin converting enzyme and 5,10-methylene-tetrahydrofolate reductase enzyme genes (Witzel et al., 2015). A recent genome-wide association study has also shown a gene encoding for the voltage-gated sodium channel (VGSC) Nav 1.2 has a protective effect upon the development of DSPN (Tang et al., 2019).

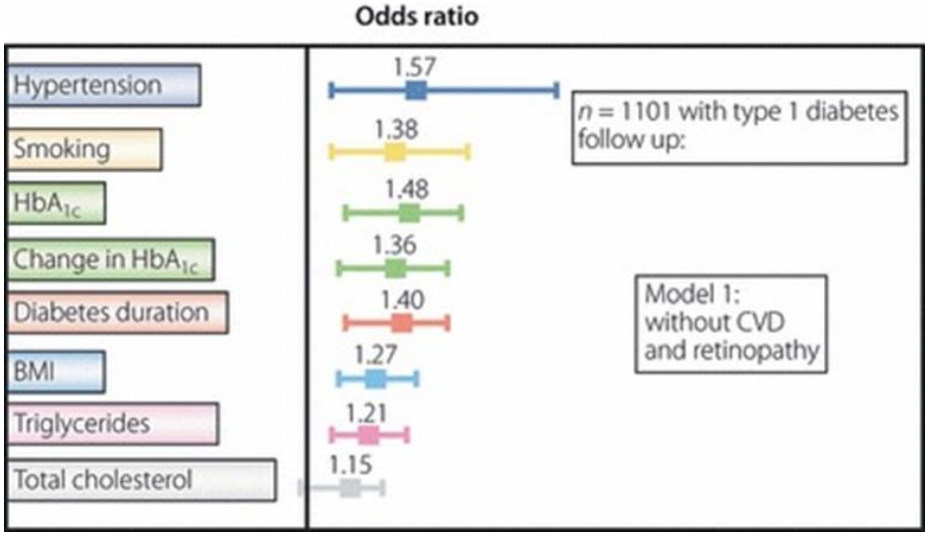

Figure 1.1. Risk factors for incident neuropathy. The EURODIAB Prospective Complications Study determined the odds ratio for the risk factors for DSPN in a cohort of 1101 patients with T1DM followed up for 7.3 ± 0.6 years. BMI, body mass index; CVD, cardiovascular disease. Reproduced from (Tesfaye, 2011), original article (Tesfaye et al., 2005).

1.3.5 Pathology and pathogenesis of DSPN

DSPN is a chronic and progressive peripheral neuropathy, affecting the most distal terminals of peripheral nerves first before spreading proximally in a length dependent manner. Sensory nerves appear to be affected before motor nerves, with peripheral autonomic and sudomotor nerves impacted also. The entire peripheral nerve system is involved in DSPN, including the nerve axon, Schwann cells, dorsal root ganglion and microvasculature (Figure 1.2). Early in the disease course there is a decline in lower-leg intra-epidermal nerve fibres, which are the end terminals for the nociceptive small sensory nerve fibres (Kennedy et al., 1996, Umapathi et al., 2007). As DSPN advances, ankle epidermal innervation may be entirely depleted and more proximal sites, such as the thigh, also have a reduction in IENF

density (IENFD) consistent with the length dependent disease process (Pittenger et al., 2004).

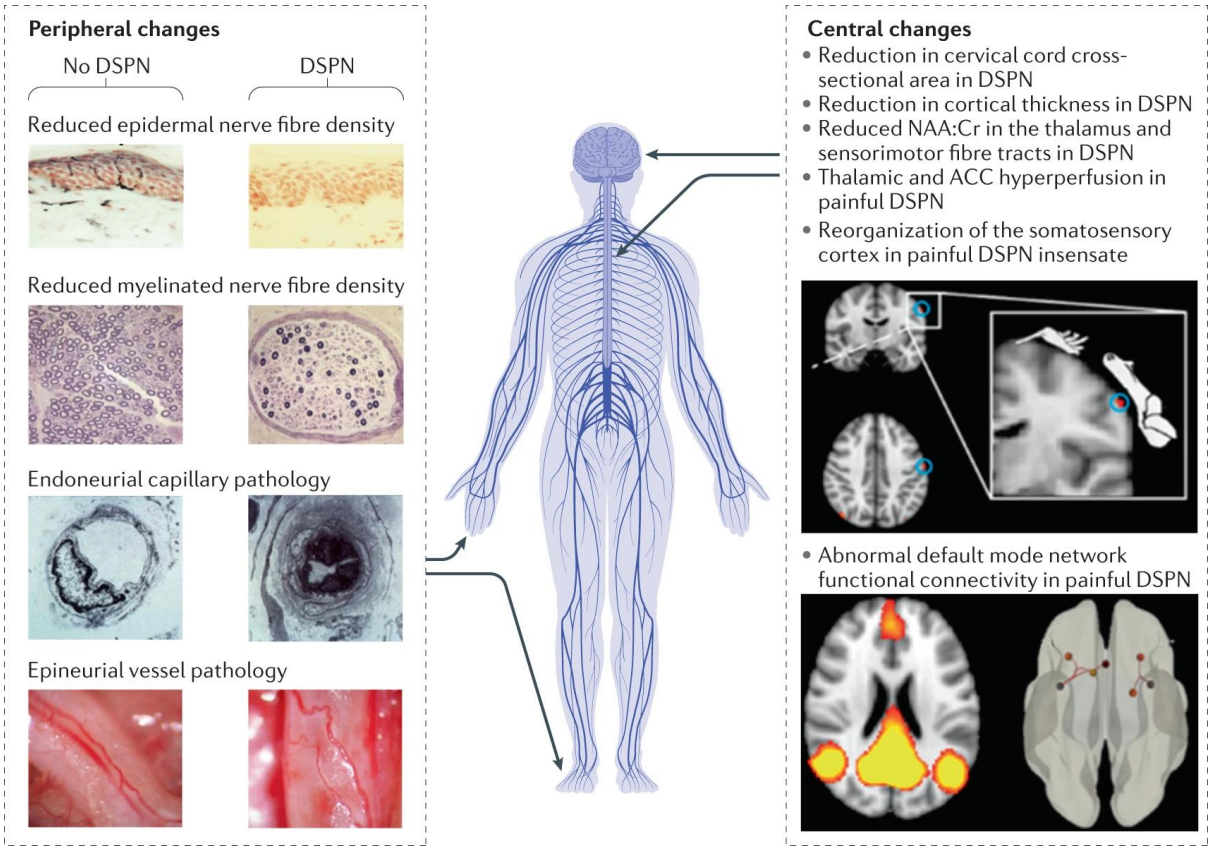

Figure 1.2. Peripheral and Central Nervous System alterations in DSPN. Peripheral alterations include a reduction in the density of intra-epidermal nerve fibres and sural nerve myelinated fibres, sural nerve endoneurial microangiopathy with increased basement membrane cell thickening, endoneurial cell proliferation and vessel occlusion, and sural nerve epineurial arterial attenuation, venous distention and tortuosity, and arteriovenous shunting. Central alterations include structural changes (such as to the spinal cord and somatosensory cortex), neurochemical changes (for example, a reduction in the N-acetylaspartate to creatine (NAA:Cr) ratio in the thalamus and white matter tracts of the parietal lobe), vascular alterations [In the anterior cingulate cortex (ACC) as well as thalamic hypervascularity] and functional alterations (such as abnormal resting and task-based functional connectivity). Reproduced from (Sloan et al., 2021).

The pathological changes in DSPN have been well studied using nerve samples obtained from amputation, autopsy, or biopsy, typically from the sural nerve. The neuronal morphological features of DSPN include axonal degeneration, demyelination, Schwann cell

pathology and microangiopathy, shown in Figure 1.2 (Malik, 1997). Endoneurial vessels develop the most advanced angiopathy, with accumulation of the basal lamina, reduced luminal area and endothelial cell hyperplasia and hypertrophy (Powell et al., 1985, Malik et al., 1993). However, epineurial blood vessels also show profound morphological abnormalities (Tesfaye et al., 1993).

The pathophysiology of DSPN is highly complex and remains incompletely understood. It involves several interrelated pathways, which target multiple cell types ultimately inducing neuronal dysfunction and nerve cell death (Figure 1.3). The vascular abnormalities seen in DSPN result in reduced neuronal blood flow, inducing nerve hypoxia and impaired neuronal function (Newrick et al., 1986, Tesfaye et al., 1992). In addition, endothelial and capillary dysfunction contribute to ischaemic injury in DSPN (Veves et al., 1998, Østergaard et al., 2015).

As a result of peripheral neurons being unable to regulate their uptake of glucose, in diabetes glucose is diverted down a number of molecular pathways which lead to downstream neuronal injury (Tomlinson and Gardiner, 2008). These key pathways include the polyol pathway, hexosamine pathway and activation of protein kinase C (Cameron et al., 2001). Glucose also undergoes irreversible enzymatic reactions with protein, lipids and nucleic acids to form advanced glycation endproducts which can be deposited throughout the peripheral nervous system, inducing permanent structural changes. Additionally, neurotrophic factors have altered expression and function in diabetes, which may result in impaired neuronal regeneration (Apfel, 1999). Insulin also acts as a neurotroph, and both reduced signalling in T1DM and insulin resistance in T2DM have been implicated in the pathogenesis of DSPN (Kim and Feldman, 2012). Fatty acids and Low-Density Lipoproteins

also have a toxic effect on the peripheral nervous system, which is consistent with obesity and dyslipidaemia being risk factors for DSPN (Vincent et al., 2011).

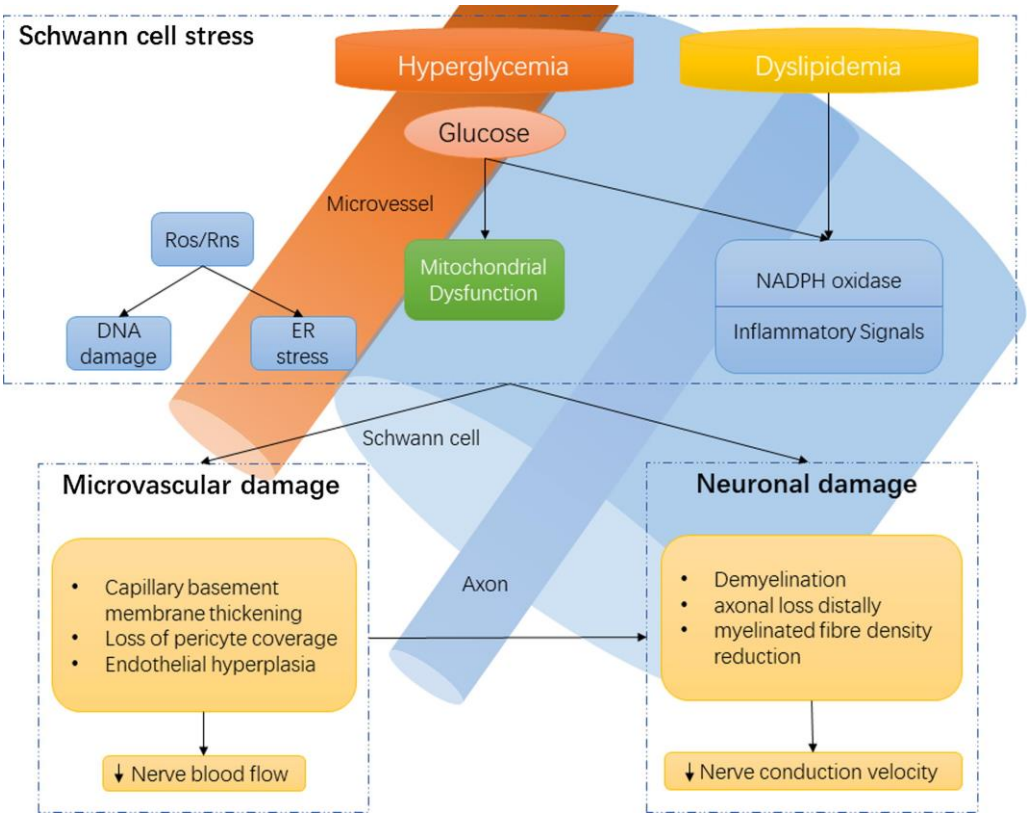

Figure 1.3 Mechanisms of microvascular and neuronal damage in DSPN. Disruption of neuronal support by Schwann cells and the vascular system contributes to neuropathy, in conjunction with the direct effects of diabetes on neurons. ER, endoplasmic reticulum; NADPH, Nicotinamide adenine dinucleotide phosphate; Ros, reactive oxygen species; Rns, reactive nitrogen species. Reproduced from (Sloan et al., 2018).

Hyperglycaemia, dyslipidaemia, impaired insulin/neurotrophic signalling culminate in downstream injurious mechanisms including oxidative stress, inflammation and mitochondrial dysfunction (Feldman et al., 2017). Mitochondrial dysfunction is a common disease mechanism in several peripheral neuropathic disorders and is described as a key factor in DSPN (Cashman and Höke, 2015). The unique bioenergetic requirements for the peripheral neurons, particularly sensory neurons, may make them vulnerable to

mitochondrial dysfunction. Structural abnormalities in mitochondria have been demonstrated in DSPN, including evidence of increased mitochondrial fission, relative to biogenesis, resulting in the production of small dysfunction mitochondria (Vincent et al., 2010). Mitochondrial dysfunction is linked to oxidative stress, which develops due to the imbalance of injurious reactive oxygen species (ROS) generation and cellular antioxidant defence mechanisms. ROS are generated as a physiological by product of electron leakage during mitochondrial oxidative phosphorylation (Naudi et al., 2012). It appears that acute hyperglycaemia results in increased ROS generation and a reduction in adenosine tri-phosphate (ATP) production due to mitochondrial dysfunction (Brownlee, 2001, Feldman et al., 2017). Whereas in chronic hyperglycaemia there is a reduction in cellular respiration and ROS generation (Fernyhough, 2015). Nutritive excess in diabetes causes down regulation of the AMP-activated protein kinase and proliferator-activated receptor γ coactivator-1α signalling pathway, which is the pathway responsible for sensing metabolic demands of the cell and regulation of mitochondrial activity (Chowdhury et al., 2013). Down regulation of this pathway leads to a shift in neuronal metabolism to the less efficient anaerobic glycolysis (Fernyhough, 2015). This maladaptation may lead to neuronal energy failure under stress, with the distal terminals most at risk of bioenergetic disruption, which may in part explain why neurons are affected in a distal-proximal gradient with the IENF impacted first (Chowdhury et al., 2013, Fernyhough, 2015).

1.3.6 Clinical consequences of DSPN

Several clinical sequalae may develop because of DSPN. Diabetic foot ulceration is a common foot diabetic foot complication, for which the loss of protective sensation in DSPN is the primary risk factor (Reiber et al., 1999). The pathway to ulceration and amputation is shown in Figure 1.4. Motor neuropathy and sudomotor can also increase the risk of foot ulceration due to foot deformity and skin dryness, respectively (Boulton et al., 2004). Diabetic foot ulcers are challenging to manage and result in enormous healthcare expenditure (Armstrong et al., 2017). Unfortunately, diabetic foot ulceration often requires lower-limb amputation, particularly when they present late. Charcot neuroarthropathy is a rarer complication of DSPN and without prompt treatment can cause chronic foot deformity, putting the foot at high risk of ulceration (Figure 1.4). Additionally, the presence of DSPN (Brownrigg et al., 2016), foot ulceration (Walsh et al., 2016) and lower limb amputation are associated with a high risk of cardiovascular disease and mortality (Dietrich et al., 2017).

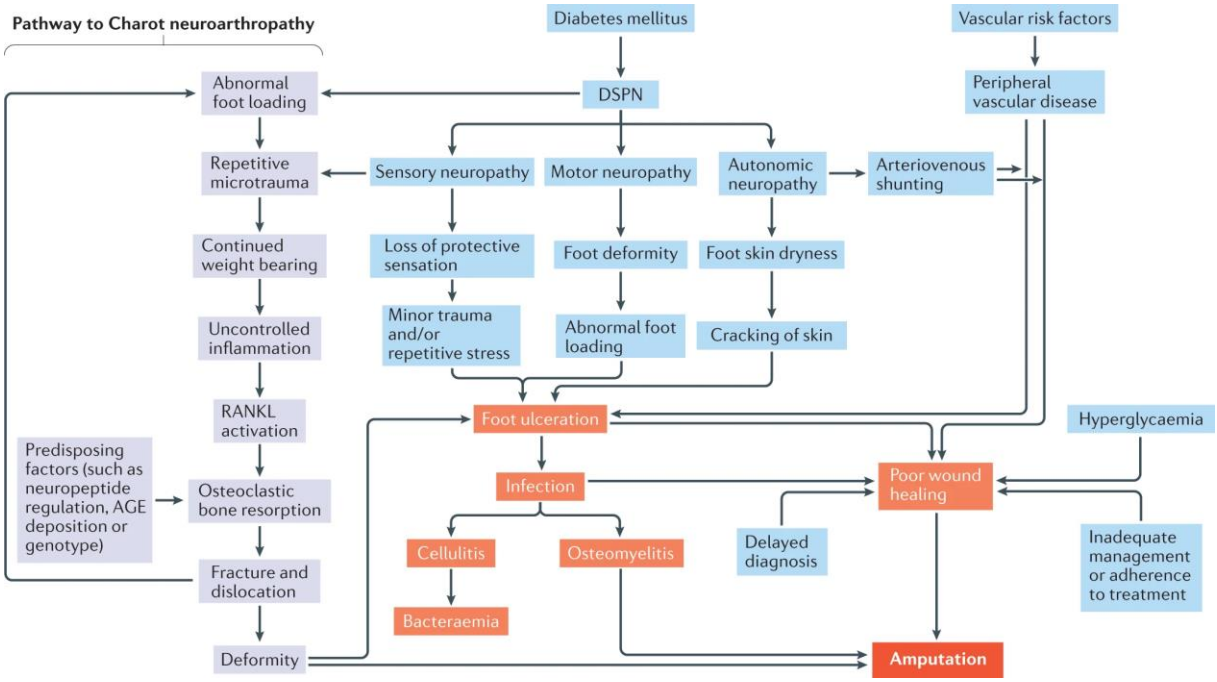

Figure 1.4. The pathways to diabetic foot ulceration and amputation. Diabetic sensorimotor peripheral neuropathy (DSPN), vascular disease and foot deformity might result in foot ulceration. In Charcot neuroarthropathy, minor trauma of the foot or ankle triggers an inflammatory cascade with a subsequent imbalance of the receptor activator of NF-κB ligand (RANKL)–osteoprotegerin axis, promoting osteoclastic bone resorption. A cycle of fracture and dislocation develops which is further compounded by weight bearing. Blue boxes signify risk factors to foot ulceration and poor wound healing. Orange boxes represent the pathway to amputation of the ulcerated foot. The grey boxes indicate the pathway to Charcot neuropathy. AGE, advanced glycation end-product. Reproduced from (Sloan et al., 2021).

DSPN is frequently asymptomatic, particularly in its early stages; as it progresses it can cause impaired balance, reduced muscle strength and altered gait, increasing the risk of falls and potential bone fractures (Alam et al., 2017). Additionally, patients with DSPN may develop peripheral neuropathic pain (painful-DSPN). This condition can have a considerable impact upon its sufferers', leading to a reduction in measures of quality of life (Benbow et al., 1998, Galer et al., 2000, Van Acker et al., 2009, Alleman et al., 2015). Moreover, patients often suffer with other diabetes related co-morbidities, most commonly related to cardiovascular disease (Sadosky et al., 2015), and are also more likely to have depression, anxiety and sleep

disruption (Gore et al., 2005, Selvarajah et al., 2014a, D'Amato et al., 2016). Data from the United States also found that patients with severe painful-DSPN have approximately three-fold greater all-cause medical costs than those with DSPN and five-fold greater than diabetes alone (Sadosky et al., 2015). In addition, painful-DSPN leads to disruption in employment, with higher rates of unemployment and absenteeism, and reduced work-based productivity for those who do work (Tölle et al., 2006, Taylor-Stokes et al., 2011).

1.4 Painful Diabetic Neuropathy

1.4.1 Epidemiology of painful diabetic neuropathy

Epidemiological studies of painful DSPN have similar limitations to those studying DSPN, with the added difficulty of the diagnosis of neuropathic pain (Ziegler et al., 2014, Hébert et al., 2017). The reported prevalence ranges from 13.3% to 34% in the Western world in patients with diabetes (Daousi et al., 2004, Davies et al., 2006, Van Acker et al., 2009, Ziegler et al., 2009, Abbott et al., 2011, Alleman et al., 2015). There may also be considerable regional variation, the prevalence has been reported to be as high as 34.5% in Qatar (Ponirakis et al., 2019), 42.2% in Eastern Libya (Garoushi et al., 2019), 53.7% in a study across the Middle East (Jambart et al., 2011), and 65.3% in Saudi Arabia (Halawa et al., 2010).

1.4.2 Risk factors of painful diabetic neuropathy

Similar to the epidemiological investigation of painful-DSPN, limitations in the methodological study of risk factors also exist (Hébert et al., 2017). Factors have been proposed to predispose to painful-DSPN, when painful-DSPN and DSPN are compared, include; obesity, age, duration of diabetes (Van Acker et al., 2009, Ziegler et al., 2009) and HbA1c (Themistocleous et al., 2016, Hébert et al., 2017). These risk factors suggest that painful-DSPN may be a manifestation of more severe peripheral nerve injury. Several studies have also found a relationship between DSPN severity and the presence and/or severity of neuropathic pain; however, others have found no such association (Shillo et al., 2019b). Moreover, female gender has been proposed as a risk factor for painful-DSPN, a finding which is consistent with other chronic pain conditions (Abraham et al., 2018a, Cardinez et al., 2018, Truini et al., 2018). Genetic factors have also been implicated in the pathogenesis of painful-DSPN, Figure 1.5. Genome-wide association studies have related polymorphisms in Chr8p21.3 and Chr1p35.1 in painful-DSPN, although the methods of case definition were inadequate (Meng et al., 2015a, Meng et al., 2015b). Whilst mutations in the voltage gated sodium channel Nav 1.7 have also been associated with painful-DSPN in smaller, studies with mechanistic investigation of the variants (Blesneac et al., 2017, Alsaloum et al., 2019).

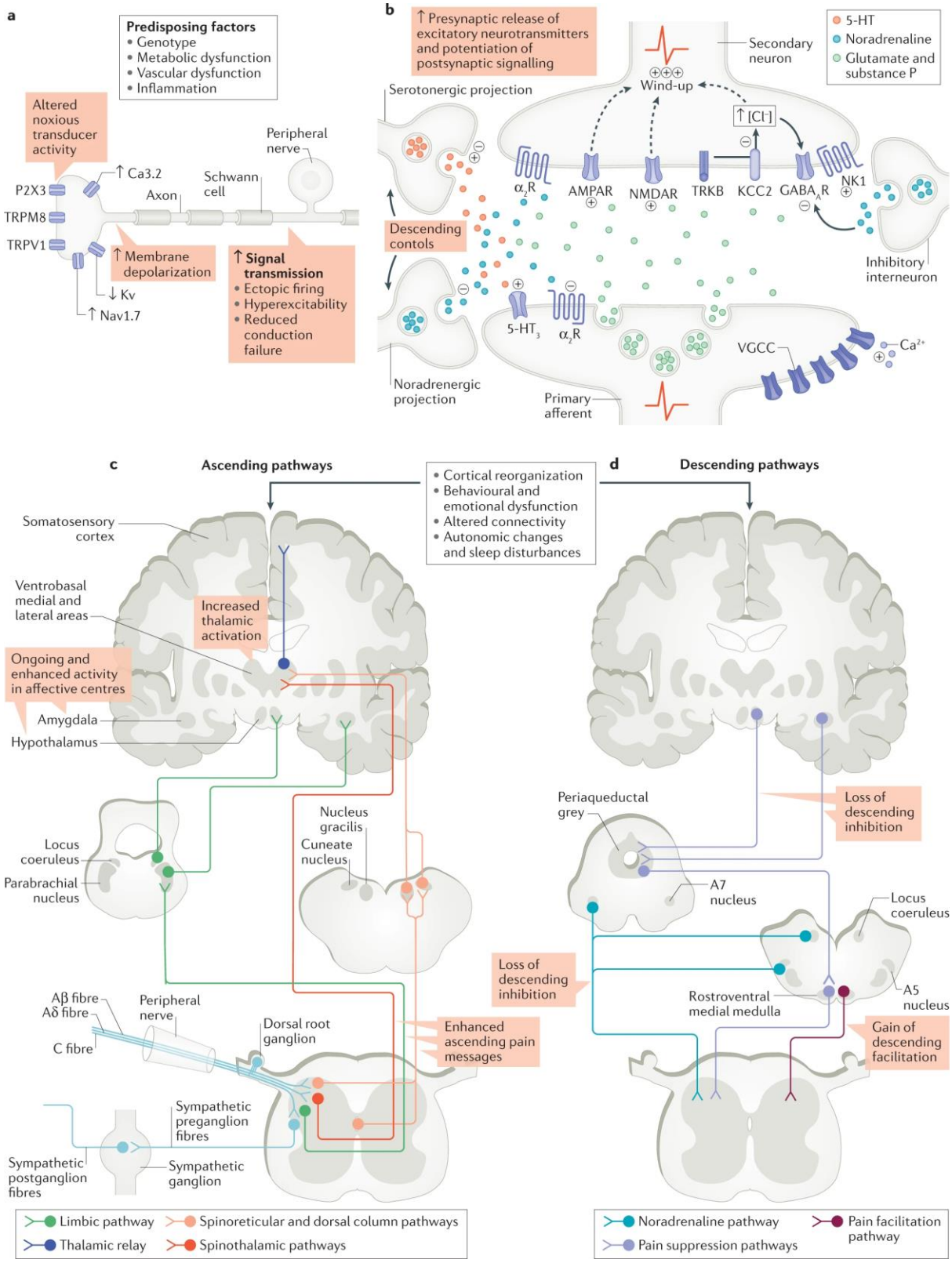
a
Predisposing factors
• Genotype
• Metabolic dysfunction
• Vascular dysfunction
• Inflammation
Altered noxious transducer activity
↑ Ca3.2
P2X3
TRPM8
TRPV1
Axon
Schwann cell
Peripheral nerve
↑ Membrane depolarization
↓ Kv
↑ Nav1.7
↑ Signal transmission
• Ectopic firing
• Hyperexcitability
• Reduced conduction failure
b
↑ Presynaptic release of excitatory neurotransmitters and potentiation of postsynaptic signalling
Secondary neuron
5-HT
Noradrenaline
Glutamate and substance P
Wind-up
Serotonergic projection
↑ [Cl-]
α2R
AMPAR
NMDAR
TRKB
KCC2
GABAAR
NK1
Descending contols
Inhibitory interneuron
5-HT3
α2R
VGCC
Ca2+
Noradrenergic projection
Primary afferent
c
Ascending pathways
• Cortical reorganization
• Behavioural and emotional dysfunction
• Altered connectivity
• Autonomic changes and sleep disturbances
Somatosensory cortex
Ventrobasal medial and lateral areas
Increased thalamic activation
Ongoing and enhanced activity in affective centres
Amygdala
Hypothalamus
Locus coeruleus
Parabrachial nucleus
Nucleus gracilis
Cuneate nucleus
Aβ fibre
Aδ fibre
C fibre
Peripheral nerve
Dorsal root ganglion
Enhanced ascending pain messages
Sympathetic preganglion fibres
Sympathetic postganglion fibres
Sympathetic ganglion
Limbic pathway
Thalamic relay
Spinoreticular and dorsal column pathways
Spinothalamic pathways
d
Descending pathways
Periaqueductal grey
Loss of descending inhibition
A7 nucleus
Locus coeruleus
Loss of descending inhibition
Rostroventral medial medulla
A5 nucleus
Gain of descending facilitation
Noradrenaline pathway
Pain suppression pathways
Pain facilitation pathway

Figure 1.5. Mechanisms of painful DSPN. Numerous alterations occur in the peripheral and central nervous system in painful diabetic sensorimotor peripheral neuropathy (DSPN), leading to an overall gain of facilitatory and loss of inhibitory signalling. Predisposing factors for painful-DSPN might include genotype, metabolic and vascular abnormalities, and inflammation. Peripheral nerve alterations: nerve injury induces nociceptor hypersensitivity through inflammation, altered distal transducer activity (for example, TRPV1, TRPM8 and P2X3) and altered expression of ion channels (for example, sodium, potassium and calcium channels) (part **a**). Alterations in synaptic transmission: persistent nociceptive input increases pre-synaptic neurotransmitter release (for example, glutamate and substance P) and the potentiation of post-synaptic signalling to the spinal cord via enhanced AMPA and NMDA receptor activation. Substance P acts on neurokinin 1 (NK1) to add to this excitation (part **b**). Reduced spinal inhibition through GABA and the transporter potassium-chloride transporter member 5 (KCC2) aids enhanced pain messages. Reduced noradrenaline descending inhibition via α_2 adrenoceptors (α_2Rs) and increased 5-hydroxytryptamine (5-HT) descending excitation via 5-HT_3 receptors add to the dominance of excitatory transmission. Central sensitization develops through an imbalance in the facilitation and inhibitory modulation of pain signals in the spinal cord (parts **c** and **d**) and brain. Autonomic alterations and sleep disturbance as well as psychological, behavioural and emotional factors further enhance pain perception. AMPAR, α-amino-3-hydroxy-5-methyl-4-isoxazolepropionic acid receptor; Ca3.2, T-type calcium channel 3.2; GABA, γ-aminobutyric acid; Kv, potassium channel; Nav1.7, sodium ion channel 1.7; NMDAR, *N*-methyl-D-aspartate receptor; P2X3, P2X purinoceptor 3; TRPM8, transient receptor potential cation channel subfamily M member 8; TRPV1, transient receptor potential cation subfamily V member 1; VGCC, voltage-gated calcium channel. Reproduced from (Sloan et al., 2021).

1.4.3 Pathophysiology of neuropathic pain

This section will firstly summarize the current understanding of the pathophysiology of general neuropathic pain states including, but not specific to, painful-DSPN. Following sections will focus solely upon the mechanisms of painful-DSPN.

Pain is defined by the IASP as ‘an unpleasant sensory or emotional experience associated with actual or potential tissue damage, or described in terms of such damage’ (IASP, 2012). Neuropathic pain occurs when lesions or disease of the somatosensory nervous system lead to altered and disordered transmission of sensory signals to the central nervous system (CNS) (Colloca et al., 2017). Painful-DSPN is a cause of neuropathic pain, with other conditions including postherpetic neuralgia, trigeminal neuralgia, spinal cord injury, cancer and radiculopathies. In neuropathic pain disorders, there is a gain of excitation and

facilitation with a loss of inhibition of pain signals throughout both the peripheral and central nervous system.

The perception of peripheral pain is mediated by specialized sensory neurons, the Aδ and C fibres. These neurons normally have a high threshold for transduction of sensory stimuli, only firing when there is the threat of tissue damage (Dubin and Patapoutian, 2010). However, this threshold is lowered in neuropathic pain conditions where the peripheral nerves become hypersensitive through altered ion channel transducer activity and neurogenic inflammation, see Figure 1.5 (Rosenberger et al., 2020). A number of ion channels are responsible for the transduction of noxious stimuli into action potentials with different channels mediating different sensory modalities, although there is considerable overlap of function (Lumpkin and Caterina, 2007). Transient receptor potential V1 (TRPV1) are polymodal receptors which are important in the transduction of noxious heat pain. When activated by heat, acid or agonists, such as capsaicin in chilli pepper, TRPV1 opens and initiates depolarization of nociceptive sensory nerves (Anand and Bley, 2011). It has been hypothesised that nociceptors in painful-DSPN may be exposed to relatively greater levels of the neurotrophin nerve growth factor, which may up-regulate the production of pro-excitatory proteins such as TRPV1, which could be why patients with neuropathic pain often exhibit burning pains (Baron et al., 2010). Other important mediators of noxious pain include TRPA1 and TRPM8 which are responsible for transduction of cold pain.

Primary afferent input from the peripheral nerves is essential for ongoing neuropathic pain. A study found that administering a peripheral nerve block with lidocaine completely abolishing ipsilateral neuropathic pain (Haroutounian et al., 2014). The electrical properties of peripheral nerves are altered in neuropathic pain, with increased spontaneous activity

and reduced levels of conduction failure (Ochoa et al., 2005, Serra et al., 2012). In painful peripheral neuropathies, it has been proposed that there are alterations in the function and expression of sodium, potassium and calcium ion channels in the peripheral and central nervous system (Colloca et al., 2017). VGSC are responsible for the transduction of sensory stimuli, initiating action potentials and neurotransmitter release at the synaptic terminal (Bennett et al., 2019). There are nine known alpha-subunits of VGSC, with Nav 1.7, 1.8 and 1.9 the most relevant to painful neuropathies. Although their role in painful neuropathies is incompletely understood, rare inheritable pain conditions, such as erythromelalgia and paroxysmal extreme pain disorder, develop as a result of gain-of-function mutations in Nav 1.7 (Bennett and Woods, 2014). Moreover, patients with painful peripheral neuropathies have been shown in genes encoding Nav 1.7 (Faber et al., 2012a), Nav 1.8 (Faber et al., 2012b) and Nav 1.9 (Huang et al., 2014). Alterations in the function and expression of voltage gated potassium channels (Kv) have also been implicated in the pathogenesis of painful neuropathies. Kv is important for the regulation of the initiation of action potentials and their frequency (Du and Gamper, 2013). In models of neuropathic pain, there has been shown to be a reduction in the function of Kv, which is related to neuronal hyperexcitability. In a study of a rodent model of painful-DSPN, the potent activator of Kv retigabine was effective at reducing mechanical hypersensitivity (Djouhri et al., 2019). Voltage gated calcium channels (VGCC) are a key target for pharmacotherapeutic agents in neuropathic pain, such as pregabalin and gabapentin. The N-type of VGCC are expressed at the presynaptic terminal and in response to an action potential they initiate the release of nociceptive neurotransmitters to the spinothalamic neurons. (Zamponi et al., 2009). N-type VGCC are crucial to the development of neuropathic pain, with rodent models lacking these channels demonstrating markedly reduced symptoms of neuropathic pain (Saegusa et al.,

2001). Pregabalin and gabapentin target the α2δ subunits from the dorsal root ganglion and reduce the number of synaptic vesicles fusing with the presynaptic membrane, thereby reducing the release of neurotransmitters into the synapse and preventing the propagation of nociceptive impulses to the peripheral nervous system.

The spinal cord is the first relay for nociceptive neurons from the peripheral nervous system, where excitatory and inhibitory interneurons modulate the output of the spinal cord (D'Mello and Dickenson, 2008). The spinal cord neurons predominantly provide output to the thalamus, via the spinothalamic tract; however, there is also output to the affective areas of the brain, which are important in the emotional response to pain (Tesfaye et al., 2013). Increased pain signal transmission from the peripheral nerve prime the spinal cord to enhance evoked responses to stimuli, which have greater effect due to increased sensitivity of peripheral nerves, see Figure 1.5 (D'Mello and Dickenson, 2008). Increased neurotransmitter release into the synapse mediates enhanced activation of *N*-methyl-D-aspartate (NMDA) and α-amino-3-hydroxy-5-methyl-4-isoxazolepropionic acid (AMPA) receptors which potentiate allodynia/hyperalgesia and the transmission of pain signals. Spinal hyperexcitability is also caused through a loss of γ-aminobutyric acid (GABA) release from inhibitory interneurons (Colloca et al., 2017). In addition, CNS immune cells, microglia, have been postulated to contribute to the maintenance and enhancement of pain signals in the spinal cord in neuropathic pain (Rosenberger et al., 2020). They activate in response to peripheral nerve injury and release pro-inflammatory mediators, which further enhance nociceptive signalling.

The cerebral involvement in pain is highly complex, also see Figure 1.5. As indicated by its definition given above, pain is a subjective experience which is influenced by not only

pathological factors, but also centrally mediated factors such as memory, emotion and cognition (Tracey and Mantyh, 2007). Imaging techniques, which will be described in subsequent sections, have identified a series of structures within the brain that are activated during the perception of acute pain (Apkarian et al., 2005). Studies have identified a range of brain regions with alterations in their structure, function, neurochemistry and vascular supply, using advanced imaging techniques (Tracey et al., 2019). Similar to the rest of the nervous system, there is a shift towards excitation and reduced inhibition of pain signals to the brain (Colloca et al., 2017). Persistent inputs to brain regions mediation emotion such as the cingulate cortex and amygdala areas are thought to mediate fear, depression and sleep problems (Tesfaye et al., 2013). In addition, there is dysfunction of descending endogenous inhibition of pain signalling, mediated by affective brain centres [e.g. anterior cintulate gyrus (ACC), amygdala and hypothalamus], the descending brain modulatory system in the brainstem and spinal noradrenergic and serotonergic pathways (D'Mello and Dickenson, 2008, Tesfaye et al., 2013, Colloca et al., 2017, Rosenberger et al., 2020).

1.4.4 Differences between painful- and painless-DSPN.

The specific mechanisms leading to neuropathic pain in DSPN are poorly understood but a number of potential contributory factors have been proposed, Table 1.3 (Shillo et al., 2019b).

Contributory Factor	Difference associated with painful-DSPN
Risk factors	Female Sex Diabetic nephropathy Nav 1.7 mutations
Small fibre dysfunction	Hyposensitivity phenotype Epidermal nerve fibre regeneration Greater peripheral and corneal small nerve fibre dysfunction
Microvascular alterations	Elevated immunostaining for blood vessels Increased serum markers of angiogenesis and endothelial dysfunction
Vitamin D	Reduced 25-hydroxyvitamin-D levels
Inflammation	Increased serum inflammatory biomarker levels (e.g. C-reactive protein, tumour necrosis factor, interleukin 6)
Spinal cord function	Impaired spinal inhibitory function
Thalamic function	Preservation of thalamic N-acetylaspartate and γ-aminobutyric acid neurochemical make-up Thalamic hyperperfusion Altered somato-thalamic functional connectivity
Descending modulatory pain dysfunction	Ventrolateral periaqueductal grey-mediated descending pain modulatory dysfunction
Higher brain centre alterations	Abnormal anterior cingulate cortex blood flow Altered functional connectivity between higher brain centres at rest and during experimental pain

Table 1.3. Reported differences between painful- and painless-DSPN, adapted from (Shillo et al., 2019b). Nav, voltage gated sodium channel.

The mechanisms involved in the generation and maintenance of painful-DSPN are believed to involve both peripheral and centrally mediated factors, see Figure 1.5 and Table 1.3. The autonomic, systemic, and peripherally mediated factors will be discussed here, whilst the central and peripheral skin biopsy and microvascular alterations will predominantly be discussed in later chapters.

Rodent models have been used for the pre-clinical study of neuropathic pain and pathogenetic mechanisms of painful-DSPN. However, these models are limited by their phenotypic and pathological disparity with human DSPN. Rodents rarely show morphological evidence of neuropathy as a result of their short life span (Obrosova, 2009). Moreover, behavioural markers suggestive of neuropathic pain often occur transiently a few weeks after the initiation of diabetes before the models then develop persisting hypoalgesia (Pabbidi et al., 2008, Cheng et al., 2009). The behaviour in these rodent models may reflect acute hyperglycaemic nerve damage, rather than a translatable model of human DSPN/painful-DSPN. Due to the differences between pre-clinical models and clinical DSPN most of the following discussion will focus on human studies.

Despite the profound clinical differences of painful-DSPN, the mechanisms for the underlying genesis of neuropathic pain remains uncertain (Veves et al., 2008, Spallone and Greco, 2013, Tesfaye et al., 2013). Studies of nerve pathology and neurophysiological testing have been unable to find discriminating features from painless-DSPN. Although more recent studies have found evidence of increased peripheral small fibre dysfunction using detailed quantitative sensory testing protocols (QST) (Themistocleous et al., 2016, Raputova et al., 2017) and corneal nerve fibre depletion using corneal confocal microscopy (Kalteniece et al., 2020).

Both CAN and painful-DSPN involve dysfunction and injury to small nerve fibres, therefore a potential relationship has been investigated. Gandhi et al. demonstrated significantly greater autonomic dysfunction, measured using spectral analysis of heart rate variability, in patients with painful- compared to painless-DSPN (Gandhi et al., 2010). Although other studies have demonstrated greater cardiac autonomic dysfunction in painful-DSPN, the

evidence is conflicting, and not all studies have shown a difference compared with painless-DSPN (Shillo et al., 2019b). Moreover, the significance of CAN in painful-DSPN is uncertain, it may reflect greater small fibre injury or perhaps a potential disease mechanism linked to peripheral vasomotor control.

The role of hyperglycaemia mediated mechanisms in painful-DSPN is also not understood. Studies using rodent models of diabetes find that neuropathic pain behaviours are related to many metabolic pathways thought to be involved in the pathogenesis of DSPN (Obrosova, 2009). However, targeting these pathways in human painful-DSPN has been largely ineffective at alleviating painful symptoms (Boulton et al., 2013). A small study found that glycaemic flux was increased in painful-DSPN (Oyibo et al., 2002); however, it is not clear whether this is a cause or an effect. Methylglyoxal, a precursor to advanced glycation endproduct formation, has been shown to induce hyperalgesia via modification of Nav 1.8 (Bierhaus et al., 2012); although a large observational study found serum levels of methylglyoxal were unrelated to painful-DSPN (Hansen et al., 2015).

Inflammation is another factor which may lead to neuropathic pain in DSPN (Shillo et al., 2019b). Several studies have shown increased serum levels of systemic acute-phase proteins and chemokines in painful-DSPN, including c-reactive protein (Doupis et al., 2009), tumour necrosis factor-α (Purwata, 2011) and interleukin-6 (Herder et al., 2015). Neuroinflammation has also been shown to contribute to neuronal hypersensitivity in rodent models of painful-DSPN (Rosenberger et al., 2020).

Vitamin D is classically recognised as a key factor in calcium metabolism and bone health. However, it has been implicated in a number of chronic pain states, including painful-DSPN. Previous studies have shown that vitamin D levels are lower in painful- compared to

painless-DSPN (Shillo et al., 2019a). The study was cross-sectional, therefore unable to determine a causal relationship; however, non-randomized studies have shown improvements in symptoms with vitamin D treatment (Basit et al., 2016).

In summary, there is clinical evidence to suggest that painful-DSPN may be a consequence of more severe neuropathic injury (Sloan et al., 2018). The risk factors for painful-DSPN (e.g. increasing age, longer duration of DM, obesity etc.) and recent findings of greater small fibre dysfunction in painful- compared to painless-DSPN (Themistocleous et al., 2016, Raputova et al., 2017), support this notion. Nociceptive nerve fibres exposed to more intense hypoxic and metabolic injury in diabetes may become sensitized in susceptible individuals, e.g. patients with VGSC gene variants (Sloan et al., 2018). Residual or regeneration nociceptive nerve fibres may lead to the generation of neuropathic pain, perhaps mediated by excessive levels of neurotrophins such as nerve growth factors.

1.5 Central nervous system mediated mechanisms of painful-DSPN

Before considering the spinal cord and cerebral alterations identified in DSPN and painful-DSPN the investigative technique of magnetic resonance imaging (MRI) will be introduced. Although there is evidence from other techniques which have investigated spinal cord and cerebral involvement in the condition, e.g. electrophysiology, autopsy and other imaging techniques, this is the predominant modality used in the recent literature and in this thesis.

1.5.1 Magnetic resonance imaging

MRI is an imaging modality which utilises non-ionising electromagnetic radiation. Clinically, it is a valuable diagnostic tool as it can produce highly detailed images of the anatomy of the patient and pathology of several medical conditions. However, the unique properties of MR susceptible nuclei and advances in imaging modalities have enabled research into the physiology of the human body and pathophysiology of diseases that is not possible with other diagnostic imaging techniques.

An MR system consists of a control centre, which houses the host computer, and the MR machine in which the patient lies. The MRI scanner contains parts of the system to generate and receive the MR signal, including magnet coils, gradient coils, shim coils and a radiofrequency transmitter coil (Wilkinson and Paley, 2008). Magnetic coils are super cooled using cryogenic liquid helium so that they may produce strong, constant magnetic fields. The strength of a magnetic field is measured in tesla (T), one T is equivalent to approximately 20,000 times the earth's magnetic field strength. Gradient coils generate magnetic fields in three orthogonal directions (x, y and z) to vary the main magnetic field for image slice localisation and phase/frequency encoding. Radiofrequency coils transmit radiofrequency energy to the tissue of interest and receive the induced signal back whereas shim coils adjust the magnetic field to improve field homogeneity. In order to construct an image, the slice is localised by gradient coils generating a gradient field across a chosen axis. The signal echo is encoded into the data matrix known as k-space. The output from the receiver coil is digitised and reconstructed by computer processors using complex mathematical computation.

1.5.2 Magnetic resonance imaging physics

Magnetic resonance describes the unique properties of susceptible nuclei. Almost all clinical MR images utilise these properties of hydrogen atoms, because of their abundance throughout the human body in water (Wilkinson and Paley, 2008). However, all nuclei, which contain an odd number of protons and/or neutrons, undergo 'non-zero nuclear spin' and are susceptible to the MR process. Other nuclei which are suitable for MR imaging, predominantly in the research environment, include 31-phosphorus (31P), 23-sodium and 13-carbon. These nuclei have a net charge and exhibit nuclear spin. They therefore have angular momentum. This moving electrical current generates a magnetic field, known as a magnetic moment which are normally randomly orientated; however, when placed within the uniform magnetic field of an MRI scanner (the direction of which is termed the z-axis), the net magnetisation aligns with the field (Wilkinson and Paley, 2008). This nuclei spin is aligned with the magnetic field and moves in a characteristic way known as precession, akin to a gyroscope spinning (Currie et al., 2013b). The frequency of this precession is proportional to the applied magnetic field, the Larmor frequency. When a patient lies is within the magnetic field of an MRI scanner, the sum magnetic vector of their tissues align with the external field and are not measurable, however.

Radiofrequency pulses are produced by radiofrequency coils. This pulse is given at the same frequency as the Larmor frequency of the target nuclei, which induces strong resonant effect (Currie et al., 2013b). The radiofrequency energy is absorbed and the net magnetization of the nuclei rotates away from the z-axis (Wilkinson and Paley, 2008), with the amount of rotation dependent on the strength and duration of the radiofrequency pulse (Pooley, 2005). When the radiofrequency pulse is turned off the magnetization of the nuclei

falls back to equilibrium, which releases radiofrequency energy and induces a voltage within an MRI receiver coil (Wilkinson and Paley, 2008). The time that it takes for restoration of longitudinal magnetization along the z-axis to revert to its equilibrium is the T1 relaxation time. T1 relaxation differs among molecules; it is typically very slow in water and fast in fat. The T1 relaxation involves the exchange of energy of higher energy nuclei and their surrounding nuclei, known as the spin-lattice relaxation time. Transverse relaxation within the x-y plane occur from magnetic field inhomogeneity within the local magnetic field (T2* relaxation) and interactions between nuclear spins (T2 relaxation) (Wilkinson and Paley, 2008, Currie et al., 2013b). Additionally, after a radiofrequency pulse is turned off T1 and T2 relaxation occur simultaneously with decreasing amplitude as protons lose phase coherence, this causes the signal produced from the high energy nuclei to decay, known as free induction decay.

To facilitate spatial encoding and improving imaging contrast by 'weighting' the signal, for example to produce T1 or T2 weighted images, radiofrequency pulses are repeated with pre-defined repetition times (TR) and echo times (TE) (Currie et al., 2013b). Spin echo and gradient echo sequences are two techniques to cause refocusing of transverse magnetization. The physical properties of protons and numerous imaging sequences offers a range of possible image contrasts (Wilkinson and Paley, 2008).

1.5.3 Magnetic resonance imaging safety

MRI scanning is generally considered a safe procedure as long as some strict safety measures are considered (Wilkinson and Paley, 2008). The strong magnetic fields generated

within the MRI scanner attracts ferromagnetic objects which may become dangerous projectiles. Therefore, only MR safe objects may be brought into the scanning room. Additionally, magnetic fields can affect certain implanted medical metallic devices or shrapnel and dislodge them. Finally, radiofrequency pulses may cause heating of metallic implanted devices causing tissue damage. Strict safety checks are therefore undergone by trained radiographers in order to prevent patients or research participants entering the MRI scanner to ensure that participants with implanted ferromagnetic objects do not enter the scan room. Intravenous contrast agents may be used for certain clinical and research purposes and are generally safe but may cause allergic reactions and potential serious complications in severe renal impairment. The MR scanners produce significant noise and can potentially cause auditory damage. Therefore, protective earwear is commonly given to the patient/research participant.

1.5.4 Central nervous system involvement in DSPN

Various lines of investigation have found alterations in the function and structure of the CNS in patients with diabetes. These patients are known to have a higher risk of cerebral diseases, such as cerebrovascular disease, subclinical cognitive impairment, and dementia syndromes. The involvement of the brain DSPN and painful-DSPN will be discussed in greater detail in later chapters, but an overview of certain concepts will be introduced here.

1.5.4.1 Spinal cord involvement in DSPN

There is now considerable evidence to support the view that DSPN involves not only the peripheral but also the CNS (Tesfaye et al., 2016). This was first recognised in the 1960's when human autopsy studies of patients with extremely advanced diabetes with macro- and microvascular complications demonstrated diffuse degenerative changes within the spinal cord and the brain (Reske-Nielsen et al., 1966, Reske-Nielsen and Lundbaek, 1968). Furthermore, cerebral and spinal conduction deficits have also been shown in humans and rodents with diabetes (Biessels et al., 1999, Suzuki et al., 2000, Kucera et al., 2005). Spinal cord involvement in DSPN was then confirmed in two MR imaging studies (Eaton et al., 2001, Selvarajah et al., 2006). Initially, a small study including 19 patients with DSPN were compared with 10 patients with diabetes without DSPN (no-DSPN) and 10 healthy volunteers (HV) (Eaton et al., 2001). Participants underwent MR imaging of the cervical and thoracic spine, which revealed a reduced cord area in those with DSPN compared to healthy controls. These findings were confirmed in a larger study of 81 patients with T1DM (19 no-DSPN, 23 subclinical-DSPN and 39 clinical-DSPN), 24 healthy volunteers and 8 disease control patients with hereditary sensory motor neuropathy type 1A (HSMN) (Selvarajah et al., 2006). In this study, the spinal cord area was corrected for age, height and weight, to calculate the spinal cord area index. This measure was reduced in those with subclinical- and clinical-DSPN compared with the other groups (Figure 1.6). Interestingly, patients with HSMN did not have a reduction in spinal cord area, despite having very severe neuropathic deficits. This therefore argues against the idea that central nervous alterations are due to a 'dying back' axonopathy and may suggest concomitant disease of the central and peripheral nervous system in DSPN.

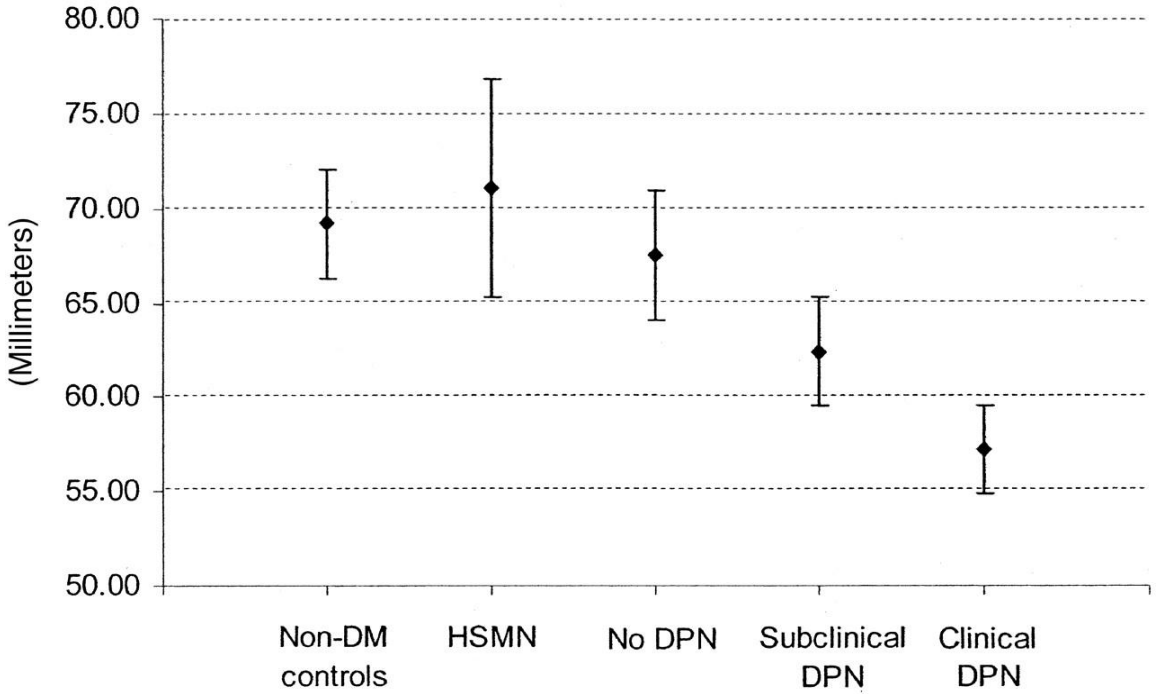

Figure 1.6. Spinal cord area measurement in five groups. The mean and 95% confidence interval spinal cord area index per group, adjusted for age, height and weight. No DSPN versus subclinical DSPN, p=0.03; subclinical versus clinical DSPN, p=0.06; clinical DSPN versus No DSPN p<0.001. DPN, DSPN; DM, diabetes mellitus; DSPN, diabetic peripheral neuropathy; HSMN, hereditary sensory motor neuropathy type 1A. Reproduced from (Selvarajah et al., 2006).

There is also evidence of functional alterations of the spinal cord in painful-DSPN. A recent study investigated the role of spinal disinhibition in experimental and clinical painful-DSPN (Marshall et al., 2017). The study used the change in amplitude of the Hoffman reflex over consecutive stimulations on electromyelograms as a measure of spinal inhibitory function. Impairment of the rate-dependent depression (RDD) is indicative of spinal disinhibition. In both experimental and clinical painful-DSPN there was evidence of deficits in RDD, suggesting impaired spinal disinhibition as a potential disease mechanism in painful-DSPN.

1.5.4.2 Cerebral involvement in DSPN

In addition to morphometric abnormalities shown in the spinal cord, there are morphometric changes in the brain in DSPN and painful-DSPN. Studies have demonstrated a reduction in grey matter volume, and/or cortical thickness, of brain regions related to somatosensory perception in patients with DSPN (Manor et al., 2012, Selvarajah et al., 2014b, Selvarajah et al., 2019, Zhang et al., 2019). A recent publication has related anatomical and functional changes in patients altered between different phenotypes of painful-DSPN (Selvarajah et al., 2019). These morphometric studies have generally been small and the morphological changes in the brain in DSPN have not been confirmed in larger studies; additionally, the differences between brain morphology in painless- and painful-DSPN are unknown.

The thalamus appears to be a key brain region involved in the pathogenesis of painful-DSPN. Thalamic neurons in rat models of painful-DSPN develop increased spontaneous activity, hyper-responsiveness and enlarged receptive fields (Fischer et al., 2009, Freeman et al., 2016). Neurochemical analysis of the brain has also shown neuronal dysfunction within the thalamus in humans with DSPN (Selvarajah et al., 2008). A follow-up, unpublished study confirmed these findings in a larger patient group; however, this study demonstrated that neuronal integrity was maintained in the somatosensory cortex and in the thalamus patients with sub-clinical and painful-DSPN (Gandhi et al., 2006). Small preliminary clinical studies have also found evidence of disrupted thalamocortical connections (Cauda et al., 2009a) and increased vascularity in the thalamus (Selvarajah et al., 2011) in patients with painful-DSPN. These findings suggest that there is preservation of function, if not overt neuronal hyperexcitability, within the thalamus in clinical painful- compared with painless-DSPN,

although this has not been confirmed. Further areas of the brain investigated in painful-DSPN include the ACC, where greater activity in this region was associated with painful-DSPN and also predicted response to pharmacological intervention (Watanabe et al., 2018). Another recent multi-modal MR study also found dysfunction within the ventrolateral periaqueductal grey-mediated descending pain modulatory system in patients with painful-DSPN (Segerdahl et al., 2018).

Overall, studies have demonstrated preliminary findings indicating that CNS changes occur in DSPN and painful-DSPN. However, these studies are generally small, and outside of our research group the included participants can have inadequate clinical characterization or case definition. Moreover, these studies generally use single modalities of neuroimaging, which often cannot determine the underlying disease processes causing the cerebral alterations.

1.6 Diagnosis and assessment of DSPN

1.6.1 Diagnosis of DSPN in the clinical environment

The minimal criteria for the diagnosis of DSPN has been proposed by the Toronto Diabetic Neuropathy Expert Group, see Table 1.4.

Definition of minimal criteria for typical DSPN
1. **Possible DSPN**: The presence of symptoms or signs of DSPN may include the following: symptoms–decreased sensation, positive neuropathic sensory symptoms (e.g., "asleep numbness," prickling or stabbing, burning or aching pain) predominantly in the toes, feet, or legs; or signs–symmetric decrease of distal sensation or unequivocally decreased or absent ankle reflexes.
2. **Probable DSPN:** The presence of a combination of symptoms and signs of neuropathy include any two or more of the following: neuropathic symptoms, decreased distal sensation, or unequivocally decreased or absent ankle reflexes.
3. **Confirmed DSPN**: The presence of an abnormality of nerve conduction and a symptom or symptoms or a sign or signs of neuropathy confirm DSPN. If nerve conduction is normal, a validated measure of SFN with class 1 evidence may be used, e.g. thermal threshold testing or skin biopsy with quantification of intra-epidermal nerve fibre density.
4. **Subclinical DSPN**: The presence of no signs or symptoms of neuropathy are confirmed with abnormal NCs or a validated measure of SFN (with class 1 evidence).

Table 1.4. Minimal diagnostic criteria for the diagnosis of DSPN, adapted from (Tesfaye et al., 2010).

Within clinical practice, most often the diagnosis of DSPN is made during Nationwide annual diabetic foot screening using simple bedside instruments (e.g. 128-Hz tuning fork and 10g monofilament). Making a 'possible' or 'probable' diagnosis of DSPN is normally sufficient in the clinical scenario (Table 1.4). Other potential causes of neuropathy and peripheral neuropathy should be excluded on clinical history and examination, and relevant investigations. The differential diagnosis of peripheral neuropathy in diabetes includes: hypothyroidism, chronic kidney disease, vasculitis, paraproteinaemia, amyloidosis, vitamin B12 deficiency, micronutrient deficiency post-bariatric surgery, industrial agent or metal exposure (e.g. arsenic, mercury, acrylamide and organophosphates), infectious disease (e.g. HIV, Hepatitis B and Lyme's disease), hereditary motor, sensory and autonomic neuropathy, and drugs (e.g. alcohol, amiodarone, colchicine etc.) (Pop-Busui et al., 2017).

1.6.2 Diagnosis and grading the severity of DSPN in the research environment

In the context of clinical research, it is essential that a confirmed diagnosis of DSPN is made with precise grading of the disease. No individual test is adequate to diagnose and grade the severity of DSPN (Dyck et al., 1987). Therefore, combining a range of different techniques is preferable to ensure accurate case definition. The Toronto Diabetic Neuropathy Expert Group recommend that a confirmed diagnosis is necessary for clinical research studies, requiring the use of objective measures of neuropathy, see Table 1.4 (Tesfaye et al., 2010). The ADA recommend that validated clinical scoring systems may be combined with electrophysiology and measures of small fibre damage in the context of DSPN trials (Pop-Busui et al., 2017). Whereas a joint report on the American Academy for Neurology, the American Association of Electrodiagnostic Medicine, and the American Academy of Physical Medicine and Rehabilitation suggested the combination of neuropathic symptoms, signs and abnormal electrodiagnostic studies provide the most accurate diagnosis of distal symmetrical polyneuropathy (England et al., 2005).

The grading of severity of DSPN is also necessary for clinical research. Research studies often use either individual or a combination of clinical scoring system or neurophysiological parameters to estimate the severity of DSPN (Pop-Busui et al., 2017). The Toronto Diabetic Neuropathy Expert Group suggest grading based on a staged or a continuous approach, the latter of which may involve the use of composite scoring systems including clinical examination findings and neurophysiological tests (Dyck et al., 2011a).

1.6.3 Clinical and composite scoring systems of DSPN

A number of clinical scoring systems have been developed and validated to measure peripheral neuropathy/DSPN severity, with widespread use in epidemiologic and clinical studies (Vas et al., 2015). The scoring systems can measure symptoms, signs or a combination of the two. The most commonly used measures of symptoms and signs are the Michigan Neuropathy Screening Instrument (Feldman et al., 1994) and the Toronto Clinical Neuropathy Score (TCNS) (Bril and Perkins, 2002b). The TCNS has been validated against sural nerve morphology and electrophysiology to determine the presence and severity of DSPN (Bril and Perkins, 2002b). More recently, the TCNS has been validated for a wide spectrum of peripheral neuropathies, showing inter- and intra-observer reliability (kappa 0.92-0.93) and an area under the receiver operating characteristics curve of 0.93 (Abraham et al., 2018b). It is a validated 19-point scoring system which grades DSPN severity according to symptom score (foot pain, numbness, tingling, weakness, imbalance and upper limb symptoms), lower limb reflex score (bilateral knee and ankle reflexes) and sensory signs (pinprick, temperature, light touch, vibration and position sense), see Appendix (Perkins et al., 2001, Bril and Perkins, 2002b).

Dyck et al. (1997) devised the Neuropathy Impairment Score of the Lower Limb (NIS-LL), which provides a summed score of clinical examination sensory and motor findings (e.g. muscle tendon reflexes and muscle group power assessment of the lower limb), see Appendix. The Neuropathy Impairment Score of the Lower Limb (NIS-LL) is able to distinguish between neuropathy and normality with 83% sensitivity and 97% specificity, although it predominantly assesses motor activity limiting its usefulness in pure small fibre neuropathy (Zilliox et al., 2015). The NIS-LL plus 7 tests (NIS-LL+7) was developed, which

combines the NIS-LL to seven neurophysiological tests, AFT, NCS measures and vibration detection thresholds (VDT) to calculate an overall measure of neuropathy severity, see Appendix (Dyck et al., 1997). The NIS-LL+7 is a continuous measure of DSPN severity and has been widely used in DSPN research studies as a clinical endpoint (Dyck et al., 2013b).

1.6.4 Nerve conduction studies

NCS have long been considered the gold standard investigation to diagnose and grade the severity of DSPN in both clinical and research settings (Dyck et al., 1985, Dyck, 1988). The procedure involves stimulation of the proximal aspect of the targeted peripheral nerve with recording electrodes placed distally either along the nerve for sensory studies or the muscle target of a motor nerve. There are several individual attributes which may be measured using NCS including: motor nerve amplitude, conduction velocity and distal motor latency, sensory nerve amplitude, distal latency, and conduction velocity and F wave latencies.

Numerous guidelines recommend NCS for case definition of distal symmetrical polyneuropathies in the research environment (England et al., 2005, Dyck et al., 2011a, Pop-Busui et al., 2017). NCS measures correlate with the severity of DSPN and nerve biopsy pathology (Behse et al., 1977, Dyck et al., 2003, Weisman et al., 2013) and are an objective measure of nerve function which are sensitive, specific and reproducible. However, there are some limitations of NCS. It can be time consuming to perform the studies and in general they are only performed by specialist neurophysiologists which limits their accessibility and raises their cost (Vas et al., 2015). Also, the 'Clinical vs Neurophysiology Investigators' have demonstrated inter-observer differences in measurement of NCS (Dyck et al., 2013a, Litchy

et al., 2014). Therefore, strict protocols should be followed to ensure the accuracy of NCS, including maintenance of limb temperature, correct and exact placement of electrodes, accurate measurement of distances, avoidance of recording spurious responses and use of just supramaximal electrical stimulation (England et al., 2005, Tesfaye et al., 2010).

There is no individual protocol that is uniformly used in the assessment of DSPN or distal symmetrical polyneuropathy, although a combination of nerve conduction attributes is more sensitive than a single measure (Dyck et al., 2003). The most frequently abnormal electrophysiological abnormalities in DSPN are present in the nerves of the lower limb, the sural, peroneal and tibial nerve (Dyck et al., 2011b, Karsidag et al., 2005). A simplified protocol by the 'Report of the American Academy of Neurology, the American Association of Electrodiagnostic Medicine, and the American Academy of Physical Medicine and Rehabilitation' recommends sural sensory and peroneal nerve measures, as these are the most sensitive markers for polyneuropathy (England et al., 2005). If either is abnormal then additional studies should be performed. The peroneal nerve compound muscle action potential, conduction velocity and distal latency, tibial nerve distal latency and sural nerve action potential are the five attributes of nerve conduction within the NIS(LL)+7 (Dyck et al., 1997).

1.6.5 Quantitative sensory testing

QST is a psychophysical measure of the perception of different external stimuli of controlled intensity to assess a range of sensory modalities (Hansson et al., 2007, Cruccu et al., 2010). QST techniques can measure large or small fibre dysfunction through a range of different

assessment modalities. Abnormal thermal thresholds of the foot are recommended to detect the presence of small fibre damage in DSPN (Tesfaye et al., 2010). Thermal threshold testing is considered a reliable, sensitive and reproducible technique, however, it is only a semi-objective measure and results may be influenced by psychological factors such as attention and motivation (Chong and Cros, 2004). Their use is further limited as abnormal results do not localise and therefore are not specific for peripheral neuropathy (Arezzo, 1999).

As part of the long-term observational follow up of the Diabetes Control and Complications Trial, the Epidemiology of Diabetes Interventions and Complications study, 1,177 adults with T1DM were tested for vibration detection thresholds (VDT) (Martin et al., 2010). VDT had a sensitivity of 80% to detect definite clinical neuropathy and 62% to detect abnormal NCS. One of the more established methods of VDT evaluation is the computer assisted sensory evaluation IV (CASE IV) device (Arezzo, 1999). A computer sets an algorithm for stimulus delivery and asks the patient to score a response. The system has a large database of results for thermal and VDT to serve as a comparison. CASE IV correlates with other means of measuring VDT such as a graduated tuning fork and the neurothesiometer (Bril and Perkins, 2002a).

The German Research Network on Neuropathic Pain (DFNS) has developed a standardised protocol from previously established QST techniques (Rolke et al., 2006). The protocol examines numerous sub modalities of the sensory system. It aims to detect both sensory loss, for small and large fibre function, and sensory gain. The protocol has a central database of reference values for various anatomical sites (Magerl et al., 2010). The QST protocol has

good inter-observer and test-re-test reliability with low heterogeneity when performed in different centres throughout Europe (Geber et al., 2011, Vollert et al., 2016).

1.6.6 Diagnosis of painful-DSPN

A flow chart for the grading of neuropathic pain has been developed by the IASP Neuropathic Pain Special Interest Group (NeupSIG) (Figure 1.7) (Finnerup et al., 2016).

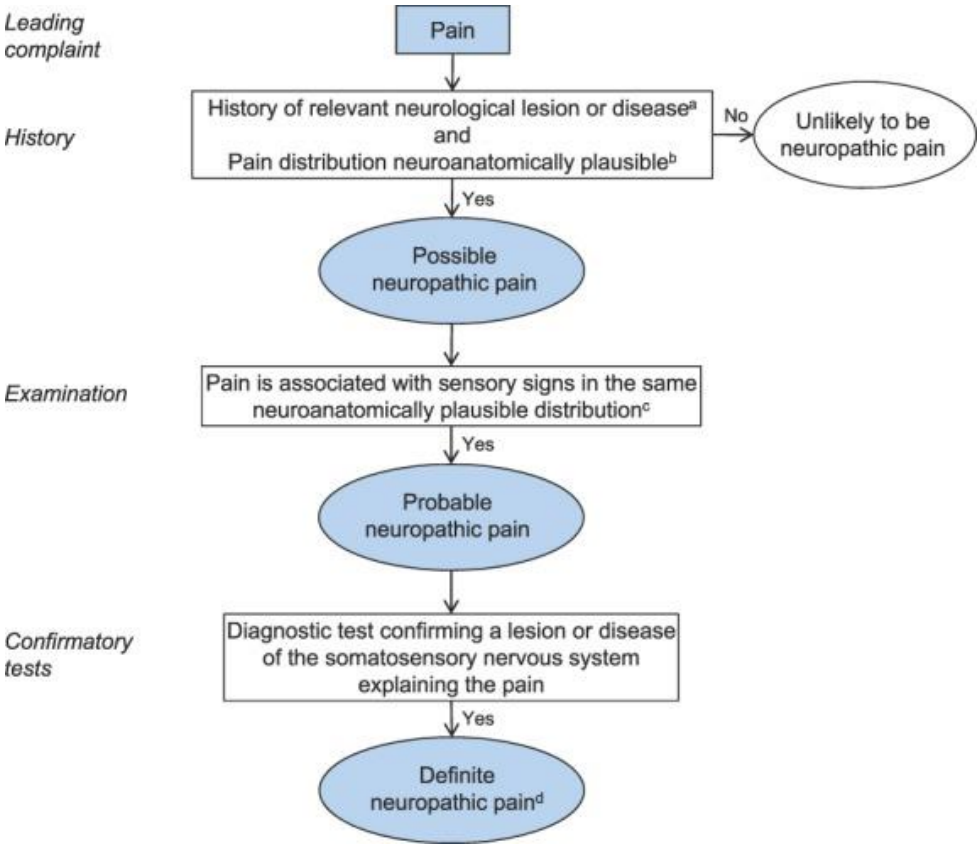

Figure 1.7. Flow chart of grading system for neuropathic pain. History, including neuropathic symptoms, suggestive of pain related to a neurological lesion and exclusion of other causes of pain. Examination, the pain distribution is consistent with the suspected lesion or disease. Confirmatory tests, e.g. sensory loss, touch-evoked or thermal allodynia. The term definite in this context means 'probable neuropathic pain with confirmatory tests'. Reproduced from (Finnerup et al., 2016).

Generally, as with DSPN, the diagnosis of painful-DSPN is a clinical one, relying on the presence of typical neuropathic symptoms in the context of a diagnosis of DSPN (according to the Toronto Diabetic Neuropathy Expert Group criteria, Table 1.4) with exclusion of other causes. Similar to the diagnosis of DSPN, in a clinical environment specialist testing is not required to diagnose painful-DSPN. In clinical research, making a 'confirmed diagnosis of DSPN' in the presence of painful neuropathic symptoms will satisfy the criteria for NeupSIG (Finnerup et al., 2016). However, there are no specific tests which distinguish DSPN from painful-DSPN. Therefore, a number of validated screening tools to detect the presence of possible neuropathic pain have been developed. The Doleur Neuropathique en 4 Questions (DN4) combines patient interview and examination findings (Bouhassira et al., 2005). The questionnaire has 10 binary items on four domains: pain description (burning, squeezing, painful cold and electric shocks), dysaesthesia symptoms (pins and needles, tingling, numbness and itching), signs of sensory deficit (touch and pricking hypoaesthesia) and evoked pain (brushing allodynia), see Appendix. It has been validated for the diagnostic work-up of painful-DSPN (Spallone et al., 2012). The severity of neuropathic pain can be reliably assessed by a simply numeric rating scale (NRS) or visual analogue scales (VAS) using an 11-point Likert scale (0=no pain, 10=worst pain imaginable) (Tesfaye et al., 2010). The Neuropathic Pain Symptom Inventory (NPSI) can also be used to evaluate different symptoms of neuropathic pain, see Appendix (Bouhassira et al., 2004).

1.7 Treatment of DSPN and painful-DSPN

1.7.1 Treatment and prevention of DSPN

Despite considerable research, there are only limited efficacious treatment options for the prevention and delay of progression of DSPN, see Figure 1.8. Intensive glucose control to achieve near normal glycaemia is strongly recommended for patients with T1DM (Pop-Busui et al., 2017). In T2DM, lifestyle interventions are recommended but intensive glucose control is only modestly effective and patient-centred goals should be targeted. Many pathogenetic pharmacotherapeutic agents have been studies but there is limited evidence for their benefit (Boulton et al., 2013).

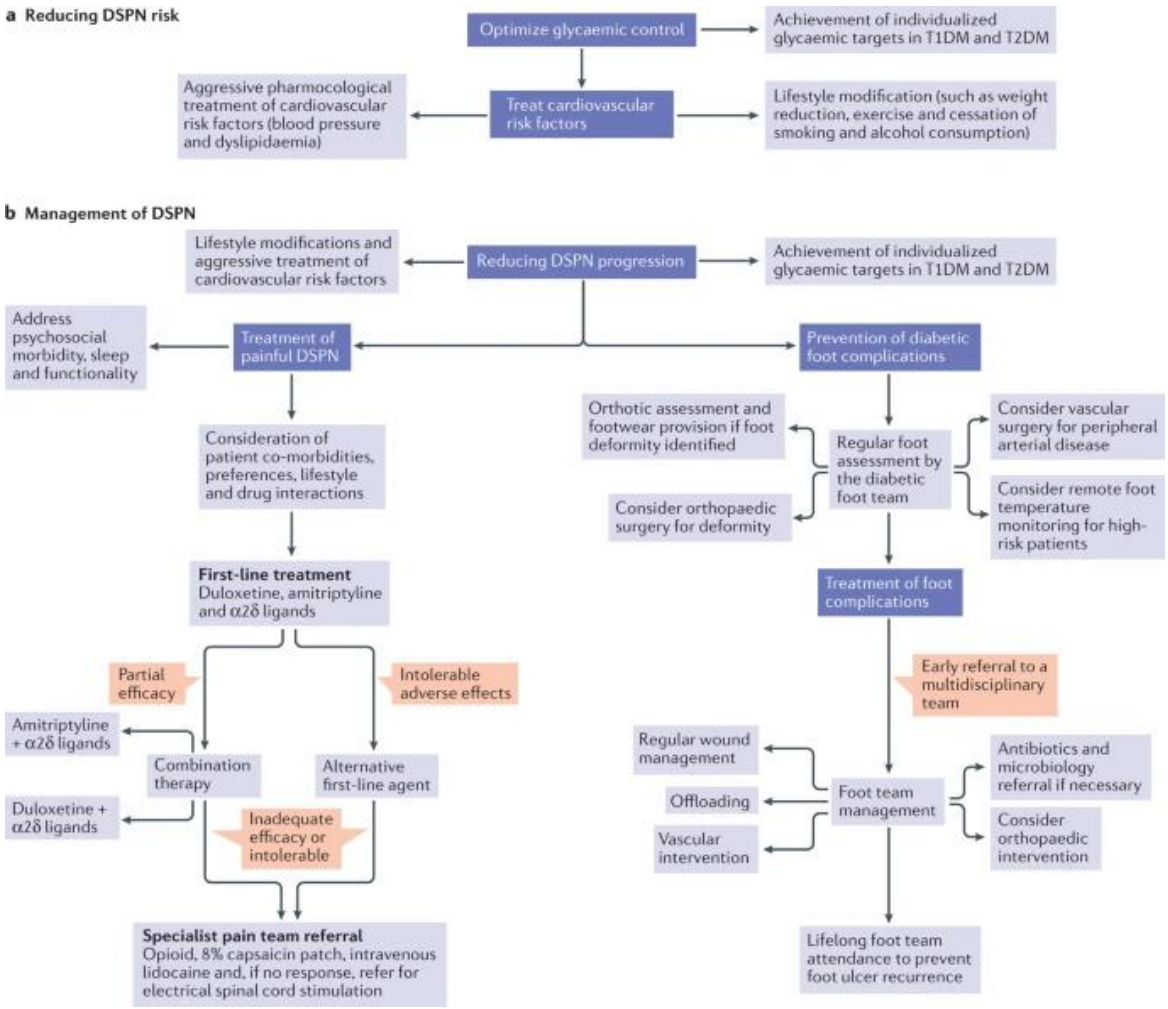

Figure 1.8. Management of DSPN. The prevention of diabetic sensorimotor peripheral neuropathy (DSPN) involves optimizing glycaemic control and achievement of cardiometabolic targets. A multidisciplinary approach aimed at the management of painful DSPN and the prevention (part a) and treatment (part b) of foot complications is vital. In the management of painful DSPN, combination treatment is recommended in instances of partial efficacy of first-line agents. If there is pain despite combination treatment, the use of opioids can be considered with caution. In refractory painful DSPN, consider a high-dose capsaicin (8%) patch, intravenous lidocaine infusion and electrical spinal cord stimulation. The management of diabetic foot ulcer disease includes the use of therapeutic footwear, early involvement of vascular surgeons, when necessary, regular podiatry (such as callus debridement and wound dressing), treatment of infection in collaboration with microbiologists, the surgical management of foot deformities in collaboration with orthopaedic surgeons, and the use of appropriate offloading and immobilization strategies (for example, casting). The management of Charcot neuroarthropathy is based on strict immobilization in the acute presentation and surgical treatment where indicated in the chronic setting. T1DM, type 1 diabetes mellitus; T2DM, type 2 diabetes mellitus. Reproduced from (Sloan et al., 2021).

1.7.2 Treatment of painful-DSPN

The treatment of painful-DSPN is largely symptomatic, there is no evidence for the benefit of achieving metabolic control although this should be encouraged as part of a holistic approach to the patient, see Figure 1.8. Pathogenetic treatments for neuropathic symptoms have received limited regional approvals but are not widely recommended by major neuropathic pain/painful-DSPN guidelines (Sloan et al., 2021). The most widely used and recommended pharmacotherapeutic agents for painful-DSPN with substantial supportive evidence include anticonvulsants (voltage gated α2δ ligands) and antidepressants (serotonin-noradrenaline reuptake inhibitors; and tricyclic antidepressants) (Alam et al., 2020). These neuropathic pain agents considered partially effective, with fewer than one half patient receiving 50% pain relief from current neuropathic pain medications (Jensen et al., 2006, Finnerup et al., 2015).

1.7.3 Pain phenotyping and treatment response

The current pharmacotherapeutic agents for neuropathic pain have not changed in over a decade. Traditionally, neuropathic pain treatments are prescribed according to the disease aetiology. However, the clinical features, and perhaps underlying disease mechanisms, of neuropathic pain may vary from individual to individual (Yang et al., 2019). Recent studies have explored whether stratification according to various patient characteristics can determine the response to treatments. These characteristics include clinical phenotype, neuroimaging and genotype. Early evidence suggests that neuropathic pain characteristics have found enhanced analgesic responses depending on pain phenotype (Sloan et al., 2021),

including in painful-DSPN (Wilkinson et al., 2020). However, there are no stratification methods which are validated for use clinically, many of these methods are only at a very early stage of investigation. Indeed, there are also no pain biomarkers available for use in clinical trials, current trials use self-reported pain scales as measures of efficacy, which are highly susceptible to confounding factors.

1.8 Conclusions

Painful-DSPN is a common and disabling complication of diabetes mellitus. As the prevalence of diabetes mellitus continues to increase, the prevalence of painful-DSPN is expected to rise also. Unfortunately, the available medications for this condition are inadequate, which is predominantly due to a lack of understanding of the underlying mechanisms of the disease. The CNS is a key component in the pathophysiology of neuropathic pain; however, it remains under-investigated in painful-DSPN. Cerebral neuroimaging has the potential to investigate two crucial areas of research: 1) The interaction between patient phenotype and peripheral and central mechanisms of DSPN and 2) whether patient stratification methods using neuroimaging can enhance mechanism-based treatment response in painful-DSPN (Sloan et al., 2021). The main objective of this thesis is to investigate the cerebral alterations in painful-DSPN. Further foci include the cerebral alterations as a result of neuropathic pain treatments in painful-DSPN and skin biopsy vascular markers in DSPN/painful-DSPN.

1.9 Aims and hypotheses

Chapter 3: Cerebral morphometric alterations in painless- and painful-DSPN

The aims of this study were to 1) define the cerebral morphological alterations in carefully phenotyped patients with painful-DSPN and painless-DSPN; 2) to explore the relationships between brain morphology and clinical/neurophysiological measures of DSPN. The hypothesis is that there will be a reduction in volume/thickness in somatomotor brain areas [e.g. primary somatosensory cortex (S1), primary motor cortex (M1), thalamus and insular cortex) with a relative preservation in somatosensory areas in painful- compared with painless-DSPN; and the final aim, 3) to determine the cerebral morphological differences in participants with irritable nociceptor (IR) and non-irritable nociceptor (NIR) painful-DSPN. The hypothesis is that there will be a relative preservation of cortical thickness/cerebral volume in somatosensory brain areas in IR- compared with NIR-painful-DSPN.

4. Cerebral Magnetic Resonance Spectroscopy alterations in DSPN: Neuronal viability in painful- and painless-DSPN

The aim of the study was to assess proton metabolite ratios of the S1 cortex and thalami, as a measure of neuronal viability, in patients with T2DM and DSPN at the S1 cortex and thalami. We hypothesised that there will be a symmetrical reduction in N-acetylaspartate to Choline (NAA:Cho) and/or NAA to creatine (Cr) in the thalami in patients with painless-DSPN.

5. Cerebral Magnetic Resonance Spectroscopy alterations in DSPN: Cerebral bioenergetics in painful- and painless-DSPN

The aim of the study was to assess 31-phosphorus metabolite ratios, as measures of cerebral bioenergetics and mitochondrial dysfunction, in patients with T2DM and DSPN in the S1 cortex and thalamus. The hypothesis was there will be altered high energy phosphorus metabolite ratios which will differentiate painful- and painless-DSPN, with evidence of mitochondrial dysfunction in painless-DSPN and increased cellular energetics in painful-DSPN.

6. The impact of optimised neuropathic pain treatment on the magnetic resonance imaging correlates of painful-DSPN 1: Neurotransmitters

The aim of the study is to assess spectroscopy neurotransmitter parameters [GABA and glutamine and glutamate (Glx)] in the ACC in patients with painful-DSPN, to determine whether changes are detectable when participants are optimally treated for their painful symptoms compared to without treatment. The hypothesis is that GABA levels will reduce and Glx levels rise after withdrawal of treatment. Moreover, another hypothesis is that patients with a greater increase in pain (i.e. responders to treatment) will have greater changes in neurotransmitters.

7. The impact of optimised neuropathic pain treatment on the magnetic resonance imaging correlates of painful-DSPN 2: Functional connectivity

The aim of the study was to perform a Resting State Functional MRI (rs-fMRI) experiment in patients with painful-DSPN, to determine differences in neuronal functional connectivity between participants on neuropathic pain treatment and after these had been discontinued. We hypothesise that there will be increased functional connectivity in nociceptive brain regions after withdrawal of treatment. We also hypothesise that patients with a greater increase in pain (i.e. responders to treatment) following treatment discontinuation will have greater changes functional connectivity.

8. Peripheral vascular markers of Painful Diabetic Peripheral Neuropathy

The aim of the study is to determine whether there are any differences in skin biopsy peripheral vascular and neural biomarkers between patients with T2DM and no neuropathy, painless-DSPN, painful-DSPN, and healthy volunteer at the level of the proximal thigh and their relationship to neuropathic pain. The hypothesis is that participants with painful-DSPN will display elevated levels of von Willebrand Factor (vWF) with correlations with pain scores and DN4.

2. General Methods

2.1 Participants

Participants were recruited from the Sheffield Teaching Hospitals NHS Foundation Trust and the University of Sheffield using a variety of sources:

1. Local Trust Diabetes Database
2. Sheffield Teaching Hospitals clinics: medical and podiatry
3. Self-referral from promotional material (posters displayed throughout the Trust; emails sent to Trust and University of Sheffield staff; and online noticeboard announcement on the Trust intranet)
4. Relatives or friends of participants recruited through the above methods

All participants gave written, informed consent before participation into the study. Studies had prior Ethics Approval by Research Ethics Committees.

Inclusion criteria

- Male and female participants aged over 18 years
- Able to give written informed consent
- Confirmed diagnosis of DM for more than one year or HV without DM
- Proficiency in the English language

- Right-handed

Exclusion criteria

- Current or history of excess alcohol intake over 14 units per week, on average
- Non-diabetic neuropathies or neurological disorder
- Diabetic neuropathies other than DSPN
- Patients with painful medical condition other than painful-DSPN in that group
- Contraindication to MRI scanning: claustrophobia, inability to lay flat and failure to comply with routine safety questions (e.g. irremovable metallic object on person)
- Pregnancy
- Major lower limb amputation
- Prescription of anti-depressants

2.2 Clinical and neurological assessment

Participants underwent a range of clinical and neurophysiological assessments, including:

- Clinical history, including collection of demographic data, medical history, medication history, diabetes and diabetes complications history, social history, and substance use habits.

- Mood and memory assessments: Hospital Anxiety and Depression Scale (HADS) (Zigmond and Snaith, 1983) and Mini-mental state examination (MMSE) (Folstein et al., 1975). The presence of depression or anxiety was defined as a score of >11 on the HADSD or HADSA scale respectively.

- Clinical examination: Height was measured to the nearest centimetre using an electronic height measure (Seca, Germany); weight was measured to the nearest 0.5kg using standard weighing scales (Seca, Germany); Waist and hip circumference obtained using a tape measure to the nearest centimetre according to the Geneva World Health Organization Expert Consultation (Organization, 2011); and blood pressure and pulse rate obtained using an automated blood pressure monitor (Omron M4-1, Hoofderp, The Netherlands) after being supine for several minutes during AFTs.

- Structured neuropathy assessments

    - TCNS (Appendix 10.1)

    - NIS (Appendix 10.2)

    - DN4 (Appendix 10.4)

    - NPSI (Appendix 10.5)

- Nerve Conduction Studies: to obtain sensory sural nerve amplitude and conduction velocity; common peroneal motor nerve amplitude, motor conduction velocity and distal latency; and tibial motor nerve distal latency. Surface electrodes were used at a stable skin surface temperature of 31°C and a room temperature of 24°C using a

Medelec electrophysiological system (Synergy Oxford Instruments, Oxford, U.K.). Patient data compared with age adjusted reference values (JA and DM, 1992).

- Autonomic function testing
    - Cardiac autonomic function tests according to the O'Brien protocol (O'Brien et al., 1986). Heart rate was measured continuously during five procedures: supine rest for 8 minutes; deep breathing, 5-seconds inhalation and 5-second exhalation; Valsalva manoeuvre; and standing for 60 seconds. Additionally, blood pressure at rest and standing were measured. Values of postural blood pressure drop, heart rate variation (rest, deep breathing and Valsalva) and heart rate variability in values of the 30^{th} and 15^{th} beats after standing (30:15 ratio). An autonomic neuropathy score for each individual test was derived from normative data and combined to calculate an autonomic neuropathy score.
    - Sudomotor function testing was performed using the SUDOSCAN device (Impeto Medical, Paris, France). A low direct voltage was applied to the hands and feet of subjects and the electrochemical skin conductance is obtained from the ratio of the current measured and voltage applied (Mayaudon et al., 2010). The device automatically calculated a quantitative result of electrochemical skin conductance (ESC).
- Quantitative sensory testing
    - Vibration detection thresholds (VDT) obtained using the 4, 2, and 1 stepping algorithm employed by the CASE IV (W.R. Electronics, Stillwater, MN, USA)

system technique (Dyck et al., 1993, Dyck et al., 1997). The results are expressed as percentile and normal deviate for age and sex.

- German Research Network on Neuropathic Pain QST protocol (Rolke et al., 2006) where the following sensory sub-modalities were tested: cold (CDT) and warm detection thresholds (WDT; TSA-II, MEDOC, Israel), cold (CPT) and heat pain (HPT), mechanical detection (MDT, von Frey hairs, Optihair2-set, Marstock Nervtest Germany) and pain (MPT, PinPrick stimulator set, Medizintechnische Systeme, Germany) thresholds, mechanical pain sensitivity (MPS), dynamic mechanical allodynia (DMA; Standardized brush, Somedic, Sweden; cotton wool tip, cotton wisp), pressure pain thresholds (PPT; Pressure gauge device, Wagner Instruments, USA), wind-up pain (WUR) and VDT (Rydel-Seiffer tuning fork, 64 Hz, 8/8 scale). As per the DFNS protocol, all modalities were tested using the same technique at the dorsum of the foot, except for: vibration detection thresholds in which the tuning fork is placed on the medial malleolus and pressure pain threshold where the pressure algometer is placed on the abductor hallucis muscle. The QST data is entered into a data analysis system, eQUISTA. This system z-transforms QST data for each parameter and compared to site, gender and age specific reference data. A positive z-score denotes a gain of function whereas a loss of function is denoted by a negative z-score. Formal training for the protocol was obtained at Bochum Hospital, Germany.

- Neuropathy Impairment Score of the Lower Limb Plus 7 Tests neuropathy composite score was derived from the NIS plus nerve conduction studies, autonomic function testing and VDT (Appendix 10.3).

- Biochemical testing: Blood and urine samples were taken from all study participants to analyse biochemistry relevant to the included studies, e.g., HbA1c, urinary albumin to creatinine ratio (ACR), creatinine, cholesterol, etc.

2.3 Magnetic resonance imaging

MRI protocols differed among the included studies; however, all scans were performed in the University of Sheffield Academic Radiology Unit at 3 Tesla (Ingenia 3.0T, Phillips Healthcare, Best, NL). Participants underwent cerebral imaging, whereby the individual is placed supine and headfirst into the scanner. All participants underwent detailed safety precautions, including completion of MR safety forms and assessment by radiographers. Pain rating scores, VAS or NRS, (0-10) were completed before the scan commenced. In participants who had diabetes a finger-prick blood glucose level was taken before the scan. If the blood glucose levels were significantly out of range (<4.0mmol/l or >25mmol/l) the participant was not scanned, and the MRI was re-arranged.

2.4 Diabetes participant grouping

Based on clinical and neurophysiological assessments and the presence of painful-DSPN participants with diabetes were divided into three subgroups according to the Toronto consensus criteria (Tesfaye et al., 2010):

- No-DSPN: Participant with DM with no symptoms of DSPN and normal clinical and neurophysiological assessments
- Painless-DSPN: Participant with DM without symptoms of painful peripheral neuropathy and confirmed- or subclinical-DSPN.
- Painful-DSPN: Participant with DM with symptoms or painful peripheral neuropathy and confirmed- or subclinical-DSPN.

2.5 Statistical analysis

Statistical advice was sought at the Statistics Service Unit, University of Sheffield. Analysis was performed using the statistical package Statistical Product and Service Solutions Version 26 (SPSS, IBM Corporation, New York, USA).

Normally distributed subgroup characteristics are presented as means and standard deviations (mean ± standard deviation). Those with a non-parametric distribution are presented as medians and inter-quartile ranges [median (IQR)]. Categorical and dichotomous variables are presented as group percentages.

Continuous data was tested for normality and appropriate parametric or non-parametric tests applied (including post-hoc corrections for multiple comparisons, where indicated). ANOVA was used to analyse group differences for continuous normally distributed data. For post hoc analysis of continuous normally distributed data the Least Significant Difference (LSD) test was used. Kruskal-Wallis (KW) was used to analyse group differences for continuous non-parametric data. For post hoc analysis of continuous non-parametric data the Mann-Whitney U test was used. For categorical data the Chi^2 test was used to determine the presence of group differences. Covariate analyses with ANCOVA was employed where appropriate.

Relationships between data types was also be tested (e.g. correlations between severity of DSPN and cerebral/skin biopsy measures) using Pearson's rank correlation and Spearman's rank correlation for parametric and non-parametric data, respectively.

3. Cerebral morphometric alterations in painless- and painful-DSPN

3.1 Introduction

3.1.1 Background

There is now clear evidence for CNS involvement in DSPN (Sloan et al., 2018). Structural and functional alterations of the spinal cord were first demonstrated in post-mortem studies in the 1960's, followed by somatosensory evoked potential studies in patients with advanced DSPN (Reske-Nielsen and Lundbaek, 1968, Reske-Nielsen et al., 1966, Kucera et al., 2005). More recent MRI studies have demonstrated spinal cord atrophy was present not only in patients with advanced DSPN but also in patients with early, subclinical DSPN (Selvarajah et al., 2006). Moreover, several studies with a relatively small number of participants have now demonstrated grey matter volume loss localised to areas associated with somatosensory/motor function, including the S1, supramarginal gyrus, cingulate cortex, insular cortex and M1 in DSPN (Frøkjær et al., 2013, Selvarajah et al., 2014b, Zhang et al., 2019). However, despite various studies showing vascular/functional alterations between painful- and painless-DSPN (Shillo et al., 2019b), no clear structural alterations have been demonstrated.

Painful-DSPN is a heterogenous condition comprising cohorts of patients with different clinical pain phenotypes (Baron et al., 2009, Themistocleous et al., 2016). Early evidence suggests that classifying participants into different phenotypes of painful-DSPN may help to

predict response to different neuropathic pain treatments (Wilkinson et al., 2020). The most common method is using QST to subdivide participants with neuropathic pain is into the IR and NIR phenotype (Demant et al., 2014, Teh et al., 2021). The IR phenotype is characterised by relatively preserved sensory function associated with thermal and/or hyperalgesia; and the NIR phenotype by thermal and mechanical sensory loss without hypersensitivity. Previous research has demonstrated alterations in functional connectivity in nociceptive brain regions between IR and NIR phenotypes in painful-DSPN; however, the morphological alterations are not known.

3.1.2 Rationale for study

The studies which have investigated the morphometric alterations in DSPN generally have had a relatively small sample size (Selvarajah et al., 2014b, Selvarajah et al., 2019). Moreover, in the largest study to date the case definition and patient phenotyping was inadequate (Zhang et al., 2019). Therefore, there is a good rationale for performing a cerebral morphometry study in a large cohort of participants with detailed clinical characterization using advanced MR analysis to enable a robust exploration of the relationships between alterations in brain morphometry and clinical/neurophysiological assessments of DSPN. Additionally, there is considerable interest in the prospect of stratification of participants into different clinical phenotypes to predict treatment response. Therefore, there is justification to explore the cerebral morphometric alterations in IR and NIR phenotypes of painful-DSPN to determine the cerebral mechanisms which might contribute to these clinical differences.

3.1.3 Aims and hypothesis

The aims of this study were to 1) define the cerebral morphological alterations in carefully phenotyped patients with painful- and painless-DSPN; 2) to explore the relationships between brain morphology and clinical/neurophysiological measures of DSPN. The hypothesis was that there will be a reduction in volume/thickness in somatosensory/motor brain areas (e.g. S1, M1, and insular cortices and the thalamus) with a relative preservation in somatosensory areas in painful- compared with painless-DSPN; and the final aim, was 3) to determine the cerebral morphological differences in participants with IR- and NIR-painful-DSPN. The hypothesis was that there will be a relative preservation of cortical thickness/cerebral volume in somatosensory brain areas in IR- compared with NIR-painful-DSPN.

3.2 Methods

3.2.1 Study Design and Participants

Two-hundred and seventy-seven participants were recruited into the study (211 with diabetes and 66 HV) from the Royal Hallamshire Hospital (Sheffield, U.K.) between 2009 and 2019. Inclusion criteria were as per the general methods and for people with diabetes type 1 or type 2 diabetes to be diagnosed for at least 6 months. Exclusion criteria were as per the general methods and recurrent severe hypoglycaemia.

The study design was a case controlled cross-sectional study.

3.2.2 Clinical and neurological assessment

History, clinical examination, structured neurological examination, nerve conduction studies were performed as described in the general methods. The neurophysiological measures analysed were sural sensory nerve action potential and conduction velocity; common peroneal nerve compound muscle action potential, conduction velocity and distal latency; tibial motor nerve distal latency.

3.2.3 Sensory phenotyping

DFNS-QST was performed as per the general methods in all participants. The QST results were used to classify participants with painful-DSPN into IR- and NIR-nociceptor phenotypes as follows (Demant et al., 2014):

- IR-painful-DSPN: presence of DMA, reduced MPT or PPT, increased MPS, lower CPT or HPT, or any combination of these signs of hyperexcitability
- NIR-painful-DSPN: patients with painful-DSPN not classified as IR phenotype, i.e. no signs of hyperexcitability described above

3.2.4 Magnetic resonance imaging protocol

3.2.4.1 Rationale for using brain volumetry

Cerebral atrophy in clinical settings normally relies on visual qualitative interpretation of structural brain images, such as an increase in cerebrospinal fluid spaces and reduced brain parenchyma (Giorgio and De Stefano, 2013). These qualitative interpretations can be quantified, for example by measuring ventricular or sulcal width (Jongen and Biessels, 2008). However, these measures will be dependent on the operator and scanner, and therefore are unlikely to be sensitive enough to detect subtle tissue loss and are therefore not suitable for use in large clinical research studies. Quantitative assessment of brain volumes has been used for nearly three decades due to advances in computer technology and MR techniques (Giorgio and De Stefano, 2013). These measures can detect subtle regional differences in brain morphology. The methods may be entirely manual, semiautomated of fully automated. Fully automated methods include voxel-based morphometry (VBM) and Freesurfer, the latter of which has been used in this study.

Brain volumetry allows the quantitation of brain tissue volume (Jongen and Biessels, 2008). Before the development of automated techniques this was previously done using manual outlining; however, this is time consuming and is not feasible for larger data sets. The Freesurfer software is a suite of tools for the analysis of neuroimaging data, including quantification of cerebral morphometry (Fischl, 2012). The software determines the boundary between white matter and grey matter and grey matter and the pial surface (Figure 3.1). Thereafter, anatomical measures are calculated including regional cortical thickness, surface area and curvature. The pipeline is mostly automated, making it ideal for

large data sets. The software is continuously improved and updated, and several studies have found it to generate robust and reliable volumetric measures of the brain (Ochs et al., 2015, Guo et al., 2019, Yim et al., 2021).

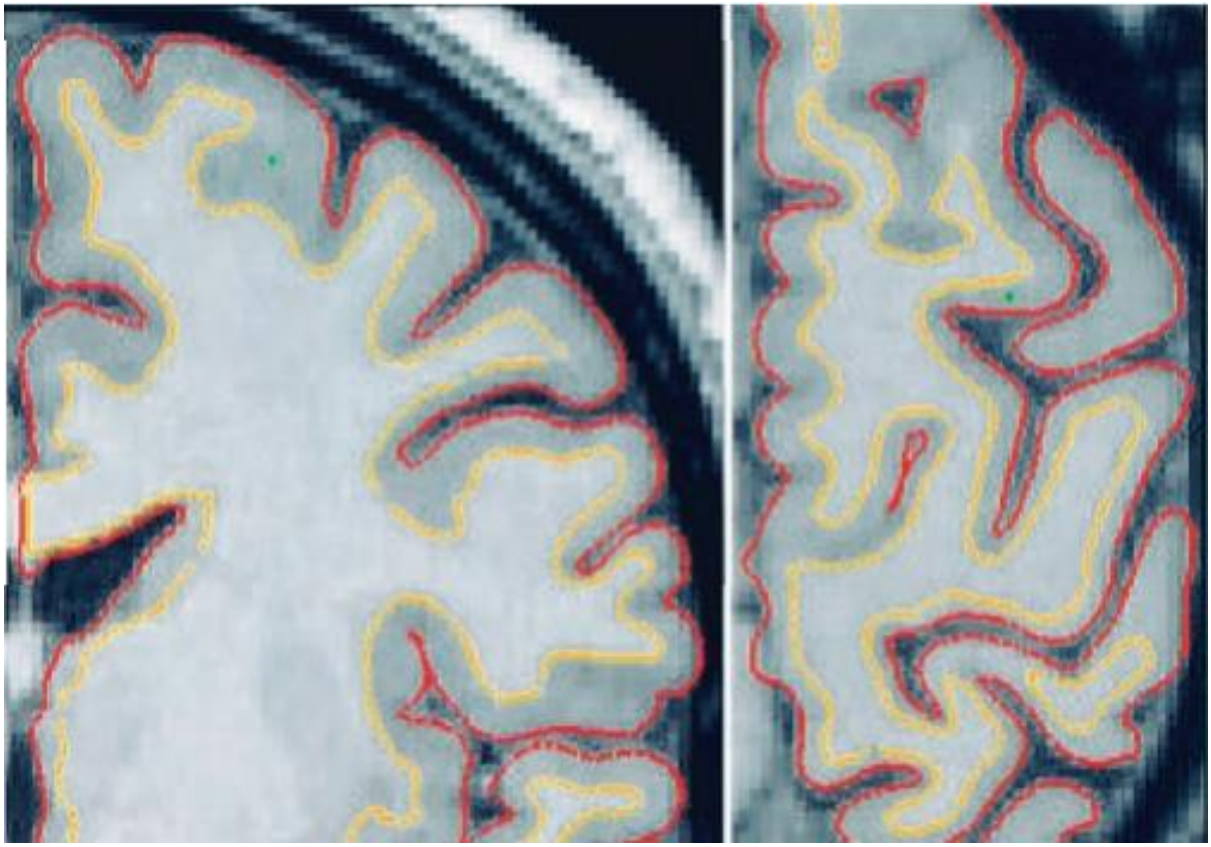

Figure 3.1. Freesurfer delineation of cerebral white and grey matter (yellow-line) and grey matter and pia (red-line), reproduced from (Fischl and Dale, 2000).

3.2.4.2 Protocol for brain volumetry

3.2.4.2.1 MR acquisition

All participants underwent MRI of the brain and anatomical data acquired with a 3D T1-weighted magnetization-prepared rapid echo sequence.

3.2.4.2.2 Cortical thickness, and global and deep brain nuclei volume

Cortical reconstruction and volumetric segmentation were performed with the Freesurfer software (https://surfer.nmr.mgh.harvard.edu). This processing included motion correction and averaging (Reuter et al., 2010) of T1 weighted images and removal of non-brain tissue using a hybrid watershed/surface deformation procedure (Figure 3.2) (Ségonne et al., 2004), affine-registration to the Talairach atlas (Fischl et al., 2002, Fischl et al., 2004), intensity normalisation, tessellation of the grey matter/white matter boundary, automated topology correction (Fischl et al., 2001, Ségonne et al., 2007), and surface deformation following intensity gradients to optimally place the grey/white and grey/cerebrospinal fluid borders at the location where the greatest shift in intensity defines the transition to the other tissue class (Figure 3.1) (Dale et al., 1999, Fischl and Dale, 2000). Surface based maps were created from the intensity and continuity information from the entire 3D MR volume in segmentation and deformation procedures to produce representations of cortical thickness, calculated as the closest distance from the grey/white boundary to the grey/CSF boundary at each vertex on the tessellated surface (Fischl et al., 2001). Global brain volumetric measures were obtained, including: total brain, cortical, subcortical, total cordial white matter and total grey volume. Regions of interest were also chosen in well-recognised brain regions involved with somatosensory/motor function (Figure 3.3). These included: S1, M1, insular and anterior cingulate cortices and the thalamus. Volumetric data for each region of interest (ROI) were averaged between the two hemispheres prior to analysis being performed.

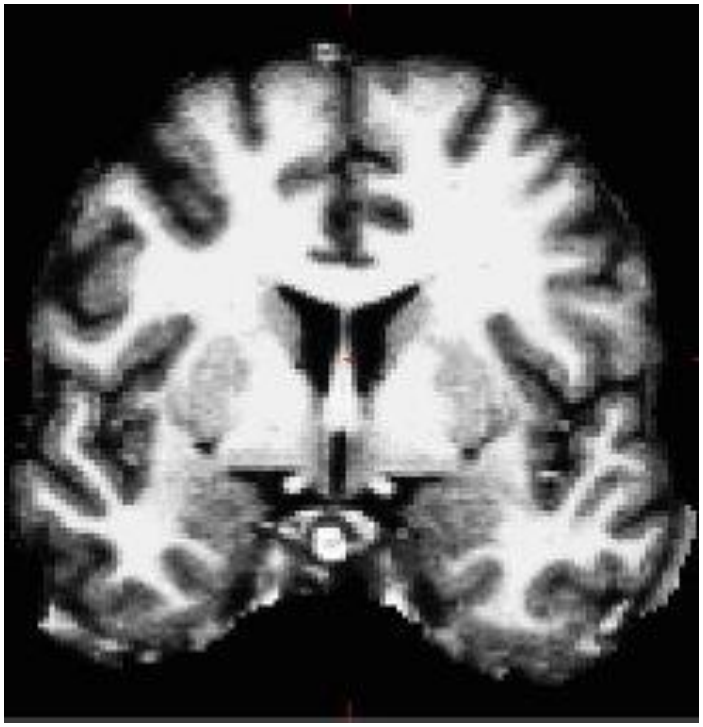

Figure 3.2. Example of skull stripped image in Freesurfer, reproduced from https://surfer.nmr.mgh.harvard.edu/fswiki/FreeSurferAnalysisPipelineOverview.

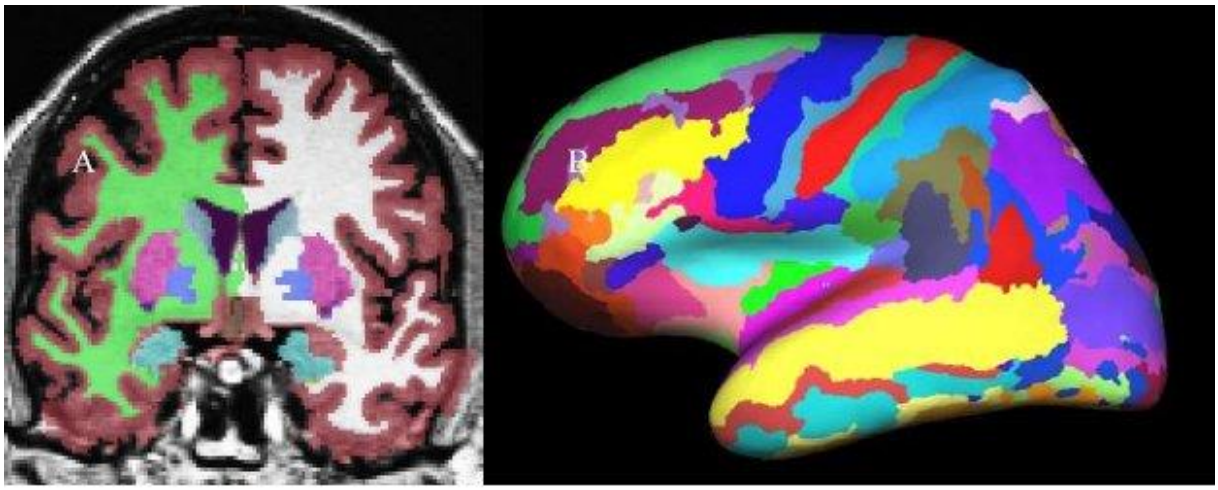

Figure 3.3. Example of Volume-based labelling in Freesurfer, reproduced from https://surfer.nmr.mgh.harvard.edu/fswiki/FreeSurferAnalysisPipelineOverview. A. Volume based labelling., B Surface based labelling.

3.2.5 Statistical Analysis

Statistical tests were applied as described within the general methods. The univariate test ANOVA was used to compare differences between groups (HV, no-DSPN, painful-DSPN, and painless-DSPN) by calculating the mean morphological parameter for each brain tissue type per group. Brain group data were also adjusted for age and sex as fixed factors. A full factorial model was used, with group difference as a contrast. The relationship between brain morphological parameters and neurological/neurophysiological attributes (e.g. nerve conductions studies, DN4 and NRS for pain) were analysed in more detail using Pearson's correlation coefficients. Group comparisons between the IR- and NIR-painful-DSPN phenotype were analysed using an independent t-test.

3.3 Results

3.3.1 Clinical and neurological assessments

Table 3.1 shows the demographic details, metabolic characteristics and results of neurophysiological assessments for all groups. There were some clinical and demographic differences seen between groups. On post hoc analysis, participants with painless-DSPN were significantly older than HV (LSD, p=0.003) and there were fewer females in the painful-DSPN group compared with HV (Chi^2 test, p=0.037) and no-DSPN (p=0.005). The duration of diabetes was longer in painless-DSPN compared with No-DSPN (LSD, p<0.001) and painful-

DSPN (p=0.004) too. There was a higher body mass index (BMI) in painful-DSPN compared with HV (p=0.001) and the HbA1c was also greater in painful-DSPN compared with no-DSPN (p=0.014). There were no group significant group differences in the presence of other microvascular complications although those with established DSPN had a greater percentage of patients with proliferative diabetic retinopathy compared with no-DSPN (no-DSPN vs. painless-DSPN, Chi^2 test p<0.001; no-DSPN vs. painful-DSPN, p=0.001).

All nerve conduction parameters confirmed neuropathy in the painless- and painful-DSPN groups compared with no-DSPN and HV (LSD, all p<0.001), as expected. Both peroneal nerve conduction velocity (p=0.020) and sural nerve action potential (p=0.002) were also reduced in no-DSPN compared with HV but remained within normal limits in the no-DSPN group. In addition, tibial distal latency was longer in painful- compared with painless-DSPN (p=0.009). As expected, the DN4 score and NRS was higher than all other groups (all p<0.001). The DN4 was also higher in painless-DSPN compared with HV and no-DSPN (both p<0.001).

	HV (n = 66)	No DSPN (n = 57)	Painless-DSPN (n = 77)	Painful-DSPN (n = 77)	P value
Age (years)	54.4 ± 12.7	56.6 ± 9.7	60.0 ± 9.3	57.7 ± 8.6	**0.030 A**
Female sex, %	53%	59.6%	44.7%	32.5%	**0.010 Chi^2**
Duration of diabetes (years)		15.5 ± 14.1	23.9 ± 14.0	17.7 ± 11.6	**0.001 A**
Type 1 Diabetes, %		36.8%	50%	32.2%	0.165 Chi^2
Body mass index (kg/m^2)‡	27.3 ± 5.2	29.3 ± 6.5	29.4 ± 5.7	30.9 ± 6.7	**0.008 A**
HbA1c (mmol/mol)		63.3 ± 17.3	68.2 ± 17.1	71.4 ± 20.5	**0.047 A**
eGFR (mL/min/1.73 m^2)		83.7 ± 10.2	80.3 ± 14.0	79.5 ± 14.8	0.190 A
No DR (%)‡		47.3%	29.4%	33%	0.057 Chi^2
Background/Pre-proliferative DR (%)‡		45.5%	36.8%	40.9%	0.621 Chi^2
Proliferative DR (%)‡		5.5%	33.8%	26.1%	**<0.001 Chi^2**
Sural amplitude (mV)‡	17.0 ± 7.2	13.3 ± 5.5	3.6 ± 5.2	4.4 ± 7.7	**<0.001 A**
Sural velocity (m/s)‡	46.2 ± 9.9	43.1 ± 6.3	35.1 ± 9.5	34.5 ± 9.3	**<0.001 A**
Peroneal amplitude (mV)‡	5.8 ± 1.9	5.0 ± 2.7	1.9 ± 2.2	1.8 ± 2.1	**<0.001 A**
Peroneal Velocity (m/s)‡	45.8 ± 4.9	43.6 ± 4.6	36.7 ± 4.8	36.3 ± 5.5	**<0.001 A**
Peroneal latency (ms)‡	4.7 ± 0.8	4.7 ± 0.9	6.2 ± 2.8	6.5 ± 2.8	**<0.001 A**
Tibial latency (ms)‡	4.4 ± 0.9	4.5 ± 0.7	6.0 ± 2.0	7.1 ± 3.7	**<0.001 A**

DN4	0.0 ± 0.0	0.1 ± 0.4	0.8 ± 1.2	6.7 ± 1.6	**<0.001 A**
NRS	0.0 ± 0.0	0.0 ± 0.0	0.0 ± 0.0	5.9 ± 3.0	**<0.001 A**

Table 3.1. Demographic details, metabolic characteristics, and results of neurophysiological assessments for the study cohort. Data are presented as mean ± standard deviation or percentages for categorical data. The statistical test used was ANOVA (A) for continuous normally distributed data or Chi^2 for categorical data. ‡ Sural nerve amplitude was undetectable in 36 patients with Painless- and 46 in Painful-DSPN. Body mass index data missing in 10 individuals; HbA1c data missing in 9 individuals; DR data missing in 14 individuals; Sural amplitude missing in 12 individuals; Sural velocity missing in 155 individuals; Peroneal amplitude missing in 16 individuals; Peroneal velocity missing in 54 individuals; Peroneal latency missing in 47 individuals; and Tibial latency missing in 70 individuals. DN4, Doleur Neuropathique en 4 questions; DR, Diabetic Retinopathy; NRS, Numeric Rating Scale for pain.

3.3.2 Global and regional brain parameters

Table 3.2 shows the global and regional brain volumes in unadjusted analysis. In global brain volume analysis, the subcortical grey volume was significantly lower in the diabetes groups compared with HV [HV vs. no-DSPN (LSD, p=0.045), painless-DSPN (p=0.010) and painful-DSPN (p=0.019)]. After adjustment for age and sex the significance was lost for subcortical grey volume (ANCOVA, p=0.065), and there remained no significant group difference in other global brain parameters.

In the ROI analysis, participants with painless-DSPN had significantly lower mean S1 cortical thickness compared to other study groups (ANOVA, p=0.003). Post hoc analysis revealed that cortical thickness was significantly lower in painless-DSPN compared with HV (LSD, p<0.001) and no-DSPN (p=0.012) (Table 3.2 and Figure 3.4). Additionally, the S1 cortical thickness was significantly reduced in painful-DSPN compared with HV (p=0.024). Group differences in mean S1 cortical thickness lost significance after adjusting for age and sex (ANCOVA, p=0.058).

M1 cortical thickness was also significantly lower in participants with painful- and painless-DSPN compared to no-DSPN and HV [ANOVA, p=0.001; Painless-DSPN vs. HV (LSD, p=0.001); painful-DSPN vs. HV (p=0.002); painless-DSPN vs. no-DSPN (p=0.18); painful-DSPN vs. no-DSPN (p=0.030)] (Table 3.2 and Figure 3.5). This group effect and post hoc analysis remained statistically significant when adjusted for age and sex (ANCOVA, p=0.025).

The insular cortical thickness was numerically the lowest in painless-DSPN, which reached significance vs. HV (LSD, p=0.003) (Table 3.2 and Figure 3.6). Additionally, in painful-DSPN the mean insular cortical thickness was significantly lower than HV (p=0.029). The group effect lost statistical significance when adjusted for age and sex (ANCOVA, p=0.223). The thalamic volume was numerically the lowest in the painless-DSPN group; however, there was no significant group effect (ANOVA, p=0.125). The ACC cortical thickness was also numerically lowest in painful-DSPN but there was no significant group difference (p=0.119).

	HV (n = 66)	No DSPN (n = 57)	Painless-DSPN (*n* = 77)	Painful-DSPN (n = 77)	P value
Global brain parameters					
Total Brain volume (cm^3)	1060.46 ± 108.23	1019.88 ± 123.80	1022.03 ± 129.92	1036.47 ± 111.11	0.182
Cortical volume (cm^3)	412.0 ± 47.79	404.23 ± 48.61	404.70 ± 48.27	403.52 ± 45.98	0.135
Subcortical grey volume (cm^3)	54.74 ± 5.39	52.76 ± 5.67	52.38 ± 5.82	52.60 ± 4.89	**0.043**
Total grey volume (cm^3)	571.31 ± 61.76	548.55 ± 63.72	550.08 ± 63.80	549.65 ± 57.20	0.098
Total cortical white matter volume (cm^3)	459.81 ± 52.48	443.45 ± 63.11	444.48 ± 68.52	458.87 ± 58.91	0.231
Regional brain parameters					
Mean Thalamic Volume (mm^3)	6.66 ± 0.79	6.42 ± 0.88	6.38 ± 0.789	6.59 ± 0.81	0.125
Mean S1 Cortical Thickness (mm)	1.93 ± 0.11	1.91 ± 0.12	1.86 ± 0.13	1.88 ± 0.11	**0.003**
Mean M1 Cortical Thickness (mm)	2.39 ± 0.14	2.37 ± 0.12	2.31 ± 0.16	2.31 ± 0.16	**0.001**
Mean Insular Cortical Thickness (mm)	2.91 ± 0.14	2.86 ± 0.15	2.83 ± 0.17	2.85 ± 0.17	**0.025**
Mean ACC Cortical Thickness (mm)	2.50 ± 0.20	2.52 ± 0.23	2.56 ± 0.25	2.47 ± 0.23	0.119

Table 3.2. Global brain volumes and regional brain volume and cortical thickness. Data are presented as mean ± standard deviation. Statistical test, ANOVA. ACC, anterior cingulate cortex; M1, primary motor; S1, primary somatosensory.

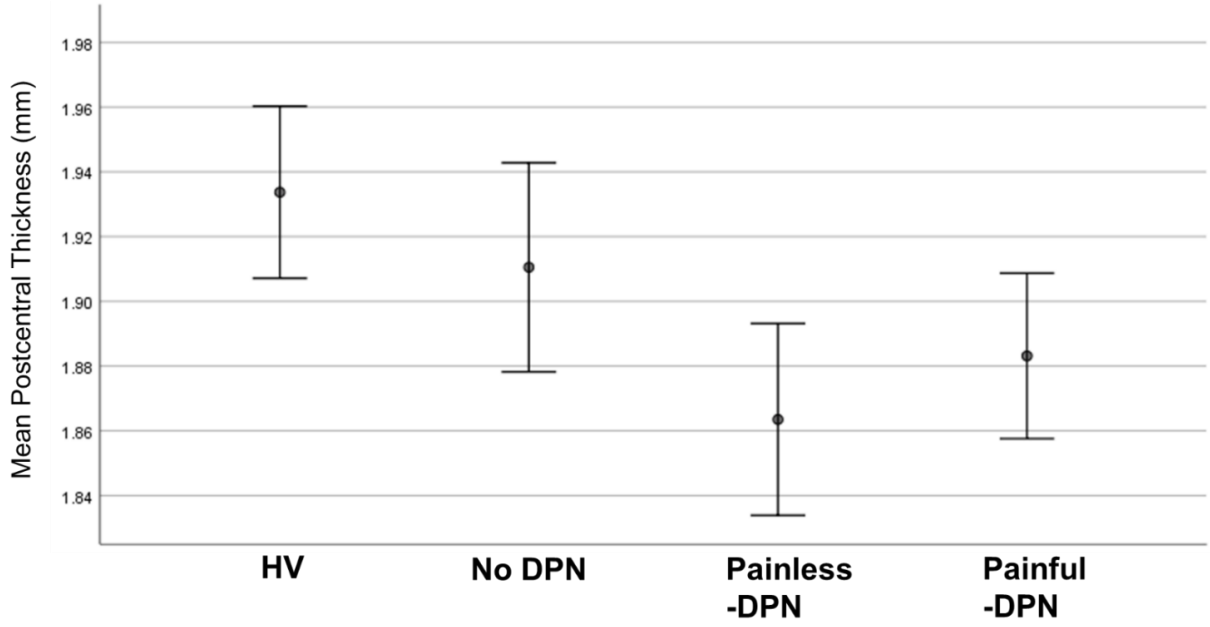

Figure 3.4. Mean Postcentral (S1) Cortical Thickness (mm) and 95% CI in participants with diabetes and HV (p=0.004, ANOVA). Painless-DSPN vs. HV (LSD, p<0.001); Painless-DSPN vs. no-DSPN (p=0.012); Painful-DSPN vs. HV (p=0.024).

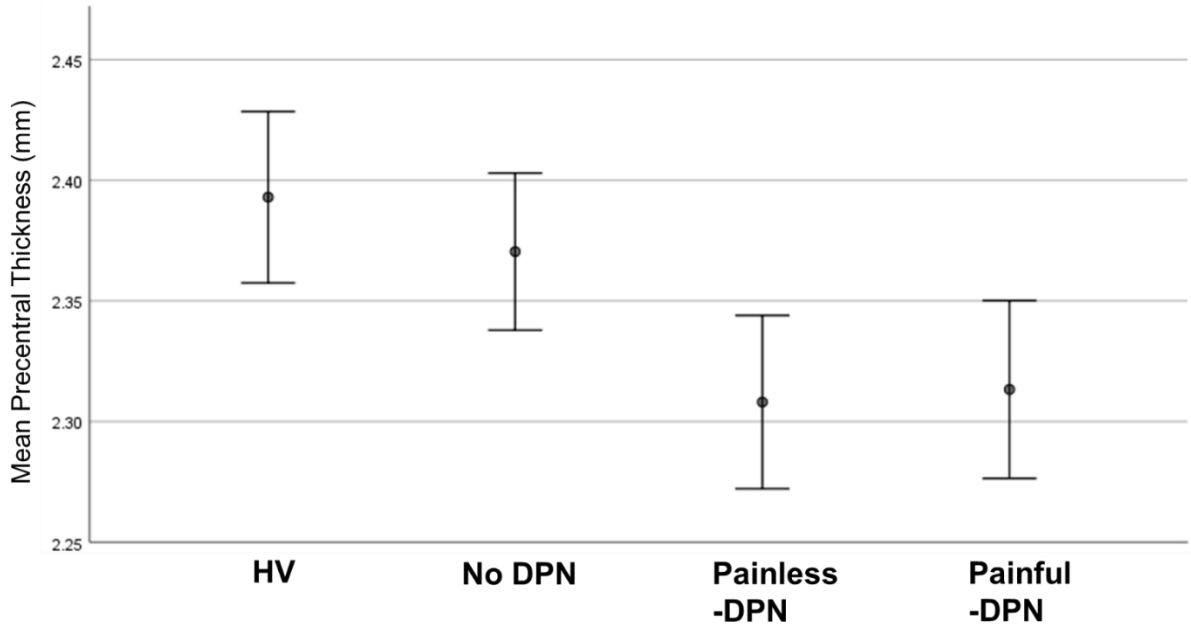

Figure 3.5. Mean Precentral (M1) Cortical Thickness (mm) and 95% CI in participants with diabetes and HV (ANOVA, p=0.001). Painless-DSPN vs. HV (LSD, p=0.001); Painful-DSPN vs. HV (p=0.002); Painless-DSPN vs. no-DSPN (p=0.18); Painful-DSPN vs. no-DSPN (p=0.030).

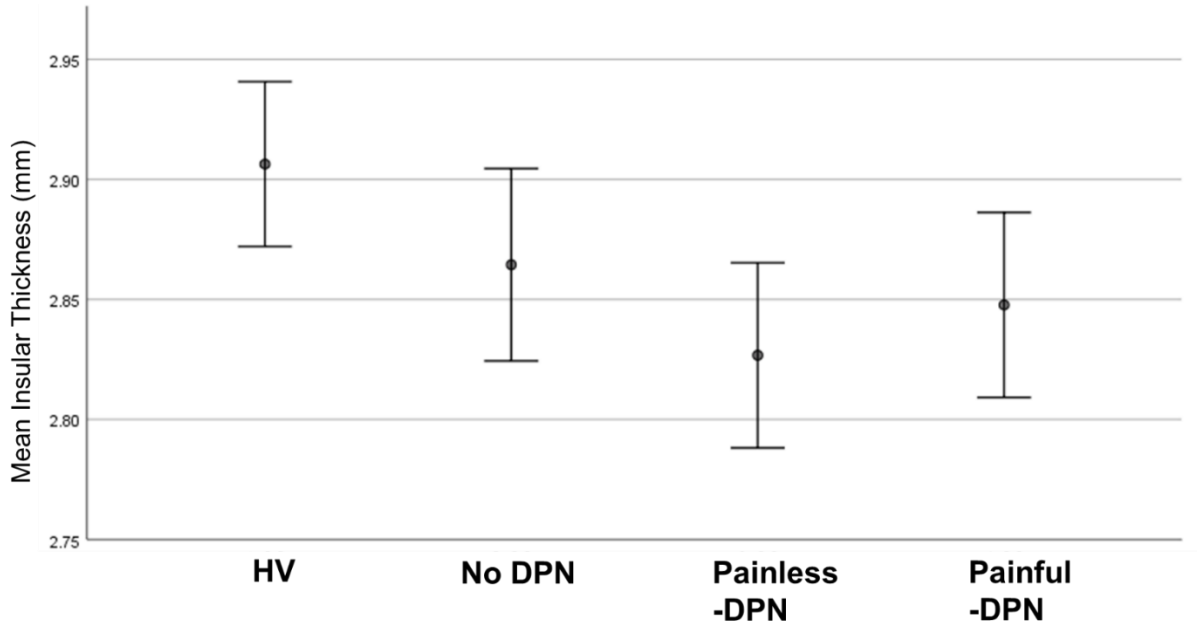

Figure 3.6. Mean Insular Cortical Thickness (mm) and 95% CI in participants with diabetes and HV (ANOVA, p=0.025). Painless-DSPN vs. HV (LSD, p=0.003); Painful-DSPN vs. HV (p=0.029).

3.3.3 Correlation analysis

The global brain parameters showed consistent mild-moderate correlations with sural nerve velocity, see Table 3.3. Additionally, as expected, age correlated with all global measures of brain volume; although there was no correlation with total cortical white matter volume (Pearson's correlation, r -0.102, p=0.090). Moreover, there were correlations with measures of DM and global brain parameters. Total brain volume correlated with duration of DM and severity of retinopathy; cortical volume correlated with duration of DM, severity of retinopathy and eGFR; total grey volume correlated with duration of DM, severity of retinopathy and eGFR; total cortical white matter correlated with duration of DM; and subcortical grey volume correlated with eGFR.

	Total brain volume		Cortical volume		Subcortical grey volume		Total grey volume	
	r	P value	r	P value	r	P value	r	P value
Sural amplitude	-0.034	0.582	0.007	0.910	0.049	0.427	0.024	0.700
Sural velocity	**-0.314**	**<0.001**	**-0.277**	**0.002**	**-0.205**	**0.024**	**-0.295**	**0.001**
Peroneal velocity	-0.096	0.154	-0.046	0.494	0.008	0.904	-0.060	0.376
Peroneal latency	0.077	0.246	0.035	0.593	-0.014	0.833	0.012	0.857
Peroneal amplitude	-0.035	0.575	-0.009	0.593	0.006	0.922	-0.003	0.967
Tibial latency	0.057	0.418	0.051	0.468	0.016	0.816	0.042	0.551
Age	**-0.159**	**0.008**	**-0.289**	**<0.001**	**-0.427**	**<0.001**	**-0.299**	**<0.001**
Body mass index	-0.023	0.707	-0.100	-0.104	0.015	0.809	-0.103	0.095
HbA1c	0.049	0.485	0.068	0.333	0.108	0.125	0.080	0.260
Duration of DM	**0.213**	**0.002**	**0.213**	**0.002**	0.085	0.218	**0.237**	**0.001**
Degree of retinopathy	**0.162**	**0.022**	**0.197**	**0.005**	0.104	0.144	**0.213**	**0.003**
eGFR	0.119	0.091	**0.151**	**0.032**	**0.176**	**0.012**	**0.149**	**0.035**

Table 3.3. Pearson's correlation between global brain parameters and clinical and neurophysiological parameters. DM, diabetes mellitus; eGFR, estimated glomerular filtration rate.

Table 3.4 shows the correlation analysis for the M1, S1 and insular cortex. As expected, M1, S1 and insular cortical thickness most strongly correlated with age. There were also weak correlations between these cerebral parameters and neurophysiological parameters, the most consistent of which was with sural nerve amplitude [M1 (Pearson's correlation r 0.256, $p<0.001$); S1 (r 0.214, $p<0.001$)]. Moreover, the ACC cortical thickness correlated with CPT (r -0.139, $p=0.030$) and MPS (r -0.250, $p<0.001$). In addition, the thalamic volume correlated with age (r -0.394, $p<0.001$), HbA1c (r -0.394, $p=0.019$), sural nerve velocity (r -0.253, $p=0.005$) and VDT (r -0.140, $p=0.030$).

	M1 cortical thickness		S1 cortical thickness		Insular cortical thickness	
	R	P value	*R*	P value	*R*	P value
Sural amplitude	**0.256**	**<0.001**	**0.214**	**<0.001**	0.104	0.092
Sural velocity	0.045	0.624	-0.035	0.704	-0.041	0.651
Peroneal velocity	0.113	0.093	0.117	0.082	**0.239**	**<0.001**
Peroneal latency	**-0.210**	**0.001**	**-0.115**	**0.019**	-0.073	0.270
Peroneal amplitude	**0.217**	**<0.001**	**0.137**	**0.027**	**0.201**	**0.001**
Tibial latency	-0.089	0.201	0.000	0.995	-0.063	0.366
Age	**-0.303**	**<0.001**	**-0.351**	**<0.001**	**-0.374**	**<0.001**
Body mass index	**-0.162**	**0.008**	**-0.128**	**0.038**	-0.088	0.151
HbA1c	0.053	0.454	0.022	0.758	0.090	0.200
Duration DM	0.072	0.302	-0.026	0.708	-0.094	0.175
CDT	0.088	0.169	0.112	0.080	-0.007	0.917
WDT	**0.175**	**0.006**	**0.134**	**0.036**	0.121	0.058
TSL	**0.153**	**0.017**	**0.141**	**0.028**	0.096	0.246
CPT	0.099	0.121	0.054	0.402	-0.024	0.710
HPT	**0.160**	**0.012**	0.098	0.123	0.004	0.947
PPT	**0.152**	**0.019**	**0.173**	**0.007**	**0.150**	**0.020**
MPT	**0.173**	**0.007**	**0.151**	**0.019**	**0.148**	**0.021**

MPS	0.048	0.454	0.030	0.644	0.021	0.740
WUR	-0.085	0.261	-0.018	0.811	-0.043	0.588
MDT	**0.153**	**0.017**	**0.160**	**0.013**	**0.221**	**<0.001**
VDT	**0.173**	**0.007**	**0.150**	**0.019**	0.123	0.056
DMA	-0.078	0.227	-0.098	0.128	-0.031	0.634

Table 3.4. Pearson's correlation between M1, S1 and insular cortical thickness and neurophysiological parameters. CDT, cold detection threshold; CPT, cold pain threshold; DM, diabetes mellitus; DMA, dynamic mechanical allodynia; eGFR, estimated glomerular filtration rate; HPT, heat pain threshold; M1, primary motor cortex; MDT, mechanical detection threshold; MPT, mechanical pain threshold; PHS, paradoxical heat sensation; PPT, pressure pain threshold; S1, primary somatosensory cortex; VDT, vibration detection threshold; WUR, wind up ratio.

3.3.4 Painful-DSPN subgroup analysis: IR and NIR stratification

The painful-DSPN group were stratified into two clinical phenotypes, IR-painful-DSPN and NIR-painful-DSPN. Table 3.5 shows the demographic, clinical and metabolic characteristics, results of neurophysiological assessments, DFNS QST assessment and cerebral measures for the two painful-DSPN phenotypes. The clinical and demographic measures were similar, although there was a greater proportion of patients with T1DM in the IR group (Chi^2, p=0.012). The sural amplitude was lower (independent samples t-test, p=0.017) and peroneal latency higher (p=0.017) in the NIR compared with IR group, suggestive of milder neuropathy severity in the latter. There were also between group differences in cold pain threshold (p=0.012), pressure pain threshold (p<0.001), mechanical pain sensitivity (p=0.001) and dynamic mechanical allodynia (p=0.045), suggestive of neuronal hypersensitivity/hyperalgesia in the IR group.

	IR Painful-DSPN (n = 34)	NIR Painful-DSPN (n = 43)	P value
Age (years)	56.4 ± 10.3	58.7 ± 8.9	0.299
Female sex, %	37.1%	28.9%	0.434*
Duration of diabetes (years)	19.8 ± 12.2	16.0 ± 11.0	0.155
Type 1 Diabetes, %	61.3%	38.7%	**0.012***
Body mass index (kg/m^2)	30.2 ± 7.3	31.6 ± 6.2	0.368
HbA1c (mmol/mol)	72.6 ± 20.6	70.5 ± 20.7	0.651
Sural amplitude (mV)	6.9 ± 9.9	2.4 ± 4.6	**0.017**
Sural velocity (m/s)	32.5 ± 9.1	38.1 ± 9.0	0.181
Peroneal amplitude (mV)	2.2 ± 2.2	1.4 ± 2.0	0.113
Peroneal velocity (m/s)	36.8 ± 5.1	35.8 ± 6.0	0.501
Peroneal latency (ms)	5.6 ± 1.1	7.3 ± 3.4	**0.017**
Tibial latency (ms)	6.2 ± 1.8	7.8 ± 4.6	0.150
DN4	7.0 ± 1.7	6.5 ± 1.5	0.186
NRS	6.1 ± 3.3	5.8 ± 2.9	0.698
CDT (z-score)	-2.13 ± 1.00	-2.57 ± 0.97	0.560
WDT (z-score)	-1.72 ± 0.84	-1.87 ± 0.53	0.328
TSL (z-score)	-1.95 ± 0.89	-2.32 ± 0.76	0.061
CPT (z-score)	-0.52 ± 0.85	-0.93 ± 0.39	**0.012**
HPT (z-score)	-0.93 ± 1.64	-1.42 ± 0.46	0.100
PPT (z-score)	2.42 ± 3.53	-0.70 ± 1.66	**<0.001**
MPT (z-score)	-1.02 ± 1.72	-1.68 ± 1.48	0.074
MPS (z-score)	-0.04 ± 1.74	-1.29 ± 1.07	**0.001**
WUR (z-score)	0.09 ± 1.69	-0.23 ± 1.51	0.537
MDT (z-score)	-2.76 ± 1.70	-2.76 ± 1.60	0.985
VDT (z-score)	-2.85 ± 2.40	-3.45 ± 2.65	0.310
DMA (z-score)	3.24 ± 9.05	0.01 ± 0.03	**0.045**

Mean Thalamic Volume (mm^3)	6660 ± 728	6539 ± 877	0.519
Mean S1 Cortical Thickness (mm)	1.89 ± 0.10	1.88 ± 0.12	0.678
Mean M1 Cortical Thickness (mm)	2.34 ± 0.14	2.29 ± 0.18	0.148
Mean Insular Cortical Thickness (mm)	2.85 ± 0.19	2.85 ± 0.16	0.887
Mean ACC Cortical Thickness (mm)	2.36 ± 0.22	2.57 ± 0.21	**<0.001**

Table 3.5. Demographic, clinical and metabolic characteristics, neurophysiological and DFNS QST assessments and cerebral measures for the two painful-DSPN phenotypes IR (Irritable nociceptor) and NIR (Non-irritable nociceptor). Data are presented as mean ± SD or percentage. Data analysed using the independent samples t-test except for * which were analysed using the Chi^2 test. ACC, anterior cingulate cortex; CDT, cold detection threshold; CPT, cold pain threshold; DMA, dynamic mechanical allodynia; DN4, Doleur Neuropathique en 4 questions; HPT, heat pain threshold; M1, primary motor; MDT, mechanical detection threshold; MPS, mechanical pain sensitivity; MPT, mechanical pain threshold; NRS, Numeric Rating Scale for pain; PPT, pressure pain threshold; S1, primary somatosensory; TSL, thermal sensory limen; VDT, vibration detection threshold; WDT, warm detection threshold; WUR, wind-up ratio.

There was no significant differences in global brain volumes between the two painful-DSPN phenotypes. However, ACC thickness was significantly lower the in IR- compared with NIR-painful-DSPN phenotype, Table 3.5 and Figure 3.7. The ACC cortical thickness negatively correlated with mechanical pain sensitivity (Pearson's correlation, r -0.281, p=0.014).

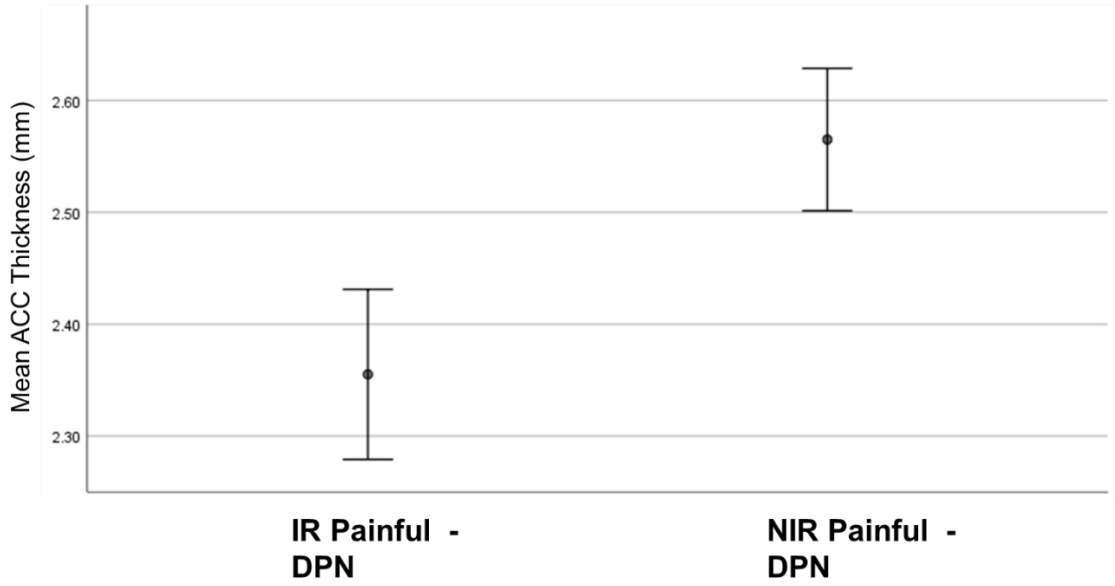

Figure 3.7. Mean ACC Thickness (mm) and 95% CI in participants with IR and NIR painful-DSPN. ACC thickness significantly lower in IR- compared with NIR-painful-DSPN (independent t-test, $p<0.001$). ACC, anterior cingulate cortex.

3.4 Discussion

To the best of our knowledge, this is the largest study to date involving well characterised participants to examine alterations in brain morphometry in DSPN. The key finding was a reduction in S1 and M1 cortical thickness in both painful- and painless-DSPN cohorts. Moreover, participants with neurophysiological evidence of more severe neuropathy had greater reductions in S1 and M1 cortical thickness. This suggests an important role in the neuropathic process which drives cortical changes in the brain. This study also demonstrated that the degree of alteration in cortical thickness was generally more marked in participants with painless- compared with painful-DSPN in regions associated with somatosensory function whereas in M1 the reduction in cortical thickness was similar. A

novel finding in the study was that ACC cortical thickness was reduced in participants with IR- compared with NIR-painful-DSPN, with greater reduction in cortical thickness in the former group. Additionally, the study also showed that global subcortical grey matter was reduced in participants with diabetes compared with HV.

Firstly, this study examined global cerebral parameters in the four patient groups. There was a significant group difference in subcortical grey volume, with all three-diabetes group showing a reduction in volume of similar magnitude, compared with HV. There were no significant group differences in the other global parameters; although there was a trend towards a reduction in the three diabetes groups in total brain volume, cortical volume and total grey volume compared with HV. Global brain volumes also correlated with sural nerve velocity, but not other measures of neurophysiological tests. However, this finding is limited by the fact that many cases had this neurophysiological variable missing from the dataset. Other global cerebral variables did not correlate with measures of neuropathy; therefore, this result may therefore be a false positive. There were correlations with global brain volumes and some clinical parameters, mostly consistently and strongly with age, as expected, but also with measures of diabetes, e.g., duration of DM and severity of microvascular complications

Large meta-analyses have previously demonstrated significant reductions in global grey matter volume in patients with T2DM compared with HV (Wu et al., 2017, Yao et al., 2021). There are fewer studies examining the differences in global brain parameters between T1DM and HV; although a 2015 meta-analysis found no differences in brain volume or total grey matter volume between these two groups (Moulton et al., 2015). Smaller studies, including our own, have found greater differences in global brain parameters in patients

with diabetes and a greater burden of microvascular complications compared to those without (Selvarajah et al., 2014b, Fang et al., 2018). However, the study in this thesis indicates that global brain volumes were similar between all three diabetes groups. Therefore, these results suggest that reductions in global brain volumes may be accelerated by the presence of diabetes but may not be significantly impacted by the presence of neuropathy. Further large meta-analyses and longitudinal analyses are required to determine the relationship between global brain measures and diabetic complications, however, to confirm this hypothesis.

On regional brain analysis there were significant group differences in S1, M1 and insular cortical thickness in DSPN groups. The cortical thickness was lowest at these regions in painless-DSPN compared with both control groups, with a lesser reduction in painful-DSPN. However, the group analysis significance was lost after correction at the S1 and insular cortex. At at these regions there was a stepwise reduction from the no-DSPN group to the DSPN groups. These results suggest that there are reductions in S1, M1 and insular cortical thickness as a result of diabetes, with an additive effect of DSPN. Overall, the data are consistent with previous smaller studies which have demonstrated reductions in brain areas associated with somatosensory and motor function in patients with DSPN compared with HV and no-DSPN, including: S1 (Selvarajah et al., 2014b), M1 (Selvarajah et al., 2019) and the insular cortices (Zhang et al., 2019).

A notable feature of this data was that the M1 cortical thickness was similar between painless- and painful-DSPN. Whereas at regions of the brain associated with somatosensory function and the pain matrix, i.e. S1 and insular cortices, there was a stepwise reduction from HV to no-DSPN, then painful-DSPN and lastly painless-DSPN which had the lowest

cortical thickness. In a previous study within our group we found that the S1 and M1 cortical thickness was lowest in an insensate painful-DSPN subgroup compared with HV, no-DSPN, painless-DSPN and sensate painful-DSPN groups (Selvarajah et al., 2019). In this prior study the sample size was smaller than the current study. Additionally, the subgrouping of painful-DSPN cohorts were different (sensate and insensate vs. IR and NIR) and the participants with insensate painful-DSPN had the most severe neuropathy, which may explain the differences in the results. Few studies have explored the morphological differences in the brain between painless- and painful-neuropathies. However, dichotomous symptom-based subgroupings were found to have distinct neuroplasticity in S1 and M1 cortices in participants with carpal tunnel syndrome (Maeda et al., 2016). Participants with carpal tunnel syndrome and paraesthesia demonstrated reduced S1/M1 cortical thickness which correlated with measures of neurophysiology; whereas those with neuropathic pain had greater S1/M1 thickness and showed correlation with pain severity. Similarly, in other chronic pain states cortical thickness appears preserved, if not increased, at the S1 cortex (Smallwood et al., 2013, Dai et al., 2015). In painful-DSPN there is a concurrent loss of peripheral sensation and peripheral neuropathic pain, sometimes referred to as the painful/painless leg (Ward, 1982). Thus, there may be a partial, but incomplete, loss of cortical thickness in areas related to somatosensory function in painful-DSPN, with larger reductions in painless-DSPN where there is greater reduction in peripheral neuronal impulse transmission, i.e. a dying back phenomenon with disuse atrophy. The cortical thickness in these regions may be partially maintained in painful-DSPN due to persistence of neuronal input from painful signalling. In our study there was no correlation between somatosensory brain regions and measures of neuropathic pain; therefore, further investigation into subgroups of painful-DSPN are necessary to explore this relationship in more detail.

Previous research within our group has demonstrated functional alterations in different phenotypes of painful-DSPN (Selvarajah et al., 2019, Wilkinson et al., 2020, Teh et al., 2021). Indeed, this study demonstrated structural alterations of the ACC in different subgroups, discussed below.

The clearest group differences in the S1, M1 and the insular cortices were between DSPN groups and HV. However, there were fewer significant differences between no-DSPN and the other groups. There were some clinical and neurophysiological variables which might explain the lack of group effect between no-DSPN and the DSPN groups. For example, the sural nerve amplitude was significantly lower in no-DSPN compared with HV. This has previously been described in participants with no-DSPN having relatively reduced peripheral neurological function compared with healthy volunteers (Gibbons et al., 2010). Also, the duration of diabetes was greater in painless- compared with painful-DSPN and no-DSPN. It is possible that these group differences may act as confounds for the cerebral results.

In this study there was no significant group differences on volumetric analysis in the thalamus. There was a trend towards a reduced volume in the painless-DSPN group with a lesser reduction in no-DSPN, which did not reach significance. This analysis measured the volume of the entire thalamus whereas only the certain areas of the thalamus, such as the ventral posterior lateral (VPL) thalamic subnucleus, are involved in somatosensory perception. Other studies have demonstrated focal reduced grey matter volume within the thalamus in DSPN using another MR analysis technique, VBM, which performs pairwise analysis between two groups (Zhang et al., 2019, Hansen et al., 2021). Therefore, the technique in this study may not have been sensitive enough to detect focal changes in thalamic subnuclei. A number of studies have also demonstrated thalamic functional

alterations between painful- and painless-DSPN (Shillo et al., 2019b), which will be explored further within this thesis in later chapters.

As this study recruited many participants, it was possible to explore the relationship of clinical and neurophysiological alterations and morphological differences within the brain. Generally, the cerebral parameters correlated with clinical measures, such as age and BMI. Indeed, age is well known to be a key determinant of morphological alterations within the brain. However, there were also correlations between cortical thickness at somatosensory/motor brain regions and neurophysiological parameters. The strongest correlations for neurophysiological parameters were with sural nerve amplitude and the S1 and M1 cortical thickness. Other brain regional morphometric parameters also correlated with measures of neurophysiology, such as the insular and anterior cingulate cortical thickness and thalamic volume. The strength of correlation between cerebral parameters and neurophysiology was relatively weak. This likely reflects the heterogeny of not only DSPN but also diabetes itself, e.g. type of diabetes, duration of diabetes and degree of other co-morbidities such as hypertension, microvascular and macrovascular disease. To definitively determine the relationship between cerebral parameters and DSPN, detailed prospective studies are necessary with baseline sensory phenotyping and longitudinal imaging.

DFNS QST was used to subgroup patients into the IR- and NIR-painful-DSPN phenotype to determine whether there were structural brain alterations between these two groups. Despite evidence of milder neuropathy in the IR group, there was a significant reduction in ACC cortical thickness compared with the NIR phenotype. Moreover, although the rating of pain was similar between groups, the ACC cortical thickness negatively correlated with MPS,

a measure of neuronal hypersensitivity. Therefore, this appears to show that there are differences in cortical thickness driven by the underlying phenotype. These findings are consistent with previous research within our group with a smaller cohort of patients (Teh et al., 2021). Zhang et al. has also demonstrated a reduced ACC cortical thickness on VBM in a paired painful-DSPN vs. HV analysis but not in painless-DSPN < HV analysis; although this study did not perform analysis on subgroups of painful-DSPN (Zhang et al., 2019).

The ACC has been highlighted as a key area for nociceptive processing of acute pain in humans (Apkarian et al., 2005). This region has been shown to be involved in the descending modulation of pain, attention to pain and emotional aspects of pain (Tracey and Mantyh, 2007). It is activated in response to noxious pain (Duerden and Albanese, 2013) accessing its sensory, cognitive and affective components (Xie et al., 2009). The ACC also shows heightened activation in chronic pain states (Bliss et al., 2016) and a number of studies have demonstrated anatomical alterations within the ACC in chronic pain states (Davis and Moayedi, 2013), suggesting a degenerative process or functional alteration (Bushnell et al., 2013). For example, reduced ACC cortical thickness has been shown in chronic lower back pain (Seminowicz et al., 2011, Kregel et al., 2015), fibromyalgia (Burgmer et al., 2009, Robinson et al., 2011), osteoarthritis (Woodworth et al., 2019) and headache disorders (Obermann et al., 2009, Gerstner et al., 2011) etc. (May, 2011). Moreover, reduced ACC cortical thickness has been shown to reverse with improvement in painful symptoms (Obermann et al., 2009, Seminowicz et al., 2011); although, these findings are not universal across the literature (Apkarian et al., 2004, Schmidt-Wilcke et al., 2006). The neurobiology causing this alteration is uncertain but may be due to neuronal loss related to excitotoxicity (Bushnell et al., 2013). The precise reason for reduced ACC cortical thickness in participants

with the IR-painful-DSPN phenotype is also unclear. ACC activation has been shown in participants with painful-DSPN, indeed it was found that increased activity within this region predicted successful treatment with duloxetine (Watanabe et al., 2018). Therefore, enhanced affective and emotional activity within the ACC may lead to excitotoxicity and consequent reduced cortical thickness in those with IR-painful-DSPN. An alternative explanation may be that degeneration within this region may be associated with reduced descending inhibition. Teh et al. demonstrated altered functional connectivity in IR and NIR phenotypes in painful-DSPN (Teh et al., 2021) and these two phenotypes have also been shown to have different responses to neuropathic pain treatments in a clinical trial (Demant et al., 2014). The finding in this study further supports the concept that different phenotypes of neuropathic pain have different underlying disease mechanisms. However, the aetiology and pathophysiology of different clinical phenotypes of neuropathic pain remain understudied. A greater understanding of this in the future may lead to improved mechanisms based management of painful-DSPN (Sloan et al., 2021).

There are many strengths to this study, to the best of our knowledge it is the largest study of cerebral morphometry in DSPN. Participants underwent detailed neurophysiological assessment as well as advanced volumetric cerebral imaging. However, the limitations of the study include the group differences in demographics, clinical characteristics, and metabolic parameters which may confound for the results. The reasons for this include that the study recruited many participants over a long period of time and incorporated 3D T1-weighted MR images from several studies. However, several of the differences between groups also reflect the well-known risk factors for DSPN and painful-DSPN. For example, age, BMI and longer duration of diabetes are risk factors for DSPN. The preponderance of

males in the painful-DSPN is difficult to explain, as female sex is a risk factor for the condition (Hébert et al., 2017). This may be due to a recruitment bias. Moreover, there were some missing data in the clinical and neurophysiological assessment of patients, which may have impacted the correlation analysis.

3.5 Conclusions and future work

This study demonstrates that key somatosensory and motor brain regions have reduced cortical thickness which relate to measures of neurophysiology, suggesting that DSPN is driving these structural alterations. This finding is consistent with our understanding that DSPN is not merely a disorder of the peripheral nerve, but the CNS also. Moreover, the cortical thickness reduction is more pronounced in somatosensory regions in painless- compared with painful-DSPN, suggesting relative preservation from cortical degeneration in the latter, which may be due to persisting neuronal impulses. Whereas the motor cortical thickness is similarly reduced in painless- and painful-DSPN. A novel finding of this study was that ACC thickness is dramatically reduced in participants with IR-painful-DSPN compared with the NIR phenotype. Maladaptation within this region therefore may reflect the changes occurring in the brain in different clinical phenotypes of painful-DSPN.

Future work is necessary to determine the mechanisms resulting in morphometric alterations in DSPN. Prospective studies in matched participants are required to longitudinally determine the factors associated with changes in cerebral morphology. Moreover, the finding of reduced ACC cortical thickness differentiating patients with IR- and

NIR-painful-DSPN phenotypes opens critical lines of future work. Further multimodal imaging studies are necessary to explore the functional role of the ACC as a determinant of different pain phenotypes in painful-DSPN. Numerous advanced imaging modalities are available which may interrogate the ACC in painful-DSPN, including blood flow haemodynamics, functional connectivity and neurotransmitter levels, which have the potential to unlock the causal relationship of morphological abnormalities in the ACC in different pain phenotypes. Exploration of the nature of different pain phenotypes is important in order to determine whether a mechanism-based approach to pain management may be feasible with painful-DSPN.

4. Cerebral Magnetic Resonance Spectroscopy alterations in DSPN: Neuronal function in painful- and painless-DSPN

4.1 Introduction

4.1.1 Background

Chapter 3 demonstrated evidence of structural changes in the brain in DSPN. Other studies have also shown brain vascular and functional alterations using a range of imaging modalities (Selvarajah et al., 2008, Cauda et al., 2009a, Cauda et al., 2009b, Selvarajah et al., 2011, Segerdahl et al., 2018, Selvarajah et al., 2019, Hansen et al., 2021, Wilkinson et al., 2020, Teh et al., 2021). Certain cerebral alterations including thalamic microvascular perfusion, somato-thalamic functional connectivity, descending pain modulatory function and ACC blood flow appear to differentiate painless- from painful-DSPN (Table 1.3) (Shillo et al., 2019b), suggesting involvement of the CNS in the aetiopathogenesis of neuropathic pain in diabetes. In Chapter 3, S1 cortical thickness was found to be reduced in painless-DSPN with lesser reductions in painful-DSPN. Other studies have highlighted the S1 cortex and the thalamus as two key brain regions thought to be involved in the pathophysiology of both DSPN and painful-DSPN. This chapter will describe the first of two Magnetic Resonance Spectroscopy (MRS) analyses exploring neurochemical differences in the S1 cortex and thalamus on the same cohort of participants. This chapter will describe the proton MRS data (1H-MRS) and Chapter 5 the 31-phosphorus MRS data (31P-MRS).

The S1 cortex is in the post-central gyrus and is responsible for processing, localizing, and discriminating of somatosensory impulses. It receives somatosensory information from the entire body; however, the proportional representation of body areas is different. The representation of the human body is known as the homunculus, with the leg and foot areas represented on the medial and superior surface of the cerebral hemisphere. In both DSPN and painful-DSPN, studies have demonstrated structural and functional alterations in the S1 cortex, including data from Chapter 3 (Selvarajah et al., 2014b, Wilkinson et al., 2020, Teh et al., 2021, Sloan et al., 2021). However, few S1 cortical alterations between painful- and painless-DSPN have been described. Recent publications from our group have shown that different pain phenotypes of painful-DSPN were associated with altered S1 cortical thickness/volume (Selvarajah et al., 2019, Wilkinson et al., 2020). Further studies in painful-DSPN have described altered functional connectivity with the S1 cortex and other key brain regions involved in the processing of pain (Cauda et al., 2009a, Selvarajah et al., 2019, Wilkinson et al., 2020, Teh et al., 2021).

The thalamus, however, is a grey matter structure of the diencephalon lying above the midbrain. It has neuronal projections to all the cerebral cortex, acting as a relay for somatosensory signals. It receives most of the peripheral somatosensory impulses from the spinal cord, where they are modulated, processed, and transmitted to higher brain centres within the pain matrix. There are numerous lines of evidence which have suggested altered function within the thalamus in painful- compared with painless-DSPN. Data from experimental models of painful-DSPN have shown hyper excitability, enhanced spontaneous activation and enlarged receptive fields in thalamic neurons (Fischer et al., 2009, Freeman et al., 2016). Moreover, the inhibitory neurotransmitter GABA was significantly elevated in the

thalamus in patients with painful- compared to painless-DSPN (Shillo et al., 2019). Also, altered thalamic blood flow has been shown in two separates studies using exogenous intravenous contrast (Selvarajah et al., 2011, Greig et al., 2017). These studies suggest preserved or heightened neuronal activity within the thalamus in painful- compared with painless-DSPN; however, this has not been confirmed in human DSPN.

The mechanisms underlying the structural and functional changes in DSPN, both with and without pain, are unclear. Studies have used 1H-MRS to investigate the underlying neurochemical alterations to gain insight into these cerebral changes in DSPN. Initially our group performed 1H-MRS in a small cohort of participants with T1DM with and without DSPN, shown in Figure 4.1 (Selvarajah et al., 2008). Patients with DSPN had a significantly lower N-acetylaspartate (NAA) to choline (Cho) ratio and NAA to creatine (Cr) ratio, as measures of neuronal function, compared with HV and no-DSPN. This finding was confirmed in a recent study which linked reduced thalamic grey matter volume loss with a reduced NAA:Cr in patients with T1DM and severe DSPN, suggesting thalamic neuronal loss (Hansen et al., 2021). A further unpublished study performed 1H-MRS in a much larger cohort of participants, and found there were no alterations in neurochemical markers of neuronal function in the S1 cortex in patients with painless- and painful-DSPN who had T1DM, shown in Figure 4.2 (Gandhi et al., 2006). However, this study found that there was a reduction in NAA:Cr in the thalamus in painless-DSPN, confirming the above findings; although, the NAA:Cr ratio in painful-DSPN was unaltered compared with no-DSPN and HV, see Figure 4.2 (Gandhi et al., 2006, Selvarajah et al., 2008).

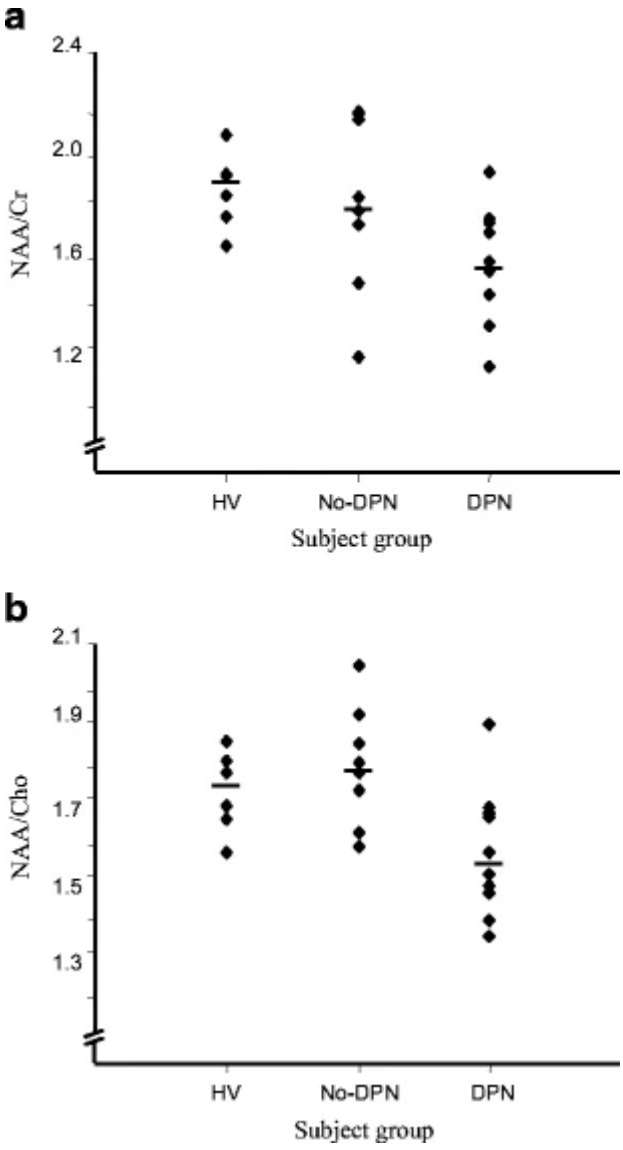

Figure 4.1. NAA:Cr (a) and NAA:Cho (b) ratio quantified using 1H-MRS in the thalamus in HV, patients with T1DM diabetes without DPN (No-DSPN) and patients with T1DM and DSPN (DPN) in a study performed by Selvarajah et al. (2008). Subgroup 1H-MRS metabolite differences: (DPN vs. No-DPN and HV) p = 0.04 (a), p = 0.02 (b). Cr, Creatine; Cho, choline; DPN, diabetic peripheral sensorimotor neuropathy; Cho, choline; Cr, creatine; NAA, N-Acetylaspartate. Reproduced from (Selvarajah et al., 2008).

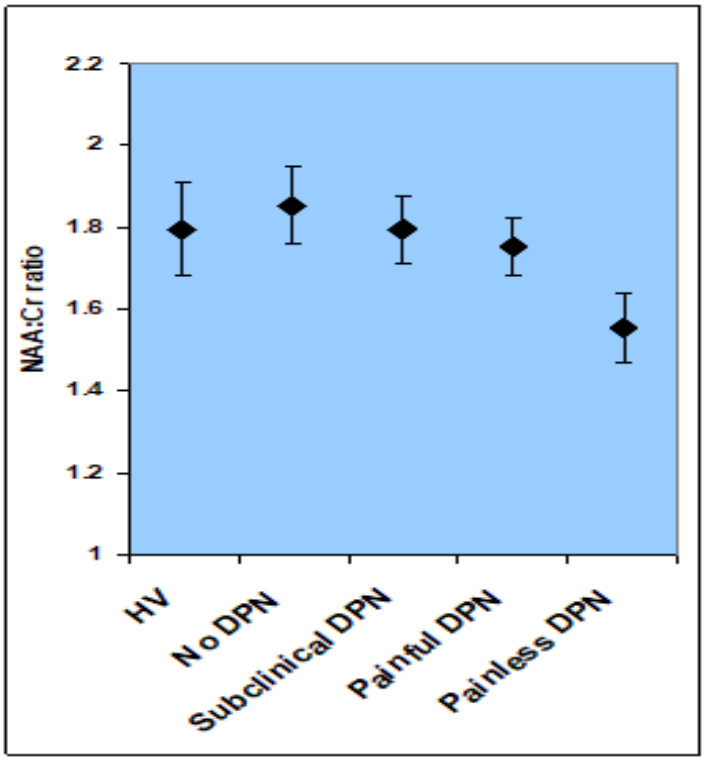

Figure 4.2 NAA:Cr ratio quantified using 1H-MRS in the thalamus in HV and four groups of patients with T1DM [No-DPN, T1DM without DSPN; subclinical DPN, T1DM with neurophysiological but not clinical evidence of DSPN; painful- and painless-DPN (DSPN)] in a study performed by Gandhi et al. (RA et al., 2006). The ratio was significantly lower in painless-DPN compared with all four other groups, $p<0.001$. Cr, Creatine; DPN, diabetic peripheral sensorimotor neuropathy; NAA, N-Acetylaspartate. DPN, diabetic peripheral sensorimotor neuropathy. Reproduced from (RA et al., 2006).

4.1.2 Rationale for study

Overall the above studies have demonstrated a reduced NAA level in participants with T1DM and painless-DSPN in the thalamus, with one study finding a normal ratio at the S1 cortex in DSPN. It therefore appears as though there may be a reduction of neuronal function in the thalamus in patients with painless-DSPN; whereas, in painful-DSPN neuronal function may be retained. However, these changes have not been demonstrated in T2DM

nor in both left and right thalami and S1 cortices. We therefore sought to 1H-MRS neurometabolite ratios in the thalamus and S1 cortices bilaterally in DSPN, with and without neuropathic pain, initially using 1H-MRS in participants with T2DM.

4.1.3 Aims and hypothesis

The aim of the study was to assess proton metabolite ratios of the S1 cortices and thalami, as a measure of neuronal function, in patients with T2DM and DSPN. We hypothesised that there will be a symmetrical reduction in NAA:Cho and/or NAA:Cr in the thalami in patients with painless-DSPN.

4.2 Methods

4.2.1 Study Design and Participants

Fifty-five participants were recruited to the study (12 HV, 11 T2DM without DSPN i.e no-DSPN, 12 with painless-DSPN and 20 with painful-DSPN). All participants with diabetes had T2DM and were diagnosed at least 6-months prior to their inclusion in the study. Inclusion and exclusion criteria were performed as described in the general methods section.

The study design was a case control cross-sectional study.

4.2.2 Clinical and neurological assessment

History, mood/memory assessment, clinical examination, structured neurological examination, nerve conduction studies and calculation of NIS-LL+7 was performed as described in the general methods.

4.2.3 Magnetic resonance spectroscopy protocol

4.2.3.1 Rationale for using Magnetic resonance spectroscopy

In vivo MRS allows the non-invasive measurement of biochemical processes within the human body in a particular region of interest, known as a voxel. This technique has been used in the research environment to examine biochemical/metabolic alterations in various neurological diseases and also has clinical applications, including the investigation of cerebral tumours. Hydrogen is the most commonly interrogated nuclei because of the sensitivity of this nucleus, its abundance within cerebral neurometabolites and the short acquisition time (Currie et al., 2013a). However, spectra from other MR sensitive endogenous nuclei such as 31-P may be detected too. It is possible to differentiate neurometabolites because of the phenomenon of chemical shift due to the shielding of different nuclei by their surrounding electron cloud. The MR spectra is a plot of signal intensities, measured along the y-axis, using an arbitrary scale; whereas the intensity of absorption, the area under spectral peaks, is proportional to the concentration of the measured metabolite (Figure 4.3). 1H-MRS detects metabolites containing protons and offers the ability to investigate neuronal function/viability.

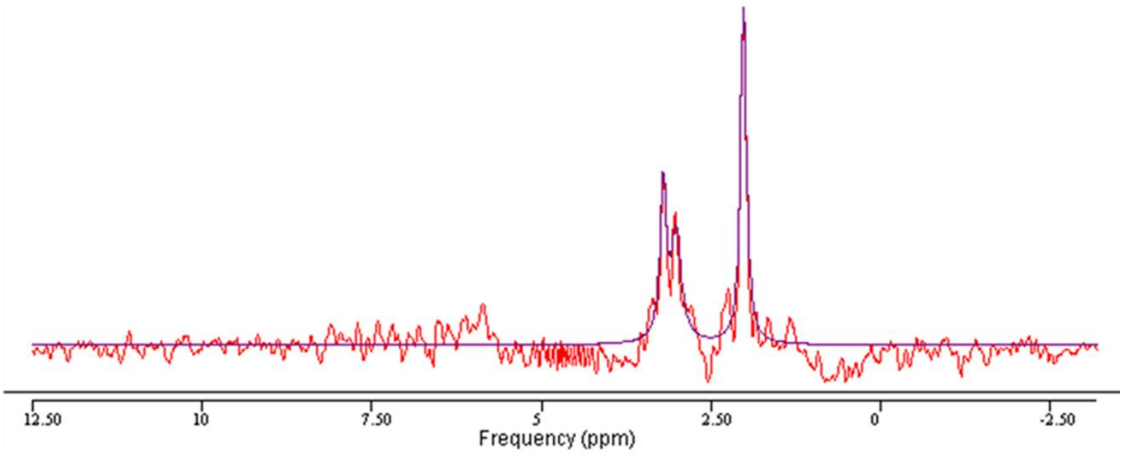

Figure 4.3. 1H-MRS spectrum as presented in jMRUI. The red line is the original spectra after pre-processing and the purple line the spectral line fitting for metabolite quantitation using AMARES. The peak on the far right represents N-acetylaspartate (located at 2.02ppm), the middle peak is creatine (3.02ppm) and the far-left peak choline (3.2ppm).

N-Acetylaspartate: The NAA peak is the most prominent peak on a 1H-MRS spectra, located at 2.02ppm (parts per million) (Figure 4.3) (Currie et al., 2013a). The function of NAA is incompletely established but it is postulated to be involved in a number of cerebral processes, including: neuronal osmoregulation, myelin lipid synthesis, nitrogen removal from the brain, facilitating energy metabolism and it is a precursor to N-acetylaspartylglutamate, a prevalent neurotransmitter (Moffett et al., 2007, Currie et al., 2013a). NAA acts as a marker for neuronal health, viability and number and is reduced in a variety of lesions and neurological disorders.

Phosphocreatine/Creatine: The creatine (Cr) resonance is a combination of creatine and phosphocreatine located at 3.02ppm, with a smaller peak at 3.9ppm (Currie et al., 2013a). Creatine and phosphocreatine are in equilibrium; therefore, creatine is commonly used as a an internal standard in MR spectroscopy from which metabolite ratios can be measured.

However, some authors advise caution as there are cases, particularly during tissue destruction, where creatine levels have fallen.

Choline: The Cho spectral peak is located at 3.2ppm, containing soluble constituents of the cell membrane (Currie et al., 2013a). Increases in this peak may be caused by rises in cell proliferation or membrane disruption. Also, this peak is greater in glial cells and within white compared to grey matter.

4.2.3.2 Protocol for 1H-MRS

Magnetic resonance spectroscopy imaging was performed using the 3T scanner described in the general methods with a dual tuned 1H/31P head coil (RAPID Biomedical GmbH, Würzburg, Germany). Initially, a multiple 2D survey scan was performed for localization of the voxel matrix (sagittal, coronal and transverse plane) with the following parameters: TR 11 ms, TE 4.6 ms, flip angle 15°, and voxel size 1.0 mm^3. The spectroscopy matrix contained a 14 x 14 grid of voxels with an individual voxel size was 25 x 25 x 40 mm^3. For 1H-MRS the TE was 288ms and TR 2000ms. The matrix was orientated to encompass the two ROIs, the foot region of the somatosensory cortex and the thalamus bilaterally (Figure 4.4).

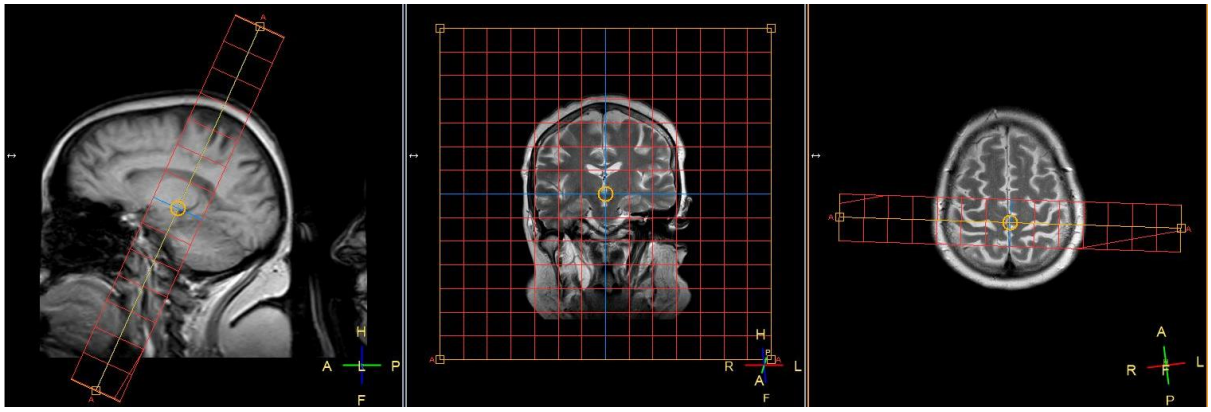

Figure 4.4 Example of the placement of spectroscopy matrix in the sagittal, coronal and transverse planes.

The 1H-MRS technique performed in the protocol was point resolved spectroscopy (PRESS) (Bottomley, 1987). PRESS is the commonest technique used for 1H-MRS. It involves the application of three concurrent radiofrequency pulses, one 90◦ excitation and two 180◦ refocusing pulses, in three orthogonal gradients (Figure 4.5). The spin echo is obtained from where the three orthogonal planes intersect, i.e. the region of interest. Additionally, the double spin-echo technique allows a much longer signal sampling window which is necessary to analyse small frequency differences in the chemical shift of 1H metabolites.

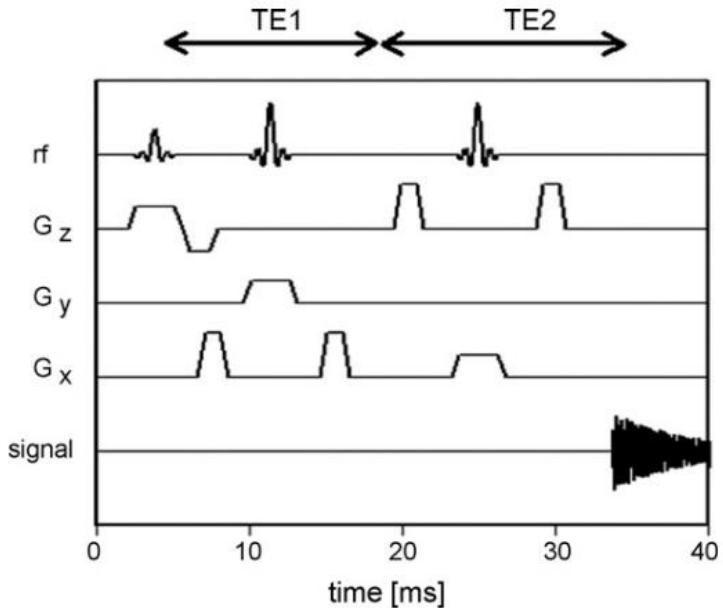

Figure 4.5. PRESS-sequence with three radiofrequency pulses (rf) applied simultaneously with field gradients along the three axes of the magnet (z, y and x). Reproduced from Klose et al. (Klose, 2008).

4.2.3.3 Magnetic resonance spectroscopy data processing

The data were processed using the software package for time-domain analysis of MRS data, java-based version of the MR user interface package (jMRUI, version 5.2) (Stefan et al., 2009). The jMRUI software allows pre-processing and quantitation of MRS spectra. The pre-processing algorithm Hankel Lanczos Squares Singular Values Decomposition (HLSVD) was used to suppress water and lipid peaks for 1H-MRS (de Beer et al., 1992). This requires the manual selection of the beginning and end of these peaks, which are then removed from the spectral analysis.

The non-least squares quantitation algorithm function of jMRUI was used, Advanced Method for Accurate, Robust, and Efficient Spectral fitting (AMARES) (Vanhamme et al.,

1997). The algorithm necessitates user input of components to be estimated into the algorithm, for which prior knowledge constraints regarding the peaks can also be imposed. Such user-input components include the weighting of the signal, which is the multiplication of the first points of the free induction delay signal. The other user components are starting values for frequencies and linewidths, which are displayed in Table 4.1 for 1H-MRS metabolites.

Neurometabolite Peak	Frequency (ppm)	Line Width (Hz)
Choline	3.22	4.4
Creatine	3.03	8.9
NAA	2.02	4.4

Table 4.1. Starting values for 1H-MRS on jMRUI. NAA, N-acetylaspartate; ppm, parts per million.

The jMRUI software provides a graphical representation of the original spectrum obtained from the MR scan (Figure 4.3 – red line). After calculation of the amplitude of the spectra the estimated signal, individual estimated components, and the remaining residue of the fitted estimated signal (i.e., difference after subtraction of the estimated signal from the original signal) are displayed (Figure 4.3 – purple line). From these graphical displays the spectra can be visually assessed for quality.

Automatically generated metabolite maps can be unreliable for several reasons, e.g movement artefact and inaccurate spectral line fitting. The individual metabolite maps in this study were assessed for quality manually with visual assessment of the line fit (Figure

4.3) and calculation of the Cramér–Rao lower bound from each spectrum, which is calculated during jMRUI processing (Stefan et al., 2009). Cramér–Rao lower bounds are an estimate of error of the concentration measurements and are the lowest possible standard deviations of model parameter estimates obtained during spectral quantification (Cavassila et al., 2001). Widely used thresholds levels of Cramér–Rao lower bounds are 20% or 50%. Levels above 50% this means the data may not be significantly different from zero and therefore may be considered unreliable (Wilson et al., 2019). However, quality filtering using Cramér–Rao lower bounds may cause bias in the estimated mean concentrations of cohort data (Kreis, 2016). Table 4.2. presents the Cramér–Rao bound values for the 1H-MRS metabolites. The spectra of the included participants in the final analysis were therefore of adequate quality, none were removed as a result of high Cramér–Rao bound values.

	Cramér–Rao bound Non-dominant hemisphere	Cramér–Rao bound Dominant hemisphere
S1 Cho	15.7 ± 17.0	16.8 ± 13.9
S1 Cr	16.0 ± 17.3	19.2 ± 17.3
S1 NAA	5.7 ± 5.4	6.3 ± 7.0
Th Cho	9.5 ± 3.7	8.3 ± 5.7
Th Cr	10.8 ± 7.8	11.9 ± 14.0
Th NAA	3.9 ± 3.0	4.1 ± 4.1

Table 4.2. Cramér–Rao bound for 1H-MRS analysis of all study participants. Data are presented as mean ± standard deviation. Cho, choline; Cr, creatine; NAA, N-acetylaspartate; Th, thalamic; S1, primary somatosensory cortex.

1H-MRS metabolites may be quantified in either absolute or relative measurements. Absolute quantification requires the correction of many factors including tissue composition of the voxel, this is not always feasible and is likely to result in higher error than relative

quantification. Moreover, the area under the spectral peak is not always proportional to the metabolite concentration, as the relationship depends on various biophysical and MR parameters (Ulmer, Backens and Ahlhelm 2015). The semi-quantitative approach involves the generation of metabolite ratios which is the most used method (Currie, et al. 2013). In this study as we assessed the metabolite ratios and the following metabolite ratios were quantified: NAA:Cho, NAA:Cr, Cho:Cr.

4.2.4 Statistical Analysis

The Shapiro-Wilk Test was used to test normality. Spectroscopy metabolites and ratios were analysed from both hemispheres of the brain and the mean ratio calculation. The dominant hemisphere (DH) refers to the left hemisphere of the brain as all participants were right-handed and the non-dominant (NDH) the right hemisphere of the brain. The mean value of ratios was calculated from the mean of each of the DH and NDH metabolites. The data was analysed otherwise as described in the general methods.

4.3 Results

4.3.1 Participant recruitment details

A total of 55 participants underwent 31P-MRS and 1H-MRS analysis; however, participants had to be removed for certain analyses because of inadequate MRS spectra, see Figure 4.6. The participants were removed from the 1H-MRS analysis due to movement artefact and/or inadequate water/fat suppression.

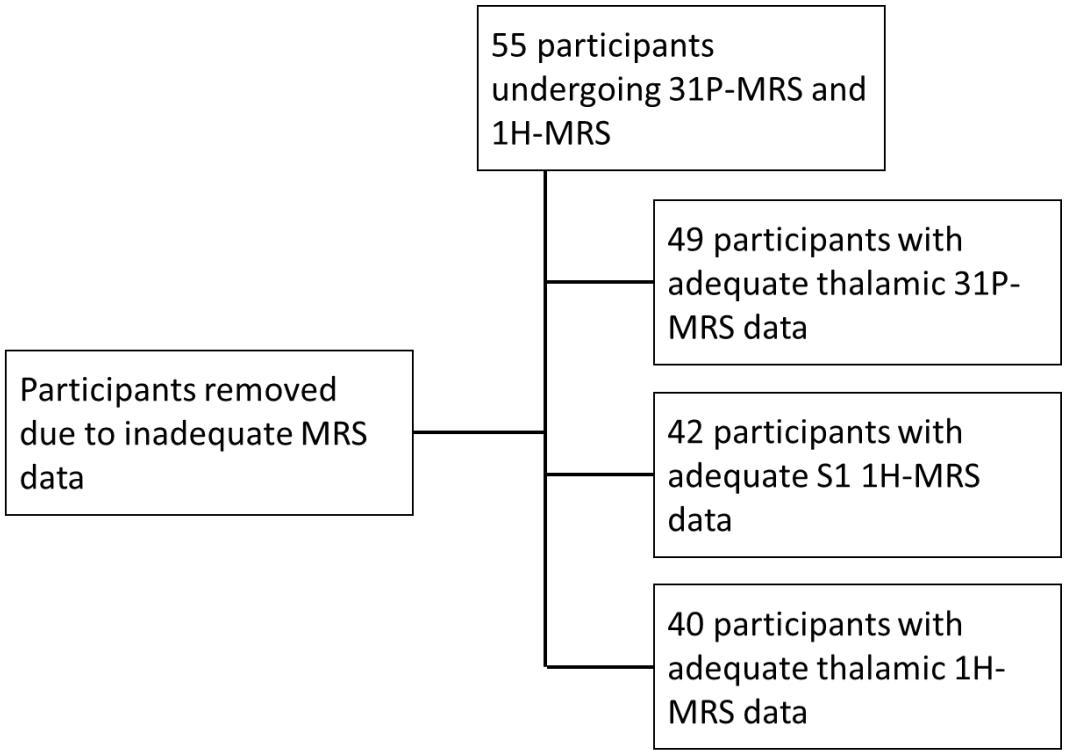

Figure 4.6. Consort flow diagram of the inclusion of patient MRS data in the final analysis. 55 participants underwent 31P-MRS; 6 participants were excluded for 31P-MRS thalamic analysis; 13 participants were excluded for 1H-MRS analysis; and 15 participants were excluded for 1H-MRS thalamic analysis. 1H-MRS, proton magnetic resonance spectroscopy; 31P-MRS, 31-phosphorus magnetic resonance spectroscopy; S1, primary somatosensory cortex.

4.3.2 Participant demographic, clinical and neurophysiological data

Table 4.3 summarises the demographic and clinical data, and biochemistry test results for all study participants. The HbA1c was greater in the diabetes groups compared with HV (all, Mann Whitney U test, $p<0.001$); however, there was no significant difference amongst the three diabetes groups. Current alcohol intake was significantly lower in the painful-DSPN group compared with other groups ($p<0.01$). Post hoc analysis revealed no other statistically significant difference in study variables in Table 4.3 between the painful- and painless-DSPN groups.

	HV (n=12)	No-DSPN (n=11)	Painless-DSPN (n=12)	Painful-DSPN (n=20)	P value
Age (years)	67 (IQR 12.8)	60.0 (7.0)	61.5 (7.8)	61.6 (8.3)	0.442 KW
Sex (% female)	33%	45%	58%	40%	0.638 Chi^2
Duration DM (years)		8.7 ± 5.6	15.8 ± 5.7	12.5 ± 8.3	0.065 A
Retinopathy presence (% present)		45%	50%	60%	0.710 Chi^2
Retinopathy score (0= No DR, 1= Bck/Pre-P, 2=Pro/Laser)		0 = 6 1 = 5 2 = 0	0 = 6 1 = 5 2 = 1	0 = 8 1 = 6 2 = 6	0.242 Chi^2
Nephropathy presence (% present)		9%	45%	53%	0.055 Chi^2
ACR (mg/mmol)		0.5 (0.8 IQR)	1.4 (1.8)	2.4 (1.7)	0.135 KW
Number of hypoglycaemic episodes in last 12 months		0.0 (0.0 IQR)	0.0 (0.0)	0.0 (2.8)	0.157 KW
Smoked ever (% Yes)	42%	73%	50%	70%	0.289 Chi^2
Pack Years smoking [Packs (1 pack = 20 cigarettes) x Number of years]	0 (18.8 IQR)	10 (24.0)	0.38 (25.9)	2.2 (33.8)	0.644 KW
Alcohol intake (units/week)	3.0 (10.5 IQR)	7.5 (12.0)	1.5 (8.5)	0.0 (0.4)	**0.006 KW**
Waist/hip ratio	0.89 ± 0.1	0.93 ± 0.1	0.98 ± 0.1	0.95 ± 0.1	0.082 A
Body mass index (kg/m^2)	28.0 ± 6.6	28.7 ± 4.1	32.2 ± 3.4	31.3 ± 5.2	0.116 A
Systolic blood pressure (mmHg)	135.3 ± 20.9	128.2 ± 11.2	142.6 ± 17.7	141.8 ± 15.6	0.126 A
Creatinine (µmol/l)	70.8 ± 7.2	72.8 ± 12.0	77.9 ± 12.6	71.2 ± 16.0	0.489 A
Total Cholesterol (mmol/l)	4.83 ± 1.0	4.86 ± 1.0	3.89 ± 1.0	4.29 ± 1.0	0.054 A
HbA1c (mmol/mol)	37.5 (IQR 14.0)	61.0 (29.0)	58.5 (26.0)	64.0 (31.5)	**<0.001 KW**

Glucose During MR (mmol/l)		9.8 (IQR 4.3)	9.0 (4.8)	8.6 (4.3)	0.955 KW
MMSE	30.0 (IQR 0.0)	30.0 (1.0)	30.0 (1.8)	29.0 (1.8)	0.164 KW
Depression (% Yes)	0%	0%	0%	15%	0.136 Chi^2
Anxiety (% Yes)	0%	0%	8%	20%	0.159 Chi^2

Table 4.3. Clinical details of participants undergoing MRS. Data are presented as mean ± standard deviation for parametric and median (IQR) for non-parametric continuous data or percentage for categorical data. The statistical test used was ANOVA (A) for continuous normally distributed data, Kruskal-Wallis (KW) for non-parametric continuous data or Chi^2 for categorical data. Retinopathy parameters: Bck, background retinopathy; DR, diabetic retinopathy; Laser, panretinal photocoagulation; Pre-P, pre-proliferative retinopathy; Pro, proliferative retinopathy. ACR, albumin creatinine ratio; DM, Diabetes Mellitus; HV, healthy volunteer; MMSE, mini-mental state examination; MR, magnetic resonance scan.

Table 4.4 summarises the neurological assessments of the study participants. The values for the clinical scoring systems for neuropathic pain, NPSI and DN4, were both statistically higher in the painful-DSPN group compared with all other groups, as expected (Mann Whitney U test, all, $p<0.001$). The values for the clinical scoring systems for peripheral neuropathy, TCNS and NIS-LL, were also both statistically higher in the DSPN groups compared with HV and no-DSPN ($p<0.001$). The TCNS was also statistically higher in the painful- compared with painless-DSPN group ($p=0.025$); although, objective measures of neuropathy, including nerve conduction parameters, ESC, CAN composite score and NIS-LL7 were not significantly different between painless- and painful-DSPN groups. However, these all indicated a greater severity of neuropathy in the DSPN groups compared with HV and no-DSPN, except for peroneal motor nerve distal latency which was not statistically different between HV and painful-DSPN.

	HV (n=12)	No-DSPN (n=11)	Painless-DSPN (n=12)	Painful-DSPN (n=20)	P value
NPSI (Total score)	0.0 (IQR 0.0)	0.0 (0.0)	0.0 (0.8)	22.58 (14.8)	**<0.001 KW**
DN4	0.0 (IQR 0.0)	0.0 (0.0)	0.0 (1.8)	6.5 (2.8)	**<0.001 KW**
TCNS	0.0 (IQR 0.0)	0.0 (2.0)	9.0 (7.0)	14.5 (4.5)	**<0.001 KW**
NIS-LL	0.0 (IQR 0.0)	0.0 (0.0)	12.0 (12)	17.5 (9.5)	**<0.001 KW**
NIS-LL+7	0.0 (IQR 0.8)	0.0 (0.0)	23.5 (14.7)	24.5 (16.8)	**<0.001 KW**
Peroneal CMAP (mV)	6.3 ± 2.4	6.2 ± 1.9	1.9 ± 2.0	3.1 ± 2.1	**<0.001 A**
Peroneal MNCV (m/s)	46.5 (IQR 3.0)	45.5 (2.3)	39.5 (9.6)	37.7 (8.1)	**<0.001 KW**
Peroneal MNDL (msec)	4.9 (IQR 0.6)	4.2 (0.5)	6.5 (3.9)	5.5 (1.6)	**0.001 KW**
Tibial MNDL (msec)	4.6 (IQR 0.9)	4.4 (0.8)	5.4 (2.4)	6.0 (2.9)	**0.001 KW**
Sural SNAP (mV)	14.1 (IQR 6.0)	12.6 (4.8)	1.8 (3.4)	0.7 (9.1)	**<0.001 KW**
CAN composite score	0.0 (IQR 0.0)	0.0 (0.5)	0.0 (0.0)	2.0 (2.5)	0.077 KW
ESC (µS)	79.0 (IQR 11.5)	78.0 (15.05)	61.0 (26.0)	53.0 (35.0)	**0.002 KW**

Table 4.4. Neurological assessments of study participants undergoing MRS. Data are presented as mean ± standard deviation for parametric and median (IQR) for non-parametric continuous data. The statistical test used was ANOVA (A) for continuous normally distributed data and Kruskal-Wallis (KW) for non-parametric continuous data. CAN, cardiac autonomic neuropathy; CMAP, compound muscle action potential; DN4, doleur neuropathique 4; ESC, electrochemical skin conductance; MNDL, motor nerve distal latency; MNCV, motor nerve conduction velocity; NIS-LL, neuropathic impairment score of the lower limb; NPSI, neuropathic pain symptom inventory; SNAP, sural nerve action potential; TCNS, Toronto clinical neuropathy score.

Appendix 10.7 provides a breakdown of the individual components of the NPSI score for participants with painful-DSPN and 10.8 the DFNS-QST results in all participants. Participants with painful- and painless-DSPN had QST evidence of small- and large-nerve fibre dysfunction in comparison to HV and no-DSPN. Moreover, DFNS-QST parameters were

similar between the two DSPN groups with no evidence of allodynia/hyperalgesia in the painful-DSPN group.

4.3.3 1H-MRS Participant demographic, clinical and neurophysiological data

Forty-two (n=42) participants had adequate S1 cortical 1H-MRS data available for analysis (HV, n=8; no-DSPN, n=7; painless-DSPN, n=9; and painful-DSPN, n=18) and 40 for thalamic analysis (HV, n=9; no-DSPN, n=8; painless-DSPN, n=9; and painful-DSPN, n=14). Therefore, 13 participants did not have somatosensory cortical 1H-MRS data available for analysis (HV: Age 59.3 ± 18.5, female 50%, BMI 27.6 ± 8.7 kg/m^2 and HbA1c 36.8 ± 6.0 mmol/mol; no-DSPN: Age 61.0 ± 3.4, female 50%, BMI 28.3 ± 2.4 kg/m^2 and HbA1c 59.0 ± 8.1 mmol/mol; painless-DSPN: Age 62.7 ± 2.1, female 67%, BMI 32.3 ± 5.5 kg/m^2 and HbA1c 67.0 ± 14.0 mmol/mol; painful-DSPN: Age 59.0 ± 8.5, female 50%, BMI 37.6 ± 2.3 kg/m^2 and HbA1c 50.0 ± 18.4 mmol/mol). Also, 15 participants did not have thalamic 1H-MRS data available for analysis (HV: Age 63.3 ± 4.9, female 33.3%, BMI 35.5 ± 4.3 kg/m^2 and HbA1c 40.7 ± 3.8 mmol/mol; no-DSPN: Age 61.7 ± 4.6, female 0%, BMI 29.9 ± 2.3 kg/m^2 and HbA1c 52.0 ± 13.7 mmol/mol; painless-DSPN: Age 61.7 ± 0.6, female 100%, BMI 32.4 ± 5.4 kg/m^2 and HbA1c 62.3 ± 16.2 mmol/mol; painful-DSPN: Age 60.0 ± 3.7, female 50%, 35.9 ± 4.8 kg/m^2 and HbA1c 60.2 ± 15.0 mmol/mol). In view of the potential for group clinical and neurophysiological characteristics to be altered after participant exclusion, their group variables were re-analysed, Appendix 10.9 – 10.12.

The group differences in those undergoing 1H-MRS were similar in HbA1c (Kruskal Wallis. P=0.001) and current alcohol intake (Kruskal Wallis, p=0.023) in comparison to all study

individuals. In this patient cohort there were additional group differences in cholesterol (ANOVA, p=0.022) and percentage of participants with nephropathy (Chi^2, p=0.046). There was a significantly greater percentage of participants with diabetic nephropathy in the neuropathy groups compared with no-DSPN; however, this was not the case for ACR. Total cholesterol was also significantly lower in the two neuropathy groups compared with no-DSPN and HV. The neurological assessments for participants undergoing S1 1H-MRS analysis were similar to the full cohort analysis.

The group differences for those undergoing 1H-MRS thalamic analysis were similar in HbA1c and current alcohol intake in comparison to participants undergoing 1H-MRS of S1. In this patient cohort there were additional group differences in waist/hip ratio (Kruskal Wallis, p=0.024), but not cholesterol and nephropathy. The waist/hip ratio was significantly higher in painless-DSPN compared with HV and no-DSPN. The waist/hip ratio was also significantly higher in painful-DSPN compared with HV but not no-DSPN. Finally, the BMI was significantly higher in the two DSPN groups compared with HV (ANOVA, p=0.017). The group differences of neurological assessments were similar to those described above for participants undergoing 31P-MRS.

4.3.3 1H-MRS Imaging results

The raw 1H-MRS metabolite values for S1 and the thalamus are presented in Table 4.5 and 4.6, respectively, and the 1H-MRS ratios for S1 are presented in Table 4.7 with the mean NAA:Cho graphically displayed in Figure 4.7. There were no significant differences among the raw metabolite values or ratios at the S1 cortex either.

	HV (n=8)	No-DSPN (n=7)	Painless-DSPN (n=9)	Painful-DSPN (n=18)	P value
NDH S1 Cho	5.65 (IQR 2.9)	6.86 (2.5)	6.00 (2.1)	6.61 (1.8)	0.118
NDH S1 Cr	5.96 (5.3)	8.45 (2.3)	7.21 (3.2)	7.64 (1.4)	0.390
NDH S1 NAA	12.54 (3.5)	16.40 (1.5)	17.21 (5.8)	16.91 (4.8)	0.190
DH S1 Cho	5.70 (3.8)	6.65 (1.8)	7.25 (3.9)	7.15 (3.5)	0.378
DH S1 Cr	6.00 (5.6)	7.45 (2.5)	7.44 (3.9)	6.3 (2.5)	0.637
DH S1 NAA	13.59 (3.5)	15.10 (3.9)	16.83 (4.2)	16.45 (3.4)	0.072

Table 4.5. 1H-MRS raw data of the S1 cortex. Data are presented as median (IQR). The statistical test used was the Kruskal-Wallis test. Cho, choline; Cr, creatine; DH, dominant hemisphere; NAA, N-acetylaspartate; NDH, non-dominant hemisphere; S1, somatosensory cortex.

	HV (n=9)	No-DSPN (n=8)	Painless-DSPN (n=9)	Painful-DSPN (n=14)	P value
NDH Th Cho	8.40 (IQR 3.7)	10.70 (1.7)	9.66 (3.4)	9.21 (2.6)	0.537 KW
NDH Th Cr	8.28 ± 2.6	8.99 ± 2.8	8.90 ± 3.2	8.07 ± 2.7	0.856 A
NDH Th NAA	17.80 (6.8)	19.91 (2.9)	17.56 (5.0)	18.0 (2.7)	0.507 KW
DH Th Cho	7.76 (3.4)	9.97 (1.6)	9.74 (3.1)	8.72 (3.0)	0.056 KW
DH Th Cr	6.27 (2.8)	8.76 (2.8)	7.88 (4.7)	7.59 (4.3)	0.568 KW
DH Th NAA	17.86 (8.1)	19.13 (3.1)	18.0 (5.4)	17.02 (4.3)	0.527 KW

Table 4.6. 1H-MRS raw data of the thalamus. Data are presented as mean ± standard deviation for parametric and median (IQR) for non-parametric continuous data. The statistical test used was ANOVA (A) for continuous normally distributed data and Kruskal-Wallis (KW) for non-parametric continuous data. Cho, choline; Cr, creatine; DH, dominant hemisphere; NAA, N-acetylaspartate; NDH, non-dominant hemisphere; S1, somatosensory cortex.

	HV (n=8)	No-DSPN (n=7)	Painless-DSPN (n=9)	Painful-DSPN (n=18)	P value
NDH S1 NAA:Cho	2.53 (IQR 0.7)	2.23 (0.8)	2.82 (0.8)	2.31 (0.6)	0.211 KW
NDH S1 NAA:Cr	2.27 ± 0.8	2.00 ± 0.3	2.60 ± 1.1	2.10 ± 0.6	0.221 A
NDH S1: Cho:Cr	0.97 ± 0.6	0.84 ± 0.2	0.97 ± 0.3	0.93 ± 0.3	0.841 A
DH S1 NAA:Cho	2.48 (1.0)	2.31 (0.3)	2.35 (0.9)	2.07 (0.7)	0.335 KW
DH S1 NAA:Cr	2.76 ± 1.1	2.54 ± 1.1	2.49 ± 0.6	2.45 ± 0.5	0.431 A
DH S1: Cho:Cr	1.08 ± 0.3	1.12 ± 0.5	1.05 ± 0.3	1.12 ± 0.2	0.955 A
Mean S1 NAA:Cho	2.50 (0.4)	2.25 (0.4)	2.64 (0.7)	2.17 (0.7)	0.127 KW
Mean S1 NAA:Cr	2.51 ± 0.7	2.27 ± 0.6	2.55 ± 0.6	2.28 ± 0.3	0.503 A
Mean S1: Cho:Cr	1.02 ± 0.4	0.98 ± 0.3	1.01 ± 0.2	1.02 ± 0.3	0.986 A

Table 4.7. 1H-MRS metabolite ratios at the S1 cortex. Data are presented as mean ± standard deviation for parametric and median (IQR) for non-parametric continuous data. The statistical test used was ANOVA (A) for continuous normally distributed data and Kruskal-Wallis (KW) for non-parametric continuous data. Cho, choline; Cr, creatine; DH, dominant hemisphere; NAA, N-acetylaspartate; NDH, non-dominant hemisphere; S1, somatosensory cortex.

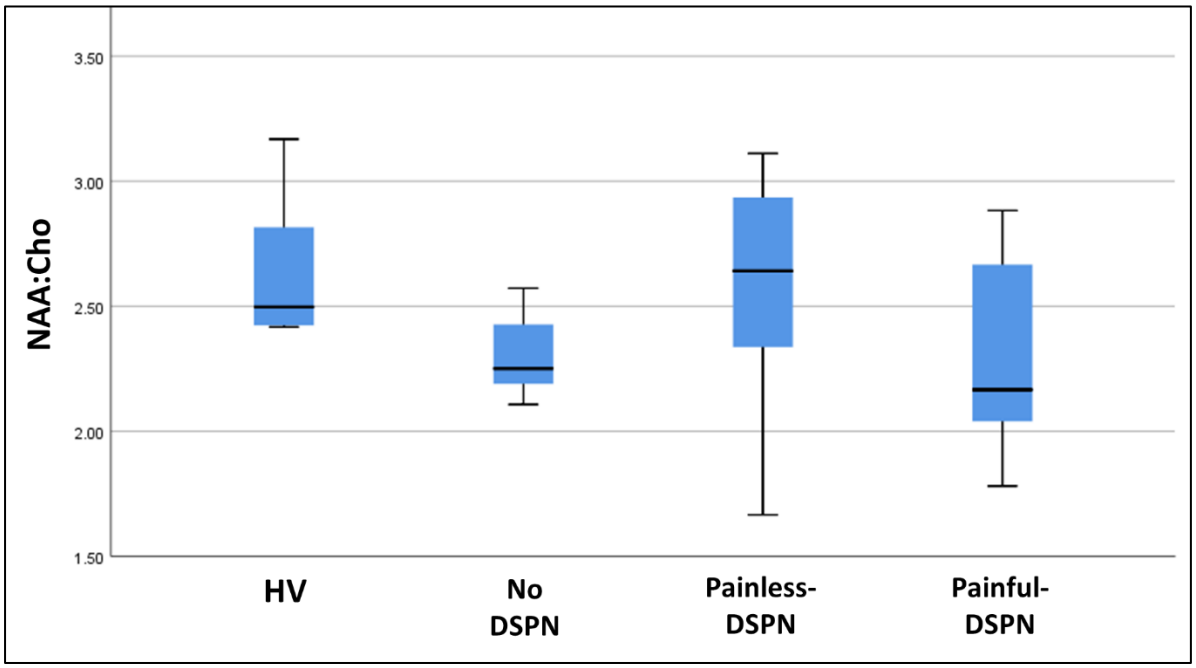

Figure 4.7. Mean somatosensory cortical NAA:Cho box and whisker plot (P=0.127, Kruskal Wallis). Cho, Choline; NAA, N-acetylaspartate.

In view of the significant group differences in HbA1c, cholesterol, alcohol intake and the presence of nephropathy for participants undergoing 1H-MRS analysis of the somatosensory cortex, these variables were added to an ANCOVA. None of these four variables had a significant impact upon the outcome of the model for the mean NAA:Cho, NAA:Cr and Cho:Cr.

On correlation analysis, the mean S1 NAA:Cho correlated with DN4 (r -0.355, p=0.021), peroneal motor nerve conduction velocity (r 0.401, p=0.017), CAN total score (r -0.432, p=0.010) and NRS during the scan (r -0.311, p=0.048), Spearman's correlation. The mean NAA:Cr correlated with age (r 0.305, p=0.049), Pearson's correlation.

Table 4.8 shows the results of 1H-MRS at the thalamus. There was a significant group effect in DH thalamic NAA:Cho (Kruskal-Wallis test, p=0.013), see Figure 4.9. The NAA:Cho was

significantly lower in no-DSPN (Mann Whitney-U test, p=0.036) and painless-DSPN (p=0.004) compared with HV. Also, this ratio was reduced in painless- compared with painful-DSPN (p=0.013). There was a trend towards a reduced NAA:Cho at the mean thalamus, with the numerical value the lowest in painless-DSPN, see Figure 4.8, which did not reach statistical significance. The NAA:Cr was numerically the lowest at the DH, NDH and mean thalamus, although there was no significant group effect. Similarly, there was no significant group difference in Cho:Cr.

	HV (n=9)	No-DSPN (n=8)	Painless-DSPN (n=9)	Painful-DSPN (n=14)	P value
NDH Th NAA:Cho	1.98 (IQR 0.3)	1.85 (0.8)	1.79 (0.3)	2.00 (0.6)	P=0.460 KW
NDH Th NAA:Cr	2.37 ± 0.7	2.36 ± 0.8	2.10 ± 0.5	2.16 ± 0.4	P=0.723 A
NDH Th Cho:Cr	1.18 ± 0.3	1.29 ± 0.6	1.20 ± 0.3	1.10 ± 0.2	P=0.941 A
DH Th NAA:Cho	2.29 (0.4)	1.8 (0.5)	1.71 (0.5)	2.00 (0.7)	**P=0.013 KW**
DH Th NAA:Cr	2.57 ± 0.7	2.44 ± 0.5	2.04 ± 0.3	2.62 ± 1.0	P=0.215 A
DH Th Cho:Cr	1.15 ± 0.3	1.40 ± 0.5	1.64 ± 1.0	1.32 ± 0.4	P=0.358 A
Mean Th NAA:Cho	2.07 (0.3)	1.79 (0.4)	1.74 (0.3)	1.93 (0.4)	P=0.060 KW
Mean Th NAA:Cr	2.47 ± 0.7	2.40 ± 0.7	2.10 ± 0.3	2.56 ± 0.7	P=0.384 A
Mean Th Cho:Cr	1.17 ± 0.3	1.35 ± 0.5	1.42 ± 0.6	1.28 ± 0.3	P=0.628 A

Table 4.8. 1H-MRS metabolite ratios at the thalamus. Data are presented as mean ± standard deviation for parametric and median (IQR) for non-parametric continuous data. The statistical test used was ANOVA (A) for continuous normally distributed data and Kruskal-Wallis (KW) for non-parametric continuous data. Cho, choline; Cr, creatine; DH, dominant hemisphere; NAA, N-acetylaspartate; NDH, non-dominant hemisphere; S1, somatosensory cortex.

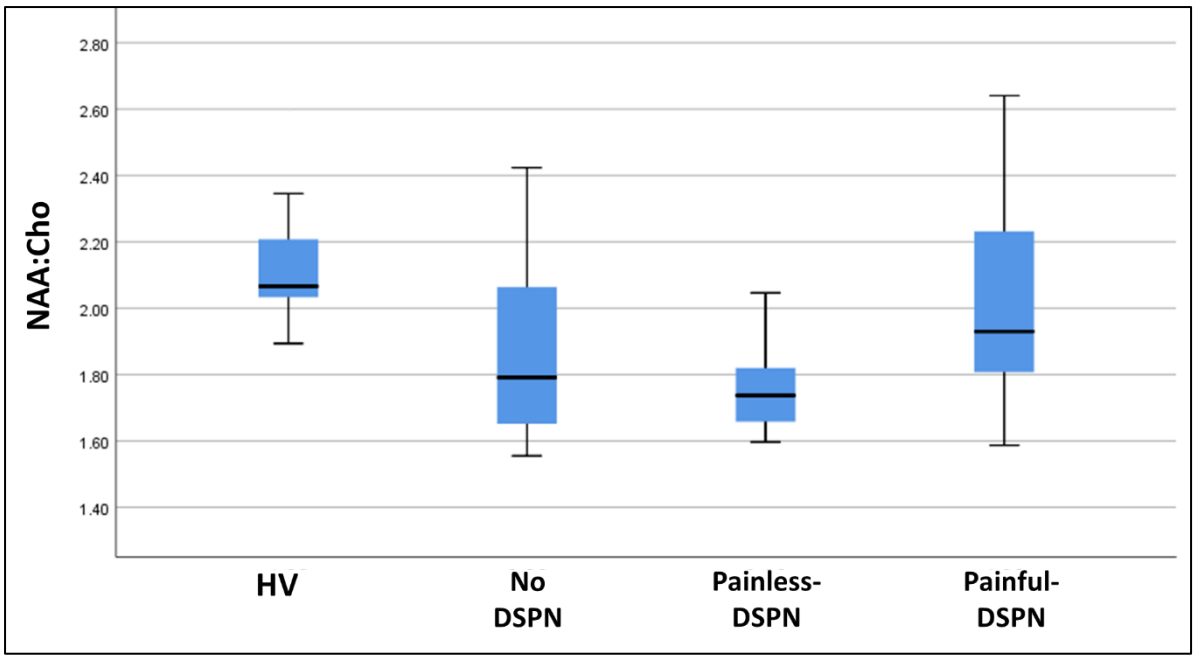

Figure 4.8. Mean thalamic NAA:Cho box and whisker plot (p=0.060, Kruskal Wallis). Cho, choline; NAA, N-acetylaspartate

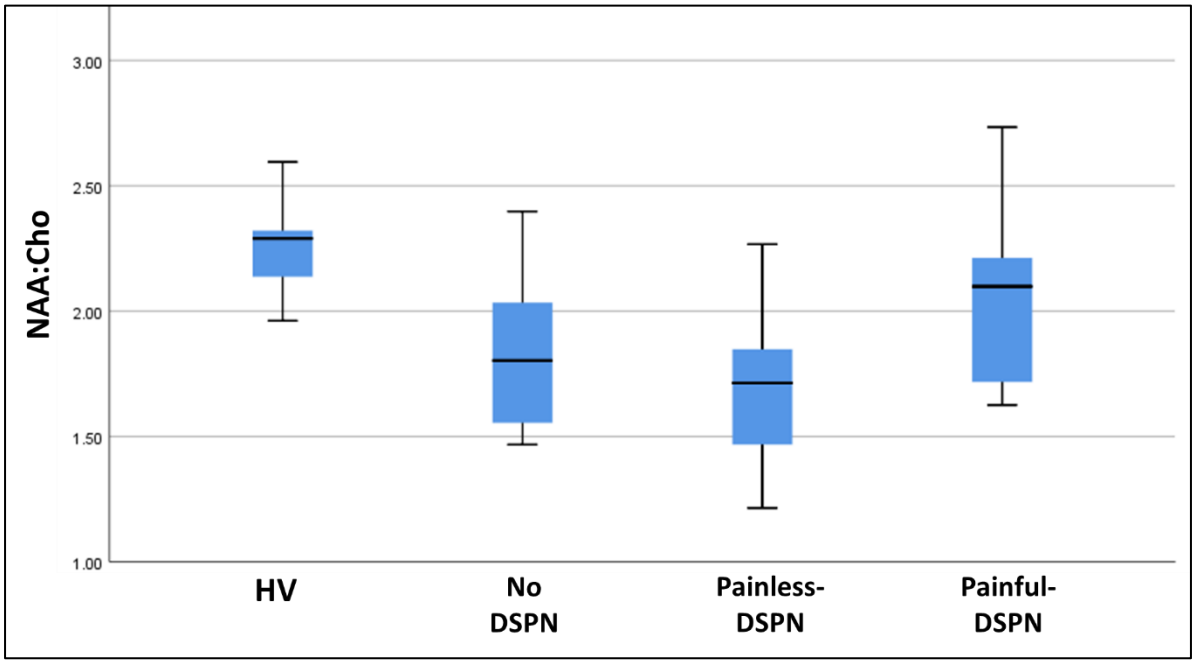

Figure 4.9. Dominant hemisphere thalamic NAA:Cho box and whisker plot (p=0.013, Kruskal Wallis). HV vs. painless-DSPN (p=0.004, Mann Whitney-U); HV vs. no-DSPN (p=0.036); Painless- vs. painful-DSPN (p=0.013). Cho, choline; NAA, N-acetylaspartate.

When HbA1c, alcohol intake and waist/hip ratio were included there remained a significant group effect in the DH thalamic NAA:Cho (ANCOVA, p=0.012). However, when BMI was added to the model the group effect lost significance (p=0.089).

In order to determine whether the alterations in neurometabolite levels were symmetrical, a paired analysis was performed and there was no significant difference between DH and NDH NAA:Cho at the level of the somatosensory cortex (p=0.187) or thalamus (Mann Whitney-U test, p=0.445).

Correlation analysis was performed to determine the cause of the reduction of NAA:Cho in the DH of the thalamus, Table 4.9. There were significant correlations between the DH thalamic NAA:Cho and the glucose level taken before the MR (Spearman's correlation, r -0.381, p=0.015) and the BMI (r -0.439, p=0.005), see Figure 4.11. There was no significant correlation seen with metabolic and neurophysiological measures except the peroneal motor nerve conduction velocity (r 0.354, p=0.043), see Figure 4.10. No other correlations were observed between other thalamic 1H-MRS metabolite ratios and metabolic or neurophysiological measures, including DFNS QST and NPSI measures. The mean thalamic NAA:Cho correlated with BMI only, (r -0.387, p=0.014, Spearman's correlation). The mean thalamic NAA:Cr and Cho:Cr did not correlated with any other variables.

DH Th NAA:Cho	r	Significance
Age	0.091	0.577
NIS-LL+7	-0.153	0.353
TCNS	-0.230	0.887
Total NPSI	0.093	0.570
NRS pain score during MRI	0.069	0.676
DN4	-0.017	0.915
HbA1c	-0.268	0.095
Glucose during MRI	-0.381	**0.015**
Peroneal motor nerve conduction velocity	0.354	**0.043**
Body mass index	-0.439	**0.005**

Table 4.9. Spearman's correlation between dominant hemisphere thalamic NAA:Cho metabolic and neurological variables. Cho, choline; DH, dominant hemisphere; DN4, doleur neuropathique 4; MRI, magnetic resonance imaging; NAA, N-acetylaspartate; NIS-LL+7, Neuropathy Impairment Score of the Lower Limb plus 7 tests; NRS, numeric rating scale; Th, thalamus; TCNS, Toronto clinical neuropathy score.

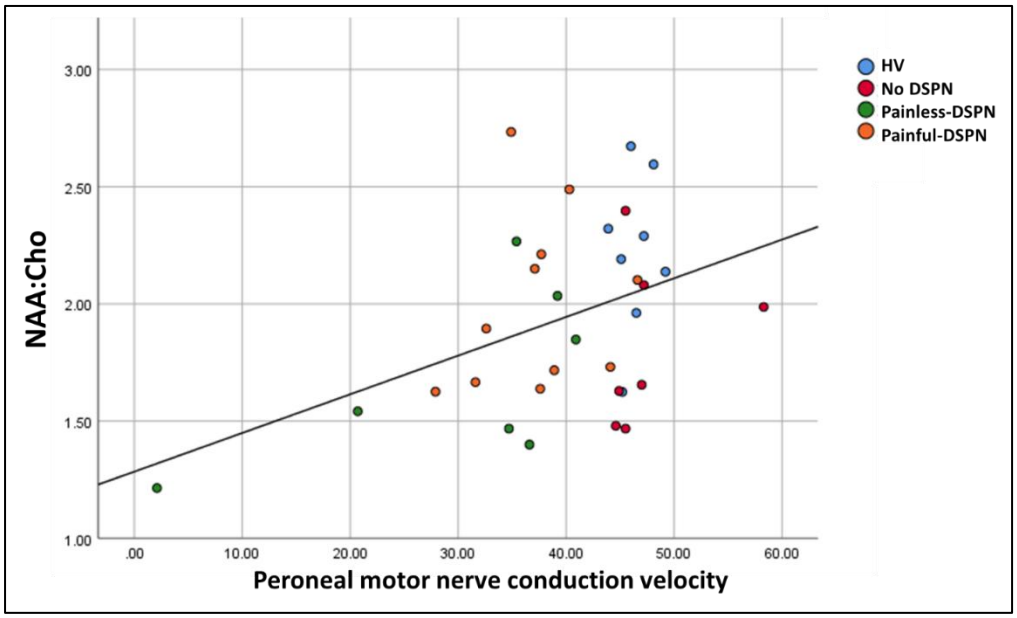

Figure 4.10. Spearman's correlation between dominant hemisphere thalamic NAA:Cho and peroneal motor nerve conduction velocity (r 0.354, p=0.043). Cho, choline; NAA, N-acetylaspartate.

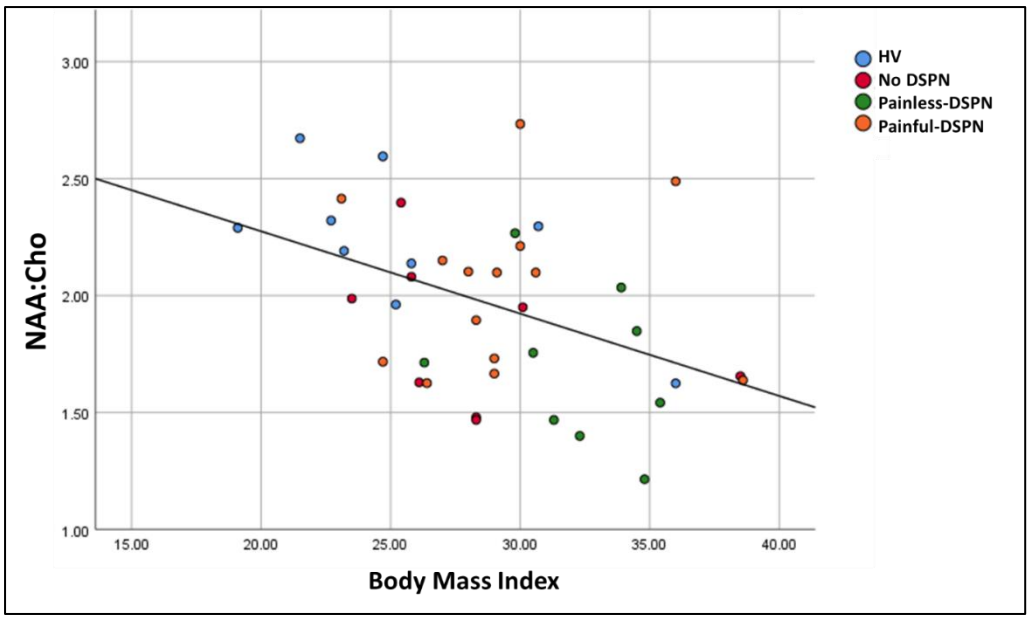

Figure 4.11. Spearman's correlation between dominant hemisphere thalamic NAA:Cho and body mass index (r -0.439, p=0.005). Cho, choline; NAA, N-acetylaspartate.

4.4 Discussion

In this study, 1H-MRS was performed to investigate proton containing cerebral neurometabolites in pain processing areas of the brain in well characterized patients with DSPN. The main finding of the study was a reduction in DH thalamic NAA:Cho in painless-DSPN compared with painful-DSPN and HV, with a lesser reduction in no-DSPN which reached significance versus HV. The DH thalamic NAA:Cho negatively correlated with fingerpick glucose before the MRI scan, BMI and peroneal motor nerve velocity. There were no group differences in the 1H-MRS 'raw' phosphorus metabolite levels and no significant differences in neurometabolite ratios at the S1 cortex.

Overall, these results suggest a reduction in NAA:Cho within the thalamus in painless-DSPN, with a lesser reduction in no-DSPN, and NAA:Cho preservation in painful-DSPN. The

NAA:Cho alterations reached statistical significance only in the thalamus in the DH; however, the pattern of NAA:Cho results, and the fact that there was no difference in NAA:Cho in pairwise analysis, suggest this is likely to be a symmetrical phenomenon. The NAA:Cho may not have reached statistical significance on the non-dominant side due to inadequate statistical power and/or methodological reasons, which will be discussed in the limitations. However, there are known to be subtle differences in right and left thalamic function, which have been noted in thalamic stroke syndromes (Schmahmann, 2003, Chen et al., 2017). For example, thalamic pain syndrome more commonly occurs following lesions of the right (NDH) thalamus. The volumetric data appeared similar in the left and right thalamus Chapter 3, which suggest the alterations to the brain in DSPN are symmetrical; however, further research is necessary to confirm this hypothesis.

NAA has one of the highest concentrations of all free amino acids within the brain (Rae, 2014). Its function is incompletely understood, but it is well recognised as a neuronal marker for 1H-MRS. There is some controversy as to whether NAA is a better marker of neuronal density or neuronal function. However, the majority of pathological conditions and diseases demonstrate a reduced NAA (Cecil, 2013). Whereas the total Cho signal arises from nine proteins in the *N*-methyl moiety of choline-containing compounds (Rae, 2014). The Cho peak is regarded as a product of myelin breakdown and increases in the Cho signal may occur due to elevations of precursors of myelin synthesis as well as products upon myelin degradation and/or destruction (Cecil, 2013). Therefore, the findings of this study suggest that there is greater neuronal dysfunction and/or membrane turnover in participants with T2DM and no-DSPN and painless-DSPN.

Previous research within the group has also demonstrated reduced NAA within the thalamus in participants with DSPN and T1DM. Selvarajah et al. conducted a study with a small number of participants performing 1H-MRS using an $8ml^3$ voxel placed within the VPL nucleus of the thalamus (Selvarajah et al., 2008) and found a lower mean NAA:Cr and NAA:Cho ratio in participants with DSPN compared with no-DSPN and HV. Similarly, Gandhi et al. demonstrated a significantly lower NAA:Cr ratio, but not NAA:Cho, at the VPL nucleus in the thalamus in patients with painless-DSPN compared with HV, no-DSPN, painful-DSPN and subclinical-DSPN in a large 1H-MRS study (20 HV and 110 with T1DM) (Gandhi et al., 2006). Although these previous research studies showed reduced NAA in the thalamus in participants with T1DM and painless-DSPN, the study in this thesis also found reduced NAA:Cho in no-DSPN. The previous studies indicated that patients with T1DM of both moderate (11.6 ± 7.7 years) and long duration of diabetes (27.0 ± 4.2 years) without DSPN (no-DSPN) had unaltered NAA levels at the thalamus (Gandhi et al., 2006, Selvarajah et al., 2008). Further, reduced cerebral NAA has been demonstrated in patients with diabetes without complications; although results are inconsistent amongst studies (Zhao et al., 2018). A potential methodological reason for the reduced NAA:Cho in no-DSPN in this study is that the voxel was larger, encompassing the whole of the thalamus, whereas in the two previous studies (Gandhi et al., 2006, Selvarajah et al., 2008) the voxel was smaller and just included the ventral posterolateral nucleus (VPL) nucleus, the main thalamic nucleus involved with somatosensory function. Therefore, there may be a generalised thalamic reduction in NAA in diabetes, but the VPL nucleus may be relatively unaffected in no-DSPN.

The correlation analysis in this study indicates that metabolic measures were driving NAA:Cho alterations more than neurophysiological alterations. Indeed, previous studies have shown that BMI, HbA1c and acute changes in glucose lead to lower cerebral levels of

NAA (Wootton-Gorges et al., 2007, Gazdzinski et al., 2008, Sahin et al., 2008, Gazdzinski et al., 2010, Zhao et al., 2018); although the mechanisms of cerebral alterations of Cho are less clear. However, Selvarajah et al. (2008) previously found that there were consistent moderately strong correlations between NAA:Cr and NAA:Cho ratios and neurophysiological measures, suggesting the reduced thalamic NAA was related to DSPN in T1DM. The reasons for the differences in results between the study by Selvarajah et al. and this thesis are unclear. The inclusion of a painful-DSPN group, larger voxel size or imaging of T2DM participants may contribute to these discrepancies. There is increasing recognition of different mechanisms underlying DSPN in T1 and T2DM (Callaghan et al., 2012). This may also be reflected in different underlying cerebral alterations in patients with DSPN. The components of the metabolic syndrome which are more prevalent in T2DM, i.e. obesity, hypertension and hyperlipidaemia, may result in greater cerebral cell membrane disruption compared with T1DM.

The finding of a higher NAA in patients with painful- compared with painless-DSPN is also consistent with the study by Gandhi et al. (2006). However, a smaller study by Sorensen et al. (2008) found that the thalamic NAA was reduced in participants with T1 and T2DM diabetes with and without painful-DSPN. However, there were a number of methodological issues with the study, such as case definition and MRS analysis techniques, which may act as confounding factors. The mechanism of a reduced NAA in the thalamus in painless- but not painful-DSPN is incompletely understood, it could reflect the neuronal 'dying-back' phenomenon in painless-DSPN which is well recognised in the peripheral nervous system in DSPN. Spinal cord atrophy has been shown in DSPN; therefore, neuronal dysfunction/loss may extend to the CNS (Selvarajah et al., 2006). Recent findings by Hansen et al. (Hansen et al., 2021) performing combined volumetric and spectroscopy analysis, found reduced

thalamic and NAA levels, suggesting thalamic neuronal loss in painless-DSPN. In contrast to the findings in painless-DSPN, in painful-DSPN there appears to be a preservation of thalamic neuronal function. It has previously been hypothesised that relative preservation of thalamic neuronal function is necessary for the transmission of painful signals to higher centres and the perception of chronic pain in DSPN (Gandhi et al., 2006). Although the cause is unclear, there is evidence suggesting that there is thalamic neuronal hyperexcitability in experimental DSPN (Fischer et al., 2009) and thalamic hypervascularity in clinical painful-DSPN (Selvarajah et al., 2011), potentially as a response to increased oxygen demand due to increased neuronal activity. Persistent neuronal activity due to sensory impulses from the peripheral nervous system in painful-DSPN may preserve thalamic sensory neuronal function. Further research is required to determine the causal and temporal nature of thalamic metabolite alterations in DSPN and its potential role in the pathogenesis of painful-DSPN. This concept will be further explored in the 31P-MRS analysis in Chapter 4.

The S1 cortical NAA levels seems to be less impacted than the thalamus as demonstrated by Gandhi et al. (2006) and this thesis. Therefore, the volume loss/reduced cortical thickness which has been described in the S1 cortex in DSPN in a previous research study (Selvarajah et al., 2014b) and Chapter 3 (Selvarajah et al., 2014b) may not be associated with underlying neuronal dysfunction; however, further research is necessary to determine the mechanisms underlying structural brain alterations in DSPN.

The strengths of this study include the use of chemical shift imaging, to quantify 1H-MRS spectra within multiple voxels. Moreover, the clinical characterization of the study participants patients was comprehensive, with neurophysiological data which was statistically similar between painful- and painless-DSPN. Despite the strengths of the study

there are some limitations. Firstly, although there are benefits to using chemical shift imaging; the technique has a lower signal to noise ratio than single voxel spectroscopy. The signal to noise ratio is determined by a number of factors including the MR field strength, voxel size and scan time. Although a longer scan can improve signal intensity the spectra are more susceptible to movement artefact. As a result of movement artefact and inadequate water/fat suppression, some patients (13 for S1 analysis and 15 for thalamic analysis) had to be excluded due to poor quality of the spectra; although removal of these patients did not lead to important clinical/neurophysiological differences in group analysis. Moreover, due to the aforementioned constraints, the voxel size in this study is relatively large ($25cm^3$). Therefore, there may be a partial volume effect, which is likely to be particularly pertinent to the thalamic voxels. Only part of the thalamus is involved in sensory perception, most notably the VPL nucleus. When the VPL nucleus was selectively imaged in aforementioned studies there was a clear reduction in NAA in painless-DSPN (Gandhi et al., 2006, Selvarajah et al., 2008). The lower signal to noise ratio also may have impacted other results, and may explain why other neurometabolite ratios were not significantly altered in this study, particularly the NAA:Cr in the thalamus. Finally, there was evidence of a greater BMI in participants with DSPN and a lower level of cholesterol and alcohol intake; the latter two are likely a consequence of the patients having treatment for cardiovascular risk factors and targeted advice to reduce alcohol intake.

4.5 Conclusions and future work

This study furthers the concept of thalamic neurochemical alterations in diabetes and DSPN. The results are largely consistent with previous findings within the study group, that NAA is reduced in the thalamus in patients with painless-DSPN but not painful-DSPN. However, in this study there was also a reduction in NAA in the thalamus in participants with no-DSPN compared with HV, suggesting a diabetes effect on the thalamus. This is contrary to previous research in participants with T1DM and this may reflect differing thalamic neuronal pathology in T2DM. Moreover, the S1 cortical 1H-MRS metabolites are unaltered in DSPN. The mechanism of these findings is unknown but suggests disruption of thalamic, but not S1 cortical, neuronal function and/or membrane turnover in patients with T2DM without painful-DSPN. These results also suggest a preservation of thalamic neuronal function/number in painful- compared with painless-DSPN, which may be related to increased thalamic neuronal activity in painful-DSPN.

The underlying mechanisms of the dichotomous 1H-MRS metabolite ratios in the thalamus in painful- and painless-DSPN are unknown. There is indirect evidence for heightened neuronal activity as demonstrated in experimental and clinical studies. 31P-MRS allows for the non-invasive measurement of cerebral bioenergetics which can inform on cellular mitochondrial function and energy usage. The following chapter will use this technique to assess whether there are altered thalamic and S1 alterations in cellular energetics to determine whether these might underly 1H-MRS abnormalities in DSPN.

5. Cerebral Magnetic Resonance Spectroscopy alterations in DSPN: Cerebral bioenergetics in painful- and painless-DSPN

5.1 Introduction

5.1.1 Background

Preceding chapters have indicated there is unaltered volume in the thalamus in participants with painful- and painless-DSPN; whereas there is neuronal dysfunction, as measured using NAA:Cho, in no-DSPN and painless- but not painful-DSPN. Moreover, there is a reduction in S1 cortical thickness in painless-DSPN but lesser reductions in those with painful-DSPN, with no alterations in NAA:Cho. This study used 31P-MRS as the investigative technique to determine whether abnormalities in cerebral bioenergetics or mitochondrial function might underly these alterations at the thalamus or S1 cortex.

31P-MRS is a non-invasive technique which allows the indirect assessment of phosphorus containing metabolites which represent markers of various biological processes including mitochondrial dysfunction and cellular energetics. Mitochondrial dysfunction has been highlighted as an important mechanism in the pathophysiology of DSPN in the peripheral nerve; although; it is unknown whether it impacts nerves within the brain too (Fernyhough, 2015). Moreover, several studies, including within Chapter 3 and 4, suggest heightened neuronal activity within the brain in painful-DSPN. Previous studies have found direct evidence of neuronal hyperexcitability in the thalamus in experimental painful-DSPN (Fischer et al., 2009) and indirect evidence in clinical DSPN, by measuring microvascular

perfusion (Selvarajah et al., 2011). However, the extent of neuroplasticity and altered function of the S1 cortex in painful-DSPN is incompletely understood. In response to noxious heat pain, patients with painful-DSPN have been reported to show activation of the S1 cortex; although these responses were similar to those seen in healthy controls in a functional magnetic resonance imaging (fMRI) study (Tseng et al., 2013). Moreover, in a rs-fMRI study there was reduced functional connectivity in patients with painful-DSPN between the S1 cortex and a number of other brain regions, including the thalamus, S1, M1 and anterior cingulate cortices (Cauda et al., 2009a). Cerebral energetics and mitochondrial dysfunction have not been explored in clinical DSPN and 31P-MRS was used in this study to determine whether this might provide an explanation for the thalamic and S1 cortical abnormalities described in previous Chapters.

5.1.2 Rationale for study

The mechanisms underlying cerebral manifestations of DSPN in the thalamus and S1 are incompletely understood. 31P-MRS is an investigative technique which provides information relating to mitochondrial function and cellular energetics. The technique has been applied to experimental DSPN (Biessels et al., 2001); but not clinical DSPN. Therefore, this study applied 31P-MRS to the brain to investigate whether phosphate metabolites as markers of mitochondrial dysfunction and cellular energetics are altered in painless- and painful-DSPN.

5.1.3 Aims and hypothesis

The aim of the study was to assess 31-phosphorus metabolite ratios, as measures of cerebral bioenergetics and mitochondrial dysfunction, in patients with T2DM and DSPN in the S1 cortex and thalamus. The hypothesis was there will be altered high energy phosphorus metabolite ratios which will differentiate painful- and painless-DSPN, with evidence of mitochondrial dysfunction in painless-DSPN and increased cellular energetics in painful-DSPN.

5.2 Methods

5.2.1 Study Design and Participants

Fifty-five participants were recruited to the study (12 HV, 11 No-DSPN, 12 with painless-DSPN and 20 with painful-DSPN). All participants with diabetes had T2DM, according to the World Health Organization criteria (https://www.who.int/diabetes/publications/Definition%20and%20diagnosis%20of%20diabetes_new.pdf) and were diagnosed at least 6-months prior to their inclusion in the study. Inclusion and exclusion criteria were performed as described in the Chapter 4 (4.2.1).

The study design was a case control cross-sectional study.

5.2.2 Clinical and neurological assessment

History, mood/memory assessment, clinical examination, structured neurological examination, nerve conduction studies and calculation of NIS-LL+7 were performed as described in the general methods.

5.2.3 Magnetic resonance spectroscopy protocol

5.2.3.1.1 Rationale for using 31P-Magnetic resonance spectroscopy

The same principles for using 1H-MRS apply to the use of 31P-MRS, described in Chapter 4. However, instead of detecting proton containing metabolites, 31P-MRS measures 31-phosphorus containing metabolites. allowing the non-invasive detection of markers of tissue bioenergetics (ATP; Phosphocreatine, PCr; and inorganic phosphate, Pi), cellular membrane composition (Phosphomonoesters, PME; and phosphodiesters, PDE) and intracellular pH.

The three markers of 31P-MRS relating to cellular metabolism (ATP, PCr and Pi) are intricately linked (Figure 5.1). During non-ischaemic conditions in normally functioning mitochondrion ATP is kept at a stable level in the process of mitochondrial phosphorylation whereby ADP is combined with Pi. During increased energy expenditure or reduced ATP generation PCr donates its high energy phosphate metabolite, Pi, to ADP in order to maintain cellular levels of ATP.

5.2.3.1.2 31P-MRS metabolites

Adenosine tri-phosphate (ATP): ATP is often referred to as the energy currency for cellular life, acting as the primary source of energy in living cells (Figure 5.1). 31P-MRS identifies three ATP isotopomers in the form of three peaks: a doublet γ-ATP, a doublet α-ATP and a triplet for β-ATP. It is often used as an internal reference standard, as cellular metabolic processes act to maintain a constant level of ATP. However, the concentration may be altered in different conditions, e.g. ischaemia, although this is often a late finding and normally occurs after alteration of other phosphorus containing metabolites (Liu et al., 2017).

Phosphocreatine: PCr is the most prominent peak in 31P-MRS and is therefore used as the reference for the location, rather than the intensity, of other peaks at 0ppm. The high energy phosphate bind serves as a buffer to maintain constant levels of ATP during periods of increased energy expenditure or reduced energy generation (Valkovič et al., 2017).

Inorganic phosphate (Pi): Pi serves as a substrate or product in chemical reactions of energy metabolism (Valkovič et al., 2017). The peak lies at 5.0ppm.

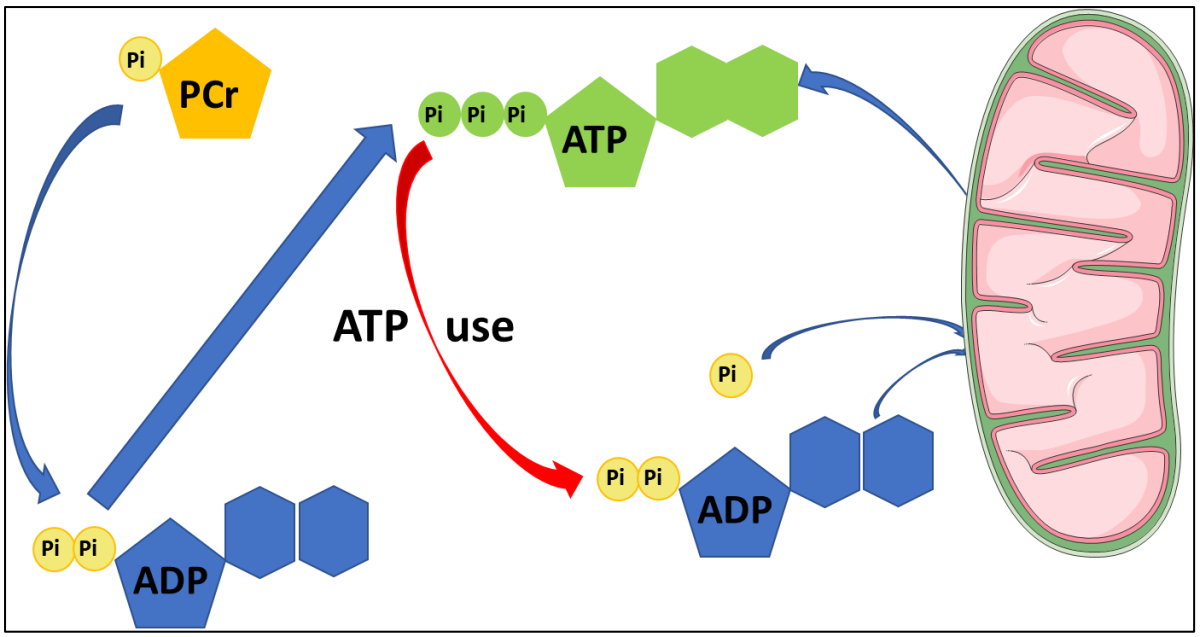

Figure 5.1. Cerebral cellular ATP metabolism. During non-ischaemic conditions, ATP is generated from oxidative phosphorylation where ADP is combined with Pi by ATP synthase in the inner mitochondrial membrane. In healthy tissues the rate of ATP production is linked to ATP hydrolysis (red line) such that ATP content remains constant. Creatinine kinase catalyses the reaction, ADP + PCr + H^+ ⇔ ATP + Cr. During increased periods of demand, or reduced ATP generation (e.g. ischaemia or hypoxia) CK allows the rapid transfer of Pi in PCr to ADP (blue line).

5.2.3.2 Protocol for Magnetic resonance spectroscopy

The protocol was the performed as described in Chapter 4 (4.2.3.2) except for the echo time, repetition time and 31P-MRS technique. The TE for 31P-MRS was 0.26ms and TR 4000ms. The 31P-MRS technique performed in the protocol was Image-Selected *in Vivo* Spectroscopy (ISIS) (Ordidge et al., 1988). ISIS is one of the most used techniques for short T2 metabolites in 31P (Figure 5.2). The spectra within a volume of interest are calculated using the free induction delay signal from several separate radio-frequency pulses cycles. The data from these cycles are added and subtracted to calculate the final spectra.

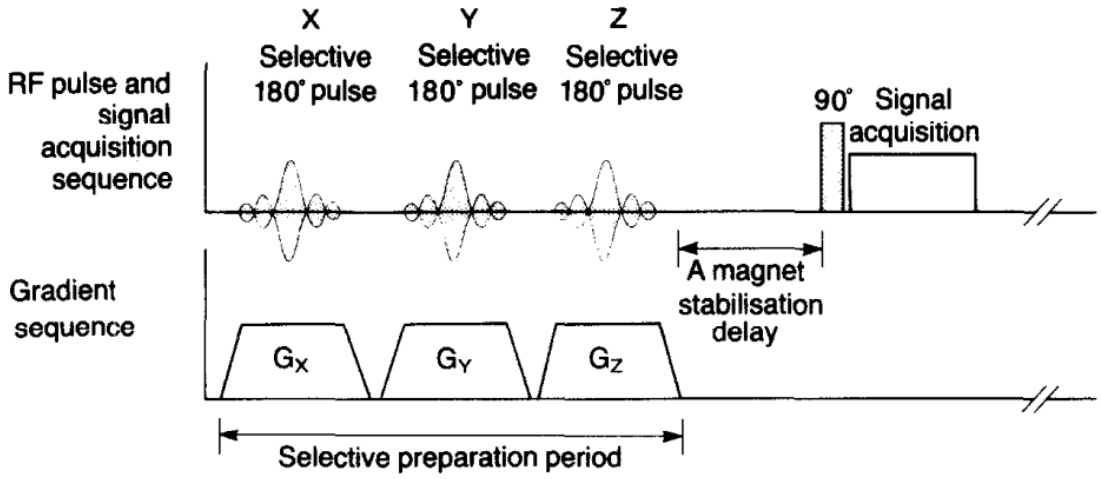

Figure 5.2. Radiofrequency pulses and magnetic field gradient sequences for ISIS. Selective inversion pulses may be applied in three orthogonal slices followed by a non-selective 90^o pulse, which excites the entire volume under the coil. The free induction delay signal is subsequently acquired. This sequence is repeated multiple times with various permutations of the inversion pulses (i.e. x=on/off, y=on/off and z=on/off). The spectrum is constructed after calculation of several ISIS cycles. G, field gradient; RF, radiofrequency. Image reproduced from Ordidge et al. (Ordidge et al., 1988).

5.2.3.3 Magnetic resonance spectroscopy data processing

Java-based version of the MR user interface package was utilised as described in Chapter 4 (4.2.3.3). However, as there are no 31P metabolites within water and lipids, the HLSVD algorithm was not required. For AMARES the starting values for frequencies and linewidths are displayed in Table 5.1. Additionally, prior knowledge was imposed upon the amplitude of the ATP peaks, the ratio of the amplitude of the 3 β-ATP peaks were fixed to 0.5:1:0.5; the two α-ATP and γ-ATP peaks amplitude ratio was also fixed in a 1:1 ratio. Soft constraints were also applied to the line width for each metabolite where the range was pre-determined for each peak.

Peak	Frequency (ppm)	Line Width (Hz)
β-ATP-1	-16.86	11.7
β-ATP-2	-16.58	29.4
β-ATP-3	-16.24	29.4
α-ATP-1	-7.75	23.5
α-ATP-2	-7.4	23.5
γ-ATP-1	-3.19	35.3
γ-ATP-2	-2.62	29.4
PCr	0.05	11.7
GPC	2.92	11.7
GPE	3.42	23.5
Pi	4.85	11.7
PE	6.52	35.3
PC	6.78	29.4

Table 5.1. Starting values for 31P-MRS on jMRUI. ATP, adenosine tri-phosphate; GPC, glycerophosphocholine; GPE, glycerophosphoethanolamine; Pi, inorganic phosphate; PC, phosphocholine; PE, phosphoethanolamine; ppm, parts per million.

The pH was calculated in jMRUI, as the chemical shifts of Pi and PCr are pH dependent. The pH was calculated with the following formula where δ is δ_{Pi} (Liu et al., 2017).

$$pH = pK + log(\frac{\delta - \delta_{H_2PO_4^-}}{\delta_{HPO_4^{2-}} - \delta})$$

A graphical illustration of 31P-MRS spectra obtained within jMRUI are reproduced in Figure 5.3.

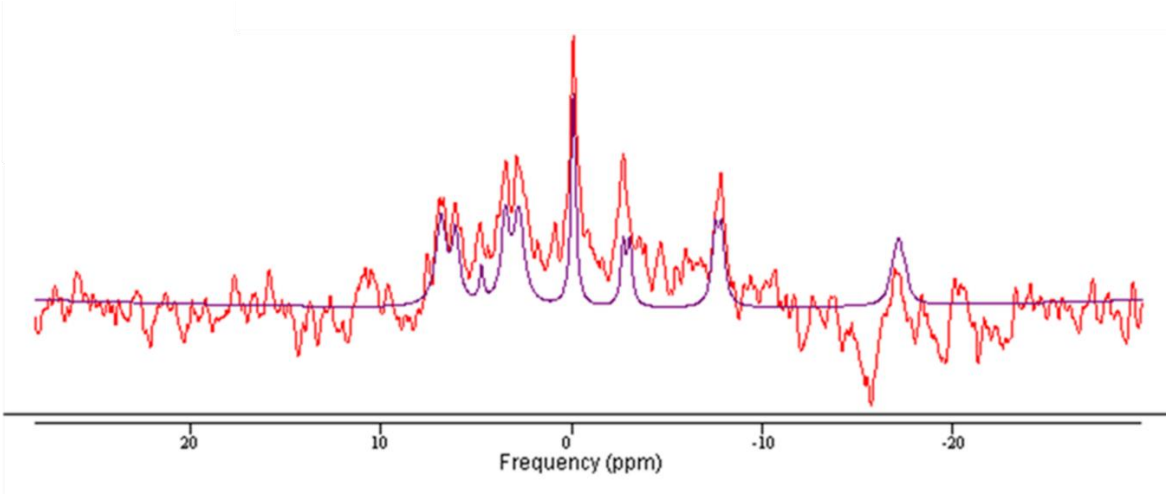

Figure 5.3. 31P-MRS as presented in jMRUI. The red line is the original spectra after pre-processing and the purple line the spectral line fitting for metabolite quantitation using AMARES.

The individual spectra were assessed for visual quality as per Chapter 4 (4.2.3.3). Also, the Cramér–Rao bands were calculated, Table 5.2.

	Cramér–Rao bound Non-dominant hemisphere	Cramér–Rao bound Dominant hemisphere
Th β-ATP	38.4 ± 16.2	36.8 ± 25.1
Th α-ATP	18.5 ± 3.6	19.1 ± 4.2
Th γ-ATP	22.4 ± 5.0	21.6 ± 3.9
Th PCr	11.2 ± 2.4	10.9 ± 2.1
Th Pi	45.4 ± 32.5	41.2 ± 15.2
Th PME	70.0 ± 43.9	72.9 ± 49.3
Th PDE	41.4 ± 18.0	44.8 ± 26.0
S1 β-ATP	49.1 ± 19.1	44.2 ± 15.6
S1 α-ATP	22.9 ± 5.9	22.9 ± 5.8
S1 γ-ATP	25.6 ± 6.8	24.2 ± 6.3
S1 PCr	13.4 ± 3.3	13.2 ± 3.1
S1 Pi	46.5 ± 12.1	44.9 ± 11.0
S1 PME	80.2 ± 69.4	64.6 ± 35.2
S1 PDE	56.4 ± 39.7	51.3 ± 22.8

Table 5.2. Cramér–Rao bound for 31P-MRS analysis of all study participants. Pi, inorganic phosphate; PDE, phosphodiesters; PCr, phosphocreatine; PME, phosphomonoesters; S1, primary somatosensory cortex; Th, Thalamus.

The β-ATP peak was poorly fit on the spectra and at times indistinguishable from the residue, on both visual assessment of spectra and the Cramér–Rao lower bound which ranged between approximately 20-200%. It is recognised that the β-ATP concentration can appear to be low due to a reduced signal to noise ratio (Meyerspeer et al., 2020). Expert consensus recommendations for 31P-MRS in skeletal muscle (none exist for 31P-MRS cerebral analysis) suggest using the γ-ATP (Meyerspeer et al., 2020), although others exclude the β-ATP peak and use the combination of the γ-ATP and α-ATP peaks (Novak et al., 2014). For this analysis β-ATP was excluded, and the γ-ATP and α-ATP peaks analysed.

The 31P-MRS metabolite ratios which were assessed in this study were: PCr:ATP (Mean γ-ATP and α-ATP), Pi:ATP, Pi:PCr, PME (PE+PC):PDE (GPC+GPE). Table 5.3 shows what the different metabolite ratios represent.

Metabolite Ratio	What the measure represents
PCr:ATP	This is a marker of cellular energetics. A reduction in the ratio signifies depletion of PCr, which occurs during increased energy usage or reduced ATP supply.
Pi:ATP	This is a measure of oxidative phosphorylation. A rise in this ratio signifies mitochondrial dysfunction
Pi:PCr	This is a marker of cellular energy reserves or energy metabolism. A rise is associated with bioenergetic defects or defective oxidative capacity.
PME:PDE	As PME includes contributions from phospholipid membrane precursors, and PDE from membrane breakdown products, the PME:PDE ratio is used as a measure of cellular membrane turnover. A reduction in the ratio signifies increased membrane turnover.

Table 5.3. 31P-MRS metabolite ratios measured in this study and what they represent (Kemp, 2000, Rango et al., 2006, Dinh et al., 2009, Ha et al., 2013, Shi et al., 2015, Walchhofer et al., 2021). Pi, inorganic phosphate; PDE, phosphodiesters; PCr, phosphocreatine; PME, phosphomonoesters.

5.2.4 Statistical Analysis

The DH refers to the left hemisphere of the brain as all participants were right-handed and the NDH the right hemisphere of the brain. The mean value of ratios was calculated from the mean of each of the DH and NDH metabolites. The data were analysed otherwise as described in the general methods.

Participants undergoing S1 31P-MRS analysis were subgrouped into those with low pain (NRS 0-2) and moderate/severe pain (NRS 3-10) on a 0-10 Likert scale. The Mann-Whitney U

test was used to compare pain scores and 31P-MRS variables between these groups as the data was non-parametric.

5.3 Results

5.3.1 Participant recruitment details

Participant recruitment details are displayed in Chapter 4 (4.3.1). Fifty-five participants underwent 31P-MRS analysis of the S1 cortex and 49 the thalamus (Figure 4.6).

5.3.2 Participant demographic, clinical and neurophysiological data

Table 4.3 summarises the demographic, clinical and biochemistry data for all study participants; Table 4.4 the neurological assessments; Appendix 10.7 the breakdown of NPSI scores for painful-DSPN; and Appendix 10.8 the DFNS-QST results.

Six patients had either inadequate voxel placement or spectra and were removed from the analysis for the thalamus (One HV: Age 60, male, BMI 40.0kg/m^2 and HbA1c 43.0mmol/mol; two No-DSPN, Patient 1: Age 59, male, BMI 27.3kg/m^2 and HbA1c 67.0mmol/mol. Patient 2: Age 67, male, BMI 28.3kg/m^2 and HbA1c 49.0 mmol/mol; Painless-DSPN: Age 61, male, BMI 31.3 kg/m^2 and HbA1c 94.0mmol/mol; Painful-DSPN, Patient 1: Age 61, female, BMI 31.6kg/m^2 and HbA1c 73.0mmol/mol. Patient 2: Age 53, male, BMI 39.2kg/m^2 and HbA1c 37.0mmol/mol). Therefore, patients who underwent thalamic 31P-MRS had re-analysis of

the demographic and clinical data, and biochemistry test results. In the group that underwent thalamic 31P-MRS, in addition to alcohol intake and HbA1c, there was significant group effect in the presence of nephropathy and total cholesterol level. Otherwise, there were no other differences in the statistical significance of group effects as described above (Table 5.4 and 5.5).

	HV (n=11)	No-DSPN (n=9)	Painless-DSPN (n=11)	Painful-DSPN (n=18)	P value
Age (years)	69 (IQR 13.0)	60.0 (7.0)	62.0 (9.0)	61.5 (8.0)	0.442 KW
Sex (% female)	36%	56%	64%	39%	0.482 Chi^2
Duration DM (years)		9.7 ± 5.8	16.5 ± 5.6	12.0 ± 7.4	0.065 A
Retinopathy presence (% present)		44.4%	54.5%	61.1%	0.713 Chi^2
Retinopathy score (0= No DR, 1= Bck/Pre-P, 2=Pro/Laser)		0 = 5 1 = 4 2 = 0	0 = 5 1 = 5 2 = 1	0 = 7 1 = 5 2 = 6	0.241 Chi^2
Nephropathy presence (% present)		0%	45.5%	47.1%	**0.040 Chi^2**
ACR (mg/mmol)		0.5 (0.1)	1.5 (1.8)	1.8 (1.7)	0.070 KW
Number of hypoglycaemic episodes in last 12 months		0.0 (0.0)	0.0 (0.0)	0.0 (3.5)	0.129 KW
Smoked ever (% Yes)	45.5%	77.8%	54.5%	66.7%	0.454 Chi^2
Pack Years smoking [Packs (1 pack = 20 cigarettes) x Number of years]	0 (20.0 IQR)	12.0 (22.5)	0.75 (31.3)	2.2 (36.3)	0.661 KW
Alcohol intake (units/week)	4.0 (11.0 IQR)	10.0 (12.0)	2.0 (10.0)	0.0 (0.13)	**0.005 KW**
Waist/hip ratio	0.88 ± 0.1	0.92 ± 0.0	0.97 ± 0.1	0.95 ± 0.1	0.055 A
Body mass index (kg/m^2)	26.8 ± 5.5	28.9 ± 4.5	32.3 ± 3.6	30.8 ± 5.1	0.056 A
Systolic blood pressure (mmHg)	134.2 ± 21.5	130.4 ± 10.7	142.6 ± 17.7	141.3 ± 15.9	0.292 A

Creatinine (µmol/l)	70.4 ± 7.4	69.1 ± 9.6	77.0 ± 12.7	71.8 ± 16.7	0.532 A
Total Cholesterol (mmol/l)	4.93 ± 1.0	4.98 ± 1.0	3.81 ± 1.0	4.33 ± 1.0	**0.028 A**
HbA1c (mmol/mol)	37.0 (IQR 5.0)	61.0 (31.5)	56.0 (20.0)	64.0 (32.8)	**<0.001 KW**
MMSE	30.0 (IQR 0.0)	30.0 (1.5)	30.0 (2.0)	29.0 (2.25)	0.206 KW
Depression (% Yes)	0%	0%	0%	17%	0.138 Chi^2
Anxiety (% Yes)	0%	0%	9%	16.7%	0.317 Chi^2

Table 5.4. Clinical details of participants undergoing 31P-MRS of the thalamus. Data are presented as mean ± standard deviation for parametric and median (IQR) for non-parametric continuous data or percentage for categorical data. The statistical test used was ANOVA (A) for continuous normally distributed data, Kruskal-Wallis (KW) for non-parametric continuous data or Chi^2 for categorical data. Retinopathy parameters: Bck, background retinopathy; DR, diabetic retinopathy; Laser, panretinal photocoagulation; Pre-P, pre-proliferative retinopathy; Pro, proliferative retinopathy. ACR, albumin creatinine ratio; DM, Diabetes Mellitus; HV, healthy volunteer; MMSE, mini-mental state examination; MR, magnetic resonance scan.

	HV (n=11)	No-DSPN (n=9)	Painless-DSPN (n=11)	Painful-DSPN (n=18)	ANOVA / KW / Chi^2
NPSI (Total score)	0.0 (IQR 0.0)	0.0 (0.0)	0.0 (1.0)	19.1 (14.8)	**0.001 KW**
DN4	0.0 (IQR 0.0)	0.0 (0.0)	0.0 (2.0)	6.0 (3.0)	**0.001 KW**
TCNS	0.0 (IQR 0.0)	0.0 (2.0)	9.0 (7.0)	14.5 (5.8)	**0.001 KW**
NIS-LL	0.0 (IQR 0.0)	0.0 (0.0)	14.0 (11.0)	17.5 (11.3)	**0.001 KW**
NIS-LL+7	0.0 (IQR 1.0)	0.0 (0.0)	25.0 (15.0)	24.5 (14.8)	**0.001 KW**
Peroneal CMAP (mV)	6.0 ± 2.4	6.0 ± 2.1	1.7 ± 1.8	2.5 ± 1.9	**0.001 A**
Peroneal MNCV (m/s)	46.7 (IQR 3.0)	45.6 (2.5)	39.2 (12.8)	37.7 (5.9)	**0.001 KW**
Peroneal MNDL (msec)	4.9 (IQR 0.6)	4.2 (0.5)	7.5 (4.5)	5.8 (2.2)	**0.002 KW**
Tibial MNDL (msec)	4.7 (IQR 0.8)	4.4 (0.8)	5.4 (2.3)	6.2 (3.5)	**0.001 KW**
Sural SNAP (mV)	13.6 (IQR 7.0)	12.6 (5.9)	1.4 (3.2)	0.7 (7.0)	**0.001 KW**
CAN composite score	0.0 (IQR 0.0)	0.0 (0.8)	0.0 (0.0)	0.0 (3.1)	0.071 KW
ESC (µS)	79.0 (IQR 13.0)	78.0 (16.0)	61.0 (26.0)	53.0 (32.0)	**0.001 KW**

Table 5.5. Neurological assessments of study participants undergoing 31P-MRS of the thalamus. Data are presented as mean ± standard deviation for parametric and median (IQR) for non-parametric continuous data. The statistical test used was ANOVA (A) for continuous normally distributed data and Kruskal-Wallis (KW) for non-parametric continuous data. CAN, cardiac autonomic neuropathy; CMAP, compound muscle action potential; DN4, doleur neuropathique 4; ESC, electrochemical skin conductance; MNDL, motor nerve distal latency; MNCV, motor nerve conduction velocity; NIS-LL, neuropathic impairment score of the lower limb; NPSI, neuropathic pain symptom inventory; SNAP, sensory nerve action potential; TCNS, Toronto clinical neuropathy score.

5.3.3 31P-MRS results

5.3.3.1 Raw metabolite data

The 'raw' metabolite values for 31P-MRS are presented in Table 5.6 and 5.7. There was no significant difference in metabolite ratios at the S1 cortex. At the DH thalamic Pi there was a significant group effect (Kruskal-Wallis test, p=0.002). The Pi was numerically the highest in painless-DSPN, reaching significance compared with HV (Mann Whitney U test, p=0.034) and painful-DSPN (p<0.001). Additionally, in no-DSPN the DH thalamic Pi levels were significantly higher compared with painful-DSPN (p=0.004).

	HV (n=12)	No-DSPN (n=11)	Painless-DSPN (n=12)	Painful-DSPN (n=20)	P value
NDH α-ATP	0.076 ± 0.02	0.098 ± 0.02	0.086 ± 0.02	0.093 ± 0.02	0.057 A
NDH γ-ATP	0.076 ± 0.01	0.081 ± 0.02	0.078 ± 0.02	0.087 ± 0.02	0.305 A
NDH PCr	0.195 (IQR 0.06)	0.188 (0.06)	0.202 (0.04)	0.185 (0.05)	0.467 KW
NDH Pi	0.072 ± 0.03	0.069 ± 0.04	0.087 ± 0.04	0.083 ± 0.03	0.567 A
DH α-ATP	0.080 ± 0.01	0.092 ± 0.02	0.082 ± 0.01	0.089 ± 0.02	0.202 A
DH γ-ATP	0.081 ± 0.01	0.085 ± 0.01	0.083 ± 0.02	0.085 ± 0.02	0.895 A
DH PCr	0.195 (IQR 0.05)	0.183 (0.04)	0.191 (0.03)	0.171 (0.05)	0.114 KW
DH Pi	0.079 ± 0.04	0.083 ± 0.03	0.087 ± 0.04	0.092 ± 0.03	0.761 A

Table 5.6. Raw 31P-MRS metabolite levels in the S1 cortex. Data are presented as mean ± standard deviation for parametric and median (IQR) for non-parametric continuous data. The statistical test used was ANOVA (A) for continuous normally distributed data and Kruskal-Wallis (KW) for non-parametric continuous data. DH, dominant hemisphere; NDH, non-dominant hemisphere; Pi, inorganic phosphate; PDE, phosphodiesters; PCr, phosphocreatine; PME, phosphomonoesters.

	HV (n=11)	No-DSPN (n=9)	Painless-DSPN (n=11)	Painful-DSPN (n=18)	P value
NDH α-ATP	0.095 (IQR 0.02)	0.086 (0.02)	0.095 (0.02)	0.1015 (0.04)	0.327 KW
NDH γ-ATP	0.080 ± 0.02	0.081 ± 0.01	0.082 ± 0.01	0.087 ± 0.01	0.374 A
NDH PCr	0.198 ± 0.02	0.200 ± 0.03	0.186 ± 0.02	0.191 ± 0.02	0.523 A
NDH Pi	0.072 ± 0.03	0.093 ± 0.05	0.104 ± 0.05	0.080 ± 0.04	0.304 A
DH α-ATP	0.089 ± 0.02	0.087 ± 0.01	0.093 ± 0.02	0.090 ± 0.02	0.848 A
DH γ-ATP	0.084 ± 0.01	0.078 ± 0.01	0.078 ± 0.01	0.081 ± 0.02	0.562 A
DH PCr	0.203 ± 0.03	0.177 ± 0.03	0.196 ± 0.03	0.179 ± 0.03	0.093 A
DH Pi	0.076 ± 0.05	0.107 ± 0.02	0.117 ± 0.02	0.076 ± 0.03	**0.002 KW**

Table 5.7. Raw 31P-MRS metabolite levels in the thalamus. Data are presented as mean ± standard deviation for parametric and median (IQR) for non-parametric continuous data. The statistical test used was ANOVA (A) for continuous normally distributed data and Kruskal-Wallis (KW) for non-parametric continuous data. DH, dominant hemisphere; NDH, non-dominant hemisphere; Pi, inorganic phosphate; PDE, phosphodiesters; PCr, phosphocreatine; PME, phosphomonoesters.

5.3.3.2 S1 cortex metabolite ratio analysis

Table 5.8 shows the 31P-MRS DH, NDH, and mean S1 cortical results for the different groups. There was a reduction in the mean PCr:ATP in the no-DSPN group compared to healthy volunteers (LSD, p=0.013) (Figure 5.4). There was a further reduction in mean PCr:ATP in patients with painful-DSPN compared to HV (p=0.001), but this did not reach statistical significance compared to no-DSPN (p=0.462). However, the mean PCr:ATP was significantly increased in patients with painless-DSPN compared with painful-DSPN (p=0.04). There were also significant differences in the PCr:ATP on the DH and NDH hemisphere. In the NDH hemisphere, PCr:ATP was lower in painful-DSPN compared with HV (p=0.003) and painless-DSPN (p=0.018). PCr:ATP was also lower in no-DSPN compared with HV (p=0.05). In the DH hemisphere, PCr:ATP was also lower in painful-DSPN (p=0.004) and no-DSPN (p=0.015) compared with HV. There were no significant group differences in Pi:ATP (Figure 5.5), Pi:PCr (Figure 5.6), PME:PDE and pH at the NDH, DH and mean S1. Adding HbA1c had no effect upon the statistical model in an ANCOVA for PCr:ATP, Pi:ATP nor Pi:PCr. The ANCOVA for the mean somatosensory cortical PCr:ATP remained significant, p=0.008.

	HV (n=12)	No-DSPN (n=11)	Painless-DSPN (n=12)	Painful-DSPN (n=20)	P value
NDH PCr:ATP	3.08 ± 1.50	2.21 ± 0.50	2.63 ± 0.60	2.15 ± 0.48	**0.019**
NDH Pi:ATP	1.03 ± 0.62	0.84 ± 0.54	1.15 ± 0.62	1.02 ± 0.57	0.643
NDH Pi:PCr	0.34 ± 0.14	0.38 ± 0.23	0.45 ± 0.28	0.44 ± 0.20	0.515
NDH PME:PDE	0.89 ± 0.42	1.04 ± 0.25	1.06 ± 0.38	1.35 ± 0.91	0.212
NDH pH	7.036 ± 0.04	7.084 ± 0.12	7.032 ± 0.05	7.043 ± 0.08	0.372
DH PCr:ATP	2.57 ± 0.83	2.12 ± 0.38	2.43 ± 0.51	1.95 ± 0.38	**0.011**
Dh Pi:ATP	1.03 ± 0.59	0.98 ± 0.49	1.06 ± 0.41	1.13 ± 0.50	0.869
Dh Pi:PCr	0.41 ± 0.20	0.48 ± 0.23	0.47 ± 0.24	0.56 ± 0.23	0.348
Dh PME:PDE	0.91 ± 0.48	1.09 ± 0.54	0.95 ± 0.55	1.05 ± 0.40	0.759
DH pH	7.035 ± 0.06	7.042 ± 0.05	7.036 ± 0.04	7.056 ± 0.11	0.875
Mean PCr:ATP	2.83 ± 1.04	2.16 ± 0.39	2.53 ± 0.52	2.05 ± 0.40	**0.006**
Mean Pi:ATP	1.03 ± 0.50	0.91 ± 0.45	1.11 ± 0.39	1.08 ± 0.48	0.740
Mean Pi:PCr	0.37 ± 0.15	0.42 ± 0.21	0.46 ± 0.22	0.50 ± 0.19	0.339
Mean PME:PDE	0.90 ± 0.41	1.07 ± 0.33	1.01 ± 0.41	1.20 ± 0.59	0.364
Mean pH	7.036 ± 0.04	7.063 ± 0.08	7.036 ± 0.04	7.047 ± 0.08	0.727

Table 5.8. 31P-MRS metabolite ratios in the S1 cortex. Data are presented as mean ± standard deviation. The statistical test used was ANOVA. DH, dominant hemisphere; NDH, non-dominant hemisphere; Pi, inorganic phosphate; PDE, phosphodiesters; PCr, phosphocreatine; PME, phosphomonoesters.

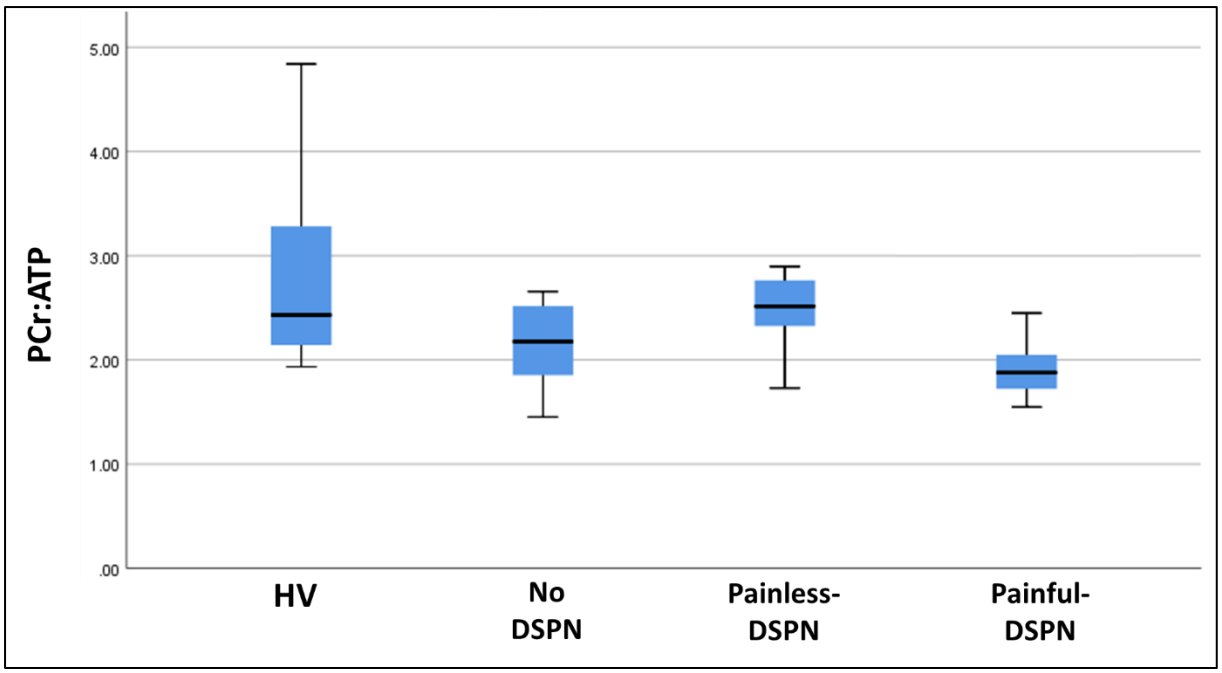

Figure 5.4. Mean S1 cortical PCr:ATP box and whisker plot (p=0.006, ANOVA). Painful-DSPN vs. HV (p=0.001, LSD); Painful-DSPN vs. painless-DSPN (p=0.04); No-DSPN vs. HV (p=0.013). PCr, phosphocreatine.

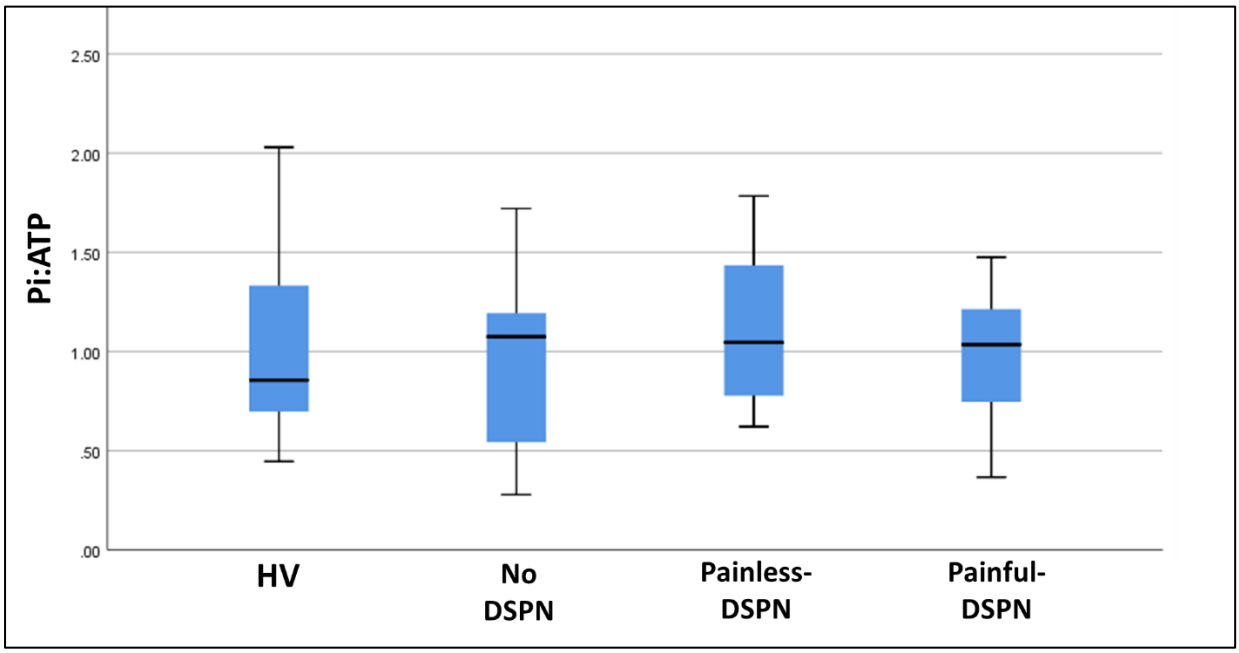

Figure 5.5. Mean S1 cortical Pi:ATP box and whisker plot (p=0.740, ANOVA). Pi, inorganic phosphate.

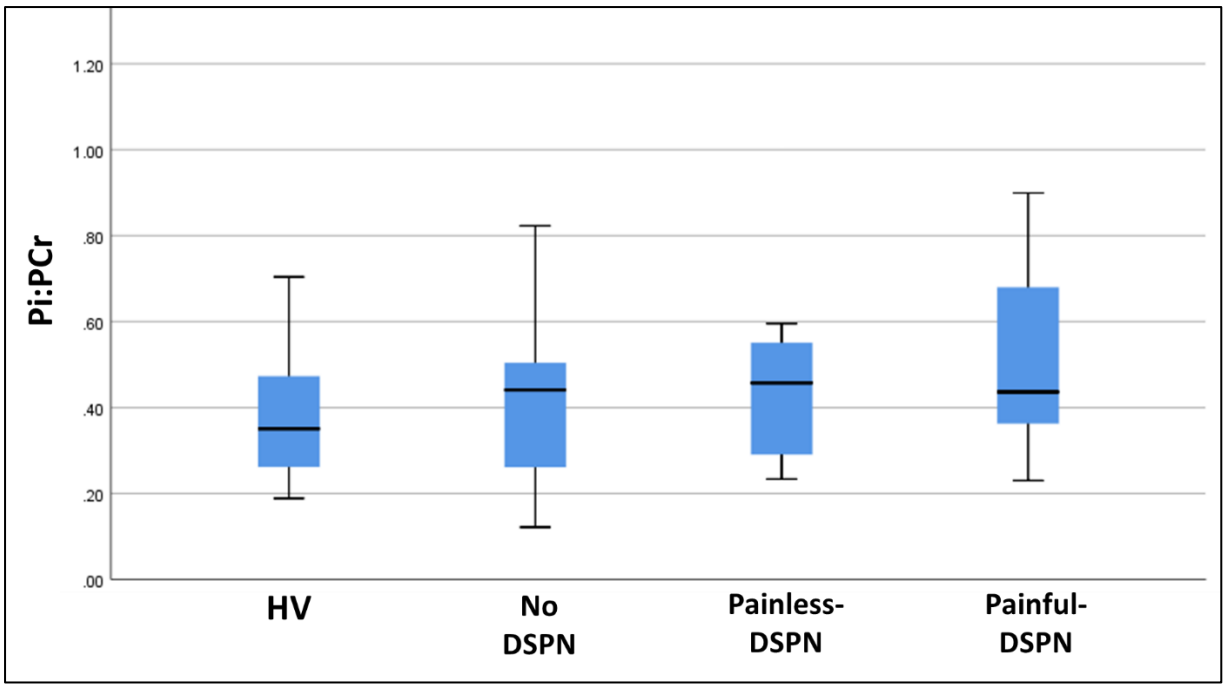

Figure 5.6. Mean S1 cortical Pi:PCr box and whisker plot (p=0.339, ANOVA). PCr, phosphocreatine; Pi, inorganic phosphate.

The correlation between mean S1 cortical PCr:ATP and clinical and neurophysiological variables is displayed in Table 5.9. The mean S1 cortical PCr:ATP did not correlate with demographic or clinical parameters, nor neurological or neurophysiological measures. However, there were significant negative correlations between this ratio and measures of neuropathic pain, such as the DN4 (Spearman's rank, r -0.326, p=0.015), NRS (r -0.424, p=0.001) and the total NPSI (r -0.391, p=0.003). Moreover, subscores of the NPSI correlated with the S1 PCr:ATP (Burning spontaneous pain r -0.342, p=0.011; pressing spontaneous pain, r -0.298, p=0.027; paroxysmal pain, r -0.448, p=0.001; evoked pain, r -0.377, p=0.005; paraesthesia/dyseasthesia r -0.408, p=0.002), with the strongest relationship shown with paroxysmal pain. There was no correlation with DFNS-QST z-scores.

The mean S1 Pi:ATP and pH did not correlate with demographic or clinical parameters, or neurological or neurophysiological parameters. The Pi:PCr correlated with the total burning

NPSI subscore (r 0.304, p=0.024), evoked pain NPSI subscore (r 0.266, p=0.050) and MMSE (r -0.310, p=0.034). The PME:PDE showed a negative correlation with number of pack years smoking and (r -0.352, p=0.008) and fingerpick blood glucose before the MRI scan (r 0.278, p=0.040), but no other variables.

Mean PCr:ATP	r	P value
Age	0.200	0.143
HbA1c	-0.041	0.765
Glucose during MR	-0.055	0.690
Body mass index	-0.036	0.792
Systolic blood pressure	-0.034	0.810
NIS-LL+7	-0.073	0.601
TCNS	-0.155	0.258
Total NPSI	-0.391	**0.003**
Total burning NPSI subscore	-0.342	**0.011**
Total pressing NPSI subscore	-0.298	**0.027**
Total paroxysmal NPSI subscore	-0.448	**0.001**
Total evoked pain NPSI subscore	-0.377	**0.005**
Total dysaesthesia NPSI subscore	-0.408	**0.002**
NRS during MR	-0.424	**0.001**
DN4	-0.326	**0.015**

Table 5.9. Spearman's correlation between mean S1 cortical PCr:ATP metabolic and neurological variables. DN4, doleur neuropathique 4; MR, magnetic resonance scan; NIS-LL+7, Neuropathy Impairment Score of the Lower Limb plus 7 tests; NPSI, neuropathic pain symptom inventory; NRS, numeric rating scale; PCr, phosphocreatine; TCNS, Toronto clinical neuropathy score.

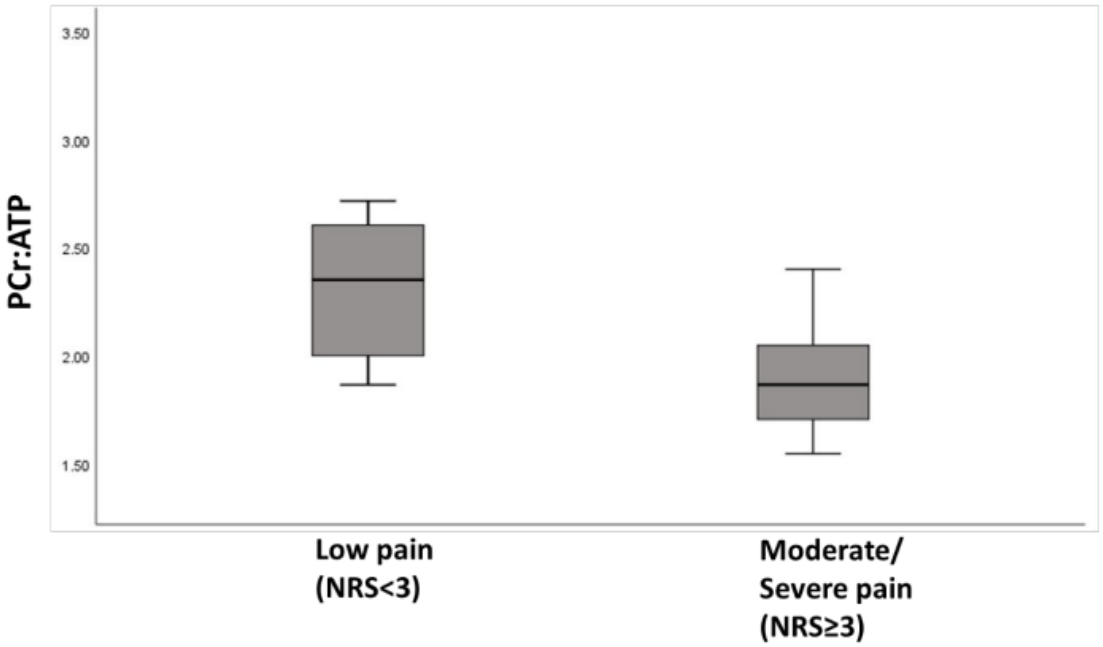

Figure 5.7. Mean S1 PCr:ATP in participants with painful-DSPN and low pain (NRS <3) and moderate/severe pain (NRS 3-10) on a 0-10 scale, box and whisker plot (p=0.033, Mann-Whitney U test). NRS, numeric rating scale; PCr, phosphocreatine.

Figure 5.7 shows mean S1 PCr:ATP for participants with painful-DSPN after stratification into those experiencing low pain (NRS <3, mean SD, 0.4 ± 0.9; n=6) and moderate to severe pain (NRS 3-10, mean ± SD, 5.6 ± 1.8; n=14) during the MR scan. The PCr:ATP was significantly higher in the moderate/severe pain group [median (IQR) 1.87(0.35)] compared with the low pain group [2.35 (0.67), p=0.033], Mann-Whitney U test. Other than NRS pain scores (Mann-Whitney U test, p<0.001) there were no other significant group differences in clinical or neurophysiological measures between the two groups.

5.3.3.3 Thalamus metabolite ratio analysis

Table 5.10 shows the 31P-MRS DH, NDH, and mean thalamic results for the different groups. There was a significant group effect at the NDH PCr:ATP ratio, shown in Figure 5.9 (ANOVA, p=0.036). The ratio was numerically the lowest in painful-DSPN, which reached significance versus HV (LSD, p=0.045) and no-DSPN (p=0.008). The PCr:ATP was numerically the lowest in painful-DSPN at the DH and mean value (Figure 5.8); however, neither reached statistical significance.

There was a significant group effect in Pi:ATP and Pi:PCr ratio at the DH and mean thalamic value (Figures 5.10 and 5.11). The mean thalamic Pi:ATP was statistically higher in painless-DSPN compared with HV (LSD, p=0.008) and painful-DSPN (p=0.005). The mean thalamic Pi:PCr was statistically lower in HV compared with no-DSPN (p=0.049) and painless-DSPN (p=0.008). Additionally, the mean Pi:PCr was lower in painful- compared with painless-DSPN (p=0.039). There was no group effect in the Pi:ATP or Pi:PCr at the NDH thalamus. There was also no difference between the groups in the PME:PDE nor the pH.

In view of the significant group differences in HbA1c, this variable was added to an ANCOVA. HbA1c had no significant effect upon the outcome of the model for PCr:ATP; however, it did for Pi:ATP and Pi:PCr. The thalamic Pi:ATP ANCOVA and post hoc group differences retained significance (ANCOVA, p=0.015; painful-DSPN vs. no-DSPN, p=0.042; painful-DSPN vs. painless-DSPN, p=0.002) but the Pi:PCr ANCOVA was no longer significant (p=0.087).

	HV (n=11)	No-DSPN (n=9)	Painless-DSPN (n=11)	Painful-DSPN (n=18)	P value
NDH PCr:ATP	2.28 ± 0.24	2.37 ± 0.35	2.13 ± 0.34	2.04 ± 0.27	**0.036 A**
NDH Pi:ATP	0.85 ± 0.39	1.10 ± 0.59	1.25 ± 0.65	0.89 ± 0.52	0.241 A
NDH Pi:PCr	0.40 (IQR 0.25)	0.40 (0.14)	0.62 (0.50)	0.41 (0.44)	0.366 KW
NDH PME:PDE	0.89 (IQR 0.60)	0.94 (0.45)	0.97 (0.41)	0.95 (0.77)	0.955 KW
NDH pH	7.110 (IQR 0.14)	7.070 (0.09)	7.0250 (0.06)	7.030 (0.08)	0.063 KW
DH PCr:ATP	2.38 ± 0.47	2.19 ± 0.45	2.33 ± 0.41	2.13 ± 0.38	0.406 A
Dh Pi:ATP	0.91 ± 0.63	1.31 ± 0.28	1.41 ± 0.41	0.90 ±0.40	**0.010 A**
Dh Pi:PCr	0.38 ± 0.26	0.61 ± 0.16	0.61 ± 0.14	0.45 ± 0.24	**0.022 A**
Dh PME:PDE	0.98 (IQR 0.92)	1.23 (0.45)	0.81 (0.7)	0.89 (0.7)	0.618 KW
DH pH	7.090 (IQR 0.11)	7.060 (0.09)	7.045 (0.08)	7.030 (0.04)	0.638 KW
Mean PCr:ATP	2.33 ± 0.30	2.28 ± 0.37	2.23 ± 0.34	2.09 ± 0.26	0.197 A
Mean Pi:ATP	0.88 ± 0.41	1.21 ± 0.30	1.33 ± 0.46	0.90 ± 0.36	**0.012 A**
Mean Pi:PCr	0.38 ± 0.19	0.55 ± 0.18	0.60 ± 0.19	0.45 ± 0.19	**0.034 A**
Mean PME:PDE	1.13 (IQR 0.58)	1.10 (0.43)	0.89 (0.45)	0.97 (0.45)	0.954 KW
Mean pH	7.095 (IQR 0.13)	7.060 (0.13)	7.0450 (0.05)	7.040 (0.07)	0.208 KW

Table 5.10. 31P-MRS metabolite ratios in the thalamus. Data are presented as mean ± standard deviation for parametric and median (IQR) for non-parametric continuous data. The statistical test used was ANOVA (A) for continuous normally distributed data and Kruskal-Wallis (KW) for non-parametric continuous data. DH, dominant hemisphere; NDH, non-dominant hemisphere; Pi, inorganic phosphate; PDE, phosphodiesters; PCr, phosphocreatine; PME, phosphomonoesters.

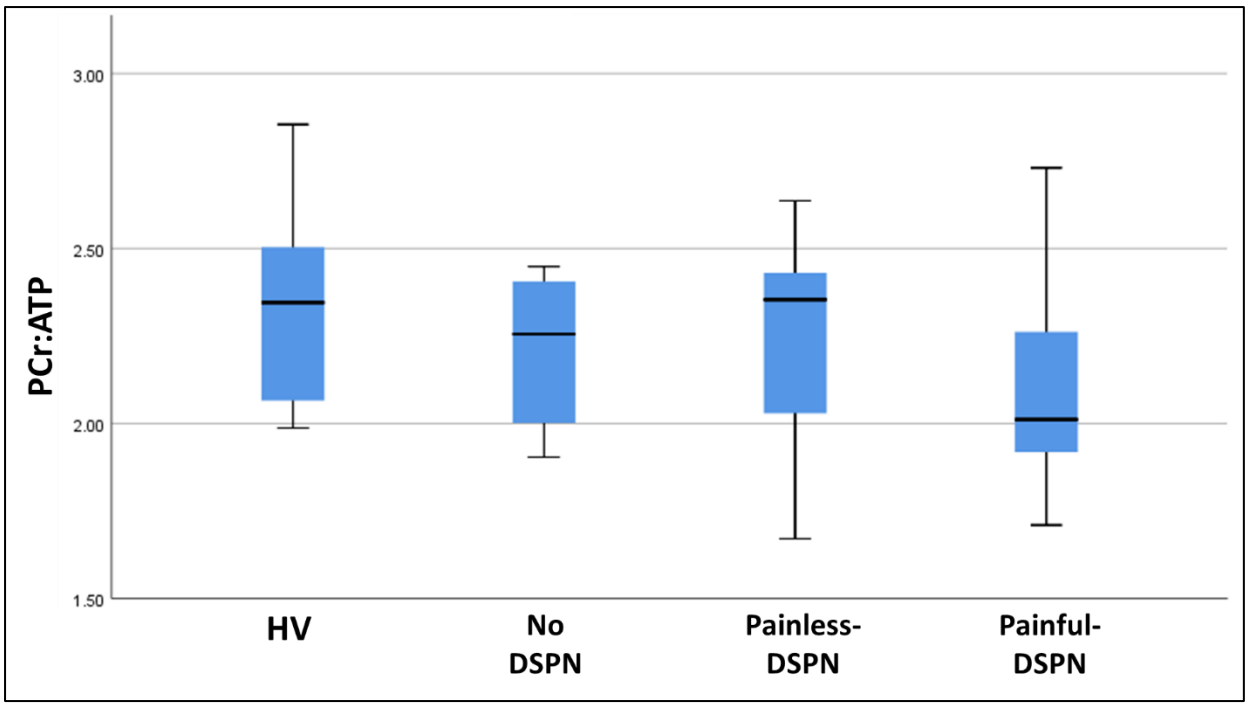

Figure 5.8. Mean thalamic PCr:ATP box and whisker plot (p=0.197, ANOVA). PCr, phosphocreatine.

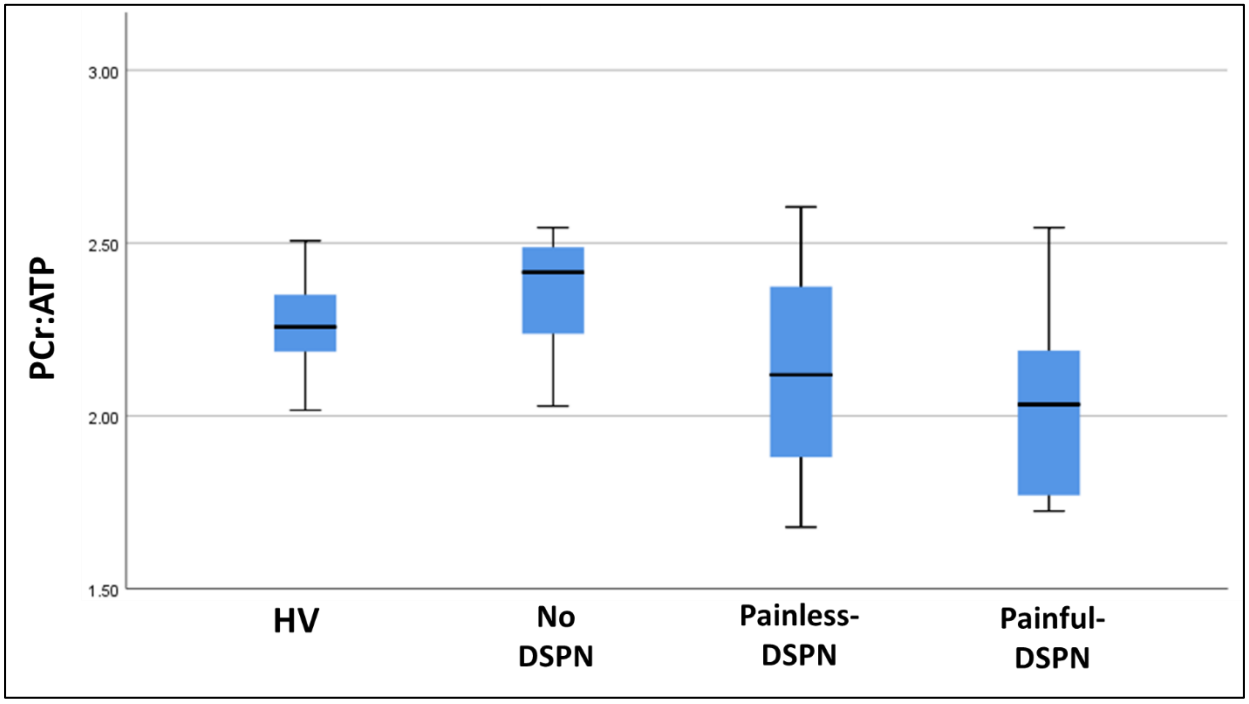

Figure 5.9. NDH thalamic PCr:ATP box and whisker plot (p=0.036, ANOVA). Painful-DSPN vs. HV (p=0.045, LSD); Painful-DSPN vs. no-DSPN (p=0.008). PCr, phosphocreatine.

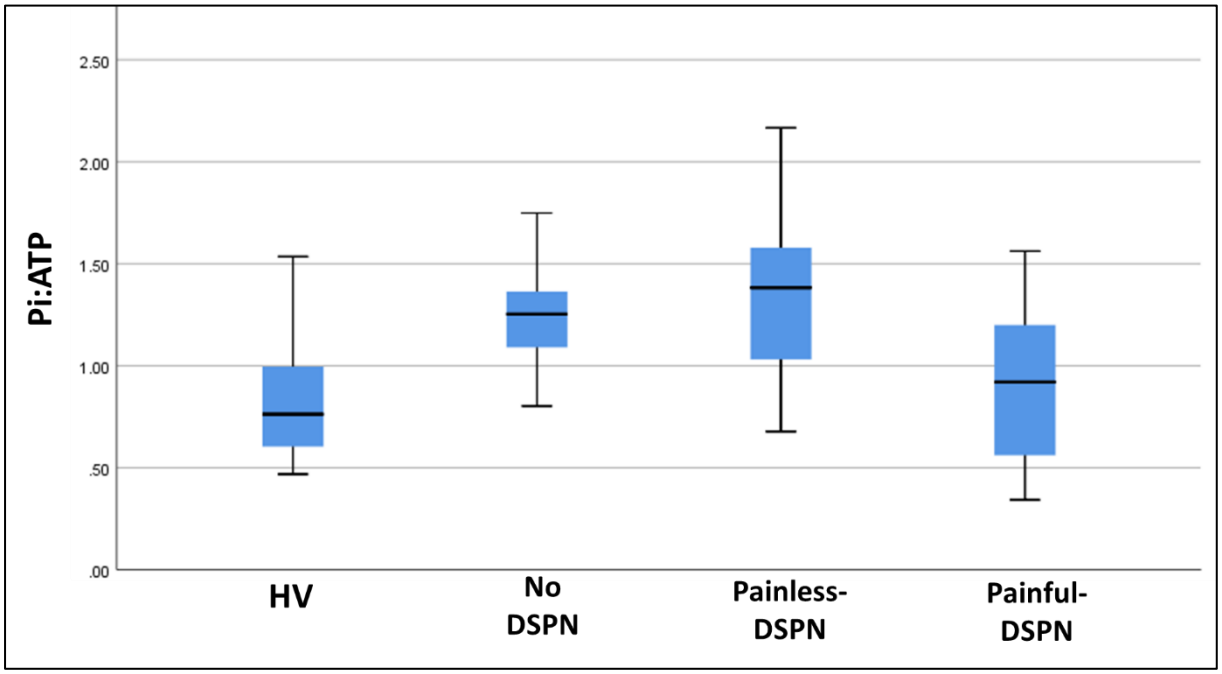

Figure 5.10. Mean thalamic Pi:ATP box and whisker plot (p=0.012, ANOVA). Painless-DSPN vs. HV (p=0.008, LSD); Painless-DSPN vs. painful-DSPN (p=0.005). Pi, inorganic phosphate.

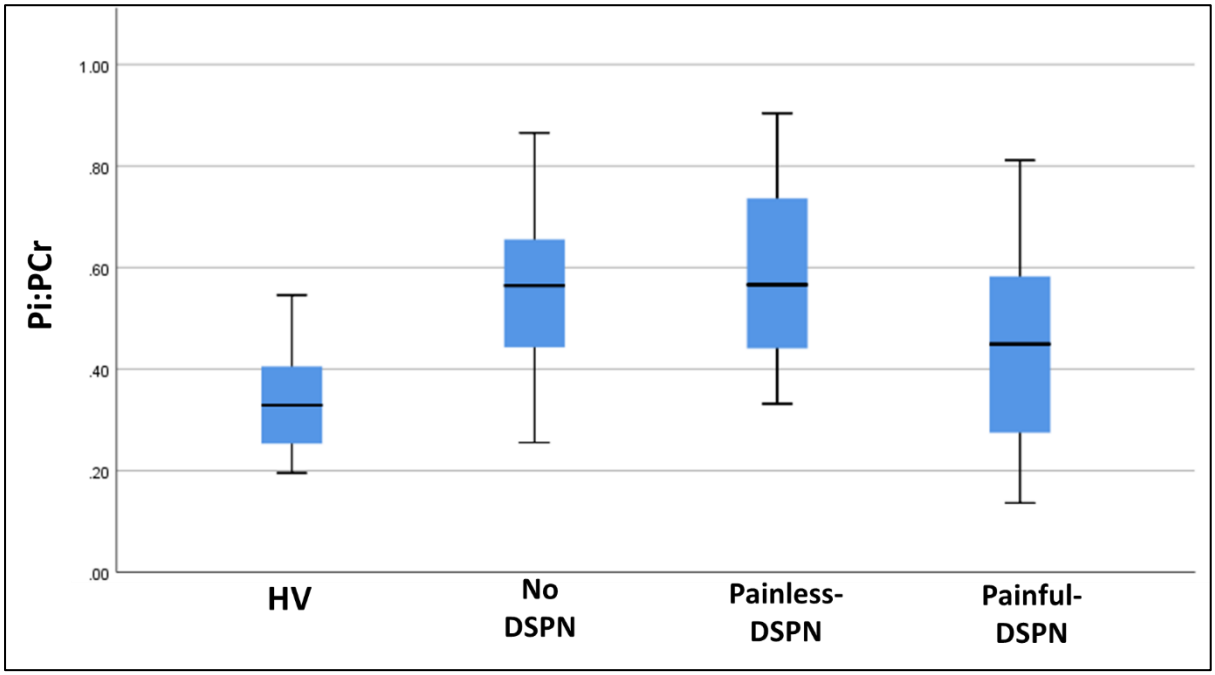

Figure 5.11. Mean thalamic Pi:PCr box and whisker plot (p=0.034, ANOVA). Painless-DSPN vs. HV (p=0.049, LSD); Painless-DSPN vs. HV (p=0.008); Painful-DSPN vs. Painless-DSPN (p=0.039). PCr, phosphocreatine; Pi, inorganic phosphate.

Correlation analysis with the NDH PCr:ATP revealed significant correlations between blood pressure (Spearman's correlation, r -0.283, p=0.049) and a number of neurological and neurophysiological measures (Table 5.11). The TCNS and NIS-LL+7 score all showed significant correlations, indicating the PCr:ATP was negatively related to increasing severity of neuropathy. Additionally, the PCr:ATP was negatively related to increasing neuropathic pain, as indicated by correlations with the pain score during the MR scan (r -0.289, p=0.046), DN4 (r -0.283, p=0.049) and total NPSI (r -0.390, p=0.006) and two subscores (Total burning pain NPSI subscore: r -0.318, p=0.026; total pressing NPSI subscore: r -0.476, p=0.001).

NDH PCr:ATP	r	Significance
Age	-0.028	0.850
HbA1c	-0.220	0.129
Glucose before MR	-0.219	0.131
Body mass index	-0.119	0.415
Systolic blood pressure	-0.283	**0.049**
NIS-LL+7	-0.470	**0.001**
TCNS	-0.400	**0.004**
Total NPSI	-0.390	**0.006**
Total burning NPSI subscore	-0.318	**0.026**
Total pressing NPSI subscore	-0.476	**0.001**
Total paroxysmal NPSI subscore	-0.387	**0.006**
Total evoked pain NPSI subscore	-0.224	0.121
Total dysaesthesia NPSI subscore	-0.273	0.058
NRS during MR	-0.289	**0.046**
DN4	-0.283	**0.049**

Table 5.11. Spearman's correlation between NDH thalamic PCr:ATP and metabolic and neurological variables. DN4, doleur neuropathique 4; MR, magnetic resonance scan; NIS-LL+7, Neuropathy Impairment Score of the Lower Limb plus 7 tests; NDH, non-dominant hemisphere; NRS, numeric rating scale; PCr, phosphocreatine; TCNS, Toronto clinical neuropathy score.

Correlation analysis with the mean thalamic Pi:ATP revealed no significant correlations with pain, neurological or neurophysiological measures (nerve conduction studies and DFNS-QST). However, Pi:ATP showed significant correlations with HbA1c (r 0.363, p=0.010), duration of diabetes (r 0.364, p=0.025) and there was a trend toward a relationship with fingerprick glucose values before the MR (r 0.261, p=0.070) (Table 5.12).

Mean Pi:ATP	r	Significance
Age	-0.163	0.262
HbA1c	0.364	**0.010**
Glucose before MR	0.261	0.070
Body mass index	0.174	0.232
Systolic blood pressure	0.173	0.236
NIS-LL+7	-0.021	0.889
TCNS	-0.041	0.780
Total NPSI	-0.117	0.224
NRS during MR	-0.266	0.068
DN4	-0.232	0.109

Table 5.12. Spearman's correlation between mean thalamic Pi:ATP and metabolic and neurological variables. DN4, doleur neuropathique 4; MR, magnetic resonance scan; NIS-LL+7, Neuropathy Impairment Score of the Lower Limb plus 7 tests; NRS, numeric rating scale; Pi, inorganic phosphate; TCNS, Toronto clinical neuropathy score.

Correlation analysis with the mean Pi:PCr was similar to the Pi:ATP, there were positive correlations between this ratio and HbA1c (Spearman's correlation, r 0.477, p=0.001), glucose during the MR (r 0.345, p=0.015) and duration of diabetes (r 0.322, p=0.049) (Table 5.13).

Mean Pi:PCr	*R*	Significance
Age	-0.193	0.184
HbA1c	0.477	**0.001**
Glucose during MR	0.345	**0.015**
Body mass index	0.174	0.232
Systolic blood pressure	0.211	0.146
NIS-LL+7	0.119	0.420
TCNS	0.094	0.520
Total NPSI	-0.008	0.955
NRS during MR	-0.123	0.406
DN4	-0.107	0.464

Table 5.13. Spearman's correlation between mean thalamic Pi:PCr and metabolic and neurological variables. DN4, doleur neuropathique 4; MR, magnetic resonance scan; NIS-LL+7, Neuropathy Impairment Score of the Lower Limb plus 7 tests; NRS, numeric rating scale; PCr, phosphocreatine; Pi, inorganic phosphate; TCNS, Toronto clinical neuropathy score.

5.3.3.4 Correlation analysis between 31P and 1H-MRS variables

At the S1 NDH there was a significant correlation between the NAA:Cho and PCr:ATP (r 0.344, p=0.026, Spearman's correlation) (Figure 5.12) and also the Cho:Cr and Pi:PCr (r -0.311, p=0.045, Pearson's correlation). For comparison, the dominant hemisphere somatosensory cortical NAA:Cho and PCr:ATP Spearman's correlation was r 0.297 (p=0.056) and the Cho:Cr and Pi:PCr Pearson's rank correlation was r -0.110 (p=0.489).

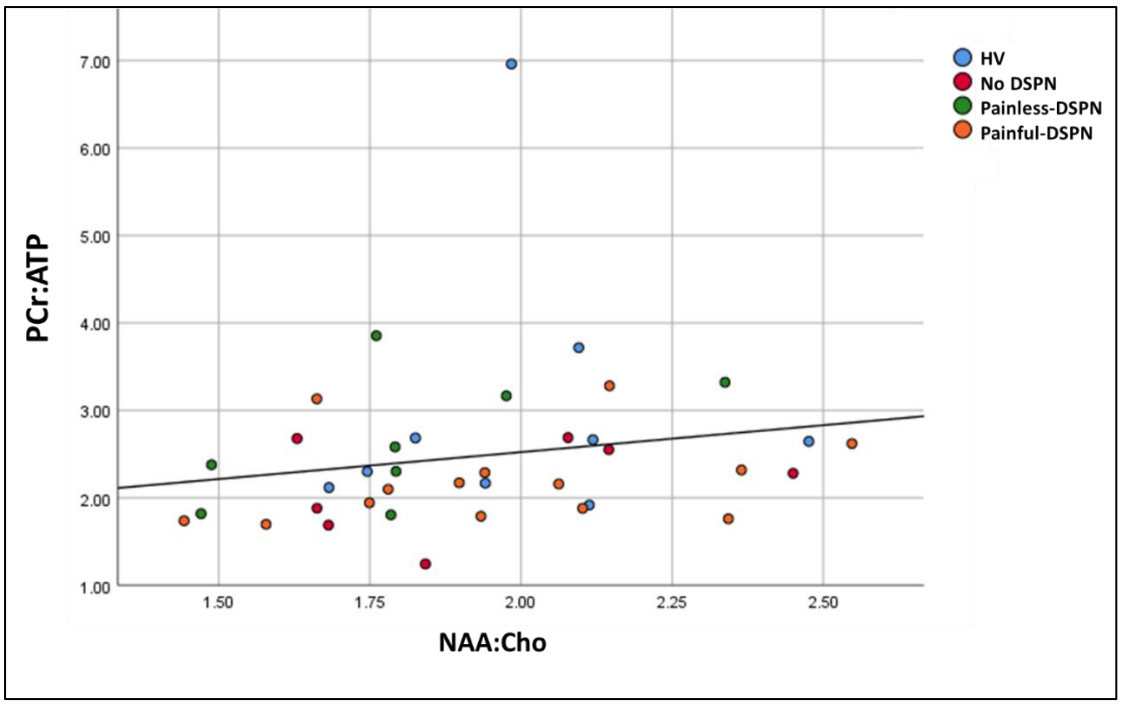

Figure 5.12. Spearman's correlation between NDH S1 cortical NAA:Cho and PCR:ATP (r 0.344, p=0.026). Cho, choline; NAA, N-acetylaspartate; PCr, phosphocreatine.

At the dominant hemisphere of the thalamus there was a significant correlation between the NAA:Cho and Pi:ATP, Figure 5.13, (r -0.383, p=0.018, Spearman's correlation) and the NAA:Cho and Pi:PCr (r -0.328, p=0.045). There was no correlation between DH thalamic NAA:Cho and PCr:ATP (r -0.008, p=0.960). At the NDH, the NAA:Cho correlated with the PCr:ATP (r -0.343, p=0.035), Figure 5.14, and the Pi:PCr (0.-381, p=0.018).

The mean thalamic PCr:ATP correlated with the mean somatosensory cortical PCr:ATP (r 0.370, p=0.009). The DH thalamic PCr:ATP correlated with the DH somatosensory cortical PCr:ATP (r 0.454, p=0.001). The NDH thalamic PCr:ATP did not significantly correlate with the NDH somatosensory cortical PCr:ATP (r 0.158, p=0.279). There was no correlation between the Pi:ATP or Pi:PCr between the thalamus and S1 cortex.

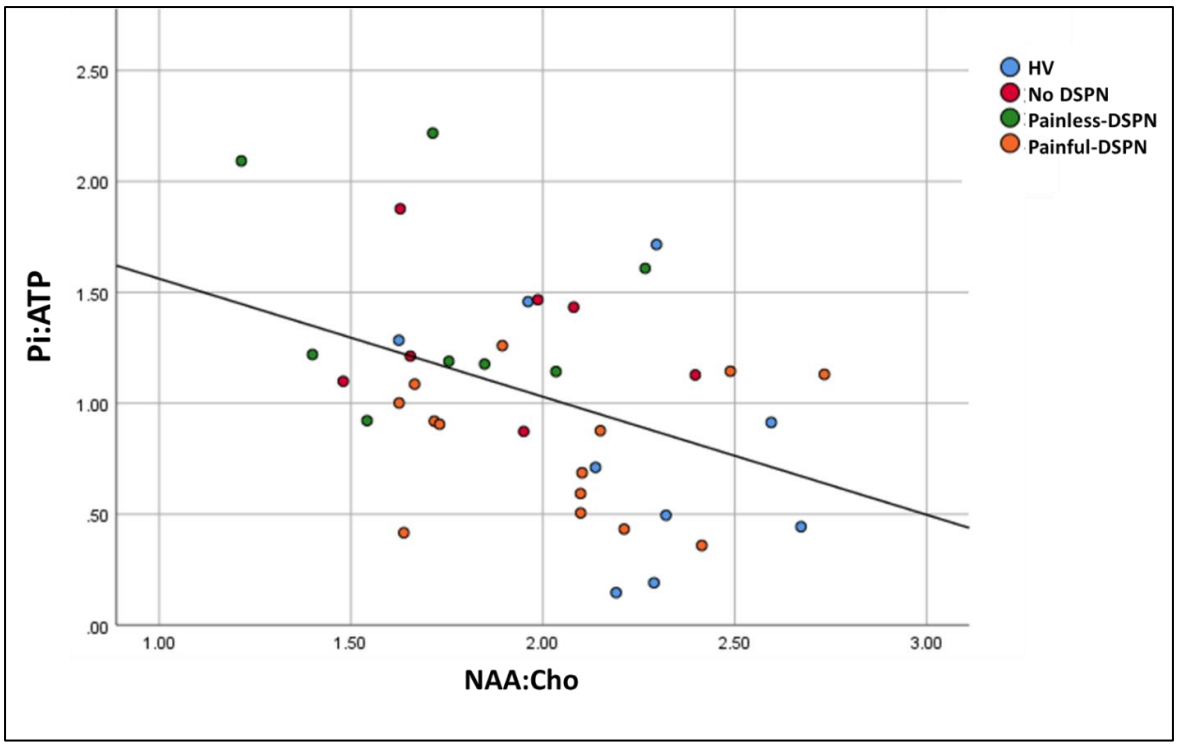

Figure 5.13. Spearman's correlation between DH thalamic NAA:Cho and Pi:ATP (r -0.383, p=0.018). Cho, choline; NAA, N-acetylaspartate; Pi, inorganic phosphate.

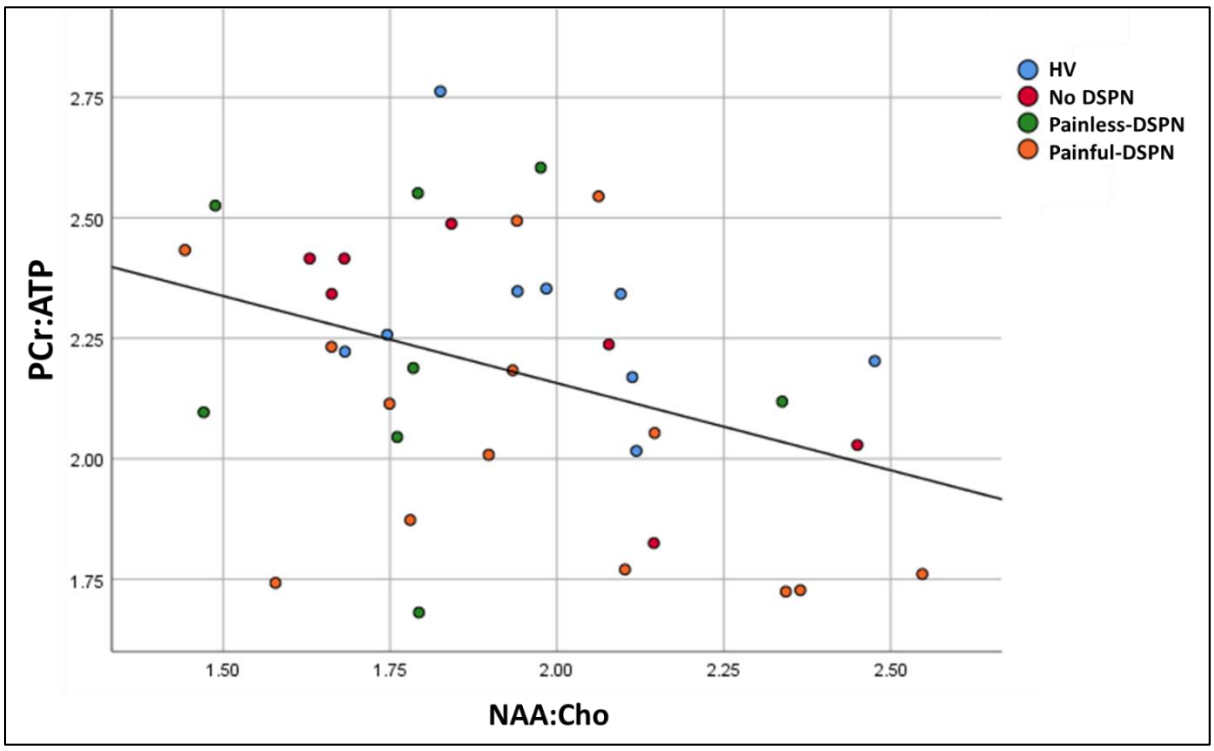

Figure 5.14. Spearman's correlation between NDH thalamic NAA:Cho and PCr:ATP (r -0.343, p=0.035). Cho, choline; NAA, N-acetylaspartate; PCr, phosphocreatine.

5.4 Discussion

In this study 31P-MRS was performed to examine phosphorus containing neurometabolites in pain processing areas of the brain in well characterized patients with DSPN. The results suggest differing bioenergetic processes occurring in the thalamus and S1 cortex. At the S1 cortex, there was a clear pattern with PCr:ATP being the lowest in painful-DSPN whilst it was significantly higher in painless-DSPN. The PCr:ATP ratio was also lower in those with no-DSPN compared to HV, but not painless-DSPN. The S1 PCr:ATP also correlated with several measures of neuropathic pain. At the thalamus, however, the mean thalamic Pi:PCr and Pi:ATP were highest in painless-DSPN compared with HV and painful-DSPN. The Pi:PCr was also statistically higher in no-DSPN compared with HV. The Pi:PCr and Pi:ATP also correlated with measures of diabetes, e.g. HbA1c and duration of diabetes. The PCr:ATP was also lower at the NDH thalamus in painful-DSPN compared with HV and no-DSPN. Additionally, there were correlations seen between the 31P and 1H-MRS parameters at the thalamus and S1 cortex where the NAA:Cho correlated with Pi:ATP and Pi:PCr at the DH thalamus and the NDH NAA:Cho with the PCr:ATP and Pi:PCr. Finally the NAA:Cho correlated with the PCr:ATP at the non-dominant hemisphere at S1.

The findings at the S1 cortex are suggestive of greater S1 cortical energy usage in painful-DSPN with higher pain scores. The S1 cortex is one of the main components of the cerebral network for processing pain, receiving ascending impulses from important pain pathways such as the spinothalamic tract (Apkarian et al., 2005). Other studies have shown that increased brain activity in this region in experimental pain is coupled with increased blood flow (Liu et al., 2013) and relates to the severity of stimulus intensity (Bornhövd et al., 2002). These studies support the findings of depleted S1 PCr in painful-DSPN. Moreover, the

findings are consistent with other studies which have shown evidence of increased cerebral neuronal activity in painful-DSPN in other brain regions (Sloan et al., 2021), for example hyperexcitable ventral posterolateral thalamic neurons in experimental conditions (Fischer et al., 2009), hyperperfusion of the thalamus (Selvarajah et al., 2011), ventrolateral periadqueductal grey-mediated pain facilitation (Segerdahl et al., 2018) and increased ACC activity (Watanabe et al., 2018) in human painful-DSPN.

PCr:ATP levels in patients with Painless-DSPN were significantly higher compared to those with painful-DSPN despite a similar severity of neuropathy. This signifies the relative lower resting state neuronal activity in the S1 cortex compared to patients with painful-DSPN. Other studies have demonstrated that painless-DSPN may be associated with reduced cerebral neuronal activity, including a reduction in the NAA levels, shown in previous work within our group (Selvarajah et al., 2008) and Chapter 4, and sensorimotor fibre tracts (Hansen et al., 2019), thalamic atrophy (Hansen et al., 2021) and altered thalamic perfusion characteristics, including reduced blood volume (Selvarajah et al., 2008)**.** Moreover, previous studies have demonstrated volume loss within the S1 cortex in participants with DSPN, but the potential pathophysiological mechanisms have been unexplained (Selvarajah et al., 2014b). This is the first study to show a marker of bioenergetics in patients with painless-DSPN, suggesting reduced neuronal activity, which may be associated with cortical atrophy or a dying back axonopathy secondary to reduced sensory input causing Wallerian degeneration. Further, there was a negative correlation between NAA:Cho and PCr:ATP at the NDH S1 indicating reduced neuronal function/viability as energy usage increases. This might be consistent with the concept of excitotoxicity in cerebral neurons in neuropathic pain (Bushnell et al., 2013); however, the mechanism of this is unclear.

Other negative results within this study provide insight into the alterations at S1 in DSPN. Although the results suggest that the energy status at this region was altered, the pH, Pi:ATP and Pi:PCr were equivocal between groups suggesting that cellular oxygen supply was adequate for activity and mitochondrial function. Finally, there were no group differences in PME:PDE although there was a significant negative correlation with pack years smoking and a positive correlation with finger prick glucose. The PME and PDE peaks were not well defined, as indicated by the higher Cramér–Rao lower bounds, and further study would be required to confirm these findings.

At the level of the thalamus, the pattern of 31P-MRS alterations was drastically different, suggesting differing bioenergetic processes occurring at this site. The results were suggestive of altered mitochondrial function in no-DSPN and painless-DSPN, which may be secondary to the effect of chronic metabolic dysfunction on the thalamus rather than DSPN. However, in participants with painful-DSPN the comparable levels of Pi:PCr and Pi:ATP with HV indicated relatively preserved mitochondrial function at the thalamus, which is consistent with previous findings of relatively normal thalamic GABA neurotransmitter levels (Shillo et al., 2016) and 1H-MRS parameters as described in Chapter 4 and in a previous study (Gandhi et al., 2006). Moreover, heightened microvascular blood flow in the thalamus in patients with painful-DSPN may also ensure adequate oxygen delivery and preserve thalamic mitochondrial function compared with patients with painless-DSPN (Selvarajah et al., 2011). NAA:Cho also correlated with Pi:PCr at both DH and NDH thalamus and Pi:ATP at the DH. This novel finding suggests that increased 31P markers of mitochondrial dysfunction are related to reduced neuronal function. The mechanisms of cerebral neuronal injury in diabetes are incompletely understood. It is believed that mechanisms of cerebral injury in cognitive dysfunction include hyperglycaemia, protein

glycation, microvascular disease, endothelial dysfunction, inflammation, etc (McCrimmon et al., 2012). These results give new insight into the aetiology of neuronal injury in the thalamus in diabetes and DSPN, indicating that mitochondrial dysfunction is a potential mechanism.

The PCr:ATP ratio was also shown to be the lowest at the NDH thalamus in painful-DSPN. This finding is suggestive of increased energy usage within the thalamus in this group compared with HV and no-DSPN. However, the meaning of this result is less clear as there was no significant group effect at the DH thalamus nor the mean values. Moreover, this ratio correlated with measures of neuropathy (NIS-LL+7) more strongly than neuropathic pain. Therefore, this finding could be suggestive of increased energy demand in the thalamus secondary to metabolic or microvascular dysfunction due to chronic diabetes and DSPN, there may be an additional effect of increased neuronal activity due to peripheral neuropathic pain. The thalamic NDH PCr:ATP positively correlated with NAA:Cho; although converse to the S1 cortex this was a negative correlation suggesting reduced energy usage was associated with reduced NAA:Cho levels. The reasons for this discrepancy are unclear, but again point towards different energetic processes in the thalamus and S1 cortex.

The strengths of this study include that it is the first to use 31P-MRS to study DSPN and chronic pain conditions affecting the periphery. 31P-MRS is a unique tool as it allows the *in vivo* assessment of tissue metabolism without ionizing radiation nor administration of contrast/radioactive tracers (Liu et al., 2017). Therefore, this technique is complimentary to other cerebral imaging methods such as blood oxygen level-dependent (BOLD) functional MRI and those which determine blood flow dynamics because 31P-MRS provides an objective measure of cellular energetics and mitochondrial function. Additionally, the

sample size is adequate and similar to other cerebral imaging studies in DSPN (Selvarajah et al., 2008, Selvarajah et al., 2011, Teh et al., 2021). We deliberately increased the numbers in painful-DSPN to ensure further exploration of this group was possible. The clear group differences in PCr:ATP justify the sample sizes. The limitations of this study are similar to the limitations of the 1H-MRS study. The ISIS MRS technique is also recognised to be particularly susceptible to movement artefact. Also, although the study sample size is greater than the 1H-MRS study, further larger studies may be recommended to confirm the findings.

5.5 Conclusions and future work

To conclude, for the first time this study used cerebral 31P-MRS to examine a peripheral neuropathic pain condition. There appears to be a diabetes effect in phosphorus metabolite ratios at both the level of the thalamus (Pi:PCr and Pi:ATP) and S1 cortex (PCr:ATP). 31P-MRS metabolite ratios reveal that mitochondrial dysfunction in the thalamus may be the cause of reduced neuronal dysfunction in no- and painless-DSPN; whereas there appears to be normal mitochondrial function in painful-DSPN, comparable to that of HV. These findings also relate to markers of neuronal function, indicating that mitochondrial function may be a key mechanism of thalamic neuronal dysfunction in diabetes. At the S1 cortex, the PCr:ATP ratio was found to be lowest in painful-DSPN due to increased S1 cortical energy metabolism. This compliments findings in other studies reporting painful-DSPN is associated with heightened pain matrix cerebral neuronal activity (Selvarajah et al., 2011, Watanabe et al., 2018, Fischer et al., 2009) and whilst conversely there was reduced activity in painless-DSPN (Selvarajah et al., 2011). The negative correlation between PCr:ATP and measures of

neuropathic pain, and the lower PCr:ATP ratios in those with higher pain scores compared to those with low pain scores, suggests S1 cortex bioenergetics are related to the severity of neuropathic pain. Exploratory studies are now required in other chronic pain conditions, and other pain processing areas of the brain. Finally, S1 cortical PCr:ATP may serve as a potential biomarker for neuropathic pain and a target for therapeutic intervention for novel treatments.

6. The impact of optimised neuropathic pain treatment on the magnetic resonance imaging correlates of painful-DSPN 1: Neurotransmitters

6.1 Introduction

6.1.1 Background

The management of painful-DSPN poses a significant treatment challenge (Alam et al., 2020). The first line treatments for painful-DSPN have remained unchanged for over a decade and are generally considered to be inadequate. The number needed to treat for 50% pain relief for neuropathic pain ranges from 4 to 10 across most positive trials, indicating only modest improvements in pain (Finnerup et al., 2015). Moreover, these treatments are often offset by intolerable adverse effects.

A potential reason for the inefficacy of analgesic agents is the lack of a pain biomarker. Current trials use self-reported pain scales as measures of efficacy, which are highly susceptible to confounding factors. Studies have investigated neuroimaging parameters to determine their suitability as biomarkers of treatment response in neuropathic pain trials, although none are validated for clinical use. One brain region which has been studied in two clinical trials of painful-DSPN is the ACC, a key brain region within the pain matrix. Increased functional connectivity from the ACC to insular cortex was demonstrated in patients with painful-DSPN who responded to intravenous lidocaine compared with non-responders

(Wilkinson et al., 2020). Another study found that increased ACC blood flow, as measured by using iodine-123-N-isopropyl-p-iodoamphetamine single-photon emission computed tomography, was associated with painful- compared with painless-DSPN (Watanabe et al., 2018). Additionally, a decrease in cerebral blood flow in this region was observed in patients gaining significant pain relief with three months of duloxetine treatment compared with non-responders. However, the effect of painful-DSPN treatments on neurotransmitters in the ACC has not been explored.

Neurotransmitters are critically involved in the modulation of pain perception in cortical structures (Quintero, 2013). GABA is the main inhibitory and glutamate the main excitatory neurotransmitter, both of which may be quantified using 1H-MRS (Yasen et al., 2017). Glutamate is often assessed spectrally as the combination of glutamine+glutamate (Glx). The balance of these neurotransmitters has been investigated to a limited extent in DSPN. Lower relative levels of GABA were observed within the thalamus of patients with DSPN (painful- and painless-DSPN combined) in comparison to those without DSPN (HV plus no-DSPN groups combined) (Shillo, 2019). GABA and glutamate are also key neurotransmitters within the ACC (Bliss et al., 2016). Healthy participants undergoing tonic noxious stimulation have been shown to have an increased glutamate and Glx at the ACC (Archibald et al., 2020b).

6.1.2 Rationale for study

GABA and Glx are key neurotransmitters involved in the processing of pain. However, the response of these neurotransmitters to analgesia have not been studied in painful-DSPN.

This study has chosen the ACC as our region of interest as blood flow changes in the ACC have been associated with a better treatment response to duloxetine.

6.1.3 Aims and hypothesis

The aim of the study is to assess MRS neurotransmitter parameters (GABA and Glx) in the ACC in painful-DSPN, to determine whether changes are detectable when participants are optimally treated for their painful symptoms compared to without treatment. The hypothesis is that GABA levels will reduce and Glx levels rise after withdrawal of treatment. Moreover, another hypothesis is that patients with a greater increase in pain (i.e. responders to treatment) will have greater changes in neurotransmitters.

6.2 Methods

6.2.1 Study Design and Participants

The study design is a pre-post observational study conducted alongside the OPTION DM [Optimal Pathway for TreatIng neuropathic paiN in Diabetes Mellitus trial (REC reference 16/YH/0459)] study. The study within this thesis aimed to include 20 patients with painful-DSPN enrolled in the OPTION-DM study at Sheffield Teaching Hospitals. Sample size calculations have not specifically been performed as this is a preliminary study.

6.2.2 Inclusion and exclusion criteria

The study inclusion and exclusion criteria for patients recruited into this study from the OPTION-DM study cohort were as presented in Chapter 2 General Methods (section 2.1.1 and 2.1.2). However, participants were only eligible for OPTION-DM if certain criteria were met (Selvarajah et al., 2018):

6.2.2.1 OPTION-DM inclusion criteria

1. Participant aged ≥18 years
2. Neuropathic pain affecting both feet and / or hands for at least 3 months or taking pain medication for neuropathic pain for at least 3 months
3. Bilateral distal symmetrical neuropathic pain confirmed by the DN4 questionnaire at screening visit
4. Bilateral distal symmetrical polyneuropathy confirmed by modified TCNS (mTCNS) > 5 at screening visit (Appendix 10.6).
5. Stable glycaemic control (HbA1c < 108mmol/mol)
6. Participants with a mean total pain intensity of at least 4 on an 11-point NRS during 1 week off pain medications.
7. Willing and able to comply with all the study requirements and be available for the duration of the study.

8. Willing to discontinue current neuropathic pain-relieving medications

9. Informed consent form for study participation signed by participant

6.2.2.2 OPTION-DM exclusion criteria

1. Non-diabetic symmetrical polyneuropathies

2. History of alcohol/substance abuse which would, in the opinion of the investigator, impair their ability to take part in the study

3. History of severe psychiatric illnesses which would, in the opinion of the investigator, impair their ability to take part in the study

4. History of epilepsy

5. Contraindications to study medications

6. Pregnancy/breast feeding or planning pregnancy during the study

7. Use of prohibited concomitant treatment that could not be discontinued with the exception of prior concomitant and safe use of selective serotonin reuptake inhibitors with study medications (duloxetine and/or amitriptyline)

8. Use of high dose morphine equivalent (>100mg/day)

9. Liver disease (aspartate transaminase/alanine aminotransferase >2 times upper limit of normal)

10. Significant renal impairment (eGFR <30mL/minute/1.73m2)

11. Heart failure New York Heart Association (New York Heart Association) ≥ class II
12. Clinically significant cardiac arrhythmias on 12 lead ECG or current history of arrhythmia
13. Patients with a recent myocardial infarction (<6 months prior to randomisation)
14. Postural hypotension (reduction of > 20mmHg on standing)
15. Prostatic hypertrophy or urinary retention to an extent which were, in the opinion of the investigator, be a contraindication to the study medication
16. Patients with other painful medical conditions where the intensity of the pain was significantly more severe than their diabetic peripheral neuropathic pain (patients were not be excluded if the pain was transient in nature)
17. Any suicide risk as judged by the investigator or as defined by a score of ≥2 on the suicide risk questionnaire
18. Significant language barriers which were likely to affect the participants understanding of the medication schedule or ability to complete outcome questionnaires
19. Concurrent participation in another clinical trial of an investigational medicinal product
20. Major amputations of the lower limbs

21. Foot ulcers, only if in the opinion of the local investigator they would have had a confounding/detrimental effect on study primary outcome or participation e.g. localised foot pain from the ulcer site

6.2.3 Study procedures

6.2.3.1 OPTION-DM study summary

A detailed description of the full OPTION-DM protocol is available elsewhere (Selvarajah et al., 2018), this section will provide a brief summary of the trial methods which are relevant to this study in the thesis.

The OPTION-DM study was a yearlong, multicentre, double-blind 3x3 Williams square crossover study of Treatment Pathways to evaluate the superiority of at least one treatment pathway (amitriptyline supplemented with pregabalin, duloxetine supplemented with pregabalin and pregabalin supplemented with amitriptyline) in reducing the 7-day average 24-hour pain in patients with painful-DSPN. Patients underwent three treatment pathways, each lasting 16-weeks and within each pathway the optimal dosing of the pharmacotherapy was achieved over several dosing visits.

Patients were initially commenced on monotherapy which was titrated over 6-weeks. If insufficient analgesia was not achieved with monotherapy, then combination therapy with a second agent commenced and titrated over a further 16-weeks, whereupon the therapies were tapered and withdrawn before commencing the next treatment pathway. Therefore, at the end of each pathway individual patients were taking monotherapy or combination

therapy. Monotherapy consisted of one of amitriptyline, duloxetine or pregabalin. Alternatively, if the patient was on combination therapy, they were taking either amitriptyline and pregabalin or duloxetine and pregabalin (Figure 6.1). At the week-16 follow-up visit, participants were advised to taper-down study medication (3 days) and stop the medication completely (4 days) before commencing the next treatment pathway. The taper dose was one dose level below the maximum tolerated dose. Participants on dose level 1 were required to stop study medication completely for 7 days.

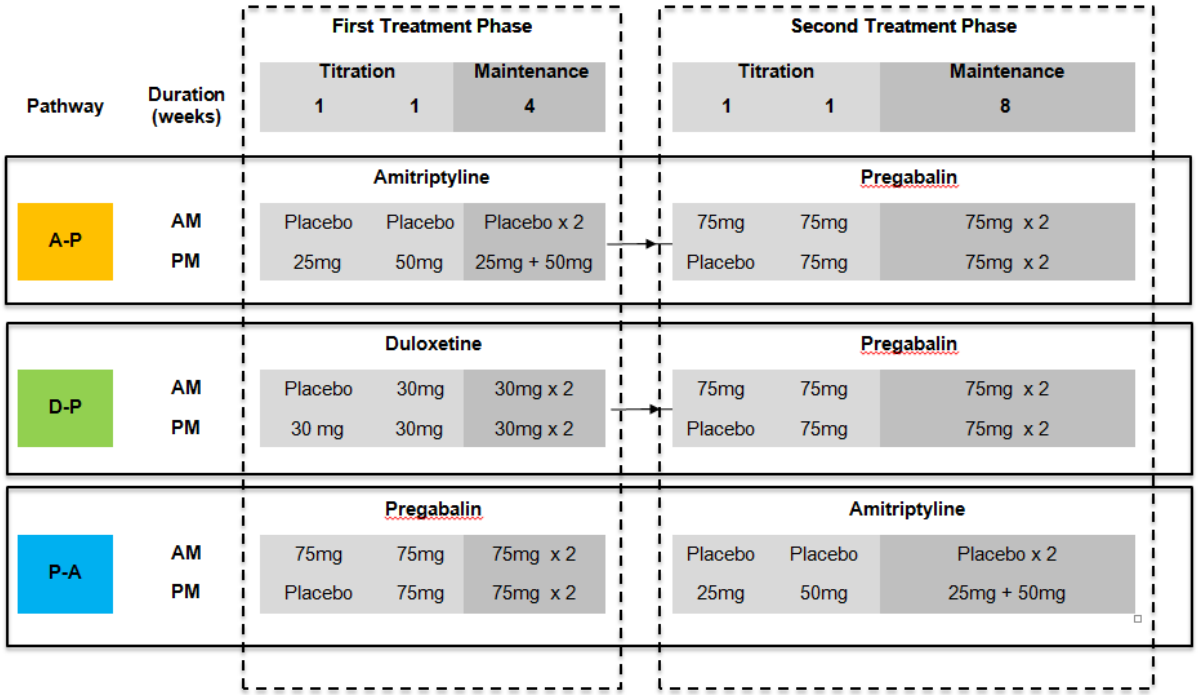

Figure 6.1. Dosing schedule for OPTION-DM. At the time of this sub-study participants were enrolled in any one of the three pathways: A-P (amitriptyline and pregabalin), D-P (duloxetine-pregabalin) or P-A (pregabalin-amitriptyline). Participants were titrated to the dose level in order to manage their pain adequately (Visual Analogue Score of pain <3/10), reproduced from (Selvarajah et al., 2018).

6.2.3.2 MRS sub-study procedures

This sub-study took place at the end of an OPTION-DM pathway, to ensure patients were on optimal analgesic therapy, to ensure uniformity and reduce the study burden on the patients. The MRI scans were performed on the study visit when patients were on optimal treatment (i.e. week-16 visit) and then a second scan when the medications had been washed out (Figure 6.2). The participants were under double-blind study conditions for the study.

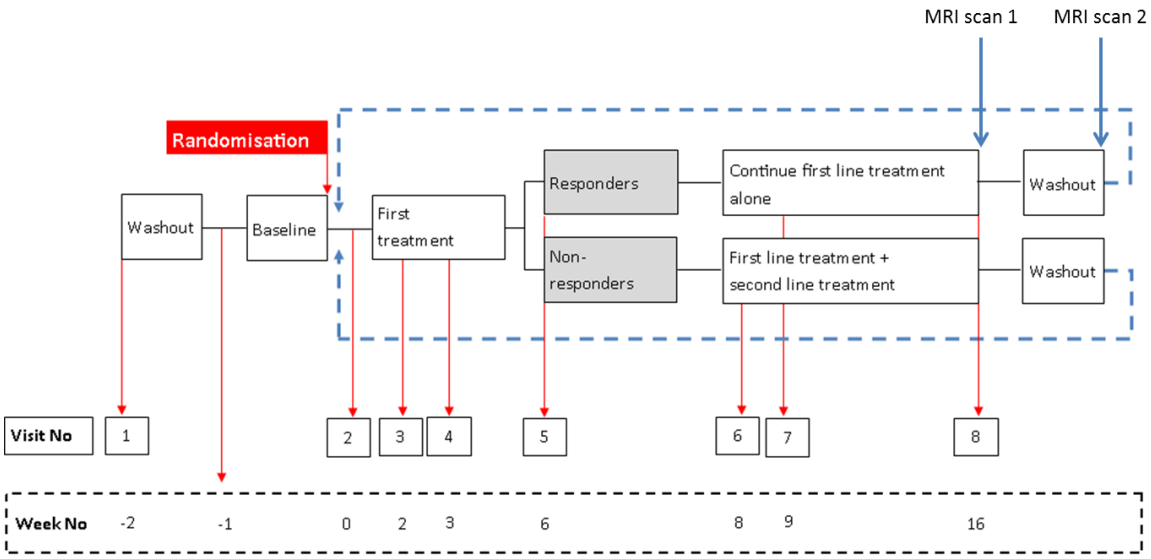

Figure 6.2. Protocol overview of OPTION-DM. Dosing and titration schedule for each pathway. Weeks 0-16 was repeated for each treatment pathway. The MRI scans were performed on week 16 of the final treatment pathway and one week subsequently after treatments had been washed out. Figure adapted from (Selvarajah et al., 2018).

6.2.4 Clinical and neurological assessment

Participants underwent a range of demographic, clinical, psychosocial, biochemical and neurological assessments as part of the OPTION-DM efficacy and safety analyses (Selvarajah et al., 2018). The assessments relevant for this study are included below:

- Clinical assessments: Height, weight, pulse rate and blood pressure.
- Neurological assessments: NPSI, mTCNS and DN4.
- Psychosocial assessments: Insomnia severity index (Morin et al., 2011), HADS (Zigmond and Snaith, 1983), EQ5D5L quality of life assessment (Herdman et al., 2011) and Pain Catastrophizing Scale (Sullivan et al., 1995).

During the visits for MRI scan 1 and 2, see Figure 6.2, the VAS scores for pain severity during the MRI were obtained.

6.2.5 Magnetic resonance spectroscopy protocol

6.2.5.1 GABA spectroscopy

Although GABA is the predominant inhibitory neurotransmitter within the brain it is still present at relatively low concentrations (Puts and Edden, 2012). Moreover, the GABA signal overlaps with other metabolites which are more abundant within the brain, obscuring the GABA signal. It is possible to tailor MRS experiments to specifically isolate GABA signals,

however. There are several methods to resolve the GABA signal, the most used is with spectral editing. The spectral editing procedure involves performing at least two MRS experiments, with and without frequency-selective pulses applied to the GABA signal, and subtracting the study without a frequency-selective pulse to isolate the GABA signal (Puts and Edden, 2012).

The MEGA-PRESS method is the most widely applied method for editing GABA signals, indeed this was the methods previously used within our group (Shillo, 2019). One limitation of such methods is that one molecule could only be targeted per scan with enough sensitivity, thereby limiting the number of molecules and brain regions measured per study (Chan et al., 2016). Therefore, the Hadamard Encoding and Reconstruction of MEGA-Edited Spectroscopy (HERMES) method was developed for dual editing to acquire more than two molecules simultaneously allowing increased signal to noise ratio compared to sequential measurements of individual molecules in the same total scan time (Chan et al., 2016). The main features of the HERMES method include: Hadamard-encoded combinations of editing pulse frequencies, which give a multiplexed experiment that simultaneously edits more than one molecule, and Hadamard reconstructions of the sub spectra, which give separate spectra for each molecule (Figure 6.3). HERMES has been successfully applied *in-vivo* to detect GABA signals (Saleh et al., 2016b, Chan et al., 2019).

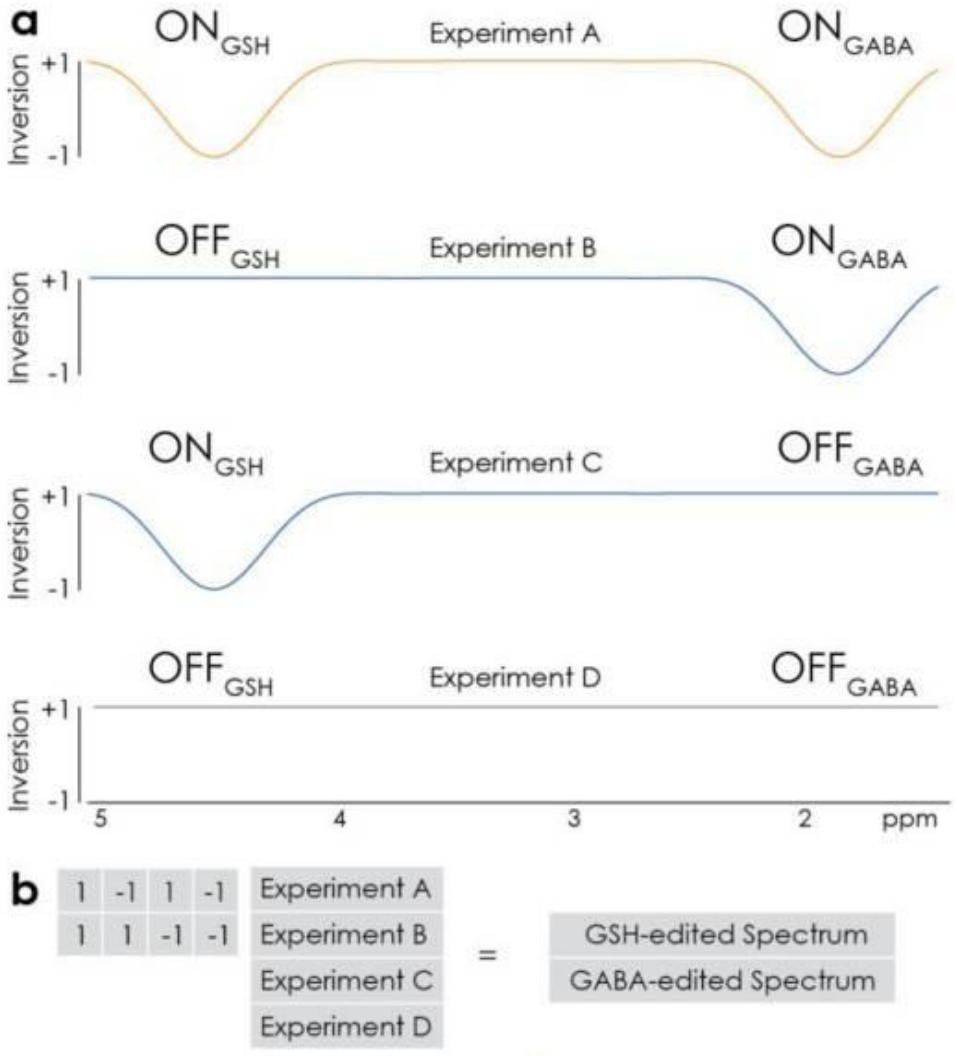

Figure 6.3. HERMES editing of GABA and glutathione (GSH). a) Inversion profiles of editing pulses applied in the four sub-experiments A-D. HERMES acquires all combinations of (ON_{GSH}, OFF_{GSH}) and (ON_{GABA}, OFF_{GABA}). b) Hadamard transformation of the sub-experiments yields the separate GSH- and GABA-edited spectra (Reproduced from (Saleh et al., 2016b)

6.2.5.2 Protocol for magnetic resonance spectroscopy acquisition

Magnetic resonance spectroscopy imaging was performed using the 3T scanner. Prior to MRS a T1 3D image was obtained for spectroscopic voxel localization (Figure 6.4). The voxel size was 35 x 40 x 20 mm^3 placed within the midline of the ACC to encompass the region

previously shown to have hyperperfusion in patients with painful-DSPN (Watanabe et al., 2018).

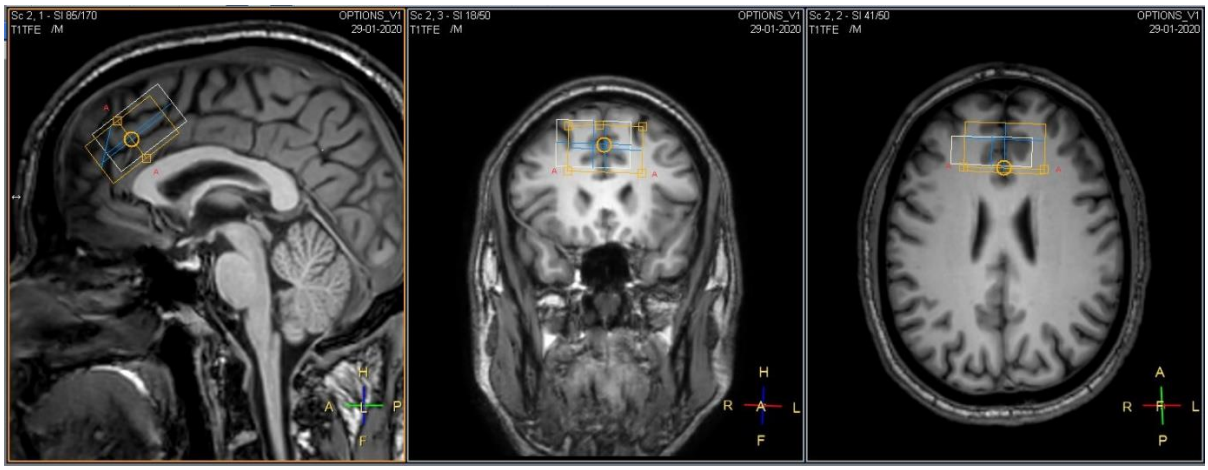

Figure 6.4. Voxel placement for the ACC MRS study.

The HERMES spectral editing method was used (Chan et al., 2016) with the following parameters: TE = 80ms; TR = 2000ms; spectral width = 2kHz; frequency selective pulse applied at 1.9 ppm (GABA); and 16 phase cycles and 320 dynamic scans were performed. The water signal was suppressed using the VAPOR method (Tkác et al., 1999).

6.2.5.3 Magnetic resonance spectroscopy data processing

Spectroscopic post-acquisition data was processed using the dedicated editing processing software pipeline Gannet (GABA-MRS Analysis Tool, Version 3.1) (Edden et al., 2014). Gannet is an open-sourced software coded within Matlab (The Mathwors, Natick, USA). It

has been designed for batch analysis of datasets with minimal user intervention specifically for GABA-edited MRS data. Although the process is automated the software provides pdf files at four steps for the user to judge the quality of the data.

The first output demonstrates the processed GABA-edited difference spectrum; the frequency of the maximum point in the spectrum plotted against time, giving quality information on the stability of the experiment; and the Cr signal before and after frequency and phase correction (Figure 6.5).

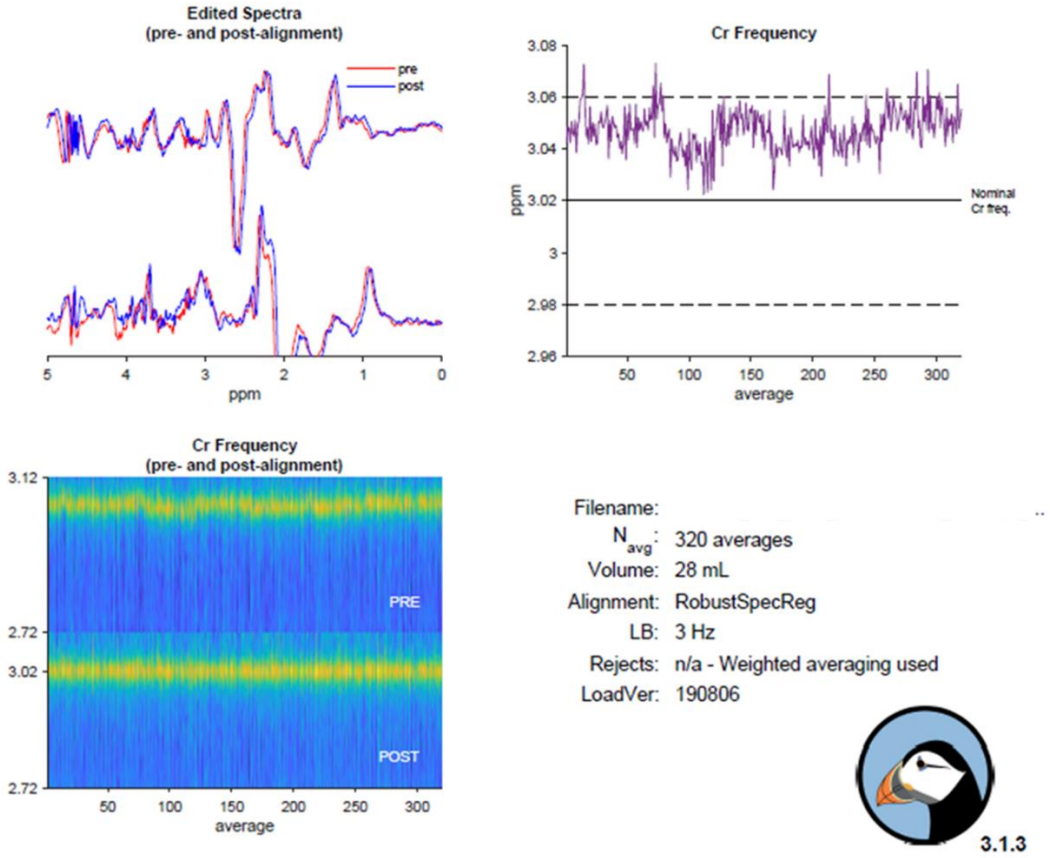

Figure 6.5. Gannet Load Output. The top-left plot demonstrates the processed GABA-edited difference spectrum with the red (pre) and blue (post) spectrum before and after frequency and phase correction. The top right plot gives quality information on the stability of experiment by showing the frequency of the maximum point in the spectrum (residual Cr signal) plotted against time. The bottom left plot demonstrates the Cr signal over the duration of the experiment, the upper half (pre) and lower half (post) shown the Cr signal before and after phase correction.

The second output demonstrates the modelling of the metabolite signal; the modelling of the signal against which the GABA is quantified; and the results of the fitting (Figure 6.6).

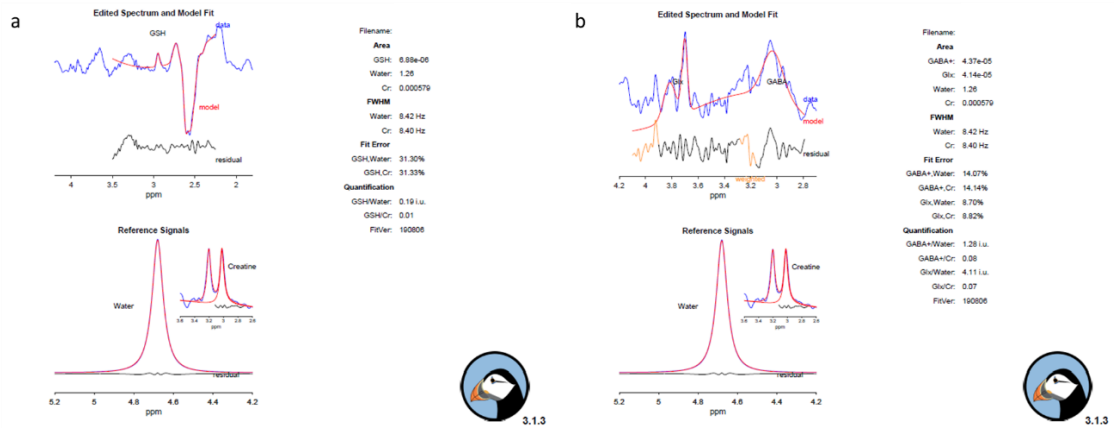

Figure 6.6. Gannet Fit Output. This output demonstrates the results of the modelling of the GSH (a) and GABA/Glx signal (b). The top left plot demonstrates the modelling of the GABA signal. The GABA-edited spectrum is shown in blue and the red overlay is the model of the best fit with the residual plot displayed in black. The bottom left output shows the modelling of the signal against which the metabolite is quantified. The right hand-panel contains the results of the fitting including: the integral area of the metabolite, water and Cr; the width of the fitted metabolite signal; and the metabolite concentration expressed in institutional units relative to water and as an integral ratio relative to Cr.

The third output registers the MRS voxel to the T1-weighted image (Figure 6.7).

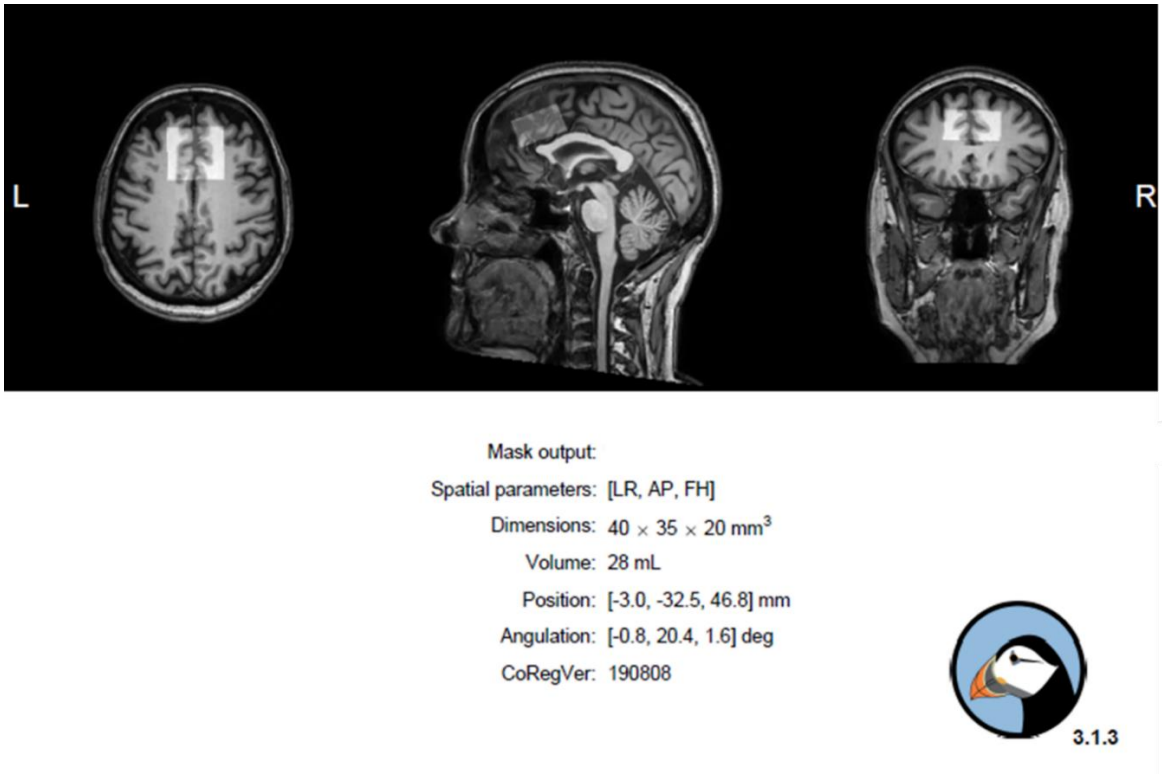

Figure 6.7. Gannet CoRegister Output. This output registers the MRS voxel (the highlighted area within the ACC) to masking software within Gannet. An image is developed with a mask of the MRS voxel with the same geometric parameters as the T1-weighted image.

The fourth and final output utilises the software toolkit Statistical Parametric Mapping version 12 [SPM12, Functional Imaging Laboratory (FIL), the Wellcome Trust Centre for NeuroImaging, Institute of Neurology, UCL, UK, https://www.fil.ion.ucl.ac.uk/spm/] (Figure 6.8). The T1-weighted image is segmented and uses these results to determine tissue fractions (grey matter, white matter and cerebrospinal fluid) for the voxel and the CSF-corrected neurometabolite estimate. These are the data used for the outcomes of the study, GABA/H_2O and Glx/H_2O.

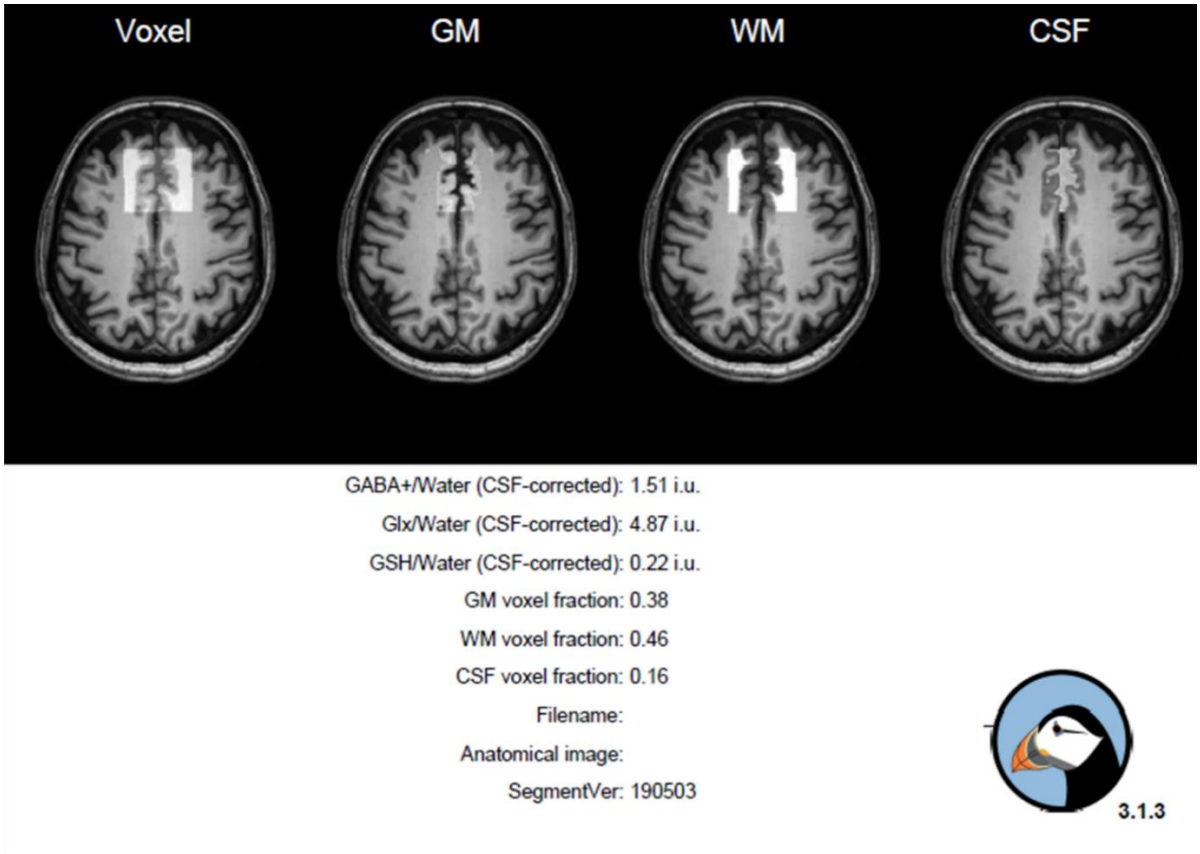

Figure 6.8. Gannet Segment Output. The top images indicate a single slice to show the voxel location and the fractions of grey matter (GM), white matter (WM) and cerebrospinal fluid (CSF). The below data panel provides the CSF-corrected metabolite concentrations, and the voxel tissue fractions.

6.2.6 Statistical Analysis

Statistical analysis was performed as per the general methods. Pairwise MRS data for pre- and post-scan variables were analysed using the paired Students t-test (parametric data) or Wilcoxon signed-rank test (non-parametric data).

After the initial analysis, participants were stratified into different subgroups. Firstly, patients were stratified into whether they had high baseline pain scores (VAS pain score ≥8) or low/moderate scores (VAS pain score ≤7) on the 11-point VAS. Subsequently, participants

were stratified according to whether they had at least a modest rise in pain scores from scan 1 to 2. A modest change in pain was defined as a pain difference of 2 or greater on the 11-point VAS. The differences in VAS pain scores and neurometabolite variables were compared between groups using students t-test. The visit 2 variable score was subtracted from the visit 1 score to determine the delta (Δ) of each variable. Finally, to explore whether there was any relationship between clinical and demographic variables and neurometabolite ratios a Pearson's correlation test was performed.

6.3 Results

6.3.1 Clinical, demographic and neurological variables

Recruitment into the study was halted early as a result of the COVID-19 pandemic. Therefore, 16 participants were recruited into the study. Four participants were then removed from the study analysis (1 patient as they were only able to complete one scan and 3 patients as the scan data was inadequate for analysis on visual inspection of Gannet output).

Table 6.1 summarises the clinical, demographic and neurological variables for study participants.

Variable	Mean value ± SD or Median (IQR)
Age (Years)	61.4 ± 9.5
Systolic blood pressure (mmHg)	140.7 ± 23.1
Body mass index (kg/m^2)	28.9 ± 4.1
Female sex (number (%)	1 (8.3%)
Type of Diabetes	Type 1 – 1 (6.25%) Type 2 – 14 (87.5%) MODY – 1 (6.25%)
Duration of Diabetes (Years)	9.5 (7.75)
HbA1c (mmol/mol)	62.6 ± 13.4
mTCNS	17.9 ± 7.3
DN4	6.5 ± 1.3
Baseline pain score (VAS)	7.9 ± 1.7
Neuropathic pain treatment	Pregabalin plus amitriptyline – 2 Duloxetine plus pregabalin – 2 Amitriptyline plus pregabalin - 2 Duloxetine monotherapy – 1 Amitriptyline monotherapy – 2 Pregabalin monotherapy - 3

Table 6.1. Clinical, demographic and neurological variables for study participants. The mean and SD (±), median and (IQR), and number and (percentage) are displayed. DN4, doleur neuropathique 4; mTCNS; Modified Toronto clinical neuropathy score; MODY, Maturity onset diabetes of the young; VAS, visual analogue score.

6.3.2 Neurometabolite variables

Table 6.2 demonstrates the pain scores on an 11-point Likert scale (0-10) VAS and neurometabolite results during visit 1, when patients were on maximal analgesia, and visit 2 after their analgesia had been withdrawn. As expected, the mean VAS pain scores rose significantly from 3.9 ± 2.2 to 6.3 ± 2.5 (students t-test, p=0.005). There were no changes in

adverse events, i.e. analgesia withdrawal symptoms, between scan 1 and 2 which might act as a confound for the study. However, for three individuals there was no change in the pain scores. Despite there being a significant change in pain scores between scans there was no accompanying significant difference in neurometabolite levels (Table 6.2).

	Scan 1	Scan 2	P value
Pain score (VAS)	3.9 ± 2.2	6.3 ± 2.5	**0.005**
GABA/H_2O	1.484 ± 0.521	1.579 ± 0.944	0.774
Glx/H_2O	4.415 (3.97)	4.215 (1.25)	0.480*
GABA/Glx	0.348 ± 0.172	0.398 ± 0.249	0.638*

Table 6.2. Pain scores and neurometabolite levels during scan 1 and 2 and pairwise group comparisons. The mean and SD (±) or median and (IQR) are displayed. Group comparisons were with paired Students t-test or Wilcoxon Signed Rank test (*). GABA, γ-aminobutyric acid; Glx, Glutamine and glutamate; VAS, visual analogue scale.

Participants were stratified into those with high baseline pain scores (VAS pain score ≥8; n=8) or low/moderate scores (VAS pain score ≤7; n=4). Although, there was a significant increase in mean VAS pain scores between Visit 1 and Visit 2 (i.e. increase in pain score from visit 2) in both two subgroups, there was no significant difference in neurometabolites profiles (Table 6.3).

	High baseline pain (n=8)	Low/moderate baseline pain (n=4)	P value
Δ pain score (VAS)	-3.5 ± 2.2	-0.25 ± 0.5	**0.004**
Δ GABA	-1.450 ± 1.309	0.005 ± 0.753	0.838
Δ Glx	1.249 ± 3.872	0.283 ± 2.180	0.657
Δ GABA/Glx	-0.472 ± 0.367	-0.0577 ± 0.241	0.960

Table 6.3. Δ of pain scores and neurometabolite levels in patients stratified according to baseline pain scores. High baseline pain was defined by a pain at baseline of 8 or greater and low baseline pain by a score of 7 or lower. The mean and SD (±) is displayed. The statistical test used was the students t-test. GABA, γ-aminobutyric acid; Glx, Glutamine and glutamate; VAS, visual analogue scale.

The participants were then grouped according to whether they had at least a modest pain rise from scan 1 to scan 2 (Table 6.4). There were 6 patients each in the two groups. There was a significant difference in the Δ VAS pain score between groups, but not in any of the neurometabolite levels.

	Modest or greater change in pain (n=6)	Small change in pain (n=6)	P value
Δ pain score (VAS)	-4.3 ± 1.86	-0.50 ± 0.5	**0.003**
Δ GABA	0.202 ± 1.109	-0.392 ± 1.144	0.383
Δ Glx	1.022 ± 4.335	0.8317 ± 2.351	0.927
Δ GABA/Glx	0.049 ± 0.292	-0.150 ± 0.338	0.300

Table 6.4. Δ of pain scores and neurometabolite levels in patients stratified according to degree of change in pain from scan 1 to scan 2. A modest change in pain was defined by a change in pain by 2 points or greater changes on 11-point VAS and a small change in pain as 1 or 0 points. The mean and SD (±) is displayed. The statistical test used was the students t-test. GABA, γ-aminobutyric acid; Glx, Glutamine and glutamate; VAS, visual analogue scale.

6.3.3 Correlation analysis

There was no relationship found between metabolite ratios and pain scores during scan 1. For scan 2, there was a correlation seen between GABA/Glx and pain scores (Pearson's correlation, *r* -606, p=0.037), see Figure 6.9. There was also a relationship between Glx/H_2O and pain scores (*r* 0.592, p=0.042), see Figure 6.10. There was also no correlation between neurometabolites during either scan and demographic, clinical and neurological measures.

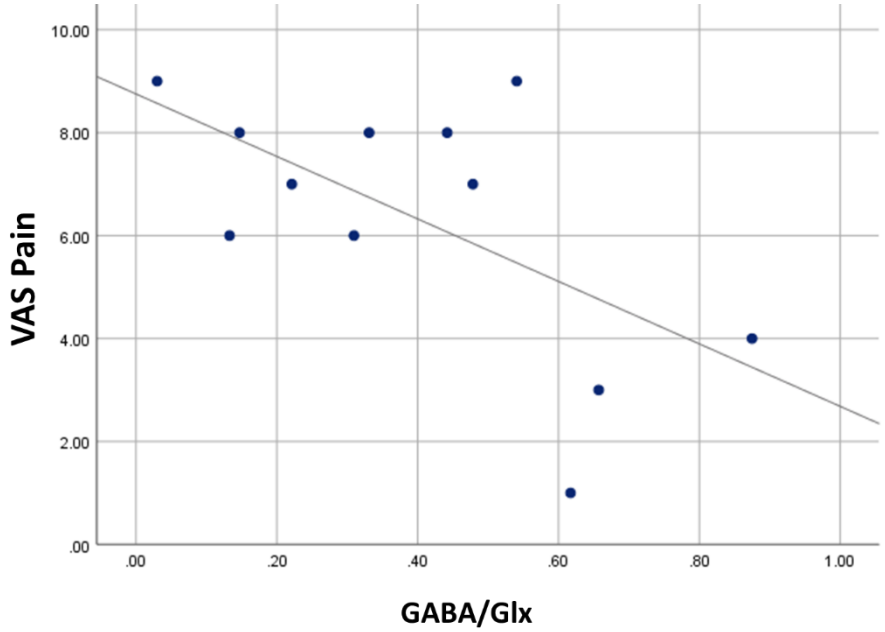

Figure 6.9. Pearson's correlation between scan 2 VAS Pain score and GABA/Glx in the ACC (r -606, p=0.037). ACC, anterior cingulate cortex; GABA, γ-aminobutyric acid; Glx, Glutamine and glutamate; VAS, visual analogue scale.

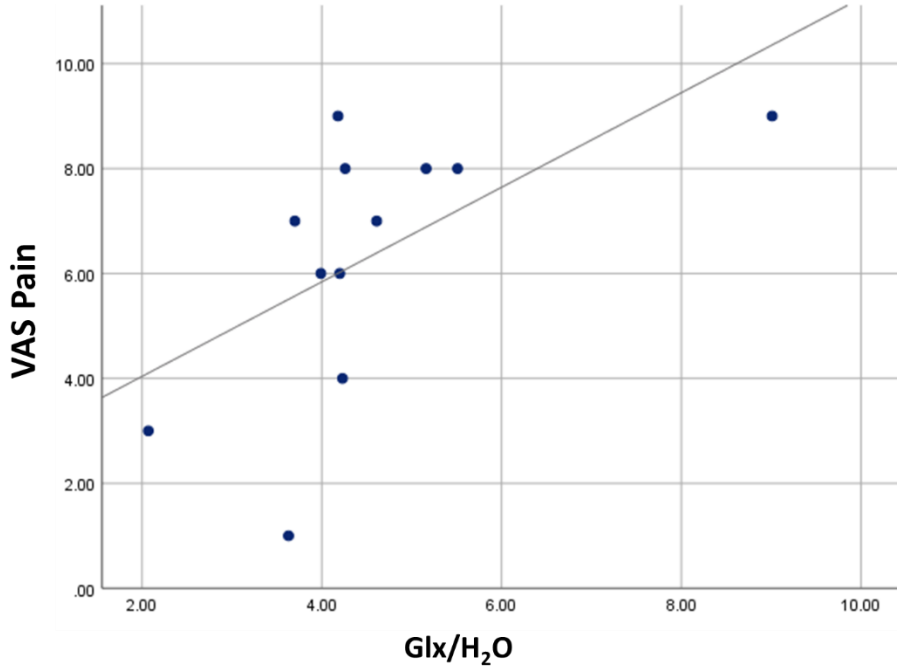

Figure 6.10. Pearson's correlation between scan 2 VAS Pain score and Glx/H_2O in the ACC (r 0.592, p=0.042). ACC, anterior cingulate cortex; Glx, Glutamine and glutamate; VAS, visual analogue scale.

6.4 Discussion

In this study, the impact of treatment on excitatory and inhibitory neurotransmitters within the ACC was examined in patients with painful-DSPN. Despite there being a significant difference in pain scores when patients were on (Scan 1) vs. off (Scan 2) medications, there were no significant differences in MR spectroscopic measures of neurotransmitter profiles. The difference in pain scores between scan 1 and 2 was not uniform among the patients; therefore, individuals were also then stratified into different subgroups: low/moderate (VAS 8≥) vs. high (VAS 8≤) baseline mean VAS pain score; and modest change in pain from between study visits (Δ VAS ≥2) or small change in pain (Δ VAS <2). There were no significant differences when patients were stratified into these subgroups. There was a significant

negative correlation between pain scores and GABA/Glx and Glx/H_2O after analgesia was withdrawn during scan 2.

GABA and glutamate are the two main signalling molecules within the brain (Harris and Clauw, 2012). Both neurotransmitters are involved in the regulation of nociceptive transmission and pain (Goudet et al., 2009). GABA is the major inhibitory neurotransmitter in pain, with receptors distributed widely throughout the brain and spinal cord (Harris and Clauw, 2012). The impact of acute and chronic pain on GABA and Glx levels in the brain is disputed. Under experimental application of pain in HV Glx has been shown to increase in various regions of the brain (Mullins et al., 2005, Cleve et al., 2015), including at the ACC (Archibald et al., 2020a). However, both increases and decreases have been shown in GABA with application of experimental pain (Archibald et al., 2020a). Further, there is considerable uncertainty as to the precise role of GABA and Glx measured using MRS in different chronic pain conditions within different regions of the brain. A meta-analysis in 2020 sought to determine GABA and Glx concentrations across pain conditions compared to pain-free controls (Peek et al., 2020). The results were not uniform, although Glx levels were elevated in some chronic pain syndromes; however, GABA was shown to be reduced in some, but not all studies. Additionally, a previous spectroscopy study in DSPN reported elevated Glx and lower GABA levels at the posterior insula in 7 participants with DSPN and sensory symptoms compared with HV (Petrou et al., 2012). There were no differences at the ACC; however, the study was limited with a small sample size and lack of a diabetes comparator groups as it is unclear whether these changes are due to diabetes, DSPN or neuropathic pain. It is therefore possible, that the results of this study are a true negative and ACC GABA and Glx are unaltered by painful-DSPN treatments.

A limitation of the study is the small sample size. The recruitment into the study had to be halted early as a result of the COVID-19 pandemic. Unfortunately, therefore only 16 participants were recruited into the study and only 12 patients had adequate data available for final statistical analysis. Another potential limitation of the study was the timing of the scans. This was a hypothesis generating opportunistic study, and as such the scans were performed at the end of a pathway in the OPTION-DM study and were one week apart. There was a statistically and clinically significant increase in VAS pain scores in participants undergoing scan 1. However, in 6 individuals there was no change in pain score or the change was minimal (1 point on an 11-point VAS). Therefore, examining mean differences in neurochemical alterations may not reflect a true difference. An alternative approach would have been to, scan patients at week-0 and again at Week 6 (when treatment was established, see Figure 6.2).

The removal of 3 patients from the final analysis due to inadequate scan data highlights another potential limitation in the study, the accuracy of the MRS spectra acquisition and analysis. GABA quantification is known to be challenging due to the presence of overlapping strong signals; coupled spin systems; and low cerebral concentration (Puts and Edden, 2012). The HERMES spectral editing method has been shown to be an efficient and reliable means to measure cerebral neurometabolites at 3T (Chan et al., 2016). However, the reproducibility is adequate but not perfect. A reproducibility study demonstrated a 16.7% coefficient of variation in measuring GABA levels using HERMES, and similar MR protocols and data analysis (Gannet) to this study, at the dorsal ACC in 12 HV (Prisciandaro et al., 2020). The coefficient of variation for Glx was 6.36%.

The Gannet processing tool is well established, but there is still variation among scans. The coefficient of variation across 10 HV in the initial publication describing the Gannet toolkit ranged from 11% in the occipital region to 17% in the dorsolateral prefrontal region (Edden et al., 2014). Further studies have found the coefficient of variation to range between 12-22% for the Gannet toolkit (Saleh et al., 2016a, Mikkelsen et al., 2017). In the study in this thesis, the percentage difference in neurometabolite levels between scan 1 and 2 was relatively low, e.g. GABA 6.1% and Glx 10.5% Even with large study numbers there is a large variation in HERMES and Gannet, so given that the study group numbers were small it may not have been possible to identify significant group differences. However, the study was hypothesis generating and correlation results do suggest that ACC Glx levels could be a tool to track pain.

6.5 Conclusions

In this pre-post sub-study of OPTION-DM, a neuropathic pain trial to determine the most efficacious pathway for the treatment of painful-DSPN, it was demonstrated that there were no differences in cerebral neurometabolites (GABA and Glx) in the ACC in patients whilst they were maximally controlled for neuropathic pain compared with after withdrawal of analgesia. However, the study did demonstrate that excitatory neurotransmitter levels Glx correlated with pain severity after analgesia had been withdrawn. This finding is consistent with the finding that elevated cerebral Glx has been observed in other chronic pain conditions and during application of experimental heat pain. It is unclear as to whether the lack of statistical difference in Glx and other neurometabolites between scan 1 and 2 is a

true negative or a false one due to methodological issues such as MRS acquisition and analysis error, sample size and scan timing.

This study indicates that the use of GABA and Glx are currently unsuitable for use as biomarkers of neuropathic pain in diabetes. However, further exploration of these measures in painful-DSPN is warranted in view of the finding of Glx and GABA/Glx correlating with pain severity. Although previous studies have demonstrated no difference in Glx levels between participants with and without painful-DSPN at various cerebral regions, including the ACC, no adequately powered study has examined neurometabolite levels at the ACC in painful-DSPN. Initially, a cross-sectional study comparing a painful-DSPN group versus HV, no-DSPN and painless-DSPN would be necessary.

7. The impact of optimised neuropathic pain treatment on the magnetic resonance imaging correlates of painful-DSPN 2: Functional connectivity

7.1 Introduction

7.1.1 Background

It is now well recognised that the CNS plays an important role in the pathogenesis and maintenance of the chronic pain state. Alterations in functional connectivity between key brain regions involved with nociception have been shown to determine clinical pain phenotype, treatment response and transformation from the acute to the chronic pain state (Wilkinson et al., 2020, Sloan et al., 2021, Teh et al., 2021). Apkarian et al. performed a systematic review and meta-analysis to determine the brain areas constituting the network for pain perception (Apkarian et al., 2005). The areas which were identified included the primary and secondary somatosensory cortex, insular cortex, ACC, prefrontal cortex and thalamus (Figure 7.1). The brain network involved in chronic pain is at least partially distinct from those involved in acute pain, with cognitive and emotional areas potentially playing a more prominent role in the former. Similar to the rest of the nervous system, there is a shift towards excitation and reduced inhibition of pain signals in the brain in chronic pain states (Colloca et al., 2017). Indeed, there is neuronal hyperexcitability in nociceptive pathways and ion channel alterations in higher brain regions in experimental neuropathic pain (Keller et al., 2007, Taylor et al., 2017, Rosenberger et al., 2020). Neuronal activity can be examined

using MR techniques, which have also been applied to the study of cerebral alterations in painful-DSPN.

A commonly used MR technique in pain research for examining neuronal activity is fMRI (Morton et al., 2016). This provides an indirect measure of neuronal activity linked to cognitive processes and has been widely used to examine areas of the brain during acute and chronic pain states (Apkarian et al., 2005). There are two applications of fMRI, task based and Resting State fMRI. In task-based fMRI experiments, neuronal activity is examined in response to an external stimulus e.g. visual or nociceptive stimulation. The technique that will be used in this study is rs-fMRI which examines brain activity at rest and can be used to determine the interaction, or functional connectivity, of different brain regions. Two recent studies have explored alterations in somatosensory network functional connectivity in painful-DSPN. Teh et al. demonstrated that individuals with IR-painful-DSPN, characterised by neuronal hypersensitivity and relatively preserved function, had greater thalamic-insular cortex and reduced thalamic-S1 cortical functional connectivity compared with the NIR-group (Teh et al., 2021). They also demonstrated that responders to intravenous lidocaine treatment had greater functional connectivity between the insular cortex and corticolimbic circuitry compared to non-responders (Wilkinson et al., 2020). However, these studies have not examined changes in neuronal functional connectivity of nociceptive brain regions before and after neuropathic pain treatments. Other studies have explored this in different conditions, such as complex regional pain syndrome, and found altered functional connectivity in regions involved in descending pain modulation (Erpelding et al., 2016) and from the amygdala (Simons et al., 2014).

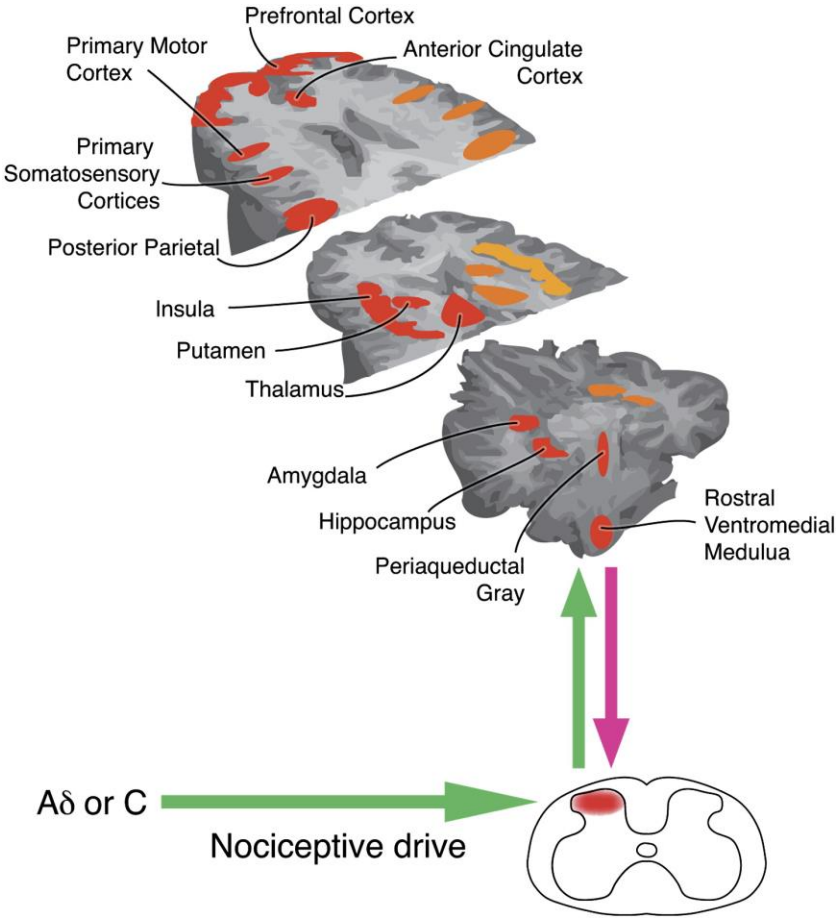

Figure 7.1. Main brain regions that activate during a painful experience, highlighted as bilaterally active but with increased activation on the contralateral hemisphere (orange), reproduced from (Tracey and Mantyh, 2007).

7.1.2 Rationale for study

A series of studies have demonstrated altered cerebral structure and function in painful-DSPN. However, the response of functional connectivity of these brain regions to analgesia has not been studied in painful-DSPN. Alterations in rs-fMRI functional connectivity have been shown to predict treatment responses in painful-DSPN, but the direct effects of treatments have not been explored. Therefore this study will examine alterations in functional connectivity before and after treatment to identify CNS biomarkers of pain relief in painful-DSPN.

7.1.3 Aims and hypothesis

The aim of the study was to perform a rs-fMRI experiment in patients with painful-DSPN, to determine differences in neuronal functional connectivity between participants on neuropathic pain treatment and after these had been discontinued. The hypothesis is that there will be increased functional connectivity in nociceptive brain regions after withdrawal of treatment and that patients with a greater increase in pain (i.e. responders to treatment) following treatment discontinuation will have greater changes in functional connectivity.

7.2 Methods

7.2.1 Study Design and Participants; inclusion and exclusion criteria; procedures; clinical and neurological assessments

The study design, methods and participants were the same as described in sections 6.2.1 to 6.2.4 in Chapter 6. However, the imaging modality analysed in these participants was rs-fMRI rather than MRS.

7.2.2 Resting State Functional MRI protocol

7.2.2.1 Rationale for using Resting-State functional MRI

Functional MRI (fMRI) is a class of imaging methods developed in order to demonstrate regional and temporal alterations in brain metabolism (Glover, 2011). There are alterations in neural activity which occur during task-based cognitive state changes or during unregulated processes during the resting brain, or the 'resting state'. Neuroimaging can identify increased neural activity by increased local cerebral blood flow, e.g. positron emission tomography and arterial spin labelling, and changes in oxygenation concentration (Glover, 2011). The latter, termed BOLD contrast is the contrast used in virtually all conventional fMRI experiments and is what was used in this study. BOLD contrast can be used to non-invasively measure in real time blood oxygenation levels within the brain in response to alterations in cerebral metabolism/blood flow (Ogawa et al., 1990). This is possible because of the different magnetic properties of oxygenated and deoxygenated haemoglobin. Oxygenated haemoglobin is diamagnetic, i.e. repelled by an applied magnetic field; whereas deoxygenated blood is highly paramagnetic, i.e. attracted by an applied magnetic field, due to its four unpaired electrons. Therefore, local endogenous gradients in magnetic fields, which are dependent upon haemoglobin concentration, modulate blood T2 and T2* relaxation times (Glover, 2011). In response to increased neural activity, increased blood flow causes an increased BOLD signal due to increased oxygenated haemoglobin supply.

There are two commonly used fMRI techniques, task-based fMRI, where participants are instructed to perform specific tasks and evaluate functional domains within the brain

(Smitha et al., 2017). In clinical pain trials, this task might involve the application of experimental heat pain during the fMRI acquisition (Selvarajah et al., 2019). The other technique is rs-fMRI, whereby spontaneous BOLD signals in the absence of explicit tasks/input are analysed (Smitha et al., 2017). Although resting state signals are generally low frequency fluctuations, the activity is greater than task-based signalling and the signal to noise ratio is better.

Resting State-fMRI is used to determine the functional connectivity between two spatial regions of interest. Functional connectivity is defined as the temporal dependence of neuronal activity patterns of anatomically separated brain regions (van den Heuvel and Hulshoff Pol, 2010). The connectivity between two brain regions is inferred based on correlations of parameters of neuronal activity with the assistance of an fMRI time series, see Figure 7.2 for a schematic illustration (Smitha et al., 2017).

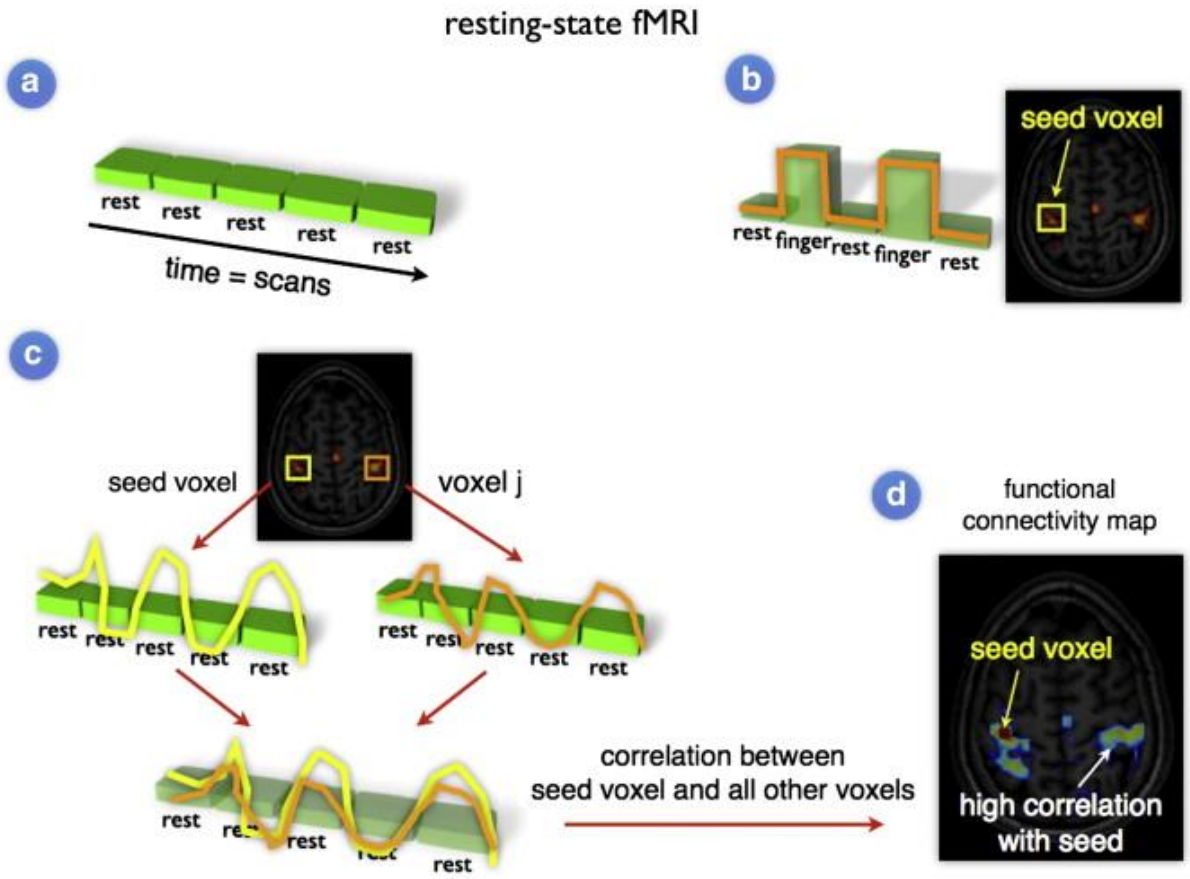

Figure 7.2 Schematic illustration of Resting-State fMRI. (a) BOLD fMRI signals are acquired throughout an experiment when the participant is at rest and asked to think of nothing. (b) Conventional task-dependent fMRI whereby a participant is asked to alternate between resting (rest) and perform a task, e.g. tapping a finger (finger), this can be used to aid selection of a seed. (c) The resting-state time-series of a seed voxel is correlated with the resting-state time-series in region j, a high correlation reflects high functional connectivity between these regions. (d) The time-series of the seed voxel can be correlated to the time-series of all other voxels within the brain, leading to a functional connectivity map reflecting the regions showing a high level of functional connectivity within a selected seed region. Figure reproduced from (van den Heuvel and Hulshoff Pol, 2010).

A commonly used technique for functional connectivity rs-fMRI analysis is 'Seed-based analysis'. This is a method in which a 'seed', or ROI, is selected and a linear correlation of this region is compared with other voxels, yielding a seed-based functional connectivity map. A typical chart showing the processing of seed-based functional connectivity analysis is displayed in Figure 7.3, reproduced from (Smitha et al., 2017). Rather than individual seeds

this study will use ROI-to-ROI measures to characterize the connectivity between pairs of ROIs among a pre-defined set of regions (Whitfield-Gabrieli and Nieto-Castanon, 2012).

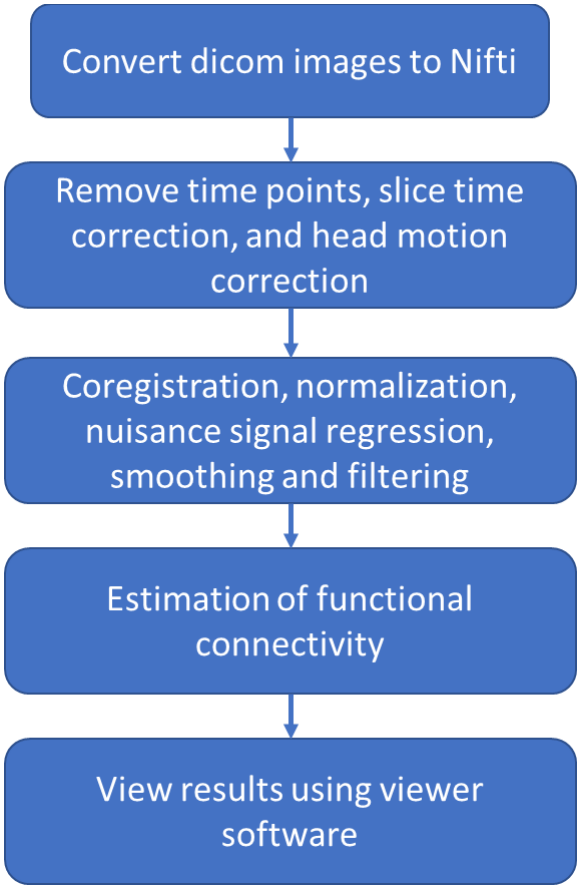

Figure 7.3. Flow chart representing the fundamental steps involved in rs-fMRI analysis using a seed-based technique (Smitha et al., 2017). Nifti, Neuroimaging Informatics Technology Initiative file.

There are benefits of fMRI in comparison to other means of performing functional assessments of the brain. Functional MRI is non-invasive and does not use radiation/radioisotopes and it provides relatively high spatial resolution and can provide anatomical scans for region of interest localization (Glover, 2011). However, like other MR modalities there are trade-offs between acquisition speed, resolution, signal to noise ratio,

signal dropout and contrasts. Moreover, acquiring resting state network data can be confounded by the scanning environment, e.g., loud noise and anxiety during the scan.

7.2.2.2 Resting State fMRI study acquisition

The acquisition and analysis protocol were similar to previous study within the research group (Wilkinson et al., 2020, Teh et al., 2021). Whilst laid supine within the MRI, individuals were asked to fixate upon a cross directly in front of them and not to think about anything, but to remain awake. A 6-minute rs-fMRI sequence was acquired using a T2*-weighted pulse sequence with in-plane pixel dimensions of 1.8mm x 1.8mm and contiguous trans axial slice thickness of 4mm orientated in the oblique axial plain, covering the whole cerebral cortex (TE=35ms, TR=2,600ms).

7.2.2.3 Resting State fMRI study analysis

The rs-fMRI data was analysed using the Functional connectivity analysis performed with the Neuroimaging Tools & Resource Collaboratory Functional Connectivity (CONN) Toolbox 18.b (www.nitrc.org/projects/conn)(Whitfield-Gabrieli and Nieto-Castanon, 2012) and SPM8 (Wellcome Centre for Human Neuroimaging, London, U.K.) in MATLAB 2014a (MathWorks, Natick, MA). CONN performs pre-processing to identify and remove confounds in the BOLD signal to prevent physiological noise and motion artefact in the data (Wilkinson et al., 2020, Teh et al., 2021). Fisher transformation converts correlation coefficients to normally distributed scores to allow second-level general linear model analysis. CONN created

subject-specific ROI files for the twenty-one ROIs and registered them to the subject space. The twenty-one ROIs involved in somatosensory and nociception were chosen: the anterior cand posterior cingulate gyrus; and the left and right thalamus, caudate, putamen, amygdala, accumbens, S1, M1, insular and frontal orbital cortex, and the Default Mode Network. Functional connectivity measures were computed between ROIs for ROI-to-ROI analysis to create ROI-to-ROI connectivity. The significant ROI-to-ROI connections were determined by $p<0.05$ following false-positive control (false discovery rate).

7.2.3 Statistical Analysis

Statistical analysis was performed as per the general methods. Paired t-tests were used to compare clinical and rs-fMRI data obtained during scan 1 and 2. In addition, z values of functional connectivity were correlated to other variables using Pearson correlation for normally distributed data and Spearman Rank correlation for non-normally distributed data (Wilkinson et al., 2020, Teh et al., 2021). The z-score was more appropriate than the magnitude of difference because it also considers the variance in the signal.

After the initial analysis, participants were stratified into various subgroups; firstly, into high baseline pain scores (VAS pain score ≥8) or low/moderate scores (VAS pain score ≤7) on the 11-point VAS. Other subgroups included Treatment Pathway, use monotherapy or combination therapy at Scan 1, type of diabetes, sex, age and presence of HTN.

7.3 Results

7.3.1 Clinical, demographic and neurological variables

All 15 of the participants who completed two scans were included within the analysis.

Clinical, demographic and neurological variables are displayed in Table 7.1.

Variable	**Mean value ± SD or Median (IQR)**
Age (Years)	62.1 ± 9.0
Systolic blood pressure (mmHg)	141.0 ± 20.6
Body mass index (kg/m^2)	30.5 ± 5.7
Female sex [number (%)]	2 (13.3%)
Type of Diabetes	Type 1 – 1 (6.66%) Type 2 – 13 (86.66%) MODY – 1 (6.66%)
Duration of Diabetes (Years)	11.0 (7.0)
HbA1c (mmol/mol)	65.3 ± 16.2
mTCNS	18.6 ± 7.3
DN4	6.5 ± 1.2
Baseline pain score (VAS)	7.9 ± 1.9
Neuropathic pain treatment	Pregabalin plus amitriptyline – 4 Duloxetine plus pregabalin – 2 Amitriptyline plus pregabalin - 3 Duloxetine monotherapy – 1 Amitriptyline monotherapy – 2 Pregabalin monotherapy – 3

Table 7.1 Clinical, demographic and neurological variables for study participants. The mean and SD (±), median and (IQR), and number (percentage) are displayed. DN4, doleur neuropathique 4; mTCNS; Modified Toronto clinical neuropathy score; MODY, Maturity onset diabetes of the young; VAS, visual analogue score.

7.3.2 fMRI results

There was a significant rise in NRS scores from scan 1 to scan 2 from 4.0 ± 2.1 (mean ± SD), to 6.1 ± 2.4 (p=0.044, paired t-test). There were no changes in adverse events, i.e. analgesia withdrawal symptoms, between scan 1 and 2 which might act as a confound factor for the study. Comparing the functional connectivity in scan 1 compared with scan 2 (Scan 2 > Scan 1); there was a significantly greater functional connectivity between the left thalamus and S1 (S1 r β -0.27, seed-level correction -3.57, *p*-FDR 0.041) and the left thalamus and Insular Cortex (S1 r β -0.18, seed-level correction -3.43, *p*-FDR 0.041). Figure 7.4 shows the change in functional connectivity between the left thalamus and S1 cortex, and 7.5 left thalamus and insular cortex, in scan 1 and 2.

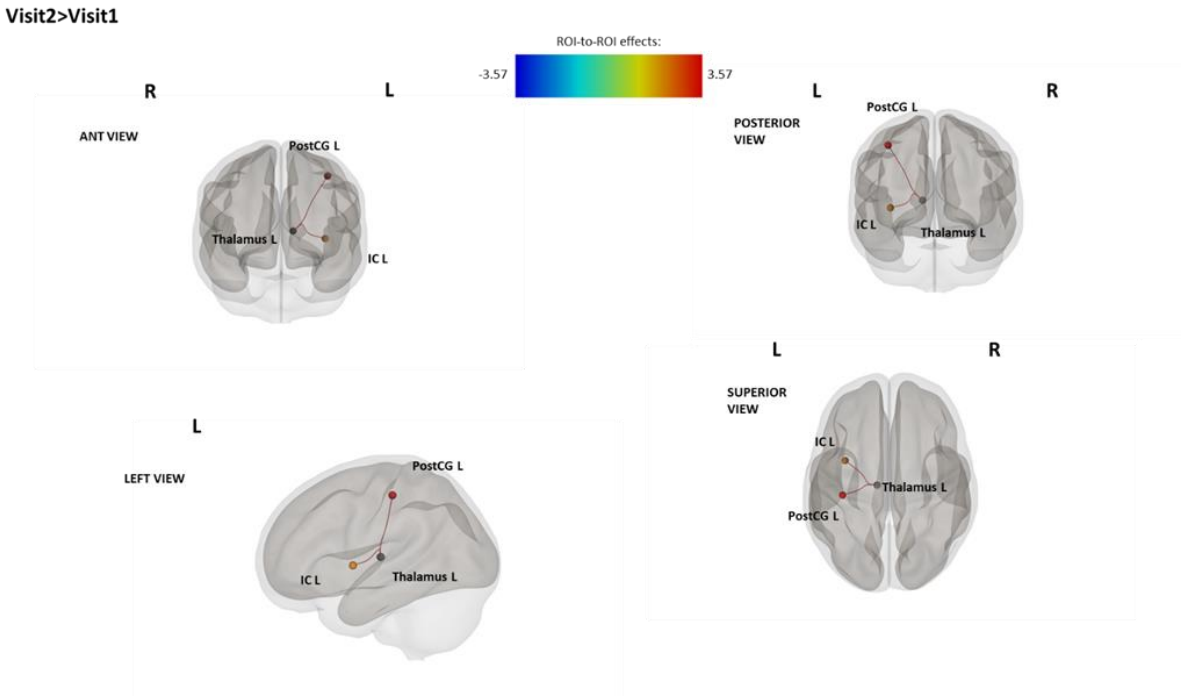

Figure 7.3. Difference in Resting-State functional connectivity between Scan 1 and Scan 2 (Scan 2 > Scan 1). Red to blue = positive to negative z-scores. IC, Insular Cortex; Post CG, primary somatosensory cortex.

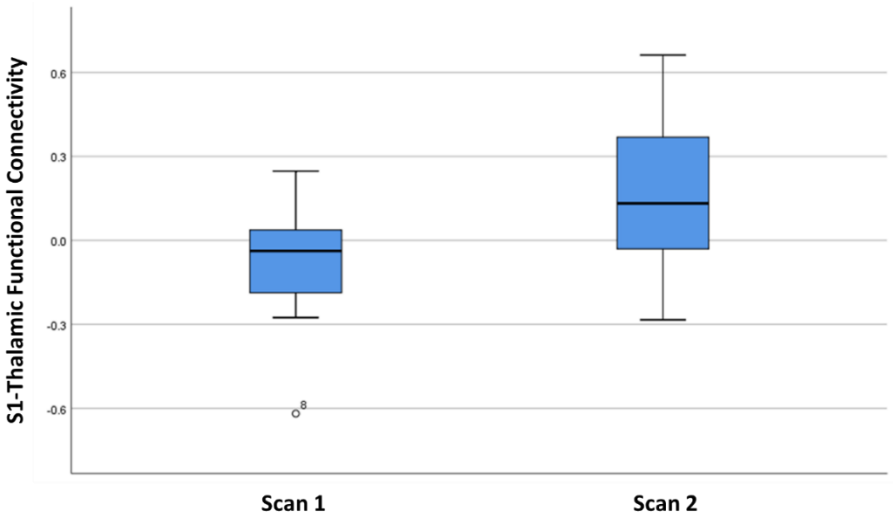

Figure 7.4. Effect size in mean S1-Thalamic functional connectivity in Scan 1 and Scan 2 (p=0.003, uncorrected paired t-test).

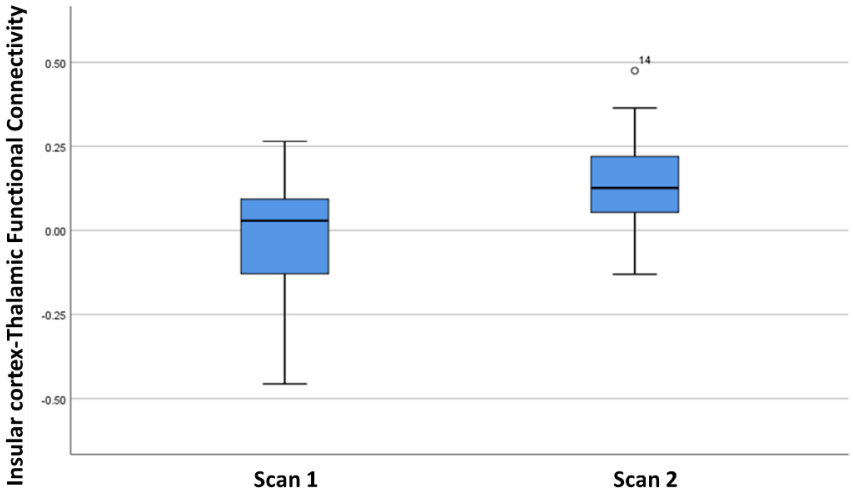

Figure 7.5. Effect size in mean Insular cortex-Thalamic functional connectivity in Scan 1 and Scan 2 (p=0.004, uncorrected paired t-test).

Correlation analysis was performed between the change in S1-Thalamic and Insular cortex-Thalamic functional connectivity between scan 1 and 2 (Δ) and pain variables, shown in Table 7.2 and 7.3, respectively.

Δ S1-Thalamic functional connectivity	r	P value
Baseline NRS pain score	-0.585	**0.022**
NRS Scan 1	0.154	0.584
NRS Scan 2	-0.303	0.173
NRS Scan 1 – Baseline NRS	-0.513	**0.050**
NRS Scan 1 – NRS Scan 2	0.475	0.074
Duration painful-DSPN	-0.489	0.064
Total NPSI	-0.597	**0.019**
Total burning NPSI subscore	-0.442	0.099
Total pressing NPSI subscore	-0.013	0.962
Total paroxysmal NPSI subscore	-0.578	**0.024**
Total evoked pain NPSI subscore	-0.187	0.504
Total dysaesthesia NPSI subscore	-0.191	0.496

Table 7.2. Pearson's correlation between Δ S1-Thalamic functional connectivity and pain variables. NPSI, neuropathic pain symptom inventory; NRS, numeric rating scale; S1, primary somatosensory cortex.

There were significant correlations between Δ S1-Thalamic functional connectivity and measures of neuropathic pain, including: baseline NRS score (Pearson's correlation r -0.585, p=0.022) see Figure 7.6., NRS Scan 1 – Baseline Scan (r -0.513, p=0.050), Total NPSI (r -0.597, p=0.019) and the Total burning NPSI subscore (r -0.578, p=0.024). There was also a trend towards a correlation between Δ S1-Thalamic functional connectivity and the duration of painful-DSPN (r -0.489, p=0.064) and the NRS Scan 1 – NRS Scan 2 (r 0.475, p=0.074).

Δ Insular cortex-Thalamic functional connectivity	r	P value
Baseline NRS	0.240	0.388
NRS Scan 1	0.353	0.197
NRS Scan 2	0.100	0.723
NRS Scan 1 – Baseline NRS	-0.121	0.688
NRS Scan 1 – NRS Scan 2	0.087	0.759
Duration painful-DSPN	0.235	0.399
Total NPSI	-0.077	0.784
Total burning NPSI subscore	-0.436	0.105
Total pressing NPSI subscore	0.042	0.882
Total paroxysmal NPSI subscore	-0.145	0.605
Total evoked pain NPSI subscore	0.239	0.392
Total dysaesthesia NPSI subscore	0.295	0.287

Table 7.3. Pearson's correlation between Δ Insular cortex-Thalamic functional connectivity and pain variables. NPSI, neuropathic pain symptom inventory; NRS, numeric rating scale.

There were no correlations between Δ Insular cortex-Thalamic functional connectivity and pain variables with only a trend towards a correlation with mTCNS (r 0.469, p=0.078).

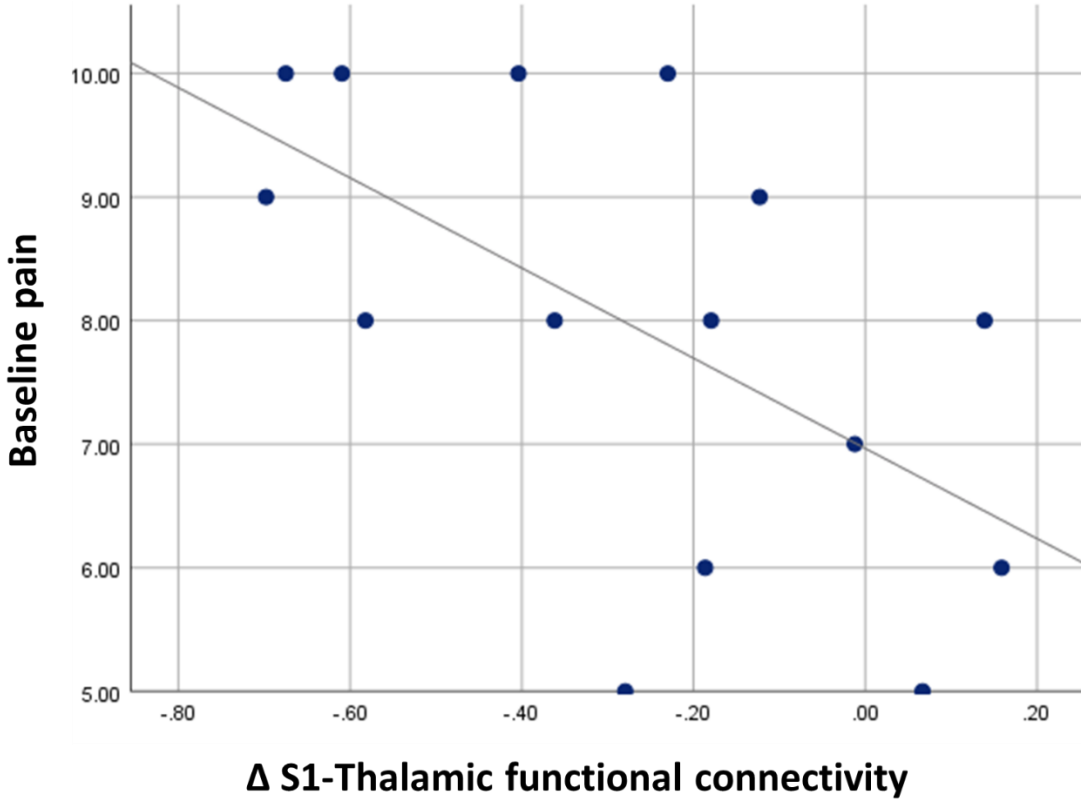

Figure 7.6. Pearson's correlation between Δ S1-Thalamic functional connectivity and baseline pain NRS score (r -0.585, p=0.022). S1, primary somatosensory cortex.

In view of the significant correlation between baseline pain and Δ S1-Thalamic functional connectivity further analysis was performed by stratifying participants into a High Baseline Pain (NRS ≥8) group and a Lower Baseline Pain (NRS ≤7) group. Table 7.4 shows the pain, clinical, demographic, metabolic and fMRI variables. As expected, there was a significantly higher baseline pain score in the High Baseline Pain group (p<0.001). Moreover, the NRS scores were greater at scan 2 (p=0.044), with a greater rise in pain from scan 1 to scan 2 in the High Baseline Pain group (p=0.002). The NPSI score at baseline was also significantly higher in the High Baseline Pain group (p=0.019). There were no other clinical or demographic differences between the two groups. The Δ S1-Thalamic functional

connectivity was significantly greater in the High compared to Lower Baseline Pain group (p=0.035), Figure 7.7.

	High Baseline Pain (8 or higher) n=10	Lower baseline pain (7 or lower) n=5	P value
Baseline NRS	9.0 ± 0.9	5.8 ± 0.8	**<0.001**
NRS scan 1	3.9 ± 2.1	4.2 ± 2.4	0.808
NRS scan 2	7.0 ± 1.8	4.4 ± 2.7	**0.044**
NRS Scan 1 – NRS Scan 2	-3.1 ± 2.1	-0.2 ± 0.4	**0.002**
Age (Years)	64.5 ± 10.1	57.4 ± 3.0	0.065
Female sex (number (%))	10%	20%	0.591*
Duration of Diabetes (Years)	17.3 ± 13.5	9.0 ± 2.5	0.203
Body mass index (kg/m^2)	30.8 ± 6.3	29.9 ±5.2	0.786
Type of Diabetes	Type 1 = 1 (10%) Type 2 = 8 (80%) MODY = 1 (10%)	Type 1 = 0 (0%) Type 2 = 5 (100%) MODY = 0 (0%)	0.562*
Systolic BP (mmHg)	139 ± 15.3	144.4 ± 30.7	0.669
HbA1c (mmol/mol)	66.0 ±11.5	64.0 ± 24.7	0.831
mTCNS	18.8 ± 6.4	18.2 ± 9.8	0.887
DN4	6.9 ± 1.1	5.6 ± 1.1	0.053
Total NPSI	29.6 ± 6.7	23.5 ± 1.4	**0.019**
Total burning NPSI subscore	6.5 ± 3.2	4.0 ± 2.3	0.145
Total pressing NPSI subscore	6.5 ± 2.7	3.8 ± 1.7	0.071
Total paroxysmal NPSI subscore	5.0 ± 3.1	4.6 ± 1.5	0.814
Total evoked pain NPSI subscore	4.9 ± 2.3	4.1 ± 2.6	0.555
Total dysaesthesia NPSI subscore	6.8 ± 2.0	7.0 ± 2.0	0.857
Insomnia severity index	21.6 ± 3.7	18.0 ± 6.0	0.172
HADS total	16.3 ± 5.8	16.2 ± 7.9	0.981
HADS Depression score	8.9 ± 2.3	8.4 ± 6.1	0.867
HADS Anxiety score	7.4 ± 4.5	7.8 ±1.8	0.811
EQ5D5L questionnaire	52.1 ±23.7	60.2 ± 16.7	0.459
Pain Catastrophising score	23.5 ± 13.4	26.4 ± 12.0	0.681
Amitriptyline mono Pregabalin mono Duloxetine mono AP combo PA combo DP combo	1 (10%) 3 (30%) 0 (0%) 1 (10%) 3 (30%) 2 (20%)	1 (20%) 0 (0%) 1 (20%) 2 (40%) 0 (0%) 1 (20%)	0.240*
Retinopathy (%)	50%	20%	0.714*
Nephropathy (%)	70%	60%	0.699*
HTN (%)	50%	33%	0.053*

Allodynia (%)	30%	0%	0.171*
S1 – Th FC Visit 1	-0.126 ± 0.217	-0.021 ± 0.186	0.374
IC – Th FC Visit 1	-0.029 ± 0.166	-0.039 ± 0.283	0.930
S1 – Th FC Visit 2	0.247 ± 0.306	0.030 ± 0.137	0.160
IC – Th FC Visit 2	0.139 ± 0.167	0.152 ± 0.155	0.893
Δ S1 – Th FC	0.372 ± 0.275	0.051 ± 0.180	**0.035**
Δ IC – Th FC	0.1678 ± 0.153	0.190 ± 0.291	0.845

Table 7.4. Pain, clinical, demographic, metabolic and rs-fMRI variables in participants stratified by severity of Baseline Pain NRS. The data are presented as mean ± standard deviation for parametric continuous data or percentage for categorical data. Statistical test was the student t-test or Chi^2 test*. AP, amitriptyline plus pregabalin; BP, blood pressure; combo, combination therapy; DP, duloxetine plus pregabalin; DN4, doleur neuropathique 4; FC, functional connectivity; HADS, hospital anxiety and depression scale; HTN, hypertension; IC, insular cortex; mono, monotherapy; mTCNS, modified Toronto clinical neuropathy score; NRS, numeric rating scale; PA, pregabalin plus amitriptyline; S1, primary somatosensory cortex; Thal, thalamus.

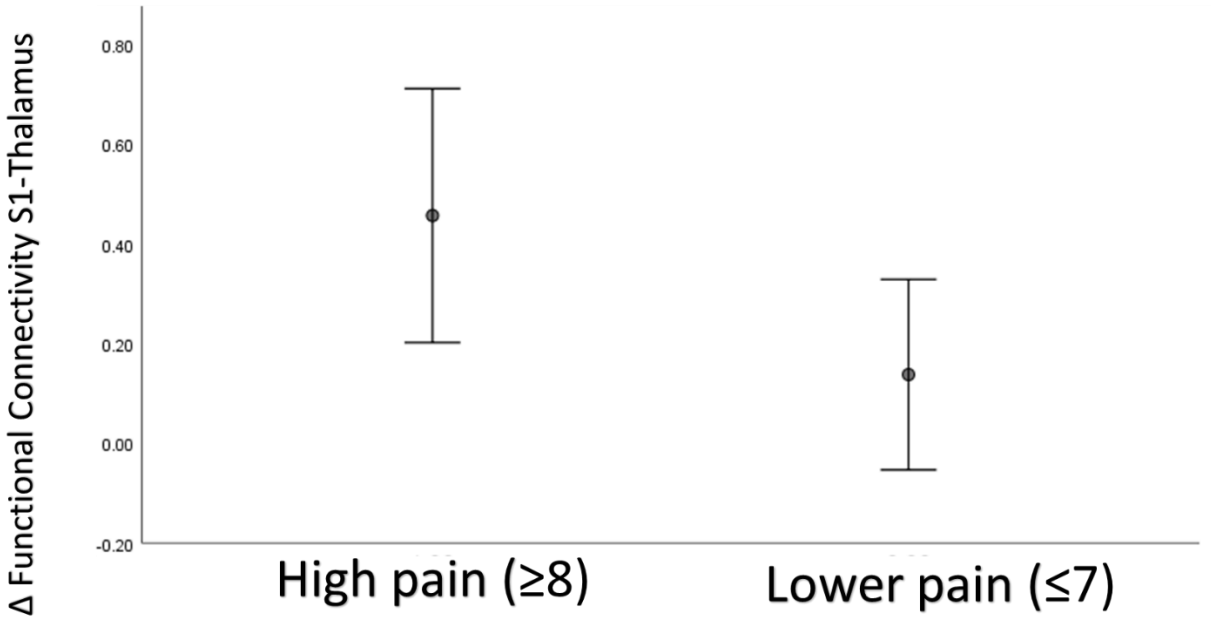

Figure 7.7. Δ S1-Thalamic functional connectivity in High Baseline Pain (NRS ≥8) group and Lower Baseline Pain (NRS ≤7) group (p=0.035, student t-test). S1, primary somatosensory cortex.

The above findings indicate that there is a relationship between rs-fMRI measures and withdrawal of treatment. Further analyses were performed to determine whether other

clinical or demographic factors or treatments were related to changes in functional connectivity or pain NRS scores between scan 1 and 2. When participants were subgrouped according to their use of monotherapy or combination therapy and their treatment pathway, there was no difference in Δ S1-Thalamic functional connectivity, Δ Insular cortex-Thalamic functional connectivity or ΔNRS. Similarly, there were no group difference in these parameters when participants were grouped according to their type of diabetes, sex, age [≥60 (mean ± SD, 55.3 ± 3.5, n=8) and <60 (68.3 ± 7.9, n=7)] and presence of HTN (n=10 with HTN, n=5 without HTN).

7.4 Discussion

In this study, rs-fMRI analysis was performed between 21 ROIs in participants during their involvement in a large clinical trial assessing the efficacy of three different treatment pathways in painful-DSPN. As expected, there was a significant rise in NRS scores from scan 1 to scan 2 when neuropathic pain medications were withdrawn. Correspondingly there was also a change in fMRI parameters comparing scan 1 to 2, with a rise in functional connectivity between the left thalamus and S1 cortex and the left thalamus and insular cortex. This indicates that these areas of the brain are more functionally linked in a higher pain state, compared with a lower pain state when still on neuropathic pain medications

Δ S1-Thalamic functional connectivity showed significant correlations with the baseline NRS, change in NRS from baseline to Scan 1, total NPSI score and the total paroxysmal NPSI subscore. Moreover, in view of the significant correlation with baseline pain NRS participants were stratified into two groups, High Baseline Pain and Lower Baseline Pain.

The cut off for pain scores in these groups were ≥8 for the Higher Baseline Pain and ≤7 for the Lower Baseline Pain. These cut-offs were used as an NRS of ≥8 may be considered to correspond to severe pain (Boonstra et al., 2016); although other cut-offs are used elsewhere (Gerbershagen et al., 2011). Further, the mean baseline pain score was approximately 8 (7.9 ± 1.9); therefore, this seemed a logical value from which to subdivide the groups. There was a significant difference in Δ S1-Thalamic functional connectivity with a greater change in connectivity in the Higher Baseline Pain group compared with the Lower Baseline Pain group. Despite the change in functional connectivity between the thalamus and insular cortex on analgesia withdrawal, there was no significant correlation between participant parameters nor was there a difference in Δ thalamic-insular cortex connectivity between the Higher and Lower Baseline Pain group. Finally, there was no relationship seen between pain, and changes in S1-Thalamic and Insular cortex-Thalamic functional connectivity between scan 1 and 2 and clinical or demographic measures.

There is biological plausibility that the changes in functional connectivity in this study between the thalamus and S1 cortex and thalamus and insular cortex are due to changes in pain intensity. All three of these regions have been identified as key components of the network activated during acute pain (Apkarian et al., 2005). The thalamus was involved in both networks highlighted in this study. Aforementioned studies have found direct evidence of hyperexcitability in the thalamus in experimental painful-DSPN (Fischer et al., 2009) and indirect evidence of preservation of function and hyperexcitability, including in preceding Chapters, Chapter 4 and 5 (Gandhi et al., 2006, Selvarajah et al., 2011, Shillo, 2019). This study further highlights the critical importance of this region of the brain in painful-DSPN. Alterations in thalamic functional connectivity with other brain regions has also been

described in other chronic pain conditions (Henssen et al., 2019, Di Pietro et al., 2020, Tu et al., 2020). Moreover, the lateral thalamus and primary somatosensory cortex are the main nodes of the lateral spinothalamocortical pathway involved in the sensory/discriminate aspect of pain detection and coding of pain intensity (Groh et al., 2018). Indeed, this pathway seems more involved in the transmission of pain impulses in normal individuals without chronic pain conditions (Apkarian et al., 2005). However, fMRI studies investigating the S1 cortex and S1-thalamic network have generally not found it to be significantly activated in acute or chronic pain (Wager et al., 2013). A small study performed by Cauda et al. (Cauda et al., 2009b) found increased connectivity within the thalamus and insular cortices but not S1 in participants with painful-DSPN. Moreover, another study in their group found reduced thalamocortical (including S1 cortex) activity in those with painful-DSPN (Cauda et al., 2009a). Both studies had small sample sizes with inadequate case definition, however. Some studies have found increased thalamic-S1 functional connectivity in chronic pain conditions (complex regional pain syndrome and orofacial pain) which was also related to severity of pain (Alshelh et al., 2016, Di Pietro et al., 2020). The reasons for the discrepancy of this study and others is unclear; although, this study has a novel design whereby resting state imaging was performed in participants optimised for treatment followed by withdrawal of treatment, where the intensity of non-evoked pain is higher. Other studies generally perform imaging in response to application of experimental heat/mechanical pain or at rest, or both, in controls and the group of interest.

This study also found increased thalamic-insular cortex functional connectivity after withdrawal of neuropathic pain treatment. The mechanism underlying this change was not clear as there was no correlation with other clinical variables. The insular cortex has been

highlighted as a key region of the brain for the processing of pain, with involvement in both the sensory and affective dimensions of pain (Lu et al., 2016). Moreover, unlike the S1 cortex several studies have identified altered insular cortex functional connectivity with other brain regions in chronic pain conditions (Ichesco et al., 2014, As-Sanie et al., 2016, Kim et al., 2017). Interestingly there were no correlations with clinical variables, including measures of pain severity. It is possible that the thalamic-insular cortex functional connectivity is more related to other psychological aspects of pain such as suffering and the emotional context of pain; although there was no relationship between baseline measures of anxiety or depression (HADS), quality of life (EQ5D5L), pain catastrophising nor sleep (Insomnia Severity Index). Other psychometrics should be considered in future studies to determine the underlying driving mechanisms of the altered thalamic-insular cortex functional connectivity shown in this study.

This study adds to previous work within the research group which has investigated alterations in functional connectivity in painful-DSPN. Wilkinson et al. performed a study to determine the phenotypic differences in painful-DSPN responders and non-responders to intravenous lidocaine (Wilkinson et al., 2020). Responders to intravenous lidocaine had greater functional connectivity between the insular cortex and the ACC, orbital frontal cortex and amygdala. Moreover, after adjustment for multiple comparisons there was a trend towards a correlation between S1-thalamic functional connectivity and Neuropathy Total Symptom Score-6 pain scores, this prior finding would be consistent with the findings of the study in this thesis. Teh et al., however, performed rs-fMRI in individuals with participants with painful-DSPN stratified into subgroups according to their clinical phenotype, irritable nociceptor or non-irritable nociceptor (Teh et al., 2021). Participants

with the IR phenotype had greater thalamic-insular cortex and reduced thalamic-S1 cortical functional connectivity. Moreover, they found a double dissociation in that self-reported neuropathic pain was more associated with thalamic-insular cortical functional connectivity and more severe nerve function deficits were more related to lower thalamic-S1 functional connectivity. The aim of the study in this thesis was different from these two studies. The correlation with severity of baseline pain and Δ S1-Thalamic functional connectivity were consistent with the correlation analysis found in Wilkinson et al. (2020) rather than Teh et al. (2021), which examined differences between IR- and NIR-painful DSPN subjects. Nevertheless, all studies identify the three regions of interest, thalamus, S1 cortex and insular cortex, as key areas involved in the cerebral mechanisms of painful-DSPN and its response to treatment.

There are currently no biomarkers which have received FDA or EMA approval for use in analgesic clinical trials. Various cerebral measures have been investigated as potential predictive or pharmacodynamic biomarkers (Wager et al., 2013, Wilkinson et al., 2020). A variety of different measures have been investigated, generally in smaller clinical studies. Further studies are necessary to validate imaging biomarkers (Smith et al., 2017). This study highlights thalamic functional connectivity, particularly to the S1 cortex, as a potential marker of neuropathic pain severity in clinical trials. This marker both altered with removal of analgesic agents and correlated with measures of pain severity. However, further study is necessary to ensure this marker is reproducible including clinical trials with baseline and prospective imaging. A particular challenge is applying pain biomarkers at an individual level, rather than a group level as in this study, in order to demonstrate clinical utility (Teh et al., 2021).

There are several strengths and limitations to this proof-of-concept study. The first strength is that it is one of the few studies to examine alterations in cerebral parameters with analgesic treatment and it is the first to do so in painful-DSPN. The technique that is used is also widely available and there are a number of validated analysis tools (Smitha et al., 2017). Additionally, the test is quick to perform, unlike aforementioned MRS studies in previous chapters, making the technique less susceptible to motion artefact with better patient acceptability. Moreover, the specific analysis tool used in this study is validated and well recognised (Whitfield-Gabrieli and Nieto-Castanon, 2012); therefore, making this investigative tool potentially clinically applicable. Ideally imaging would be performed at baseline and after optimisation of treatment, although there are also strengths to the study design in this thesis. There was a significant rise in pain scores 1-week after treatment withdrawal associated with identifiable alterations in resting state networks. If a study were performed prospectively, the scans may have to be several weeks apart, which could lead to the introduction of confounding factors. Moreover, as painful-DSPN is notably difficult to treat there is no guarantee pain scores change as they did after withdrawal of treatment. The study numbers were small overall, and smaller still in subgroup analysis, as recruitment was halted due to the COVID-19 pandemic. However, the numbers were adequate to identify changes in functional connectivity between visits, as well as Δ S1-thalamic functional connectivity correlations with other variables. However, the study numbers were not adequate to identify the underlying mechanism of Δ thalamic-insular cortex functional connectivity alterations. Also, larger study numbers would have been necessary to determine the impact of different neuropathic pain treatments upon rs-fMRI measures.

7.5 Conclusions

In this study, cerebral networks involving the thalamus demonstrated increased connectivity after withdrawal of analgesic agents in patients participating in a clinical trial for painful-DSPN. The study further confirms not only the importance of the thalamus in the pathophysiology of painful-DSPN, but the pharmacology of its treatments. Moreover, rs-fMRI functional connectivity of the thalamus, S1 and insular cortex are also again shown to be key components of the cerebral mechanisms of painful-DSPN, consistent with recent studies in this research group. Further research is ongoing in a large dataset to determine the rs-fMRI networks involved in painful-DSPN and machine-learning approaches to classify individuals into different pain phenotypes. Finally, there are no current biomarkers for pain in analgesic trials which are clinically validated but this study gives early indication that functional connectivity from the thalamus to other ROIs could act as biomarkers of pain severity in painful-DSPN. This would need further validation in prospective studies but warrants further investigation.

8. Peripheral vascular markers of painful-DSPN: A Pilot Study

8.1 Introduction

8.1.1 Background

The focus of the thesis thus far has been on the CNS alterations in DSPN; however, the peripheral mechanisms are clearly important also. A particular area of research interest is the alterations of small nerve fibres, as these are the nerves responsible for the transmission of nociceptive impulses from the periphery. The function of small nerve fibres may be investigated using QST measures; however, skin biopsy offers a minimally invasive means to examine the structure and function of the most peripheral aspect of the nociceptive sensory system in health and disease. Early research used the pan-neuronal marker (Protein Gene Product) PGP 9.5 antibodies to examine epidermal innervation and found a reduction in IENFD in peripheral neuropathies, such as DSPN, compared to control subjects (McCarthy et al., 1995, Holland et al., 1997). A reduction in epidermal innervation may be detected in those with early, often asymptomatic, DSPN (Umapathi et al., 2007, Løseth et al., 2008, Ragé et al., 2011) and IENFD linearly reduces with increasing severity of DSPN (Kennedy et al., 1996, Quattrini et al., 2007b, Arimura et al., 2013). It has been hypothesised that because small fibres are responsible for nociception they may be preferentially depleted in painful neuropathies. However, the relationship between pain and IENFD appears not to be simple. Early findings suggested IENFD may be lower in subjects with positive neuropathic symptoms, i.e. pain, compared with negative symptoms, e.g. Sorensen et al. (2006). However, multiple other studies have found no difference

between IENFD in subjects with painful compared with painless neuropathies (Shun et al., 2004, Quattrini et al., 2007b, Vlcková-Moravcová et al., 2008, Scherens et al., 2009, Cheng et al., 2013, Cheung et al., 2015, Themistocleous et al., 2016, Bönhof et al., 2017, Smith et al., 2017). Moreover, other characteristics of IENF may be altered in painful-DSPN such as markers of regeneration (Bönhof et al., 2017) and degeneration (Cheng et al., 2013).

Various lines of investigation have discovered differences in endothelial dysfunction, blood flow and blood flow regulation between painful- and painless-DSPN (Archer et al., 1984, Eaton et al., 2003, Quattrini et al., 2007a, Doupis et al., 2009). Epineurial oxygenation and blood flow is higher in painful-DSPN, which may be as a result of arterio-venous shunting (Eaton et al., 2003). Profound abnormalities in epineurial vasculature are found in subjects with insulin neuritis, in which subjects suffer severe pain (Tesfaye et al., 1996). The vessels in these subjects formed a fine network resembling neovascularisation in retinopathy. They also showed arterial attenuation and arterio-venous shunting. Such findings in painful-DSPN may render the endoneurium ischaemic, which may play a role in neuropathic pain. Indeed, small clinical trials have also demonstrated that symptoms of painful-DSPN improve with topical application of vasodilator treatment, providing indirect evidence for the involvement of cutaneous vascular factors in painful-DSPN (Agrawal et al., 2007, Agrawal et al., 2009, Shillo et al., 2019b).

A preliminary cross-sectional study within our group performed skin biopsies 10cm above the ankle with immunohistochemical staining of neural and vascular markers (Shillo, 2019). Von Willebrand factor (vWF) immunoreactivity was significantly elevated in subjects with painful-DSPN compared with all other groups (Figure 8.1) and correlated with DN4. IENFD

was severely depleted in cases of DSPN, and levels of other potential biomarkers were low in these groups, with no differences between painful-DSPN and painless-DSPN.

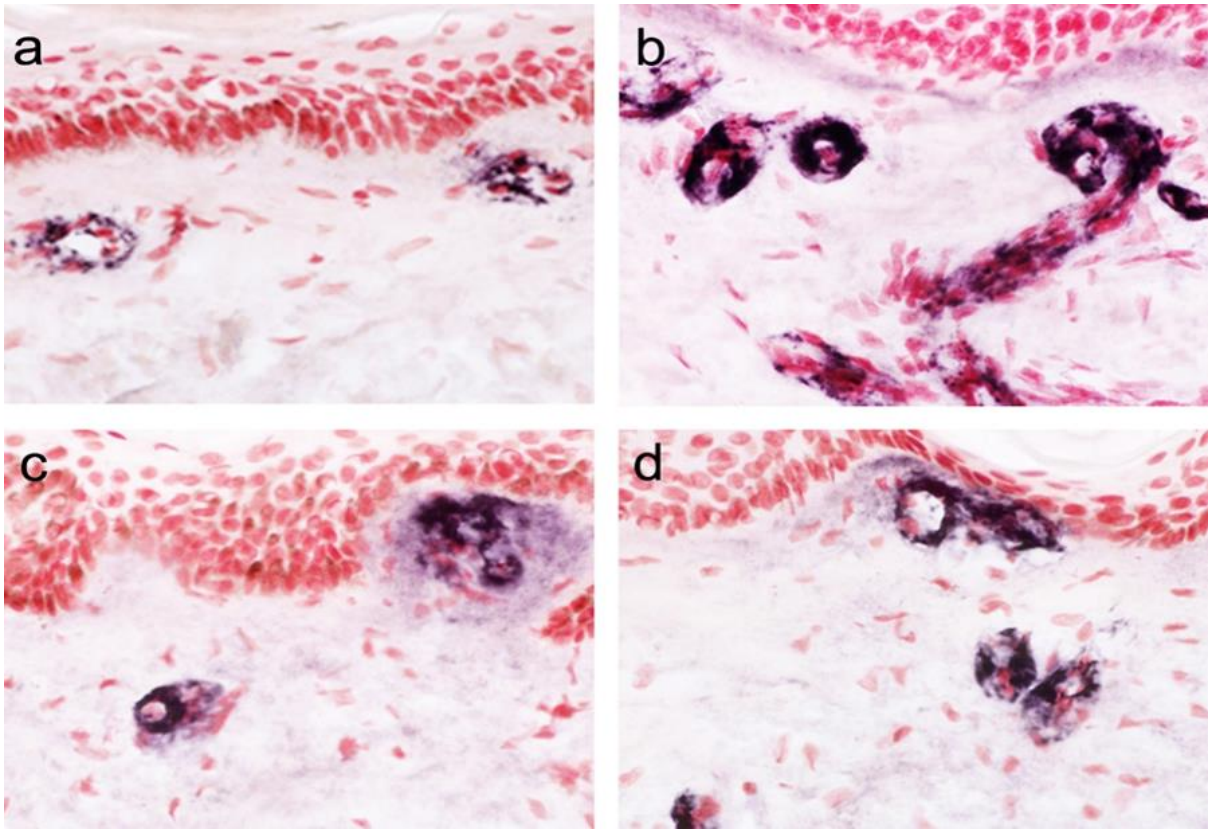

Figure 8.1. Von Willebrand Immunoreactivity in skin biopsy samples in four groups. A: healthy volunteers. B: painful-DSPN. C: painless-DSPN; D: no-DSPN. vWF immunoreactivity was significantly elevated in those with painful-DSPN compared with painless-DSPN (ANOVA, $p < 0.001$) and all other groups (Shillo et al., 2017).

8.1.2 Rationale for study

As evidenced from previous work within the research group in participants with T2DM and advanced DSPN, increased dermal vasculature and its ratio to nociceptors may differentiate painful-from painless-DSPN (Shillo, 2019). However, in this study IENF were almost entirely

depleted in participants with DSPN. Thus, it was not possible to explore the relationship of IENF to vascular markers. We therefore performed skin biopsy at the proximal thigh to investigate vascular and neural biomarkers in DSPN and their relationship to one another and the presence of neuropathic pain.

8.1.4 Aims and hypothesis

The aim of the study was to determine whether there were any differences in skin biopsy peripheral vascular and neural biomarkers between patients with T2DM and no neuropathy, painless-DSPN, painful-DSPN, and HV at the level of the proximal thigh and their relationship to neuropathic pain. The hypothesis was that participants with painful-DSPN would display elevated levels of vWF with correlations with pain scores and DN4.

8.2 Methods

8.2.1 Study Design and Participants

Forty-three participants were recruited to the study (13 HV, 5 no-DSPN, 8 painless-DSPN and 17 painful-DSPN). All participants with diabetes had T2DM, according to the World Health Organization criteria, and were diagnosed at least 6-months prior to their inclusion in the study. Inclusion and exclusion criteria were performed as described in the General Methods section. Moreover, additional exclusion criteria included:

- Contraindication to skin biopsy: infection at proposed site of biopsy, anticoagulation, bleeding disorder and allergy to anaesthetic agent
- Absent pedal pulses

The study design was a case control cross-sectional study.

8.2.2 Clinical and neurological assessment

History, mood/memory assessment, clinical examination, structured neurological examination, nerve conduction studies and calculation of NIS-LL+7 were performed as described in the general methods.

8.2.3 Skin biopsy protocol and analysis

8.2.3.1 Rationale for using skin biopsy with IENFD

Although different markers for small nerve fibres terminating within the skin have been tested, the discovery of antibodies to PGP 9.5 provided the means to detect nerve fibres with much greater efficacy than previously possible (Rode et al., 1985, Lauria, 1999). Protein gene product 9.5 (PGP 9.5) is a tissue specific ubiquitin carboxyl-terminal hydrolase that is present throughout the nervous and neuroendocrine system in humans and other species (Thompson et al., 1983, Wilson et al., 1988, Wilkinson et al., 1989). PGP 9.5 positive nerve

fibres densely innervate the epidermis (IENF) and dermis (DNF) throughout the human body (Dalsgaard et al., 1989, Wang et al., 1990, Kennedy and Wendelschafer-Crabb, 1993, Johansson et al., 1999). They are most numerous in the trunk and reduce in number proximo-distally (Johansson et al., 1999, Lauria et al., 1999). Transient receptor potential cation channel subfamily V member 1 (TRPV1), is an ion channel present throughout the nociceptive pathway that co-localises with PGP 9.5 (Lauria et al., 2006). TRPV1 is involved in the sensation of heat and pain; as a result of its co-localization with IENF, IENF are considered nociceptive nerve end-terminals.

Skin samples suitable for immunohistochemical analysis can be obtained from 3mm punch skin biopsy (Lauria et al., 2010b). The procedure causes minimal discomfort, does not require a suture and wound healing takes 7—10 days (Chien et al., 2001). Punch biopsies are typically taken at the distal leg (10cm proximal to the ankle) for the diagnosis of length dependent neuropathies. Other sites may be used, for example, the proximal thigh if this may provide information regarding the presence of a length dependent process (Lauria et al., 1998, Chien et al., 2001, Lauria et al., 2010b). Performing proximal biopsy at the thigh reduces the sensitivity of IENFD to diagnose neuropathy, compared with distal leg biopsy, but improves the specificity (Devigili et al., 2008, Timar et al., 2016). The sensitivity of thigh biopsy ranges from 47% to 57.5% and the specificity is 95%.

Quantification of the linear density of intra-epidermal nerve fibres is the commonest method of assessing epidermal innervation (Lauria et al., 2010b). It is recommended for clinical practice by International and European Guidelines (Lauria et al., 2010b, Haanpää et al., 2011) for the diagnosis of small fibre neuropathy and American guidelines for the diagnosis of distal symmetrical polyneuropathy (England et al., 2009). IENFD quantification

using immunohistochemistry and immunofluorescence correlate well and normative data are available for both methods (Lauria et al., 2010a, Nolano et al., 2015, Provitera et al., 2016).

8.2.3.2 Rationale for using skin biopsy with von Willebrand Factor

Von Willebrand Factor (vWF) is considered one of the mandatory criteria for identifying the purity of endothelial cell culture (Goncharov et al., 2020). It is a glycoprotein mediating the attachment of platelets to damaged endothelial cells (Lip and Blann, 1997, Goncharov et al., 2020). Arteries of different sizes stain for vWF, including small arteries within the skin (Pusztaszeri et al., 2006). Antibodies to vWF on skin biopsy samples have been used in recent studies to determine whether there are alterations in dermal vasculature in trench foot (Anand et al., 2017) and painful-DSPN (Shillo, 2019).

8.2.3.3 Skin biopsy protocol

The skin was anaesthetised by local infiltration of 2% lidocaine. A punch biopsy tool (Meditech Systems Ltd., Dorset) was used to obtain a 3mm depth skin biopsy. Skin biopsy specimens were obtained from the upper lateral aspect of the thigh 20cm below the anterior iliac spine in accordance with EFNS guidelines and similar studies in the field (Smith et al., 2006, Lauria et al., 2010b, Cheng et al., 2013, Timar et al., 2016). The test site was then covered with a dressing and patients given written and verbal wound care advice.

8.2.3.3 Immunohistochemistry analysis

The skin biopsy specimen was fixed for 12-18 hours in Zamboni fixative and cryprotected overnight (15% sucrose in 0.1M phosphate buffer) at 4°C, then snap frozen in liquid nitrogen.

50-µm sections for PGP 9.5 staining were floated onto PBS in 12-well plates, dehydrated with alcohol/hydrogen peroxide solution for 30 minutes, washed with PBS, and incubated with PGP 9.5 antibodies overnight. They were then washed and incubated with second antibody for 1 hour, and washed again, before sites of primary antibody attachment were revealed using nickel-enhanced, avidin–biotin peroxidase (Vector Laboratories, Peterborough, UK) (Facer et al., 1998, Anand et al, 2017).

In PGP 9.5-stained 50 µm sections, the IENF quantification method used followed the EFNS guidelines (Lauria et al., 2010). IENF counts included all nerve fibres crossing the dermal epidermal junction. PGP 9.5 control values for 50 µm thickness sections were within the range of published values recommended by European Federation of Neurological Societies/Peripheral Nerve Society Guidelines (Lauria et al., 2010), and in other studies (Gøransson et al., 2004; McArthur et al., 1998; Pan et al., 2001). Intraepidermal fibres were expressed as fibres per millimetre length of the epidermis.

8.2.3.5 vWF staining and analysis

15-µm sections for vWF staining were collected onto glass slides coated with poly-l-lysine (Sigma, Poole, UK). Endogenous peroxidase was blocked by incubation in methanol containing 0.3% w/v hydrogen peroxide for 30 minutes. After rehydration, sections were incubated overnight with primary antibody. Following these procedures, the sections were treated the same as with PGP9.5 antibodies, described above.

Quantification of the abundance of sub-epidermal vessels stained by vWF was measured by image analysis (Anand et al, 2017). Digital photomicrographs were captured via video link to an Olympus BX50 microscope with a depth of 200µm below the basal epidermis, using analySIS FIVE software (Olympus, Watford, Hertfordshire, UK). The grey-shade detection threshold was set at a constant level to allow detection of positive immunostaining, and the area of highlighted immunoreactivity was obtained as a percentage (% area) of the field scanned. Images were captured (×40 objective magnification) along the entire length, and the mean values were used for statistical analysis.

8.2.4 Statistical Analysis

Data were analysed as per the general methods. A sample size of 15 in each group was calculated to have 90% power to detect a probability of 0.852 that an observation in Group 1 is less than an observation in Group 2 using a Wilcoxon (Mann-Whitney) rank-sum test with a 0.050 two-sided significance level.

8.3 Results

8.3.1 PGP 9.5 immunoreactivity

A total of 43 participants underwent skin biopsy of the thigh. All participants had analysis of PGP 9.5 immunoreactivity and 33 had analysis of vWF immunoreactivity.

Table 8.1 demonstrates the demographic, clinical and biochemical results from the participants who underwent skin biopsy and analysis of PGP 9.5 immunoreactivity in thigh skin. There was a greater proportion of participants with retinopathy in no-DSPN (Chi^2 test, $p=0.019$) and painful-DSPN ($p<0.001$) compared with painless-DSPN. Moreover, there was a greater proportion of patients with nephropathy in painless-DSPN compared with no-DSPN ($p=0.027$) and the urinary ACR was greater in all diabetes groups compared with HV, as expected. The waist/hip ratio and HbA1c was also statistically higher in all the diabetes groups compared with HV (all; LSD, $p<0.05$). Finally, the cholesterol level was statistically lower in painless- ($p=0.001$) and painful-DPSN ($p=0.007$) compared with HV.

	HV (n=13)	No-DSPN (n=5)	Painless-DSPN (n=8)	Painful-DSPN (n=17)	P value
Age (years)	63.0 ± 12.3	64.4 ± 4.7	63.1 ± 5.9	65.0 ± 10.2	0.944 A
Sex (% female)	53.8	40.0	25.0	47.1	0.620 Chi^2
Duration DM (years)		9.8 ± 5.8	16.3 ± 7.7	11.2 ± 6.8	0.177 A
Retinopathy presence (% present)		80%	62.5%	76.5%	**<0.001 Chi^2**
Retinopathy score (0= No DR, 1= Bck/Pre-P, 2=Pro/Laser)		0 = 20% 1 = 80% 2 = 0%	0 = 37.5% 1 = 37.5% 2 = 25.0%	0 = 23.5% 1 = 47.1% 2 = 29.4%	**<0.001 Chi^2**
Nephropathy presence (% present)		20%	50%	47.1%	**<0.001 Chi^2**
ACR (mg/mmol)	0.0 (0.2)	1.5 (1.7)	0.9 (1.9)	1.4 (4.0)	**<0.001 KW**
Number of hypoglycaemic episodes in last 12 months		0 ± 0	3.7 ± 7.5	4.7 ± 12.8	0.791 A
Smoked ever (% Yes)	38.5%	40%	75%	76.5%`	0.110 Chi^2
Pack Years smoking [Packs (1 pack = 20 cigarettes) x Number of years]	14.2 ± 9.7	15.3 ± 20.9	31.2 ± 22.2	32.1 ± 23.7	0.298 A
Alcohol intake (units/week)	4.4 ± 5.1	10.7 ± 3.1	6.3 ± 4.8	6.5 ± 5.6	0.337 A
Waist/hip ratio	0.86 ± 0.07	0.95 ± 0.07	1.00 ± 0.08	0.96 ± 0.07	**<0.001 A**
Body mass index (kg/m^2)	27.1 ± 6.1	30.8 ± 4.1	30.1 ± 3.2	30.6 ± 6.6	0.362 A
Systolic blood pressure (mmHg)	132.5 ± 21.0	124.2 ± 10.3	137.4 ± 19.7	136.0 ± 14.2	0.538 A

Creatinine (µmol/l)	71.8 ± 8.1	77.4 ± 8.6	72.8 ± 11.2	77.6 ± 22.3	0.746 A
Total Cholesterol (mmol/l)	5.1 ± 1.0	4.1 ± 1.2	3.5 ± 0.7	4.1 ± 0.9	**0.004 A**
HbA1c (mmol/mol)	37.4 ± 4.4	56.6 ± 10.6	63.1 ± 16.8	67.4 ± 18.9	**0.001 A**

Table 8.1. Clinical details of participants. Data are presented as mean ± standard deviation for parametric and median (IQR) for non-parametric continuous data or percentage for categorical data. The statistical test used was ANOVA (A) for continuous normally distributed data, Kruskal-Wallis (KW) for non-parametric continuous data or Chi^2 for categorical data. Retinopathy parameters: Bck, background retinopathy; DR, diabetic retinopathy; Laser, panretinal photocoagulation; Pre-P, pre-proliferative retinopathy; Pro, proliferative retinopathy. ACR, albumin creatinine ratio; DM, Diabetes Mellitus; HV, healthy volunteer.

Table 8.2 demonstrates the neurological assessments of participants undergoing the study, including the PGP 9.5 immunoreactivity results. As expected, measures of neuropathic pain, i.e. NPSI and DN4, were higher in painful-DSPN. The TCNS was also statistically higher in painful-DSPN vs. painless-DSPN. Measures of neuropathy were all statistically higher in DSPN groups compared with non-DSPN groups. Although there was no significant difference in sural nerve action potential between no-DSPN and DSPN groups. The CAN composite score was also significantly raised in painful-DSPN compared with non-neuropathy groups, but there was no difference in painless-DSPN compared with other groups.

PGP 9.5	HV (n=13)	T2DM (n=5)	Painless-DSPN (n=8)	Painful-DSPN (n=17)	P value
NPSI (Total score)	0.0 (0.0)	0.0 (0.0)	0.0 (0.0)	20.8 (18.6)	**<0.001 KW**
DN4	0.0 (0.0)	0.0 (0.0)	2.0 (1.5)	6.0 (3.5)	**<0.001 KW**
TCNS	0.0 (0.0)	2.0 (1.0)	8.0 (10.0)	15.0 (4.0)	**<0.001 KW**
NIS-LL	0.0 (0.0)	0.0 (3.0)	9.0 (19.3)	16.5 (10.0)	**<0.001 KW**
NIS-LL+7	0.0 (1.0)	0.0 (1.5)	17.0 (23.7)	25.2 (13.0)	**<0.001 KW**
Peroneal CMAP (mV)	5.1 ± 1.7	5.4 ± 2.7	2.8 ± 3.2	2.1 ± 1.7	**0.002 A**
Peroneal MNCV (m/s)	47.3 ± 3.3	46.7 ± 2.9	37.4 ± 9.7	38.9 ± 6.7	**<0.001 A**
Peroneal MNDL (msec)	4.9 (0.8)	4.5 (0.9)	6.6 (2.6)	6.1 (4.7)	**0.005 KW**
Tibial MNDL (msec)	4.4 (1.2)	4.7 (0.5)	7.4 (2.9)	6.8 (2.6)	**<0.001 KW**
Sural SNAP (mV)	16.0 ± 6.4	11.1 ± 3.9	5.6 ± 4.9	2.9 ± 5.7	**<0.001 A**
CAN composite score	0.0 (0.0)	0.0 (0.0)	0.0 (0.0)	1.6 (6.9)	**0.002 KW**
Foot ESC (µS)	75.1 ± 10.9	74.2 ± 13.5	54.1 ± 19.8	43.4 ± 18.9	**<0.001 A**
PGP 9.5 IENF fibres/mm	17.4 ± 3.2	17.7 ± 3.6	7.9 ±4.2	5.4 ± 5.2	**<0.001 A**

Table 8.2. Neurological assessments of study participants undergoing skin biopsy. Data are presented as mean ± standard deviation for parametric and median (IQR) for non-parametric continuous data. The statistical test used was ANOVA (A) for continuous normally distributed data and Kruskal-Wallis (KW) for non-parametric continuous data. CAN, cardiac autonomic neuropathy; CMAP, compound muscle action potential; DN4, doleur neuropathique 4; ESC, electrochemical skin conductance; IENF, intra-epidermal nerve fibres; MNDL, motor nerve distal latency; MNCV, motor nerve conduction velocity; NIS-LL, Neuropathy impairment score of the lower limb; NPSI, neuropathic pain symptom inventory; SNAP, sensory nerve action potential; TNCS, Toronto clinical neuropathy score.

Table 8.2 and Figure 8.2 demonstrate the PGP 9.5 immunoreactivity in the thigh skin from all four study groups. There was a reduction in PGP immunoreactivity in the DSPN groups

compared with non-neuropathy groups (all; LSD, p<0.001). However, there was no significant difference between painless- and painful-DSPN (p=0.208).

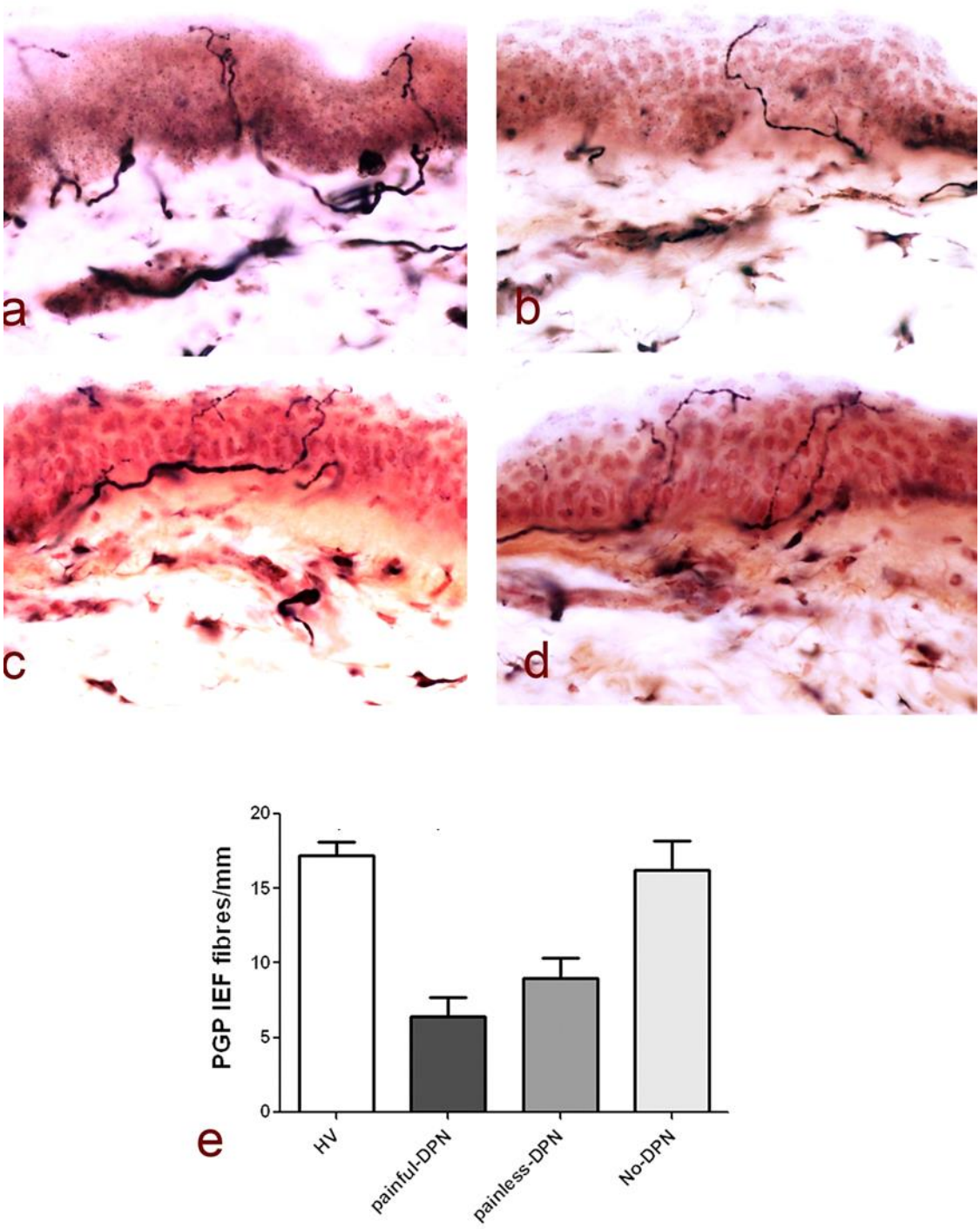

Figure 8.2. PGP 9.5 immunoreactivity in thigh skin from (a) HV, (b) painful-DSPN, (c) painless-DSPN, and (d) no-DSPN. (e) Mean ± standard error of the mean of the PGP 9.5 intra-epidermal fibres

(fibres/mm). PGP immunoreactivity in the DSPN groups significantly lower than non-neuropathy groups (ANOVA, $p<0.001$; Painless- and Painful-DSPN vs. HV and No-DSPN, all, LSD, $p<0.001$).

Table 8.3 demonstrates the DFNS QST parameters of all study participants. As expected, there was evidence of loss of sensory function in DSPN groups compared with the non-neuropathy groups although MDT was not significantly different from painless-DSPN and other groups. Also, there were no differences in painless- and painful-DSPN.

PGP 9.5	HV (n=13)	T2DM (n=5)	Painless-DSPN (n=8)	Painful-DSPN (n=17)	P value
CDT z-score	-0.82 ± 1.12	-0.78 ± 0.43	-2.21 ± 1.18	-2.13 ± 1.26	**0.006 A**
CDT % abnormal	7.7%	0.0%	50%	76.5%	**0.001 Chi^2**
WDT z-score	-1.13 ± 0.87	-0.54 ± 0.77	-1.68 ± 1.12	-2.03 ± 0.49	**0.002 A**
WDT % abnormal	23.1%	0%	50%	58.8%	0.051 Chi^2
TSL z-score	-1.48 ± 1.09	-1.09 ± 0.27	-2.25 ± 1.30	-2.23 ± 0.59	**0.027 A**
TSL % abnormal	30.8%	0%	37.5%	64.7%	**0.047 Chi^2**
CPT z-score	-0.89 (1.03)	-0.98 (0.64)	-0.87 (1.03)	-0.98 (0.71)	0.990 KW
CPT % abnormal	0%	0%	0%	0%	N/A
HPT z-score	-0.73 ± 1.01	-0.79 ± 0.98	-0.62 ± 1.62	-1.34 ± 0.52	0.253 A
HPT % abnormal	7.7%	0%	37.5%	23.5%	0.229 Chi^2
PPT z-score	0.77 ± 0.93	1.31 ± 2.19	0.55 ± 1.89	1.19 ± 1.81	0.751 A
PPT % abnormal	7.7%	60%	25.0%	64.7%	**0.009 Chi^2**
MPT z-score	1.24 ± 1.54	1.23 ± 1.57	-1.60 ± 2.11	-1.91 ± 2.02	**0.001 A**
MPT % abnormal	23.1%	60%	62.5%	82.4%	**0.013 Chi^2**
MPS z-score	-0.08 (1.53)	0.14 (2.53)	-1.72 (1.56)	-1.43 (1.31)	**0.014 KW**
MPS % abnormal	38.5%	20.0%	75.0%	76.5%	**0.040 Chi^2**
WUR z-score	-0.22 ± 1.03	-0.21 ± 1.49	-0.08 ± 0.86	-0.64 ± 0.95	0.919 A
WUR % abnormal	0%	20.0%	0%	0%	0.244 Chi^2
MDT z-score	0.64 (1.97)	0.26 (1.72)	-1.31 (5.46)	-1.74 (3.39)	**0.002 KW**
MDT % abnormal	38.5%	20.0%	50.0%	47.1%	0.492 Chi^2
VDT z-score	0.11 (1.53)	-0.04 (2.16)	-2.20 (3.83)	-2.80 (1.94)	**0.009 KW**

VDT % abnormal	15.4%	20.0%	62.5%	64.7%	**0.023 Chi^2**
DMA % abnormal	0%	0%	0%	17.6%	0.177
PHS % abnormal	7.7%	60.0%	25.0%	47.1%	0.065 Chi^2

Table 8.3. German pain research network QST results in study participants. Data are presented as mean ± standard deviation for parametric and median (IQR) for non-parametric continuous data or percentage for categorical data. The statistical test used was ANOVA (A) for continuous normally distributed data, Kruskal-Wallis (KW) for non-parametric continuous data or Chi^2 for categorical data. CDT, cold detection threshold; CPT, cold pain threshold; DMA, dynamic mechanical allodynia; HPT, heat pain threshold; MDT, mechanical detection threshold; MPT, mechanical pain threshold; PHS, paradoxical heat sensation; PPT, pressure pain threshold; VDT, vibration detection threshold; WUR, wind up ratio.

To further explore the reasons for the reduction in PGP 9.5 immunoreactivity, Table 8.4 demonstrates the correlation analysis between PGP 9.5 immunoreactivity at the thigh and clinical, demographic and neurological variables. There was no correlation with clinical and demographic variables; although there was a negative correlation with HbA1c (Pearson's correlation, r -0.546, p=0.001). PGP 9.5 immunoreactivity correlated with most neuropathy measures, other than peroneal MNDL. The strongest correlation was with NIS-LL+7 (r -0.719, p<0.001). The PGP 9.5 immunoreactivity also correlated with measures of neuropathic pain, including NPSI total and its subscores and DN4 but not the VAS. Finally, PGP 9.5 immunoreactivity correlated with certain measures of DFNS QST, including CDT, WDT, TSL, HPT, MPT, MDT, VDT and DMA, but not WUR, MPS, PPT nor CPT.

	r	P value
Age	0.049	0.754
Duration of DM	0.091	0.650
ACR	-0.144	0.423
Pack Years smoking	-0.253	0.155
Waist/hip ratio	-0.263	0.139
Body mass index	-0.182	0.310
Systolic blood pressure	-0.278	0.123
Creatinine	-0.158	0.378
Total Cholesterol	0.207	0.247
HbA1c	-0.546	**0.001**
Burning spontaneous pain NPSI subscore	-0.509	**0.002**
Pressing spontaneous pain NPSI subscore	-0.389	**0.025**
Paroxysmal pain NPSI subscore	-0.540	**0.001**
Evoked pain NPSI subscore	-0.468	**0.006**
Paraesthesia/dysaesthesia NPSI subscore	-0.581	**0.001**
NPSI (Total score)	-0.574	**<0.001**
DN4	-0.644	**<0.001**
TCNS	-0.690	**<0.001**
NIS-LL	-0.692	**<0.001**
NIS-LL+7	-0.719	**<0.001**
Peroneal CMAP	0.391	**0.029**
Peroneal MNCV	0.613	**0.001**
Peroneal MNDL	-0.113	0.559
Tibial MNDL	-0.496	**0.005**
Sural SNAP	0.496	**0.020**
CAN composite score	-0.588	**<0.001**

Foot ESC	0.484	**0.004**
VAS pain score	-0.308	0.163
CDT z-score	0.490	**0.001**
WDT z-score	0.573	**<0.001**
TSL z-score	0.501	**0.001**
CPT z-score	0.021	0.891
HPT z-score	0.334	**0.028**
PPT z-score	-0.019	0.904
MPT z-score	0.587	**<0.001**
MPS z-score	0.297	0.053
WUR z-score	0.033	0.889
MDT z-score	0.520	**<0.001**
VDT z-score	0.574	**<0.001**
DMA z-score	N/A	N/A
PHS z-score	N/A	N/A

Table 8.4. Pearson's correlation between PGP 9.5 immunoreactivity in thigh skin and clinical, demographic and neurological variables in study participants. ACR, albumin to creatinine ratio; CAN, cardiac autonomic neuropathy; CDT, cold detection threshold; CMAP, compound muscle action potential; CPT, cold pain threshold; DMA, dynamic mechanical allodynia; DN4, doleur neuropathique 4; ESC, electrochemical skin conductance; HPT, heat pain threshold; IENF, intra-epidermal nerve fibres; MDT, mechanical detection threshold; MNDL, motor nerve distal latency; MNCV, motor nerve conduction velocity; MPT, mechanical pain threshold; NIS-LL, Neuropathy impairment score of the lower limb; NPSI, neuropathic pain symptom inventory; PHS, paradoxical heat sensation; PPT, pressure pain threshold; SNAP, sensory nerve action potential; TNCS, Toronto clinical neuropathy score; VDT, vibration detection threshold; VAS, visual analogue scale; WUR, wind up ratio.

8.3.2 vWF immunoreactivity

The demographic, clinical and biochemical results were re-analysed for the 33 participants with vWF immunohistochemistry from the 43 who had a skin biopsy from the thigh, see Appendix 10.13. Therefore, 10 participants who had PGP 9.5 immunohistochemistry did not have vWF immunohistochemistry (HV: Age 57.3 ± 12.2, female 57%, BMI 26.7 ± 6.3 kg/m^2 and HbA1c 37.3 ± 5.1 mmol/mol; and painful-DSPN: Age 67.7 ± 6.1, female 66.6%, BMI 28.9

± 2.9 kg/m^2 and HbA1c 67.0 ± 17.3 mmol/mol). The results were similar to the analysis for all 43 participants. Although there was a lower proportion of participants with retinopathy in painless-DSPN compared with no-DSPN (Chi^2 test, p=0.002), but not painful-DSPN. There also was a higher waist/hip ratio and HbA1c in the neuropathy groups compared with HV. The neurological assessments for participants undergoing vWF analysis were similar to the full cohort analysis (Appendix 10.14); although numerical differences in some measures of neuropathy severity did not meet statistical significance in neuropathy compared with non-neuropathy groups, including: peroneal CMAP, sural SNAP and foot ESC.

	HV (n=6)	T2DM (n=5)	Painless-DSPN (n=8)	Painful-DSPN (n=14)	P value
PGP 9.5 IENF fibres/mm	18.1 ± 3.8	17.7 ± 3.6	7.9 ± 4.2	6.1 ± 5.5	**<0.001 A**
vWF % area	2.4 (1.0)	2.7 (1.1)	3.1 (1.8)	4.7 (0.9)	**<0.001 KW**

Table 8.5. Immunohistochemical results of study participants undergoing skin biopsy and vWF analysis. Data are presented as mean ± standard deviation for parametric and median (IQR) for non-parametric continuous data. The statistical test used was ANOVA (A) for continuous normally distributed data and Kruskal-Wallis (KW) for non-parametric continuous data. vWF, von Willebrand Factor.

Table 8.5 and Figure 8.3 demonstrate the vWF immunoreactivity in the thigh skin from all four study groups. There was an increase in vWF immunoreactivity in painful-DSPN compared with all three other study groups [Statistically higher in painful-DSPN compared with HV (Mann Whitney-U test, p<0.001), no-DSPN (p=0.005) and painless-DSPN (p=0.001)].

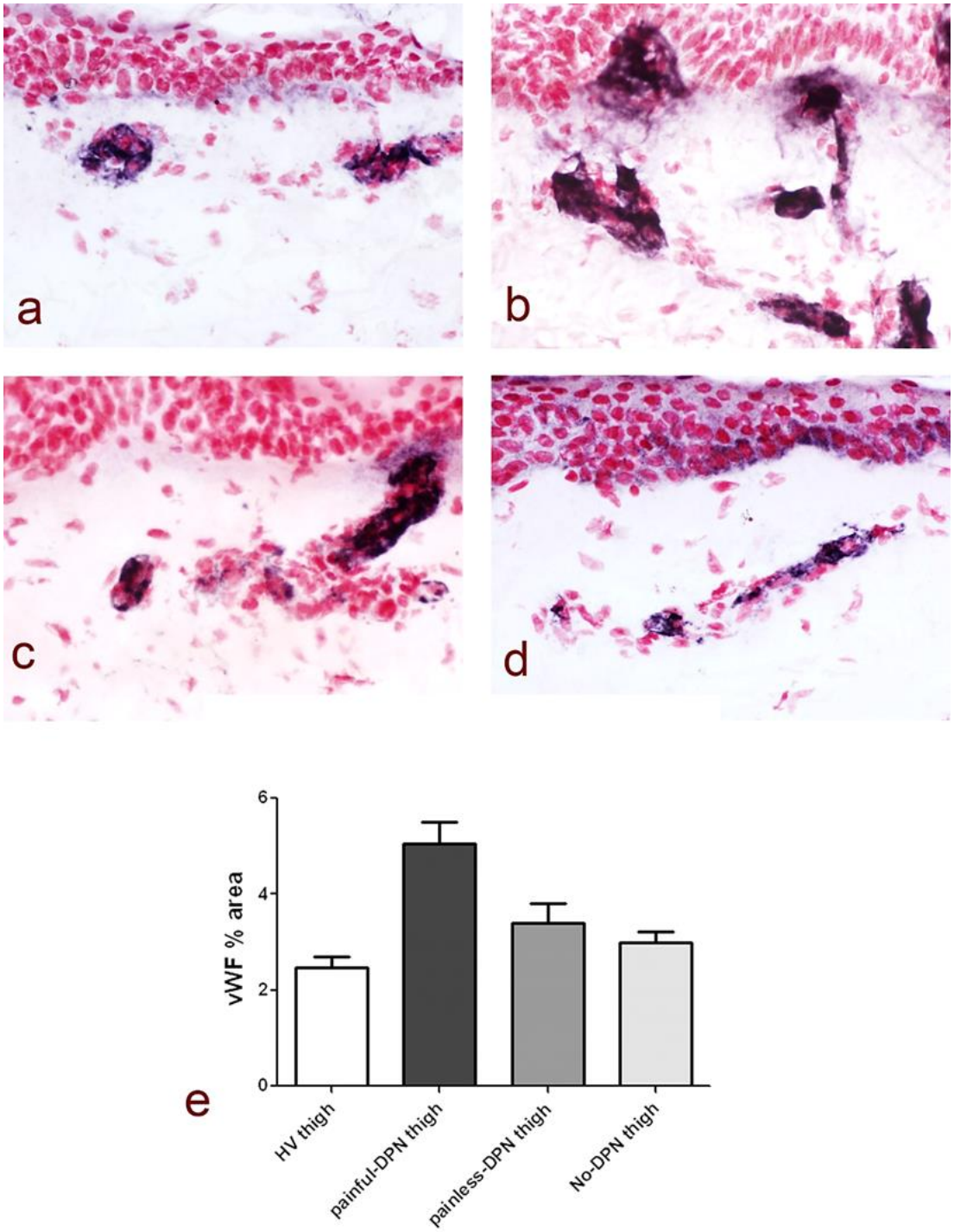

Figure 8.3. vWF immunoreactivity in thigh skin from (a) HV, (b) painful-DSPN, (c) painless-DSPN, and (d) no-DSPN, (e) image analysis of vWF sub-epithelial endothelial staining (% immunoreactivity). vWF immunoreactivity in painful-DSPN significantly higher compared with all three other study groups [painful-DSPN vs. HV (Mann Whitney-U test, $p<0.001$), vs. no-DSPN ($p=0.005$) and vs. painless-DSPN ($p=0.001$)].

Appendix 10.15 demonstrates the DFNS QST results in study participants undergoing vWF immunohistochemical analysis. Compared with the full 43 patient analysis, a number of QST parameters no longer had a group effect, including: CDT, TSL and VDT. The group significance was retained for WDT, MPT, MPS and MDT. In general, there was a reduction in sensory function in these parameters in both painless- and painful-DSPN, with no differences between these two groups. The MDT was only statistically lower in painful-DSPN compared with non-neuropathy groups, however.

Table 8.6 demonstrates the correlation analysis between vWF immunoreactivity at the thigh and clinical, demographic and neurological variables. vWF immunoreactivity positively correlated with clinical variables, including the waist/hip ratio and HbA1c. Additionally, vWF immunoreactivity also positively correlated with neuropathy measures including the clinical scoring systems (TCNS and NIS-LL), objective measures (nerve conduction studies and QST measures) and the composite score NIS-LL+7 (Spearman's correlation, r 0.641, $p<0.001$). vWF also correlated with measures of neuropathic pain, including all the subscores of the NPSI and the total NPSI score (r 0.642, $p<0.001$), DN4 (r 0.659, $p<0.001$) and VAS (r 0.585, $p=0.004$). Finally, vWF also correlated with PGP 9.5 immunoreactivity (r -0.571, $p=0.001$).

	r	P value
Age	-0.154	0.392
Duration of DM	-0.120	0.552
ACR	0.318	0.071
Pack Years smoking	0.308	0.082
Waist/hip ratio	0.352	**0.044**
Body mass index	-0.032	0.859
Systolic blood pressure	0.212	0.245
Creatinine	0.115	0.526
Total Cholesterol	-0.179	0.319
HbA1c	0.531	**0.001**
Burning spontaneous pain NPSI subscore	0.545	**0.001**
Pressing spontaneous pain NPSI subscore	0.536	**0.001**
Paroxysmal pain NPSI subscore	0.661	**<0.001**
Evoked pain NPSI subscore	0.590	**<0.001**
Paraesthesia/dysaesthesia NPSI subscore	0.482	**0.004**
NPSI	0.642	**<0.001**
DN4	0.659	**<0.001**
TCNS	0.752	**<0.001**
NIS-LL	0.713	**<0.001**
NIS-LL+7	0.641	**<0.001**
Peroneal CMAP	-0.352	0.052
Peroneal MNCV	-0.154	0.444
Peroneal MNDL	0.182	0.344
Tibial MNDL	0.472	**0.007**
Sural SNAP	-0.576	0.001
CAN composite score	0.636	**<0.001**
Foot ESC	0.605	**<0.001**
VAS pain score	0.585	**0.004**

CDT z-score	-0.373	**0.033**
WDT z-score	-0.499	**0.003**
TSL z-score	-0.414	**0.017**
CPT z-score	-0.078	0.666
HPT z-score	-0.437	**0.011**
PPT z-score	0.148	0.410
MPT z-score	-0.488	**0.004**
MPS z-score	-0.221	0.217
WUR z-score	0.227	0.502
MDT z-score	-0.531	**0.001**
VDT z-score	-0.548	**0.001**
DMA z-score	N/A	N/A
PHS z-score	N/A	N/A
PGP 9.5 IENF	-0.571	**0.001**

Table 8.6. Spearman's correlation between vWF immunoreactivity in thigh skin and clinical, demographic and neurological variables in study participants. ACR, albumin to creatinine ratio; CAN, cardiac autonomic neuropathy; CDT, cold detection threshold; CMAP, compound muscle action potential; CPT, cold pain threshold; DMA, dynamic mechanical allodynia; DN4, doleur neuropathique 4; ESC, electrochemical skin conductance; HPT, heat pain threshold; IENF, intra-epidermal nerve fibres; MDT, mechanical detection threshold; MNDL, motor nerve distal latency; MNCV, motor nerve conduction velocity; MPT, mechanical pain threshold; NIS-LL, Neuropathy impairment score of the lower limb; NPSI, neuropathic pain symptom inventory; PHS, paradoxical heat sensation; PPT, pressure pain threshold; SNAP, sensory nerve action potential; TNCS, Toronto clinical neuropathy score; VDT, vibration detection threshold; VAS, visual analogue scale; WUR, wind up ratio.

8.4 Discussion

In this study skin biopsies were taken from the upper thigh in study participants to determine whether neuronal and vascular markers were altered in patients with painful-DSPN. Firstly, 43 participants had skin biopsies from the thigh and underwent IENFD analysis. As expected, there was a reduction in PGP immunoreactivity in the DSPN groups compared with non-neuropathy groups. IENFD has previously been described to be lower in

participants with diabetes without neuropathy; however, in this cohort there was no significant difference. This is likely reflective of the fact that IENFD decline in a proximo-distal gradient with thigh nerve fibres being affected later than ankle biopsies. In painful-DSPN the IENFD was numerically the lowest, but this did not reach statistical significance vs. painless-DSPN. Therefore, these data supports previous studies which have indicated that the IENFD does not discriminate between painless- and painful-DSPN (Shun et al., 2004, Quattrini et al., 2007b, Vlcková-Moravcová et al., 2008, Scherens et al., 2009, Cheng et al., 2013, Cheung et al., 2015, Themistocleous et al., 2016, Bönhof et al., 2017, Smith et al., 2017).

PGP immunoreactivity correlated with measures of neuropathy including nerve conduction studies and QST, as expected. The negative correlation between the NIS-LL+7 was particularly strong, supporting the use of this composite score as a measure of neuropathy severity. There was no correlation between the severity of pain (VAS) and PGP immunoreactivity. The DN4 did correlate with PGP immunoreactivity; however, this measure is predominantly used to assess the presence of pain due to neuropathy and some of the questions are unrelated to pain severity and are measures of neuropathy (e.g. hypoaesthesia to touch/pinprick and tingling, pins and needles, numbness and itching). Of note, all NPSI subscores negatively correlated with PGP immunoreactivity. Previous studies have demonstrated that there may be a greater IENFD in patients with painful-DSPN and painful neuropathies of varying aetiologies with provoked pain/allodynia, compared to those without (Truini et al., 2014, Galosi et al., 2018). These other studies had considerably larger sample sizes than this study; therefore, this study may not have statistical power to detect such correlations.

Group differences were as expected, for example greater HbA1c, waist/hip ratio and ACR in participants with diabetes compared with HV. Moreover, measures of peripheral neuropathy were greater in neuropathy compared with non-neuropathy groups. CAN was more severe in painful-DSPN, as previously described (Gandhi et al., 2010). There also appeared to be a greater proportion of patients with nephropathy in those with DSPN compared to no-DSPN, reaching significance with painless- versus no-DSPN. However, the presence of any retinopathy was significantly lower in those with painless-DSPN compared to painful- and no-DSPN groups. This finding is contrary to what was expected as neuropathy and retinopathy measures generally correlate. Finally, the total cholesterol was lower in DSPN groups compared with neuropathy groups. This is likely because the neuropathy groups are under tertiary centres and well treated for cardiovascular risk factors. The cholesterol blood test was a one-off blood test is unlikely to reflect the life-long cholesterol burden of these patients. Most importantly, there were no significant differences in measures of neuropathy severity between painful- and painless-DSPN; however, TCNS was greater in painful- compared with painless-DSPN. The TCNS includes symptom scores, which may account for the greater value in those with painful-DSPN. (Bril et al., 2009).

A total of 33 participants underwent vWF immunohistochemical analysis from skin biopsy taken at the thigh. Due to the 10-patient difference compared with those having PGP 9.5 immunoreactivity measured the patient group differences in clinical and neurological variables were re-analysed. The patient characteristics were similar to those having PGP 9.5 immunoreactivity analysed. The main study findings were that the vWF immunoreactivity was significantly higher in painful-DSPN compared with all three other study groups. There

was no significant difference in vWF immunoreactivity between the other three groups. However, there were significant correlations with various clinical and neurophysiological measures and negatively correlated with PGP 9.5 immunoreactivity, suggesting a link between neuronal and vascular alterations in the skin in DSPN.

The finding of elevated vWF in participants with painful-DSPN compared to HV, no-DSPN and painless-DSPN is the same as demonstrated in the previous study within our group (Shillo, 2019). Shillo et al. (2019) demonstrated that sub-epidermal vWF immunoreactivity from skin biopsies taken at the ankle was higher in painful-DSPN compared with all other subgroups. Similarly, vWF correlated with QST parameters (CDT and HDT) and DN4. Moreover, Shillo et al. (2019) found that the calcitonin gene related peptide to vWF ratio was lower in painful- compared with painless-DSPN. Anand et al. (2017) have also previously demonstrated elevated vWF immunoreactivity in patients with painful non-freezing cold injury (i.e. trench foot) compared with healthy controls. This study also found increased VEGF in those with trench foot compared with controls too.

Shillo et al. (2019) hypothesized that hypoxia-induce increase of blood vessels may expose associated nociceptor fibres to a relative excess of algogens leading to painful-DSPN. The literature supporting this includes the fact that more severe neuropathy appears to be associated with neuropathic pain (Shillo et al., 2019b). Other skin biopsy studies have also found that markers of axonal regeneration/degeneration may be associated with painful-DSPN (Cheng et al., 2013, Bönhof et al., 2017). Various other studies have found alterations suggestive of vascular dysfunction in painful-DSPN too (Shillo et al., 2019b). Moreover, peripheral blood flow regulation has been found to be altered in painful- compared with painless-DSPN (Archer et al., 1984, Tsigos et al., 1992, Tack et al., 2002, Eaton et al., 2003,

Shillo et al., 2019b). However, the mechanisms underlying these alterations in vWF immunoreactivity, as a marker of dermal vasculature, remains unclear. Studies have also demonstrated evidence of hypoxia and abnormal angiogenesis in patients with painful-DSPN. Most relevant to this, the study by Quattrini et al. (2008) found hypoxia inducible factor 1 α (HIF-1α), a measure of tissue hypoxia, immunostaining correlated with measures of pain in individuals with DSPN. However, a validated scale of neuropathic pain was not used nor was the data supplied in the article. Despite the underlying cause of vWF in painful-DSPN being uncertain, this study highlights skin vWF staining as a potential biomarker of neuropathic pain in diabetes. As previously discussed, other than clinical features there are no current discriminatory markers of painful-DSPN.

The findings of this pilot study require replication in larger, ideally prospective studies, to confirm vWF staining of dermal blood vessels as a potential biomarker of painful-DSPN. However, they do present a possible mechanistic link explaining the efficacy of topical vasodilatory agents in treating painful-DSPN (Agrawal et al., 2007, Agrawal et al., 2009). Although, vWF has been used as a vascular marker in normal human tissues (Pusztaszeri et al., 2006); vWF has also been found to be raised in conditions causing endothelial damage (Mannucci, 1998) and is also up-regulated in angiogenesis (Zanetta et al., 2000, Randi and Laffan, 2017). Therefore, further study necessary to determine the mechanistic link between vWF elevation and painful-DSPN and whether increased vWF staining is as a result of a greater number of blood vessels, as it appears to be, or due to vascular alterations such as increased endothelial damage or greater angiogenesis.

This study is mainly limited by its participant numbers. Indeed, the sample size calculation indicates that at least 15 per group are necessary for 90% power. The biopsy analysis was

limited by factors such as the COVID pandemic and the discontinuation of clinical, non-Covid related research. However, the group differences despite small study numbers suggest that previous findings from our group are valid. Moreover, the participants are well characterized, and the investigative technique is well recognised.

This thigh skin biopsy study confirms our previous findings at the ankle (Shillo et a. 2019). The initial plan of the study was to perform more detailed immunohistochemical analysis on the skin biopsies to include further neural and vascular markers to potentially determine a mechanistic cause for vWF alterations. However, this has been delayed and limited due to the COVID pandemic and further analysis will follow before publication in peer-reviewed journals.

8.5 Conclusions

This study has demonstrated that PGP 9.5 immunoreactivity from skin biopsy taken at the thigh does not discriminate between painful- and painless-DSPN; however, vWF is significantly higher in painful-DSPN compared with all study groups. These findings confirm the results of our previous study with skin biopsies performed at the ankle. The results suggest that vWF immunoreactivity in the skin of the lower limb may act as a potential biomarker, e.g. for diagnostics/predictor, of painful-DSPN. However, further mechanistic and prospective studies are necessary to determine the causality of raised vWF immunoreactivity in painful-DSPN.

9. Conclusions

There has been considerable research into the mechanisms underlying DSPN, painful-DSPN and potential therapeutic approaches. However, pathogenic orientated treatments have almost all failed in Phase III trials (Sloan et al., 2021). There is strong evidence that tight glycaemic control can reduce the incidence of DSPN; however, other than this there are no effective treatments or prevention strategies for DSPN. The treatment of painful-DSPN has not changed in over a decade and revolves around management of symptoms, rather than treatment of the underlying disease mechanisms. The divide between experimental and clinical DSPN is a major factor in explaining the failure of translation of DSPN/painful-DSPN treatments (Sloan et al., 2021). Unfortunately, no one animal model mimics the human condition (Yorek, 2016). Therefore, there is a clear rationale for investigating the underlying mechanisms of the disease and/or effect of treatments in the human condition. Neuroimaging and skin biopsy are two investigative techniques, the former non-invasive the latter minimally invasive, which have been used in the included studies in this thesis to explore the underlying disease mechanisms of clinical painful-DSPN.

In Chapter 3 the largest cerebral morphometric study in DSPN was conducted. The predominant aim of the study was to determine the cerebral morphological alterations in DSPN and painful-DSPN and two of its phenotypes (IR- and NIR-painful-DSPN). The study demonstrated that global brain parameters other than subcortical grey matter volume were not different among the studied groups; although there was a trend towards a reduction in the three diabetes groups in total brain volume, cortical volume and total grey matter volume compared with HV. The subcortical grey volume was significantly lower in all three

diabetes groups compared with healthy volunteers. This is consistent with previous research suggesting that diabetes may have an impact on global brain volumes; however, there appeared to be no additional effect of DSPN, contrary to previous findings. Regional brain analysis revealed reduced cortical thickness at the S1, M1 and insular cortex in participants with DSPN compared with HV. There appeared to be a stepwise reduction from HV, to no-DSPN to those with DSPN. Moreover, the reduction in cortical thickness was similar at M1 cortex in painless- and painful-DSPN; whereas, at pain matrix areas, such as the insular cortex and S1, there was a stepwise reduction from diabetes, to painful- and finally painless-DSPN with the lowest thickness. This could be consistent with painful-DSPN having a relative preservation of cortical thickness/grey matter volume in regions associated with somatosensory function due to persistence of painful neuronal impulses. Finally, there was a stark reduction in ACC cortical thickness in the IR-painful-DSPN phenotype compared with NIR-phenotype. This finding furthers the concept of differing disease processes in different phenotypes of neuropathic pain.

The volumetric analysis of participants with painless- and painful-DSPN is somewhat limited by the group differences, which may have a confound on the results. However, the results suggest that DSPN does have a significant impact upon cerebral morphometry, predominantly localised to key somatosensory/motor brain regions, showing a relationship with measures of neurophysiology. DSPN has been generally considered a disease of the peripheral nerve, whereby this finding, along with others in the last two decades, suggest the brain is affected also. To definitively determine the impact and aetiology of cerebral morphometric alterations in DSPN, longitudinal study with prospective neuroimaging is now necessary. The reduction in ACC cortical thickness in IR-painful-DSPN also opens new

avenues of research, as this region may act as a key component in determining neuropathic pain phenotypes, and therefore response to treatments.

The morphometric abnormalities found in Chapter 3 led on to the cerebral neurochemical studies in Chapters 4 and 5. In Chapter 4 the proton containing neurometabolites were examined in the thalamus and S1 cortex in a cohort of participants with T2DM. There was no evidence of S1 cortical neurochemical abnormalities among the diabetes groups. However, in participants with painless-DSPN, and to a lesser extent no-DSPN, there was a reduced NAA:Cho at the DH thalamus which may be as a result of greater neuronal dysfunction. The preservation of NAA:Cho in participants with painful- compared with painless-DSPN may be secondary to persisting painful neuronal impulses.

Chapter 5 explored the potential mechanisms underlying thalamic and S1 alterations, using 31P-MRS. At the S1 cortex there was a reduction of PCr:ATP, a marker of cerebral energy usage, in painful-DSPN compared with painless-DSPN and HV. There was also a reduction in this ratio in no-DSPN compared with HV. The PCr:ATP also correlated with a number of measures of neuropathic pain. The ratio in painless-DSPN was similar to HV, suggesting that there is reduced energy usage in this group at the S1 cortex. The relationship between neuropathic pain and PCr:ATP at the S1 cortex suggests increased energy usage at this brain region in painful-DSPN, indicating a potential mechanism of relative cortical thickness preservation in this group from Chapter 3.

Chapter 5 also measured the 31P neurometabolites at the level of the thalamus. There appeared to be a diabetes effect upon the thalamus; however, there was an increase in Pi:PCr and Pi:ATP (measures of mitochondrial function), apparently driven by an increase in Pi, in no-DSPN and painless-DSPN. These ratios were similar to HV in the painful-DSPN group

and these measures also both correlated with HbA1c. Furthermore, there was a correlation with thalamic NAA:Cho and Pi:PCr. Overall, these results further the concept from Chapter 4 that there is a diabetes effect on the functioning of the thalamus, which may be secondary to impairment in cellular mitochondrial function. Moreover, the preservation in neuronal function in Chapter 4 is consistent with preservation of mitochondrial function in painful-DSPN. Therefore, mitochondrial dysfunction is a potential mechanism of thalamic neuronal injury in diabetes and painless-DSPN which is preserved in painful-DSPN.

The current neuropathic pain treatments for painful-DSPN are currently inadequate. The reasons for this may include the limitations of pain clinical trials. The primary outcome in clinical pain trials is currently with self-rated tools, most commonly pain severity using NRS/VAS. Various neuroimaging markers have been tested as biomarkers for pain; however, they are at the early stage of study, and none are validated for clinical use. Moreover, no studies have evaluated the change in neuroimaging markers in response to neuropathic pain treatments in painful-DSPN. In Chapters 6 and 7, two pre-post neuroimaging studies were undertaken in participants undergoing the OPTION-DM trial, a neuropathic pain trial to determine the most efficacious pathway for the treatment of painful-DSPN. Cerebral images were taken during the end of a treatment pathway within the study when participants were optimally treated for their neuropathic pain, and again one-week later after medication had been withdrawn. These studies therefore aimed to determine the impact of neuropathic pain pharmacotherapeutic agents on cerebral markers.

In Chapter 6, MRS was performed and using spectral editing software the neurotransmitters GABA and Glx were measured within the ACC as a hypothesis generating study. There were no differences in any neurotransmitters when participants were optimally treated for pain,

or again after withdrawal of pain. The excitatory neurotransmitter Glx did correlate with pain severity after withdrawal of analgesia, consistent with other studies showing Glx can be elevated in various brain regions in response to pain. However, GABA and Glx at the ACC did not alter after withdrawal of neuropathic pain treatments in painful-DSPN; although, methodological limitations may have contributed to the negative findings in the study.

In Chapter 7, after withdrawal of pain-relieving medications there was a significant increase in functional connectivity of the thalamus to the S1 cortex and the insular cortex. The change in S1 cortical to thalamic functional connectivity between treatment and withdrawal scans was greater in those with higher baseline pain scores and correlated with measures of pain. The study further highlights the importance of the thalamus as a key component of the central mechanisms of painful-DSPN and also the pharmacology of its treatments. Functional connectivity of the thalamus to other brain regions as measured by rs-fMRI may act as a biomarker of neuropathic pain treatment in painful-DSPN in the future after validation studies.

Finally in Chapter 8, skin biopsy with analysis of nerve (IENFD) and vascular (vWF) markers was performed. Thigh skin biopsies were obtained as previous research within the group found nerve markers to be entirely depleted at the level of the ankle in a cohort with advanced neuropathy. In this study, IENFD did not differentiate participants with painless- and painful-DSPN. However, vWF stained dermal microvessels were significantly higher in painful-DSPN compared with all other groups, as shown in previous research within our group. These findings are consistent with the importance of peripheral vascular factors in painful-DSPN. Due to the COVID pandemic, however, immunostaining to explore the

mechanisms underlying these changes was not possible and further analysis will follow before publication in peer-reviewed journals.

There are some limitations of the included studies. Other than Chapter 3, the studies had a modest sample size. The sample sizes for research involving MR imaging are often relatively small, due to the expense involved in performing the technique. Further, the COVID-19 pandemic impacted the recruitment of studies in Chapters 6 and 7 and completing the histochemistry analysis in Chapter 8. However, the included studies were generally proof of concept, except for Chapter 3, and require follow-up with studies with larger sample sizes. A further limitation was the group differences in the included studies. Precise matching was not achieved; however, many of the group differences were due to well recognised risk factors of DSPN/painful-DSPN. These group differences may act as confounders for the included results. Finally, some of the MRS spectra were of inadequate quality necessitating their removal from the final analysis. These techniques are particularly susceptible to movement artefact. The spectral quality may only become apparent after processing and the scan duration is quite long; therefore, repeating this modality during the scanning visit was not possible. A further limitation of these studies is the cross-sectional design, so causality cannot be determined from the results.

These studies open numerous lines of future research. Importantly, both the MR and skin biopsy Chapters require follow-up in longitudinal studies. The causality of cerebral alterations is unknown and needs confirmation in studies with a prospective study design. Moreover, the underlying mechanisms of these cerebral alterations may come to light with longitudinal and multi-modal imaging. ACC alterations in different phenotypes of painful-DSPN may also be investigated using multi-modal imaging, indeed the 31P metabolite

alterations would be important to explore. The 31P-MRS alterations found in the thalamus and S1 cortex can be examined in more detail using magnetization transfer resonance spectroscopy, which allows measurement of 31P metabolic rates and fluxes and may confirm the hypotheses relating to alterations in metabolite ratios. There is currently a large rs-fMRI study in progress within the group which is analysing the alterations in functional connectivity in painful- and painless-DSPN which may further inform on the results of Chapter 7. However, the changes in functional connectivity with thalamic networks needs investigation in both longitudinal studies and clinical trials to validate the potential biomarkers highlighted in the chapter. Further analysis is going to occur from the study presented in Chapter 8, which intends to inform on the mechanisms underlying vWF alterations in painful-DSPN.

To conclude, these studies add to our understanding of the cerebral alterations in DSPN and painful-DSPN and the cerebral response to neuropathic pain medications. Painless-DSPN is characterized by structural and functional loss, as indicated by a reduction in cerebral volume/cortical thickness in key areas of somatomotor function; reduced S1 neuronal energy usage; and reduced thalamic neuronal function which is associated with mitochondrial dysfunction. Painful-DSPN however, demonstrates relative preservation of morphology and function, with lesser cortical thickness reductions in somatosensory areas of the brain, and preserved neuronal function and mitochondrial function at the thalamus. Moreover, there is increased energy usage at the S1 cortex. Also, different phenotypes of painful-DSPN demonstrate structural alterations with preferentially reduced ACC cortical thickness in the IR phenotype of painful-DSPN. Finally, the thalamic connectivity to the

insular cortex and S1 cortex increases with medication withdrawal and has the potential to act as a biomarker of neuropathic pain in DSPN.

10. Appendix

Symptom scores	Reflex scores	Sensory test scores
Foot Pain Numbness Tingling Weakness	**Knee reflexes**	**Pinprick**
Ataxia	**Ankle reflexes**	**Temperature**
Upper-limb symptoms		**Light touch**
		Vibration
		Position

Appendix 10.1. Toronto Clinical Neuropathy Scoring System. Sensory testing performed on the first toe. Symptoms scores: present = 1; absent = 0. Reflex scores: absent = 2, reduced = 1, normal = 0. Sensory test score: abnormal =1, normal =0. Total scores range from 0 to a maximum of 19 (Bril and Perkins, 2002b).

LOWER LIMB FUNCTION TEST (LLF)

Preliminary Functional Tests Before Doing NIS

Persons up to 75 years old usually are able to carry their weight in walking on toes or heels unless they are markedly overweight. Patients over 60 years of age may not be able to arise from a kneeled position when they are overweight, physically unfit, or have knee disease. Do not score as abnormal if the disability is due to age, physical unfitness or knee disease.

	RIGHT		LEFT	
1. Walk on toes	Normal ○	Abnormal ○	Normal ○	Abnormal ○
2. Walk on heels	Normal ○	Abnormal ○	Normal ○	Abnormal ○
3. Arise from kneeled position	Normal ○	Abnormal ○	Normal ○	Abnormal ○

NEUROPATHY IMPAIRMENT SCORE (NIS)

OBJECTIVE: To provide a single score of neuropathic deficits and subset scores: cranial nerve, muscle weakness, reflexes and sensation. Abnormalities are abstracted from a neurologic examination in which all of the assessments are made.

SCORING : The examiner scores deficits by what he (she) considers to be normal considering test, anatomical site, age, gender, height, weight, and physical fitness.

SCORING, MUSCLE WEAKNESS

0 = NORMAL	3.25 = MOVE AGAINST GRAVITY
1 = 25% WEAK	3.5 = MOVEMENT, GRAVITY ELIMINATED
2 = 50% WEAK	3.75 = MUSCLE FLICKER, NO MOVEMENT
3 = 75% WEAK	4 = PARALYSIS

		RIGHT								LEFT							
	Cranial Nerves	0	1	2	3	3.25	3.5	3.75	4	0	1	2	3	3.25	3.5	3.75	4
1	3rd Nerve	○	○	○	○	○	○	○	○	○	○	○	○	○	○	○	○
2	6th Nerve	○	○	○	○	○	○	○	○	○	○	○	○	○	○	○	○
3	Facial weakness	○	○	○	○	○	○	○	○	○	○	○	○	○	○	○	○
4	Palate weakness	○	○	○	○	○	○	○	○	○	○	○	○	○	○	○	○
5	Tongue weakness	○	○	○	○	○	○	○	○	○	○	○	○	○	○	○	○
	Muscle Weakness																
6	Respiratory	○	○	○	○	○	○	○	○	○	○	○	○	○	○	○	○
7	Neck flexion	○	○	○	○	○	○	○	○	○	○	○	○	○	○	○	○
8	Shoulder abduction	○	○	○	○	○	○	○	○	○	○	○	○	○	○	○	○
9	Elbow flexion	○	○	○	○	○	○	○	○	○	○	○	○	○	○	○	○
10	Brachioradialis	○	○	○	○	○	○	○	○	○	○	○	○	○	○	○	○
11	Elbow extension	○	○	○	○	○	○	○	○	○	○	○	○	○	○	○	○
12	Wrist flexion	○	○	○	○	○	○	○	○	○	○	○	○	○	○	○	○
13	Wrist extension	○	○	○	○	○	○	○	○	○	○	○	○	○	○	○	○
14	Finger flexion	○	○	○	○	○	○	○	○	○	○	○	○	○	○	○	○
15	Finger spread	○	○	○	○	○	○	○	○	○	○	○	○	○	○	○	○
16	Thumb abduction	○	○	○	○	○	○	○	○	○	○	○	○	○	○	○	○
17	Hip flexion	○	○	○	○	○	○	○	○	○	○	○	○	○	○	○	○
18	Hip extension	○	○	○	○	○	○	○	○	○	○	○	○	○	○	○	○
19	Knee flexion	○	○	○	○	○	○	○	○	○	○	○	○	○	○	○	○
20	Knee extension	○	○	○	○	○	○	○	○	○	○	○	○	○	○	○	○
21	Ankle dorsiflexors	○	○	○	○	○	○	○	○	○	○	○	○	○	○	○	○
22	Ankle plantar flexors	○	○	○	○	○	○	○	○	○	○	○	○	○	○	○	○
23	Toe extensors	○	○	○	○	○	○	○	○	○	○	○	○	○	○	○	○
24	Toe flexors	○	○	○	○	○	○	○	○	○	○	○	○	○	○	○	○

NEUROPATHY IMPAIRMENT SCORE (NIS)

For patients 50-69 years old, ankle reflexes which are decreased are graded 0 and when absent are graded 1.
For patients ≥ 70 years, absent ankle reflexes are graded 0.

SCORING, REFLEXES
0 = NORMAL; 1 = DECREASED; 2 = ABSENT

	RIGHT			LEFT		
Reflexes:	0	1	2	0	1	2
25. Biceps brachii	○	○	○	○	○	○
26. Triceps brachii	○	○	○	○	○	○
27. Brachioradialis	○	○	○	○	○	○
28. Quadriceps femoris	○	○	○	○	○	○
29. Triceps surae	○	○	○	○	○	○

Touch-pressure, pin-prick and vibration sensation are tested on the dorsal surface, at the base of the nail, of the terminal phalanx of the index finger and great toe. Touch-pressure is assessed with long fiber cotton wool. Pin-prick is assessed with straight pins. Vibration sensation is tested with a 165 hz tuning fork (V. Mueller, Chicago, length 25 cm, made from 1/2" x 1 1/4 " stock; 165 hz with counterweights). Joint motion is tested by moving the terminal phalanx of the index finger and great toe.

SCORING, SENSATION
0 = NORMAL; 1 = DECREASED; 2 = ABSENT

	RIGHT			LEFT		
Sensation - Index Finger	0	1	2	0	1	2
30. Touch pressure	○	○	○	○	○	○
31. Pin-prick	○	○	○	○	○	○
32. Vibration	○	○	○	○	○	○
33. Joint position	○	○	○	○	○	○
Sensation - Great Toe	0	1	2	0	1	2
34. Touch pressure	○	○	○	○	○	○
35. Pin-prick	○	○	○	○	○	○
36. Vibration	○	○	○	○	○	○
37. Joint position	○	○	○	○	○	○

Appendix 10.2. Neuropathy Impairment Score. Reproduced from (Dyck et al., 1997). The areas

highlighted in blue compose the NIS-LL.

1	Sum individual scores of the NIS for the lower limbs NIS-LL
2	In NISS-LL substitute transformed points for percentile abnormality* of VDT for each great toe (obtained with CASE IV) for the clinical vibration sensation point score of great toes
3	Add transformed points for percentile abnormality* of variability of heart beat to deep breathing
4	Summate transformed points for percentile abnormality* of the five attributes of nerve conduction study of the lower limb (peroneal nerve, sural nerve and tibial nerve) divided by the number of attributes with obtainable values. Multiple by 5 (the number of attributes) and add this to the global score

Appendix 10.3. Calculation of the NIS (LL) + 7 (Neuropathy Impairment Score of the lower limb plus 7 tests). *Percentile abnormality: $<95^{th}$ = 0, $>95^{th}$-99^{th} = 1, $>99^{th}$-99.9^{th} = 2, > 99^{th} =3 (and the converse for opposite tail of distribution) (Dyck et al., 1997). CASE, computer assisted sensory evaluation; VDT, vibration detection threshold.

Interview questions for the patient:
Question 1: Does your pain have one or more of the following characteristics?

	Yes (1)	No (0)
1. Burning		
2. Cold is painful		
3. Electric shocks		

Question 2: Is the pain associated with one or more of the following symptoms in the same area?

	Yes (1)	No (0)
4. Tingling		
5. Pins and needles		
6. Numbness		
7. Itching		

Examination of the patient:
Question 3: Is the pain located in an area where the physical examination had one or both of the following characteristics?

	Yes (1)	No (0)
8. Hypoaesthesia to touch		
9. Hypoaesthesia to pinprick		

Hypoaesthesia: decreased sensitivity

Question 4: In the painful area, can the pain be caused or increased by:

	Yes (1)	No (0)
10. Brushing		
Total score =		

Total score ≥ 4: 90% probability of neuropathic pain.

Appendix 10.4. English translation of the Douleur neuropathique en 4 questions (DN4) (Bouhassira et al., 2005).

You may be suffering from pain due to injury or disease of the nervous system. This pain may be of several types. You may have spontaneous pain, i.e. pain in the absence of any stimulation, which may be long-lasting or occur as brief attacks. You may also have pain provoked or increased by brushing, pressure, or contact with cold in the painful area. You may feel one or several types of pain. This questionnaire has been developed to help your doctor to better evaluate and treat various types of pain you feel.

We wish to know if you feel spontaneous pain, that is pain without any stimulation. For each of the following questions, please select the number that best describes your *average spontaneous pain severity during the past 24 h.* Select the number 0 if you have not felt such pain (circle one number only).
Q1. Does your pain feel like burning?

No burning.	0	1	2	3	4	5	6	7	8	9	10	Worst burning imaginable.

Q2. Does your pain feel like squeezing?

No squeezing.	0	1	2	3	4	5	6	7	8	9	10	Worst squeezing imaginable.

Q3. Does your pain feel like pressure?

No pressure.	0	1	2	3	4	5	6	7	8	9	10	Worst pressure imaginable.

Q4. *During the past 24 h*, your spontaneous pain has been present:

Select the *response* that best describes your case

Permanently	
Between 8 and 12h	
Between 4 and 7h	
Between 1 and 3h	
Less than 1h	

We wish to know if you have brief attacks of pain. For each of the following questions, please select the number that best describes the *average severity of your painful attacks during the past 24 h*. Select the number 0 if you have not felt such pain (circle one number only).

Q5. Does your pain feel like electric shocks?

No electric shocks.	0	1	2	3	4	5	6	7	8	9	10	Worst electric shocks imaginable.

Q6. Does your pain feel like stabbing?

No stabbing.	0	1	2	3	4	5	6	7	8	9	10	Worst stabbing imaginable.

Q7. *During the past 24 h*, how many of these pain attacks have you had?

Select the *response* that best describes your case:

More than 20.	
Between 11 and 20.	
Between 6 and 10.	
Between 1 and 5.	
No pain	

We wish to know if you feel pain provoked or increased by brushing, pressure, contact with cold or warmth on the painful area. For each of the following questions, please select the number that best describes the *average severity of your provoked pain during the past 24 h*. Select the number 0 if you have not felt such pain (circle one number only).

Q8. Is your pain provoked or increased by brushing on the painful area?

No pain.	0	1	2	3	4	5	6	7	8	9	10	Worst pain imaginable.

Q9. Is your pain provoked or increased by pressure on the painful area?

No pain.	0	1	2	3	4	5	6	7	8	9	10	Worst pain imaginable.

Q10. Is your pain provoked or increased by contact with something cold on the painful area?

No pain.	0	1	2	3	4	5	6	7	8	9	10	Worst pain imaginable.

We wish to know if you feel abnormal sensations *in the painful area*. For each of the following questions, please select the number that best describes the *average severity of your abnormal sensations during the past 24 h*. Select the number 0 if your have not felt such sensation (circle one number only).

Q11. Do you feel pins and needles?

No pins and needles.	0	1	2	3	4	5	6	7	8	9	10	Worst pins and needles imaginable.

Q12. Do you feel tingling?

No tingling.	0	1	2	3	4	5	6	7	8	9	10	Worst tingling imaginable.

-END-

Appendix 10.5. The Neuropathic Pain Symptom Inventory. Reproduced from (Bouhassira et al., 2004).

Symptom scores	Sensory test scores
Foot pain	Pinprick
Numbness	Temperature
Tingling	Light touch
Weakness	Vibration
Ataxia	Position Sense
Upper limb symptoms	
Symptom scores graded as	Sensory test scores graded as
0 = absent	0 = normal
1 = present but no interference with sense of well-being or activities of daily living	1 = reduced at the toes only
2 = present, interferes with sense of well-being but not with activities of daily living	2 = reduced to a level above the toes, but only up to the ankles
3 = present and interferes with both sense of well-being and activities of daily living (both)	3 = reduced to a level above the ankles and/or absent at the toes

Maximum mTCNS is 33.
Symptoms and signs (sensory tests) are considered present if as a result of diabetic sensorimotor polyneuropathy (DSP) in the opinion of the investigator.

Appendix 10.6. The modified Toronto Clinical Neuropathy Score. Reproduced from (Bril et al., 2009)

Painful-DSPN NPSI score breakdown	Score
Total burning	5.0 (IQR 6.5)
Total Pressing	2.5 (5.0)
Total Paroxysmal pain	5.75 ± 2.4
Total Evoked pain	4.67 (5.9)
Total Paraesthesia/dysaesthesia	6.25 (3.25)

Appendix 10.7. Breakdown of the NPSI score in participants with painful-DSPN. Data are presented as mean ± standard deviation for parametric and median (IQR) for non-parametric continuous data or percentage for categorical data. NPSI, neuropathic pain symptom inventory.

	HV (n=12)	No-DSPN (n=11)	Painless-DSPN (n=12)	Painful-DSPN (n=20)	P value
CDT z-score	-0.51 ± 1.45	-0.51 ± 0.86	-2.33 ± 1.19	-2.59 ± 0.80	**<0.001 A**
CDT % abnormal	8.3%	0%	66.7%	84.2%	**<0.001 Chi^2**
WDT z-score	-0.61 ± 0.89	-0.45 ± 0.89	-1.91 ± 0.95	-1.96 ± 0.57	**<0.001 A**
WDT % abnormal	8.3%	0%	58.3%	52.6%	**0.001 Chi^2**
TSL z-score	-1.02 ± 1.32	-0.70 ± 0.82	-2.37 ± 1.26	-2.31 ± 0.73	**<0.001 A**
TSL % abnormal	25%	0%	50%	68.4%	**0.002 Chi^2**
CPT z-score	-1.02 (IQR 0.48)	-1.02 (0.13)	-1.08 (0.32)	-1.02 (0.16)	0.473 KW
CPT % abnormal	0%	0%	0%	0%	N/A
HPT z-score	-0.14 (2.91)	-0.55 (1.48)	-1.88 (1.48)	-1.46 (0.82)	**0.002 KW**
HPT % abnormal	8.3%	9.1%	41.7%	21.1%	0.151 Chi^2
PPT z-score	0.92 ± 0.81	1.29 ± 0.90	0.91 ± 1.98	0.16 ± 1.92	0.590 A
PPT % abnormal	0%	9.1%	33.3%	36.8%	0.52 Chi^2
MPT z-score	1.37 ± 2.08	1.24 ± 1.58	-2.35 ± 1.33	-1.88 ± 1.80	**<0.001 A**
MPT % abnormal	41.7%	45.5%	75%	68.4%	0.078 Chi^2
MPS z-score	-0.61 (2.02)	-0.96 (1.12)	-1.93 (0.51)	-1.94 (0.47)	**0.001 KW**
MPS % abnormal	33.3%	27.3%	91.7%	78.9%	**0.001 Chi^2**
WUR z-score	0.44 ± 1.14	-0.40 ± 1.03	0.39 ± 1.33	-	0.638 A
WUR % abnormal	0%	9.1%	0%	0%	0.473 Chi^2
MDT z-score	1.95 (2.04)	1.17 (2.00)	-2.23 (3.36)	-2.05 (2.93)	**<0.001 KW**
MDT % abnormal	58.3%	45.5%	58.3%	52.6%	0.925 Chi^2
VDT z-score	0.40 (1.44)	-0.33 (2.19)	-2.20 (3.93)	-2.96 (2.38)	**0.001 KW**
VDT & abnormal	8.3%	9.1%	50%	68.4%	**0.001 Chi^2**

DMA score	0	0	0	0	N/A
DMA % abnormal	0%	0%	0%	0%	N/A
PHS %	0 – 83.3% 1 – 8.3% 2 – 0% 3 – 8.3%	0 – 27.3% 1 – 18.2% 2 – 0% 3 – 54.5%	0 – 91.7% 1 – 0% 2 – 0% 3 – 8.3%	0 – 57.9% 1 – 5.3% 2 - 15.8% 3 – 21.1%	**0.018 Chi^2**
PHS % abnormal	8.3%	72.7%	8.3%	36.8%	**0.002 Chi^2**

Appendix 10.8. German pain research network QST results in study participants. Data are presented as mean ± standard deviation for parametric and median (IQR) for non-parametric continuous data or percentage for categorical data. The statistical test used was ANOVA (A) for continuous normally distributed data, Kruskal-Wallis (KW) for non-parametric continuous data or Chi^2 for categorical data. CDT, cold detection threshold; CPT, cold pain threshold; DMA, dynamic mechanical allodynia; HPT, heat pain threshold; MDT, mechanical detection threshold; MPT, mechanical pain threshold; PHS, paradoxical heat sensation; PPT, pressure pain threshold; VDT, vibration detection threshold; WUR, wind up ratio.

	HV (n=8)	No-DSPN (n=7)	Painless-DSPN (n=9)	Painful-DSPN (n=18)	P value
Age (years)	69.5 (IQR 11.0)	63.0 (8.0)	61.0 (13.5)	61.0 (8.0)	0.368 KW
Sex (% female)	25%	43%	56%	39%	0.641 Chi^2
Duration DM (years)		10 ± 6.2	16.4 ± 6.0	13.1 ± 8.5	0.247 A
Retinopathy presence (% present)		28.6%	33.3%	61.1%	0.216 Chi^2
Retinopathy score (0= No DR, 1= Bck/Pre-P, 2=Pro/Laser)		0 = 5 1 = 2 2 = 0	0 = 6 1 = 2 2 = 1	0 = 7 1 = 6 2 = 5	0.380 Chi^2
Nephropathy presence (% present)		0%	50%	53%	**0.046 Chi^2**
ACR (mg/mmol)		0.8 (0.77 IQR)	1.3 (1.8)	1.8 (1.6)	0.210 KW
Number of hypoglycaemic episodes in last 12 months		0.0 (1.3 IQR)	0.0 (0.0)	0.0 (3.5)	0.085 KW
Smoked ever (% Yes)	50%	57.1%	55.6%	72.2%	0.679 Chi^2
Pack Years smoking (Packs [1 pack = 20 cigarettes] x Number of years)	6.25 (18.75 IQR)	9.0 (30.0)	0.8 (20.6)	2.2 (36.3)	0.853 KW
Alcohol intake (units/week)	3.0 (11.3 IQR)	5.0 (12.0)	1.0 (11.0)	0.0 (0.1)	**0.023 KW**
Waist/hip ratio	0.90 ± 0.1	0.93 ± 0.02	0.97 ± 0.07	0.96 ± 0.08	0.208 A
Body mass index (kg/m^2)	28.0 ± 6.6	28.7 ± 4.1	32.2 ± 3.4	31.3 ± 5.2	0.116 A
Systolic blood pressure (mmHg)	137.1 ± 22.7	126.3 ± 13.3	144.8 ± 19.6	140.1 ± 15.5	0.229 A

Creatinine (µmol/l)	71.4 ± 7.7	75.4 ± 11.3	76.6 ± 14.3	71.0 ± 16.9	0.746 A
Total Cholesterol (mmol/l)	5.18 ± 0.9	5.21 ± 0.7	4.04 ± 1.0	4.32 ± 1.0	**0.022 A**
HbA1c (mmol/mol)	37.9 (IQR 4.5)	61.0 (IQR 34.0)	56.0 (30.5)	65.0 (32.8)	**0.001 KW**
Glucose During MR (mmol/l)		6.8 (IQR 7.4)	9.6 (8.3)	9.5 (5.1)	0.763 KW
MMSE	30.0 (IQR 0.0)	30.0 (0.0)	30.0 (1.0)	29.0 (2.3)	0.108 KW
Depression (% Yes)	0%	0%	0%	16.7%	0.230 Chi^2
Anxiety (% Yes)	0%	0%	11.1%	16.7%	0.445 Chi^2

Appendix 10.9. Clinical details of participants undergoing 1H-MRS in Chapter 4. Data are presented as mean ± standard deviation for parametric and median (IQR) for non-parametric continuous data or percentage for categorical data. The statistical test used was ANOVA (A) for continuous normally distributed data, Kruskal-Wallis (KW) for non-parametric continuous data or Chi^2 for categorical data. Retinopathy parameters: Bck, background retinopathy; DR, diabetic retinopathy; Laser, panretinal photocoagulation; Pre-P, pre-proliferative retinopathy; Pro, proliferative retinopathy. ACR, albumin to creatinine ratio; DM, diabetes mellitus; MMSE, mini-mental state examination.

	HV (n=8)	No-DSPN (n=7)	Painless-DSPN (n=9)	Painful-DSPN (n=18)	P value
NPSI (Total score)	0.0 (IQR 0.0)	0.0 (0.0)	0.0 (0.0)	19.1 (15.8)	**<0.001 KW**
DN4	0.0 (IQR 0.0)	0.0 (0.0)	0.0 (1.5)	6.0 (2.3)	**<0.001 KW**
TCNS	0.0 (IQR 0.0)	0.0 (2.0)	9.0 (5.0)	14.0 (5.8)	**<0.001 KW**
NIS-LL	0.0 (IQR 0.0)	0.0 (0.0)	12.0 (13.0)	18.0 (11.3)	**<0.001 KW**
NIS-LL+7	0.0 (IQR 0.8)	0.0 (0.0)	22.0 (19.8)	26.2 (17.8)	**<0.001 KW**
Peroneal CMAP (mV)	6.0 ± 2.4	6.0 ± 2.1	1.7 ± 1.8	2.5 ± 1.9	**<0.001 A**
Peroneal MNCV (m/s)	46.9 (IQR 2.9)	45.6 (2.3)	36.6 (20.2)	37.6 (7.2)	**<0.001 KW**
Peroneal MNDL (msec)	4.9 (IQR 1.0)	4.1 (0.3)	7.1 (9.5)	5.8 (1.8)	**0.001 KW**
Tibial MNDL (msec)	4.8 (IQR 0.4)	4.4 (0.9)	5.6 (2.9)	6.5 (3.3)	**0.004 KW**
Sural SNAP (mV)	12.8 (IQR 8.2)	12.5 (7.6)	1.6 (3.7)	0.7 (7.0)	**0.001 KW**
CAN composite score	0.0 (IQR 0.0)	0.0 (1.3)	0.0 (0.0)	0.0 (3.8)	0.175 KW
ESC (µS)	82.0 (IQR 11.8)	68.0 (22.0)	58.5 (32.0)	53.0 (34.5)	**0.002 KW**

Appendix 10.10. Neurological assessments of study participants undergoing 1H-MRS in Chapter 4. Data are presented as mean ± standard deviation for parametric and median (IQR) for non-parametric continuous data. The statistical test used was ANOVA (A) for continuous normally distributed data and Kruskal-Wallis (KW) for non-parametric continuous data. CAN, cardiac autonomic neuropathy; CMAP, compound muscle action potential; DN4, doleur neuropathique 4; ESC, electrochemical skin conductance; MNDL, motor nerve distal latency; MNCV, motor nerve conduction velocity; NIS-LL, neuropathic impairment score of the lower limb; NPSI, neuropathic pain symptom inventory; SNAP, sural nerve action potential; TCNS, Toronto clinical neuropathy score; vWF, von Willebrand Factor.

	HV (n=9)	No-DSPN (n=8)	Painless-DSPN (n=9)	Painful-DSPN (n=14)	P value
Age (years)	70.0 (IQR 17.0)	61.5 (6.8)	61.0 (13.5)	60.5 (15.0)	0.615 KW
Sex (% female)	33.3%	63%	44.4%	35.7%	0.594 Chi^2
Duration DM (years)		8.6 ± 5.8	16.2 ± 6.1	11.9 ± 7.0	0.067 A
Retinopathy presence (% present)		25.0%	44.4%	71.4%	0.098 Chi^2
Retinopathy score (0= No DR, 1= Bck/Pre-P, 2=Pro/Laser)		0 = 6 1 = 2 2 = 0	0 = 5 1 = 3 2 = 1	0 = 4 1 = 5 2 = 5	0.172 Chi^2
Nephropathy presence (% present)		0%	50%	46.2%	0.054 Chi^2
ACR (mg/mmol)		0.5 (0.6 IQR)	1.8 (1.7)	2.0 (1.3)	0.067 KW
Number of hypoglycaemic episodes in last 12 months		0.0 (0.0 IQR)	0.0 (0.0)	0.0 (3.5)	0.338 KW
Smoked ever (% Yes)	55.6%	62.5%	66.7%	57.1%	0.958 Chi^2
Pack Years smoking (Packs [1 pack = 20 cigarettes] x Number of years)	12.5 (20.0 IQR)	9.5 (14.3)	1.0 (38.1)	0.4 (30.0)	0.943 KW
Alcohol intake (units/week)	4.0 (10.0 IQR)	7.5 (12.0)	1.0 (7.0)	0.0 (0.6)	**0.024 KW**
Waist/hip ratio	0.87 ± 0.06	0.91 ± 0.04	0.98 ± 0.08	0.94 ± 0.08	**0.013 A**
Body mass index (kg/m^2)	25.4 ± 5.1	28.3 ± 4.6	32.1 ± 2.9	29.3 ± 4.0	**0.017 A**

Systolic blood pressure (mmHg)	128.0 ± 18.5	129.3 ± 11.2	137.9 ± 14.5	140.9 ± 17.0	0.196 A
Creatinine (µmol/l)	71.1 ± 8.0	71.0 ± 13.0	79.0 ± 13.8	73.9 ± 16.1	0.573 A
Total Cholesterol (mmol/l)	4.66 ± 0.8	5.14 ± 0.6	3.88 ± 1.0	4.41 ± 1.1	0.060 A
HbA1c (mmol/mol)	36.0 (IQR 6.5)	62.5 (IQR 28.0)	61.0 (30.5)	61.5 (39.5)	**<0.001 KW**
Glucose During MR (mmol/l)		9.04 (IQR 6.6)	9.6 (8.5)	9.5 (5.6)	0.964 KW
MMSE	30.0 (IQR 0.0)	30.0 (1.8)	30.0 (1.5)	29.0 (2.0)	0.240 KW
Depression (% Yes)	0%	0%	0%	14.3%	0.271 Chi^2
Anxiety (% Yes)	0%	0%	11.1%	14.3%	0.480 Chi^2

Appendix 10.11. Clinical details of participants undergoing 1H-MRS of the thalamus only in Chapter 4. Data are presented as mean ± standard deviation for parametric and median (IQR) for non-parametric continuous data or percentage for categorical data. The statistical test used was ANOVA (A) for continuous normally distributed data, Kruskal-Wallis (KW) for non-parametric continuous data or Chi^2 for categorical data. Retinopathy parameters: Bck, background retinopathy; DR, diabetic retinopathy; Laser, panretinal photocoagulation; Pre-P, pre-proliferative retinopathy; Pro, proliferative retinopathy. ACR, albumin to creatinine ratio; MMSE, mini-mental state examination.

	HV (n=9)	No-DSPN (n=8)	Painless-DSPN (n=9)	Painful-DSPN (n=14)	P value
NPSI (Total score)	0.0 (IQR 0.0)	0.0 (0.0)	0.0 (0.0)	17.9 (14.8)	**<0.001 KW**
DN4	0.0 (IQR 0.0)	0.0 (0.0)	0.0 (1.5)	7.0 (2.5)	**<0.001 KW**
TCNS	0.0 (IQR 0.0)	0.0 (1.5)	9.0 (7.0)	16.0 (5.0)	**<0.001 KW**
NIS-LL	0.0 (IQR 0.0)	0.0 (0.0)	14.0 (12.0)	18.0 (6.5)	**<0.001 KW**
NIS-LL+7	0.0 (IQR 1.0)	0.0 (0.0)	25.0 (17.0)	27.7 (17.0)	**<0.001 KW**
Peroneal CMAP (mV)	5.5 ± 3.5	4.7 ± 3.0	0.7 ± 3.3	2.6 ± 3.7	**<0.001 A**
Peroneal MNCV (m/s)	46.3 (IQR 2.8)	45.5 (2.3)	35.4 (18.5)	37.6 (7.7)	**<0.001 KW**
Peroneal MNDL (msec)	4.8 (IQR 0.9)	4.1 (0.2)	7.5 (7.8)	6.0 (2.2)	**0.001 KW**
Tibial MNDL (msec)	4.6 (IQR 0.9)	4.4 (0.9)	5.4 (2.9)	6.1 (3.3)	**0.004 KW**
Sural SNAP (mV)	15.4 (IQR 9.0)	12.5 (6.7)	1.4 (2.7)	1.6 (7.6)	**0.001 KW**
CAN composite score	0.0 (IQR 0.0)	0.0 (1.3)	0.0 (0.0)	0.0 (2.8)	0.175 KW
ESC (µS)	79.0 (IQR 11.0)	72.0 (21.0)	58.0 (28.8)	53.0 (29.0)	**0.002 KW**

Appendix 10.12. Neurological assessments of study participants undergoing 1H-MRS of the thalamus only in Chapter 4. Data are presented as mean ± standard deviation for parametric and median (IQR) for non-parametric continuous data or percentage for categorical data. The statistical test used was ANOVA (A) for continuous normally distributed data, Kruskal-Wallis (KW) for non-parametric continuous data or Chi^2 for categorical data. CAN, cardiac autonomic neuropathy; CMAP, compound muscle action potential; DN4, doleur neuropathique 4; ESC, electrochemical skin conductance; MNDL, motor nerve distal latency; MNCV, motor nerve conduction velocity; NIS-LL, neuropathic impairment score of the lower limb; NPSI, neuropathic pain symptom inventory; SNAP, sural nerve action potential; TCNS, Toronto clinical neuropathy score; vWF, von Willebrand Factor.

vWF	HV (n=6)	T2DM (n=5)	Painless-DSPN (n=8)	Painful-DSPN (n=14)	P value
Age (years)	69.7 ± 9.3	64.4 ± 4.7	63.1 ± 5.9	64.4 ± 10.9	0.597 A
Sex (% female)	50.0	40.0	25.0	42.9	0.790 Chi^2
Duration DM (years)		9.8 ± 5.8	16.3 ± 7.7	11.2 ± 7.1	0.200 A
Retinopathy presence (% present)		80%	62.5%	78.6%	**<0.001 Chi^2**
Retinopathy score (0= No DR, 1= Bck/Pre-P, 2=Pro/Laser)		0 = 20% 1 = 80% 2 = 0%	0 = 37.5% 1 = 37.5% 2 = 25.0%	0 = 21.4% 1 = 42.9% 2 = 35.7%	**<0.001 Chi^2**
Nephropathy presence (% present)		20%	50%	42.9%	**<0.001 Chi^2**
ACR (mg/mmol)	0.0 (0.2)	1.5 (1.7)	0.9 (1.9)	1.5 (3.5)	**0.013 KW**
Number of hypoglycaemic episodes in last 12 months		0 ± 0	3.7 ± 7.5	5.4 ± 14.2	0.768 A
Smoked ever (% Yes)	50%	40%	75%	78.6%`	0.322 Chi^2
Pack Years smoking (Packs [1 pack = 20 cigarettes] x Number of years)	10.0 ± 11.4	6.1 ± 13.4	23.4 ± 23.7	25.0 ± 24.5	0.248 A
Alcohol intake (units/week)	4.8 ± 5.0	10.7 ± 3.1	6.3 ± 4.8	6.5 ± 5.6	0.337 A
Waist/hip ratio	0.87 ± 0.06	0.95 ± 0.07	1.00 ± 0.08	0.96 ± 0.08	**0.028 A**
Body mass index (kg/m^2)	27.5 ± 6.4	30.8 ± 4.1	30.1 ± 3.2	31.0 ± 5.7	0.679 A
Systolic blood pressure (mmHg)	139.8 ± 21.7	124.2 ± 10.3	137.4 ± 19.7	137.0 ± 12.9	0.404 A

Creatinine (µmol/l)	70.0 ± 9.9	77.4 ± 8.6	72.8 ± 11.2	75.4 ± 23.9	0.892 A
Total Cholesterol (mmol/l)	5.0 ± 1.2	4.1 ± 1.2	3.5 ± 0.7	4.2 ± 1.0	0.084 A
HbA1c (mmol/mol)	37.5 ± 4.0	56.6 ± 10.6	63.1 ± 16.8	67.4 ± 18.8	**0.005 A**

Appendix 10.13. Clinical details of study participants undergoing skin biopsy and vWF analysis. Data are presented as mean ± standard deviation for parametric and median (IQR) for non-parametric continuous data or percentage for categorical data. The statistical test used was ANOVA (A) for continuous normally distributed data, Kruskal-Wallis (KW) for non-parametric continuous data or Chi^2 for categorical data. Retinopathy parameters: Bck, background retinopathy; DR, diabetic retinopathy; Laser, panretinal photocoagulation; Pre-P, pre-proliferative retinopathy; Pro, proliferative retinopathy. ACR, albumin to creatinine ratio; MMSE, mini-mental state examination.

vWF	HV (n=6)	T2DM (n=5)	Painless-DSPN (n=8)	Painful-DSPN (n=14)	P value
NPSI (Total score)	0.0 (0.0)	0.0 (0.0)	0.0 (0.0)	20.5 (18.8)	**<0.001 KW**
DN4	0.0 (0.0)	0.0 (1.0)	2.0 (1.5)	6.0 (3.3)	**<0.001 KW**
TCNS	0.0 (0.3)	2.0 (1.0)	8.0 (10.0)	15.5 (3.0)	**<0.001 KW**
NIS-LL	0.0 (0.5)	0.0 (1.0)	9.0 (19.3)	17.5 (8.5)	**<0.001 KW**
NIS-LL+7	0.0 (0.8)	0.0 (1.5)	17.0 (23.7)	27.3 (15.1)	**P <0.001 KW**
Peroneal CMAP (mV)	5.0 ± 1.9	5.4 ± 2.7	2.8 ± 3.2	2.3 ± 1.8	**0.035 A**
Peroneal MNCV (m/s)	46.6 ± 1.9	46.7 ± 2.9	37.4 ± 9.7	39.0 ± 5.0	**0.015 A**
Peroneal MNDL (msec)	4.9 (0.7)	4.5 (0.9)	6.6 (2.6)	5.7 (1.9)	**0.033 KW**
Tibial MNDL (msec)	4.8 (1.4)	4.7 (0.5)	7.4 (2.9)	6.6 (2.8)	**0.001 KW**
Sural SNAP (mV)	13.2 ± 7.9	11.1 ± 3.9	5.6 ± 4.9	2.9 ± 4.9	**0.012 A**
CAN composite score	0.0 (0.0)	0.0 (0.0)	0.0 (0.0)	2.0 (7.5)	**0.010 KW**
Foot ESC (µS)	71.2 ± 11.1	74.2 ± 13.5	54.1 ± 19.8	43.1 ± 20.8	**0.005 A**
PGP 9.5 IENF fibres/mm	18.1 ± 3.8	17.7 ± 3.6	7.9 ± 4.2	6.1 ± 5.5	**<0.001 A**
vWF % area	2.4 (1.0)	2.7 (1.1)	3.1 (1.8)	4.7 (0.9)	**<0.001 KW**

Appendix 10.14. Neurological assessments of study participants undergoing skin biopsy and vWF analysis. Data are presented as mean ± standard deviation for parametric and median (IQR) for non-parametric continuous data. The statistical test used was ANOVA (A) for continuous normally distributed data and Kruskal-Wallis (KW) for non-parametric continuous data. CAN, cardiac autonomic neuropathy; CMAP, compound muscle action potential; DN4, doleur neuropathique 4; ESC, electrochemical skin conductance; MNDL, motor nerve distal latency; MNCV, motor nerve conduction velocity; NIS-LL, neuropathic impairment score of the lower limb; NPSI, neuropathic pain symptom inventory; SNAP, sural nerve action potential; TCNS, Toronto clinical neuropathy score; vWF, von Willebrand Factor.

vWF	HV (n=6)	T2DM (n=5)	Painless-DSPN (n=8)	Painful-DSPN (n=14)	P value
CDT z-score	-0.75 ± 1.53	-0.78 ± 0.43	-2.21 ± 1.18	-2.13 ± 1.40	0.052 A
CDT % abnormal	16.7%	0.0%	50%	71.4%	**0.018 Chi²**
WDT z-score	-0.85 ± 1.08	-0.54 ± 0.77	-1.68 ± 1.12	-2.03 ± 0.46	**0.004 A**
WDT % abnormal	16.7%	0%	50%	57.1%	0.080 Chi²
TSL z-score	-1.34 ± 1.53	-1.09 ± 0.27	-2.25 ± 1.30	-2.20 ± 0.59	0.077 A
TSL % abnormal	33.3%	0%	37.5%	64.3%	0.082 Chi²
CPT z-score	-1.05 (0.19)	-0.98 (0.64)	-0.87 (1.03)	-1.0 (0.73)	0.645 KW
CPT % abnormal	0%	0%	0%	0%	N/A
HPT z-score	-0.43 ± 1.37	-0.79 ± 0.98	-0.62 ± 1.62	-1.39 ± 0.47	0.235 A
HPT % abnormal	16.7%	0%	37.5%	21.4%	0.442 Chi²
PPT z-score	0.35 ± 0.78	1.31 ± 2.19	0.55 ± 1.89	1.14 ± 1.96	0.724 A
PPT % abnormal	0.0%	60%	25.0%	71.4%	**0.014 Chi²**
MPT z-score	1.84 ± 1.90	1.23 ± 1.57	-1.60 ± 2.11	-1.96 ± 2.03	**0.0001 A**
MPT % abnormal	50%	60%	62.5%	85.7%	0.359 Chi²
MPS z-score	-1.85 (1.54)	0.14 (2.53)	-1.72 (1.56)	-1.94 (0.47)	**0.031 KW**
MPS % abnormal	66.7%	20.0%	75.0%	85.7%	0.053 Chi²
WUR z-score	-1.2 ± 1.02	-0.21 ± 1.49	-0.08 ± 0.88	-N/A ± N/A	0.592 A
WUR % abnormal	0%	20.0%	0%	0%	0.504 Chi²
MDT z-score	0.16 (2.13)	0.26 (1.72)	-1.31 (5.46)	-2.00 (3.25)	**P=0.032 KW**
MDT % abnormal	33.3%	20.0%	50.0%	50.0%	0.626 Chi²
VDT z-score	0.00 (2.12)	0.46 (2.16)	-2.20 (3.83)	-2.83 (1.85)	0.055 KW
VDT % abnormal	16.7%	20.0%	62.5%	64.3%	0.108 Chi²

DMA % abnormal	0%	0%	0%	7.1%	0.706
PHS % abnormal	0%	60.0%	25.0%	35.7%	0.172 Chi^2

Appendix 10.15. German pain research network QST results in Chapter 8 study participants. Data are presented as mean ± standard deviation for parametric and median (IQR) for non-parametric continuous data or percentage for categorical data. The statistical test used was ANOVA (A) for continuous normally distributed data, Kruskal-Wallis (KW) for non-parametric continuous data or Chi^2 for categorical data. CDT, cold detection threshold; CPT, cold pain threshold; DMA, dynamic mechanical allodynia; HPT, heat pain threshold; MDT, mechanical detection threshold; MPT, mechanical pain threshold; PHS, paradoxical heat sensation; PPT, pressure pain threshold; VDT, vibration detection threshold; WUR, wind up ratio.

References

ABBOTT, C. A., MALIK, R. A., VAN ROSS, E. R., KULKARNI, J. & BOULTON, A. J. 2011. Prevalence and characteristics of painful diabetic neuropathy in a large community-based diabetic population in the U.K. *Diabetes Care,* 34**,** 2220-4.

ABRAHAM, A., BARNETT, C., KATZBERG, H. D., LOVBLOM, L. E., PERKINS, B. A. & BRIL, V. 2018a. Sex differences in neuropathic pain intensity in diabetes. *J Neurol Sci,* 388**,** 103-106.

ABRAHAM, A., BARNETT, C., KATZBERG, H. D., LOVBLOM, L. E., PERKINS, B. A. & BRIL, V. 2018b. Toronto Clinical Neuropathy Score is valid for a wide spectrum of polyneuropathies. *Eur J Neurol,* 25**,** 484-490.

ADLER, A. I., BOYKO, E. J., AHRONI, J. H., STENSEL, V., FORSBERG, R. C. & SMITH, D. G. 1997. Risk factors for diabetic peripheral sensory neuropathy. Results of the Seattle Prospective Diabetic Foot Study. *Diabetes Care,* 20**,** 1162-7.

AGRAWAL, R. P., CHOUDHARY, R., SHARMA, P., SHARMA, S., BENIWAL, R., KASWAN, K. & KOCHAR, D. K. 2007. Glyceryl trinitrate spray in the management of painful diabetic neuropathy: a randomized double blind placebo controlled cross-over study. *Diabetes Res Clin Pract,* 77**,** 161-7.

AGRAWAL, R. P., GOSWAMI, J., JAIN, S. & KOCHAR, D. K. 2009. Management of diabetic neuropathy by sodium valproate and glyceryl trinitrate spray: a prospective double-blind randomized placebo-controlled study. *Diabetes Res Clin Pract,* 83**,** 371-8.

ALAM, U., RILEY, D. R., JUGDEY, R. S., AZMI, S., RAJBHANDARI, S., D'AOÛT, K. & MALIK, R. A. 2017. Diabetic Neuropathy and Gait: A Review. *Diabetes Ther,* 8**,** 1253-1264.

ALAM, U., SLOAN, G. & TESFAYE, S. 2020. Treating Pain in Diabetic Neuropathy: Current and Developmental Drugs. *Drugs,* 80**,** 363-384.

ALLEMAN, C. J., WESTERHOUT, K. Y., HENSEN, M., CHAMBERS, C., STOKER, M., LONG, S. & VAN NOOTEN, F. E. 2015. Humanistic and economic burden of painful diabetic peripheral neuropathy in Europe: A review of the literature. *Diabetes Res Clin Pract,* 109**,** 215-25.

ALSALOUM, M., ESTACION, M., ALMOMANI, R., GERRITS, M. M., BÖNHOF, G. J., ZIEGLER, D., MALIK, R., FERDOUSI, M., LAURIA, G., MERKIES, I. S., FABER, C. G., DIB-HAJJ, S., WAXMAN, S. G. & GROUP, P. S. 2019. A gain-of-function sodium channel β2-subunit mutation in painful diabetic neuropathy. *Mol Pain,* 15**,** 1744806919849802.

ALSHELH, Z., DI PIETRO, F., YOUSSEF, A. M., REEVES, J. M., MACEY, P. M., VICKERS, E. R., PECK, C. C., MURRAY, G. M. & HENDERSON, L. A. 2016. Chronic Neuropathic Pain: It's about the Rhythm. *J Neurosci,* 36**,** 1008-18.

ANAND, P. & BLEY, K. 2011. Topical capsaicin for pain management: therapeutic potential and mechanisms of action of the new high-concentration capsaicin 8% patch. *Br J Anaesth,* 107**,** 490-502.

ANAND, P., PRIVITERA, R., YIANGOU, Y., DONATIEN, P., BIRCH, R. & MISRA, P. 2017. Trench Foot or Non-Freezing Cold Injury As a Painful Vaso-Neuropathy: Clinical and Skin Biopsy Assessments. *Front Neurol,* 8**,** 514.

ANDERSEN, S. T., WITTE, D. R., DALSGAARD, E. M., ANDERSEN, H., NAWROTH, P., FLEMING, T., JENSEN, T. M., FINNERUP, N. B., JENSEN, T. S., LAURITZEN, T., FELDMAN, E. L., CALLAGHAN, B. C. & CHARLES, M. 2018. Risk Factors for Incident Diabetic Polyneuropathy in a Cohort With Screen-Detected Type 2 Diabetes Followed for 13 Years: ADDITION-Denmark. *Diabetes Care,* 41**,** 1068-1075.

APFEL, S. C. 1999. Neurotrophic factors in the therapy of diabetic neuropathy. *Am J Med,* 107**,** 34S-42S.

APKARIAN, A. V., BUSHNELL, M. C., TREEDE, R. D. & ZUBIETA, J. K. 2005. Human brain mechanisms of pain perception and regulation in health and disease. *Eur J Pain,* 9**,** 463-84.

APKARIAN, A. V., SOSA, Y., SONTY, S., LEVY, R. M., HARDEN, R. N., PARRISH, T. B. & GITELMAN, D. R. 2004. Chronic back pain is associated with decreased prefrontal and thalamic gray matter density. *J Neurosci,* 24**,** 10410-5.

ARCHER, A. G., ROBERTS, V. C. & WATKINS, P. J. 1984. Blood flow patterns in painful diabetic neuropathy. *Diabetologia,* 27**,** 563-7.

ARCHIBALD, J., MACMILLAN, E. L., ENZLER, A., JUTZELER, C. R., SCHWEINHARDT, P. & KRAMER, J. L. K. 2020a. Excitatory and inhibitory responses in the brain to experimental pain: A systematic review of MR spectroscopy studies. *Neuroimage,* 215**,** 116794.

ARCHIBALD, J., MACMILLAN, E. L., GRAF, C., KOZLOWSKI, P., LAULE, C. & KRAMER, J. L. K. 2020b. Metabolite activity in the anterior cingulate cortex during a painful stimulus using functional MRS. *Sci Rep,* 10**,** 19218.

AREZZO, J. C. 1999. New developments in the diagnosis of diabetic neuropathy. *Am J Med,* 107**,** 9S-16S.

ARIMURA, A., DEGUCHI, T., SUGIMOTO, K., UTO, T., NAKAMURA, T., ARIMURA, Y., ARIMURA, K., YAGIHASHI, S., NISHIO, Y. & TAKASHIMA, H. 2013. Intraepidermal nerve fiber density and nerve conduction study parameters correlate with clinical staging of diabetic polyneuropathy. *Diabetes Res Clin Pract,* 99**,** 24-9.

ARMSTRONG, D. G., BOULTON, A. J. M. & BUS, S. A. 2017. Diabetic Foot Ulcers and Their Recurrence. *N Engl J Med,* 376**,** 2367-2375.

AS-SANIE, S., KIM, J., SCHMIDT-WILCKE, T., SUNDGREN, P. C., CLAUW, D. J., NAPADOW, V. & HARRIS, R. E. 2016. Functional Connectivity is Associated With Altered Brain Chemistry in Women With Endometriosis-Associated Chronic Pelvic Pain. *J Pain,* 17**,** 1-13.

BARON, R., BINDER, A. & WASNER, G. 2010. Neuropathic pain: diagnosis, pathophysiological mechanisms, and treatment. *Lancet Neurology,* 9**,** 807-819.

BARON, R., TÖLLE, T. R., GOCKEL, U., BROSZ, M. & FREYNHAGEN, R. 2009. A cross-sectional cohort survey in 2100 patients with painful diabetic neuropathy and postherpetic neuralgia: Differences in demographic data and sensory symptoms. *Pain,* 146**,** 34-40.

BASIT, A., BASIT, K. A., FAWWAD, A., SHAHEEN, F., FATIMA, N., PETROPOULOS, I. N., ALAM, U. & MALIK, R. A. 2016. Vitamin D for the treatment of painful diabetic neuropathy. *BMJ Open Diabetes Res Care,* 4**,** e000148.

BEHSE, F., BUCHTHAL, F. & CARLSEN, F. 1977. Nerve biopsy and conduction studies in diabetic neuropathy. *J Neurol Neurosurg Psychiatry,* 40**,** 1072-82.

BENBOW, S. J., WALLYMAHMED, M. E. & MACFARLANE, I. A. 1998. Diabetic peripheral neuropathy and quality of life. *QJM,* 91**,** 733-7.

BENNETT, D. L., CLARK, A. J., HUANG, J. Y., WAXMAN, S. G. & DIB-HAJJ, S. D. 2019. The Role of Voltage-Gated Sodium Channels in Pain Signaling. *Physiological Reviews,* 99**,** 1079-1151.

BENNETT, D. L. & WOODS, C. G. 2014. Painful and painless channelopathies. *Lancet Neurol,* 13**,** 587-99.

BIERHAUS, A., FLEMING, T., STOYANOV, S., LEFFLER, A., BABES, A., NEACSU, C., SAUER, S. K., EBERHARDT, M., SCHNÖLZER, M., LASITSCHKA, F., LASISCHKA, F., NEUHUBER, W. L., KICHKO, T. I., KONRADE, I., ELVERT, R., MIER, W., PIRAGS, V., LUKIC, I. K., MORCOS, M., DEHMER, T., RABBANI, N., THORNALLEY, P. J., EDELSTEIN, D., NAU, C., FORBES, J., HUMPERT, P. M., SCHWANINGER, M., ZIEGLER, D., STERN, D. M., COOPER, M. E., HABERKORN, U., BROWNLEE, M., REEH, P. W. & NAWROTH, P. P. 2012. Methylglyoxal modification of Nav1.8 facilitates nociceptive neuron firing and causes hyperalgesia in diabetic neuropathy. *Nat Med,* 18**,** 926-33.

BIESSELS, G. J., BRAUN, K. P., DE GRAAF, R. A., VAN EIJSDEN, P., GISPEN, W. H. & NICOLAY, K. 2001. Cerebral metabolism in streptozotocin-diabetic rats: an in vivo magnetic resonance spectroscopy study. *Diabetologia,* 44**,** 346-53.

BIESSELS, G. J., CRISTINO, N. A., RUTTEN, G. J., HAMERS, F. P., ERKELENS, D. W. & GISPEN, W. H. 1999. Neurophysiological changes in the central and peripheral nervous system of

streptozotocin-diabetic rats. Course of development and effects of insulin treatment. *Brain,* 122 (Pt 4)**,** 757-68.
BLESNEAC, I., THEMISTOCLEOUS, A. C., FRATTER, C., CONRAD, L. J., RAMIREZ, J. D., COX, J. J., TESFAYE, S., SHILLO, P. R., RICE, A. S. C., TUCKER, S. J. & BENNETT, D. L. H. 2017. Rare Nav1.7 variants associated with painful diabetic peripheral neuropathy. *Pain*.
BLISS, T. V., COLLINGRIDGE, G. L., KAANG, B. K. & ZHUO, M. 2016. Synaptic plasticity in the anterior cingulate cortex in acute and chronic pain. *Nat Rev Neurosci,* 17**,** 485-96.
BÖNHOF, G. J., STROM, A., PÜTTGEN, S., RINGEL, B., BRÜGGEMANN, J., BÓDIS, K., MÜSSIG, K., SZENDROEDI, J., RODEN, M. & ZIEGLER, D. 2017. Patterns of cutaneous nerve fibre loss and regeneration in type 2 diabetes with painful and painless polyneuropathy. *Diabetologia,* 60**,** 2495-2503.
BOONSTRA, A. M., STEWART, R. E., KÖKE, A. J., OOSTERWIJK, R. F., SWAAN, J. L., SCHREURS, K. M. & SCHIPHORST PREUPER, H. R. 2016. Cut-Off Points for Mild, Moderate, and Severe Pain on the Numeric Rating Scale for Pain in Patients with Chronic Musculoskeletal Pain: Variability and Influence of Sex and Catastrophizing. *Front Psychol,* 7**,** 1466.
BORNHÖVD, K., QUANTE, M., GLAUCHE, V., BROMM, B., WEILLER, C. & BÜCHEL, C. 2002. Painful stimuli evoke different stimulus-response functions in the amygdala, prefrontal, insula and somatosensory cortex: a single-trial fMRI study. *Brain,* 125**,** 1326-36.
BOTTOMLEY, P. A. 1987. Spatial localization in NMR spectroscopy in vivo. *Ann N Y Acad Sci,* 508**,** 333-48.
BOUHASSIRA, D., ATTAL, N., ALCHAAR, H., BOUREAU, F., BROCHET, B., BRUXELLE, J., CUNIN, G., FERMANIAN, J., GINIES, P., GRUN-OVERDYKING, A., JAFARI-SCHLUEP, H., LANTÉRI-MINET, M., LAURENT, B., MICK, G., SERRIE, A., VALADE, D. & VICAUT, E. 2005. Comparison of pain syndromes associated with nervous or somatic lesions and development of a new neuropathic pain diagnostic questionnaire (DN4). *Pain,* 114**,** 29-36.
BOUHASSIRA, D., ATTAL, N., FERMANIAN, J., ALCHAAR, H., GAUTRON, M., MASQUELIER, E., ROSTAING, S., LANTERI-MINET, M., COLLIN, E., GRISART, J. & BOUREAU, F. 2004. Development and validation of the Neuropathic Pain Symptom Inventory. *Pain,* 108**,** 248-57.
BOULTON, A. J., KEMPLER, P., AMETOV, A. & ZIEGLER, D. 2013. Whither pathogenetic treatments for diabetic polyneuropathy? *Diabetes Metab Res Rev,* 29**,** 327-33.
BOULTON, A. J., KIRSNER, R. S. & VILEIKYTE, L. 2004. Clinical practice. Neuropathic diabetic foot ulcers. *N Engl J Med,* 351**,** 48-55.
BRIL, V. & PERKINS, B. A. 2002a. Comparison of vibration perception thresholds obtained with the Neurothesiometer and the CASE IV and relationship to nerve conduction studies. *Diabet Med,* 19**,** 661-6.
BRIL, V. & PERKINS, B. A. 2002b. Validation of the Toronto Clinical Scoring System for diabetic polyneuropathy. *Diabetes Care,* 25**,** 2048-52.
BRIL, V., TOMIOKA, S., BUCHANAN, R. A., PERKINS, B. A. & GROUP, M. S. 2009. Reliability and validity of the modified Toronto Clinical Neuropathy Score in diabetic sensorimotor polyneuropathy. *Diabet Med,* 26**,** 240-6.
BROWNLEE, M. 2001. Biochemistry and molecular cell biology of diabetic complications. *Nature,* 414**,** 813-20.
BROWNRIGG, J. R., HUGHES, C. O., BURLEIGH, D., KARTHIKESALINGAM, A., PATTERSON, B. O., HOLT, P. J., THOMPSON, M. M., DE LUSIGNAN, S., RAY, K. K. & HINCHLIFFE, R. J. 2016. Microvascular disease and risk of cardiovascular events among individuals with type 2 diabetes: a population-level cohort study. *Lancet Diabetes Endocrinol,* 4**,** 588-97.
BURGMER, M., GAUBITZ, M., KONRAD, C., WRENGER, M., HILGART, S., HEUFT, G. & PFLEIDERER, B. 2009. Decreased gray matter volumes in the cingulo-frontal cortex and the amygdala in patients with fibromyalgia. *Psychosom Med,* 71**,** 566-73.
BUSHNELL, M. C., CEKO, M. & LOW, L. A. 2013. Cognitive and emotional control of pain and its disruption in chronic pain. *Nat Rev Neurosci,* 14**,** 502-11.

CALLAGHAN, B. C., LITTLE, A. A., FELDMAN, E. L. & HUGHES, R. A. 2012. Enhanced glucose control for preventing and treating diabetic neuropathy. *Cochrane Database Syst Rev***,** CD007543.
CAMERON, N. E., EATON, S. E., COTTER, M. A. & TESFAYE, S. 2001. Vascular factors and metabolic interactions in the pathogenesis of diabetic neuropathy. *Diabetologia,* 44**,** 1973-88.
CARDINEZ, N., LOVBLOM, L. E., BAI, J. W., LEWIS, E., ABRAHAM, A., SCARR, D., LOVSHIN, J. A., LYTVYN, Y., BOULET, G., FAROOQI, M. A., ORSZAG, A., WEISMAN, A., KEENAN, H. A., BRENT, M. H., PAUL, N., BRIL, V., CHERNEY, D. Z. & PERKINS, B. A. 2018. Sex differences in neuropathic pain in longstanding diabetes: Results from the Canadian Study of Longevity in Type 1 Diabetes. *J Diabetes Complications,* 32**,** 660-664.
CASHMAN, C. R. & HÖKE, A. 2015. Mechanisms of distal axonal degeneration in peripheral neuropathies. *Neurosci Lett,* 596**,** 33-50.
CAUDA, F., SACCO, K., D'AGATA, F., DUCA, S., COCITO, D., GEMINIANI, G., MIGLIORATI, F. & ISOARDO, G. 2009a. Low-frequency BOLD fluctuations demonstrate altered thalamocortical connectivity in diabetic neuropathic pain. *BMC Neurosci,* 10**,** 138.
CAUDA, F., SACCO, K., DUCA, S., COCITO, D., D'AGATA, F., GEMINIANI, G. C. & CANAVERO, S. 2009b. Altered resting state in diabetic neuropathic pain. *PLoS One,* 4**,** e4542.
CAVASSILA, S., DEVAL, S., HUEGEN, C., VAN ORMONDT, D. & GRAVERON-DEMILLY, D. 2001. Cramér-Rao bounds: an evaluation tool for quantitation. *NMR Biomed,* 14**,** 278-83.
CECIL, K. M. 2013. Proton magnetic resonance spectroscopy: technique for the neuroradiologist. *Neuroimaging Clin N Am,* 23**,** 381-92.
CHAN, K. L., OELTZSCHNER, G., SALEH, M. G., EDDEN, R. A. E. & BARKER, P. B. 2019. Simultaneous editing of GABA and GSH with Hadamard-encoded MR spectroscopic imaging. *Magn Reson Med,* 82**,** 21-32.
CHAN, K. L., PUTS, N. A., SCHÄR, M., BARKER, P. B. & EDDEN, R. A. 2016. HERMES: Hadamard encoding and reconstruction of MEGA-edited spectroscopy. *Magn Reson Med,* 76**,** 11-9.
CHEN, X. Y., WANG, Q., WANG, X. & WONG, K. S. 2017. Clinical Features of Thalamic Stroke. *Curr Treat Options Neurol,* 19**,** 5.
CHENG, H. T., DAUCH, J. R., HAYES, J. M., HONG, Y. & FELDMAN, E. L. 2009. Nerve growth factor mediates mechanical allodynia in a mouse model of type 2 diabetes. *J Neuropathol Exp Neurol,* 68**,** 1229-43.
CHENG, H. T., DAUCH, J. R., PORZIO, M. T., YANIK, B. M., HSIEH, W., SMITH, A. G., SINGLETON, J. R. & FELDMAN, E. L. 2013. Increased axonal regeneration and swellings in intraepidermal nerve fibers characterize painful phenotypes of diabetic neuropathy. *J Pain,* 14**,** 941-7.
CHEUNG, A., PODGORNY, P., MARTINEZ, J. A., CHAN, C. & TOTH, C. 2015. Epidermal axonal swellings in painful and painless diabetic peripheral neuropathy. *Muscle Nerve,* 51**,** 505-13.
CHIEN, H. F., TSENG, T. J., LIN, W. M., YANG, C. C., CHANG, Y. C., CHEN, R. C. & HSIEH, S. T. 2001. Quantitative pathology of cutaneous nerve terminal degeneration in the human skin. *Acta Neuropathol,* 102**,** 455-61.
CHONG, P. S. & CROS, D. P. 2004. Technology literature review: quantitative sensory testing. *Muscle Nerve,* 29**,** 734-47.
CHOWDHURY, S. K., SMITH, D. R. & FERNYHOUGH, P. 2013. The role of aberrant mitochondrial bioenergetics in diabetic neuropathy. *Neurobiol Dis,* 51**,** 56-65.
CHRISTENSEN, D. H., KNUDSEN, S. T., GYLFADOTTIR, S. S., CHRISTENSEN, L. B., NIELSEN, J. S., BECK-NIELSEN, H., SØRENSEN, H. T., ANDERSEN, H., CALLAGHAN, B. C., FELDMAN, E. L., FINNERUP, N. B., JENSEN, T. S. & THOMSEN, R. W. 2020. Metabolic Factors, Lifestyle Habits, and Possible Polyneuropathy in Early Type 2 Diabetes: A Nationwide Study of 5,249 Patients in the Danish Centre for Strategic Research in Type 2 Diabetes (DD2) Cohort. *Diabetes Care*.
CLEVE, M., GUSSEW, A. & REICHENBACH, J. R. 2015. In vivo detection of acute pain-induced changes of GABA+ and Glx in the human brain by using functional 1H MEGA-PRESS MR spectroscopy. *Neuroimage,* 105**,** 67-75.

COLLOCA, L., LUDMAN, T., BOUHASSIRA, D., BARON, R., DICKENSON, A. H., YARNITSKY, D., FREEMAN, R., TRUINI, A., ATTAL, N., FINNERUP, N. B., ECCLESTON, C., KALSO, E., BENNETT, D. L., DWORKIN, R. H. & RAJA, S. N. 2017. Neuropathic pain. *Nat Rev Dis Primers,* 3**,** 17002.

CORCÓSTEGUI, B., DURÁN, S., GONZÁLEZ-ALBARRÁN, M. O., HERNÁNDEZ, C., RUIZ-MORENO, J. M., SALVADOR, J., UDAONDO, P. & SIMÓ, R. 2017. Update on Diagnosis and Treatment of Diabetic Retinopathy: A Consensus Guideline of the Working Group of Ocular Health (Spanish Society of Diabetes and Spanish Vitreous and Retina Society). *J Ophthalmol,* 2017**,** 8234186.

CRUCCU, G., SOMMER, C., ANAND, P., ATTAL, N., BARON, R., GARCIA-LARREA, L., HAANPAA, M., JENSEN, T. S., SERRA, J. & TREEDE, R. D. 2010. EFNS guidelines on neuropathic pain assessment: revised 2009. *Eur J Neurol,* 17**,** 1010-8.

CURRIE, S., HADJIVASSILIOU, M., CRAVEN, I. J., WILKINSON, I. D., GRIFFITHS, P. D. & HOGGARD, N. 2013a. Magnetic resonance spectroscopy of the brain. *Postgrad Med J,* 89**,** 94-106.

CURRIE, S., HOGGARD, N., CRAVEN, I. J., HADJIVASSILIOU, M. & WILKINSON, I. D. 2013b. Understanding MRI: basic MR physics for physicians. *Postgrad Med J,* 89**,** 209-23.

D'AMATO, C., MORGANTI, R., GRECO, C., DI GENNARO, F., CACCIOTTI, L., LONGO, S., MATALUNI, G., LAURO, D., MARFIA, G. A. & SPALLONE, V. 2016. Diabetic peripheral neuropathic pain is a stronger predictor of depression than other diabetic complications and comorbidities. *Diab Vasc Dis Res,* 13**,** 418-428.

D'MELLO, R. & DICKENSON, A. H. 2008. Spinal cord mechanisms of pain. *Br J Anaesth,* 101**,** 8-16.

DAI, Z., ZHONG, J., XIAO, P., ZHU, Y., CHEN, F., PAN, P. & SHI, H. 2015. Gray matter correlates of migraine and gender effect: A meta-analysis of voxel-based morphometry studies. *Neuroscience,* 299**,** 88-96.

DALE, A. M., FISCHL, B. & SERENO, M. I. 1999. Cortical surface-based analysis. I. Segmentation and surface reconstruction. *Neuroimage,* 9**,** 179-94.

DALSGAARD, C. J., RYDH, M. & HAEGERSTRAND, A. 1989. Cutaneous innervation in man visualized with protein gene product 9.5 (PGP 9.5) antibodies. *Histochemistry,* 92**,** 385-90.

DAOUSI, C., MACFARLANE, I. A., WOODWARD, A., NURMIKKO, T. J., BUNDRED, P. E. & BENBOW, S. J. 2004. Chronic painful peripheral neuropathy in an urban community: a controlled comparison of people with and without diabetes. *Diabet Med,* 21**,** 976-82.

DAVIES, M., BROPHY, S., WILLIAMS, R. & TAYLOR, A. 2006. The prevalence, severity, and impact of painful diabetic peripheral neuropathy in type 2 diabetes. *Diabetes Care,* 29**,** 1518-22.

DAVIS, K. D. & MOAYEDI, M. 2013. Central mechanisms of pain revealed through functional and structural MRI. *J Neuroimmune Pharmacol,* 8**,** 518-34.

DE BEER, R., VAN DEN BOOGAART, A., VAN ORMONDT, D., PIJNAPPEL, W. W., DEN HOLLANDER, J. A., MARIEN, A. J. & LUYTEN, P. R. 1992. Application of time-domain fitting in the quantification of in vivo 1H spectroscopic imaging data sets. *NMR Biomed,* 5**,** 171-8.

DEMANT, D. T., LUND, K., VOLLERT, J., MAIER, C., SEGERDAHL, M., FINNERUP, N. B., JENSEN, T. S. & SINDRUP, S. H. 2014. The effect of oxcarbazepine in peripheral neuropathic pain depends on pain phenotype: a randomised, double-blind, placebo-controlled phenotype-stratified study. *Pain,* 155**,** 2263-73.

DEVIGILI, G., TUGNOLI, V., PENZA, P., CAMOZZI, F., LOMBARDI, R., MELLI, G., BROGLIO, L., GRANIERI, E. & LAURIA, G. 2008. The diagnostic criteria for small fibre neuropathy: from symptoms to neuropathology. *Brain,* 131**,** 1912-25.

DI PIETRO, F., LEE, B. & HENDERSON, L. A. 2020. Altered resting activity patterns and connectivity in individuals with complex regional pain syndrome. *Hum Brain Mapp,* 41**,** 3781-3793.

DIETRICH, I., BRAGA, G. A., DE MELO, F. G. & DA COSTA SILVA SILVA, A. C. C. 2017. The Diabetic Foot as a Proxy for Cardiovascular Events and Mortality Review. *Curr Atheroscler Rep,* 19**,** 44.

DINH, T., DOUPIS, J., LYONS, T. E., KUCHIBHOTLA, S., JULLIARD, W., GNARDELLIS, C., ROSENBLUM, B. I., WANG, X., GIURINI, J. M., GREENMAN, R. L. & VEVES, A. 2009. Foot muscle energy

reserves in diabetic patients without and with clinical peripheral neuropathy. *Diabetes Care,* 32**,** 1521-4.
DJOUHRI, L., MALKI, M. I., ZEIDAN, A., NAGI, K. & SMITH, T. 2019. Activation of Kv7 channels with the anticonvulsant retigabine alleviates neuropathic pain behaviour in the streptozotocin rat model of diabetic neuropathy. *J Drug Target,* 27**,** 1118-1126.
DOUPIS, J., LYONS, T. E., WU, S., GNARDELLIS, C., DINH, T. & VEVES, A. 2009. Microvascular reactivity and inflammatory cytokines in painful and painless peripheral diabetic neuropathy. *J Clin Endocrinol Metab,* 94**,** 2157-63.
DU, X. & GAMPER, N. 2013. Potassium channels in peripheral pain pathways: expression, function and therapeutic potential. *Curr Neuropharmacol,* 11**,** 621-40.
DUBIN, A. E. & PATAPOUTIAN, A. 2010. Nociceptors: the sensors of the pain pathway. *J Clin Invest,* 120**,** 3760-72.
DUERDEN, E. G. & ALBANESE, M. C. 2013. Localization of pain-related brain activation: a meta-analysis of neuroimaging data. *Hum Brain Mapp,* 34**,** 109-49.
DYCK, P. J. 1988. Detection, characterization, and staging of polyneuropathy: assessed in diabetics. *Muscle Nerve,* 11**,** 21-32.
DYCK, P. J., ALBERS, J. W., ANDERSEN, H., AREZZO, J. C., BIESSELS, G. J., BRIL, V., FELDMAN, E. L., LITCHY, W. J., O'BRIEN, P. C., RUSSELL, J. W. & NEUROPATHY, T. E. P. O. D. 2011a. Diabetic polyneuropathies: update on research definition, diagnostic criteria and estimation of severity. *Diabetes Metab Res Rev,* 27**,** 620-8.
DYCK, P. J., ALBERS, J. W., WOLFE, J., BOLTON, C. F., WALSH, N., KLEIN, C. J., ZAFFT, A. J., RUSSELL, J. W., THOMAS, K., DAVIES, J. L., CARTER, R. E., MELTON, L. J., LITCHY, W. J. & INVESTIGATORS, C. V. N. T. 2013a. A trial of proficiency of nerve conduction: greater standardization still needed. *Muscle Nerve,* 48**,** 369-74.
DYCK, P. J., BUSHEK, W., SPRING, E. M., KARNES, J. L., LITCHY, W. J., O'BRIEN, P. C. & SERVICE, F. J. 1987. Vibratory and cooling detection thresholds compared with other tests in diagnosing and staging diabetic neuropathy. *Diabetes Care,* 10**,** 432-40.
DYCK, P. J., CARTER, R. E. & LITCHY, W. J. 2011b. Modeling nerve conduction criteria for diagnosis of diabetic polyneuropathy. *Muscle Nerve,* 44**,** 340-5.
DYCK, P. J., DAVIES, J. L., LITCHY, W. J. & O'BRIEN, P. C. 1997. Longitudinal assessment of diabetic polyneuropathy using a composite score in the Rochester Diabetic Neuropathy Study cohort. *Neurology,* 49**,** 229-39.
DYCK, P. J., HERRMANN, D. N. & STAFF, N. P. 2013b. Assessing decreased sensation and increased sensory phenomena in diabetic polyneuropathies. *Diabetes,* 62**,** 3677-86.
DYCK, P. J., KARNES, J. L., DAUBE, J., O'BRIEN, P. & SERVICE, F. J. 1985. Clinical and neuropathological criteria for the diagnosis and staging of diabetic polyneuropathy. *Brain,* 108 (Pt 4)**,** 861-80.
DYCK, P. J., KRATZ, K. M., KARNES, J. L., LITCHY, W. J., KLEIN, R., PACH, J. M., WILSON, D. M., O'BRIEN, P. C., MELTON, L. J. & SERVICE, F. J. 1993. The prevalence by staged severity of various types of diabetic neuropathy, retinopathy, and nephropathy in a population-based cohort: the Rochester Diabetic Neuropathy Study. *Neurology,* 43**,** 817-24.
DYCK, P. J., LITCHY, W. J., DAUBE, J. R., HARPER, C. M., DAVIES, J. & O'BRIEN, P. C. 2003. Individual attributes versus composite scores of nerve conduction abnormality: sensitivity, reproducibility, and concordance with impairment. *Muscle Nerve,* 27**,** 202-10.
EATON, S. E., HARRIS, N. D., IBRAHIM, S., PATEL, K. A., SELMI, F., RADATZ, M., WARD, J. D. & TESFAYE, S. 2003. Increased sural nerve epineurial blood flow in human subjects with painful diabetic neuropathy. *Diabetologia,* 46**,** 934-9.
EATON, S. E., HARRIS, N. D., RAJBHANDARI, S. M., GREENWOOD, P., WILKINSON, I. D., WARD, J. D., GRIFFITHS, P. D. & TESFAYE, S. 2001. Spinal-cord involvement in diabetic peripheral neuropathy. *Lancet,* 358**,** 35-6.

EDDEN, R. A., PUTS, N. A., HARRIS, A. D., BARKER, P. B. & EVANS, C. J. 2014. Gannet: A batch-processing tool for the quantitative analysis of gamma-aminobutyric acid–edited MR spectroscopy spectra. *J Magn Reson Imaging,* 40**,** 1445-52.

ENGLAND, J. D., GRONSETH, G. S., FRANKLIN, G., CARTER, G. T., KINSELLA, L. J., COHEN, J. A., ASBURY, A. K., SZIGETI, K., LUPSKI, J. R., LATOV, N., LEWIS, R. A., LOW, P. A., FISHER, M. A., HERRMANN, D., HOWARD, J. F., LAURIA, G., MILLER, R. G., POLYDEFKIS, M., SUMNER, A. J., NEUROLOGY, A. A. O., MEDICINE, A. A. O. N. A. E. & REHABILITATION, A. A. O. P. M. A. 2009. Evaluation of distal symmetric polyneuropathy: the role of autonomic testing, nerve biopsy, and skin biopsy (an evidence-based review). *Muscle Nerve,* 39**,** 106-15.

ENGLAND, J. D., GRONSETH, G. S., FRANKLIN, G., MILLER, R. G., ASBURY, A. K., CARTER, G. T., COHEN, J. A., FISHER, M. A., HOWARD, J. F., KINSELLA, L. J., LATOV, N., LEWIS, R. A., LOW, P. A., SUMNER, A. J., NEUROLOGY, A. A. O., MEDICINE, A. A. O. E. & REHABILITATION, A. A. O. P. M. A. 2005. Distal symmetric polyneuropathy: a definition for clinical research: report of the American Academy of Neurology, the American Association of Electrodiagnostic Medicine, and the American Academy of Physical Medicine and Rehabilitation. *Neurology,* 64**,** 199-207.

ERPELDING, N., SIMONS, L., LEBEL, A., SERRANO, P., PIELECH, M., PRABHU, S., BECERRA, L. & BORSOOK, D. 2016. Rapid treatment-induced brain changes in pediatric CRPS. *Brain Struct Funct,* 221**,** 1095-111.

FABER, C. G., HOEIJMAKERS, J. G., AHN, H. S., CHENG, X., HAN, C., CHOI, J. S., ESTACION, M., LAURIA, G., VANHOUTTE, E. K., GERRITS, M. M., DIB-HAJJ, S., DRENTH, J. P., WAXMAN, S. G. & MERKIES, I. S. 2012a. Gain of function Nav1.7 mutations in idiopathic small fiber neuropathy. *Ann Neurol,* 71**,** 26-39.

FABER, C. G., LAURIA, G., MERKIES, I. S., CHENG, X., HAN, C., AHN, H. S., PERSSON, A. K., HOEIJMAKERS, J. G., GERRITS, M. M., PIERRO, T., LOMBARDI, R., KAPETIS, D., DIB-HAJJ, S. D. & WAXMAN, S. G. 2012b. Gain-of-function Nav1.8 mutations in painful neuropathy. *Proc Natl Acad Sci U S A,* 109**,** 19444-9.

FANG, F., ZHAN, Y. F., ZHUO, Y. Y., YIN, D. Z., LI, K. A. & WANG, Y. F. 2018. Brain atrophy in middle-aged subjects with Type 2 diabetes mellitus, with and without microvascular complications. *J Diabetes*.

FELDMAN, E. L., NAVE, K. A., JENSEN, T. S. & BENNETT, D. L. 2017. New Horizons in Diabetic Neuropathy: Mechanisms, Bioenergetics, and Pain. *Neuron,* 93**,** 1296-1313.

FELDMAN, E. L., STEVENS, M. J., THOMAS, P. K., BROWN, M. B., CANAL, N. & GREENE, D. A. 1994. A practical two-step quantitative clinical and electrophysiological assessment for the diagnosis and staging of diabetic neuropathy. *Diabetes Care,* 17**,** 1281-9.

FERNYHOUGH, P. 2015. Mitochondrial dysfunction in diabetic neuropathy: a series of unfortunate metabolic events. *Curr Diab Rep,* 15**,** 89.

FINNERUP, N. B., ATTAL, N., HAROUTOUNIAN, S., MCNICOL, E., BARON, R., DWORKIN, R. H., GILRON, I., HAANPÄÄ, M., HANSSON, P., JENSEN, T. S., KAMERMAN, P. R., LUND, K., MOORE, A., RAJA, S. N., RICE, A. S., ROWBOTHAM, M., SENA, E., SIDDALL, P., SMITH, B. H. & WALLACE, M. 2015. Pharmacotherapy for neuropathic pain in adults: a systematic review and meta-analysis. *Lancet Neurol,* 14**,** 162-73.

FINNERUP, N. B., HAROUTOUNIAN, S., KAMERMAN, P., BARON, R., BENNETT, D. L., BOUHASSIRA, D., CRUCCU, G., FREEMAN, R., HANSSON, P., NURMIKKO, T., RAJA, S. N., RICE, A. S., SERRA, J., SMITH, B. H., TREEDE, R. D. & JENSEN, T. S. 2016. Neuropathic pain: an updated grading system for research and clinical practice. *Pain,* 157**,** 1599-606.

FISCHER, T. Z., TAN, A. M. & WAXMAN, S. G. 2009. Thalamic neuron hyperexcitability and enlarged receptive fields in the STZ model of diabetic pain. *Brain Res,* 1268**,** 154-61.

FISCHL, B. 2012. FreeSurfer. *Neuroimage,* 62**,** 774-81.

FISCHL, B. & DALE, A. M. 2000. Measuring the thickness of the human cerebral cortex from magnetic resonance images. *Proc Natl Acad Sci U S A,* 97**,** 11050-5.

FISCHL, B., LIU, A. & DALE, A. M. 2001. Automated manifold surgery: constructing geometrically accurate and topologically correct models of the human cerebral cortex. *IEEE Trans Med Imaging,* 20**,** 70-80.

FISCHL, B., SALAT, D. H., BUSA, E., ALBERT, M., DIETERICH, M., HASELGROVE, C., VAN DER KOUWE, A., KILLIANY, R., KENNEDY, D., KLAVENESS, S., MONTILLO, A., MAKRIS, N., ROSEN, B. & DALE, A. M. 2002. Whole brain segmentation: automated labeling of neuroanatomical structures in the human brain. *Neuron,* 33**,** 341-55.

FISCHL, B., SALAT, D. H., VAN DER KOUWE, A. J., MAKRIS, N., SÉGONNE, F., QUINN, B. T. & DALE, A. M. 2004. Sequence-independent segmentation of magnetic resonance images. *Neuroimage,* 23 Suppl 1**,** S69-84.

FOLSTEIN, M. F., FOLSTEIN, S. E. & MCHUGH, P. R. 1975. "Mini-mental state". A practical method for grading the cognitive state of patients for the clinician. *J Psychiatr Res,* 12**,** 189-98.

FORBES, J. M. & COOPER, M. E. 2013. Mechanisms of diabetic complications. *Physiol Rev,* 93**,** 137-88.

FREEMAN, O. J., EVANS, M. H., COOPER, G. J., PETERSEN, R. S. & GARDINER, N. J. 2016. Thalamic amplification of sensory input in experimental diabetes. *Eur J Neurosci,* 44**,** 1779-86.

FRØKJÆR, J. B., BROCK, C., SØFTELAND, E., DIMCEVSKI, G., GREGERSEN, H., SIMRÉN, M. & M DREWES, A. 2013. Macrostructural brain changes in patients with longstanding type 1 diabetes mellitus - a cortical thickness analysis study. *Exp Clin Endocrinol Diabetes,* 121**,** 354-60.

GALER, B. S., GIANAS, A. & JENSEN, M. P. 2000. Painful diabetic polyneuropathy: epidemiology, pain description, and quality of life. *Diabetes Res Clin Pract,* 47**,** 123-8.

GALOSI, E., LA CESA, S., DI STEFANO, G., KARLSSON, P., FASOLINO, A., LEONE, C., BIASIOTTA, A., CRUCCU, G. & TRUINI, A. 2018. A pain in the skin. Regenerating nerve sprouts are distinctly associated with ongoing burning pain in patients with diabetes. *Eur J Pain,* 22**,** 1727-1734.

GANDHI, R. A., SELVARAJAH, D., WILKINSON I.D.W., EMERY, C. J., SHAW, P., GRIFFITHS, P.D., & TESFAYE, S. 2006. Preservation of thalamic neuronal function may be a prerequisite for pain perception in diabetic neuropathy. Diabetologia.

GANDHI, R. A., MARQUES, J. L., SELVARAJAH, D., EMERY, C. J. & TESFAYE, S. 2010. Painful diabetic neuropathy is associated with greater autonomic dysfunction than painless diabetic neuropathy. *Diabetes Care,* 33**,** 1585-90.

GAROUSHI, S., JOHNSON, M. I. & TASHANI, O. A. 2019. A cross-sectional study to estimate the point prevalence of painful diabetic neuropathy in Eastern Libya. *BMC Public Health,* 19**,** 78.

GAZDZINSKI, S., KORNAK, J., WEINER, M. W. & MEYERHOFF, D. J. 2008. Body mass index and magnetic resonance markers of brain integrity in adults. *Ann Neurol,* 63**,** 652-7.

GAZDZINSKI, S., MILLIN, R., KAISER, L. G., DURAZZO, T. C., MUELLER, S. G., WEINER, M. W. & MEYERHOFF, D. J. 2010. BMI and neuronal integrity in healthy, cognitively normal elderly: a proton magnetic resonance spectroscopy study. *Obesity (Silver Spring),* 18**,** 743-8.

GEBER, C., KLEIN, T., AZAD, S., BIRKLEIN, F., GIERTHMÜHLEN, J., HUGE, V., LAUCHART, M., NITZSCHE, D., STENGEL, M., VALET, M., BARON, R., MAIER, C., TÖLLE, T. & TREEDE, R. D. 2011. Test-retest and interobserver reliability of quantitative sensory testing according to the protocol of the German Research Network on Neuropathic Pain (DFNS): a multi-centre study. *Pain,* 152**,** 548-56.

GERBERSHAGEN, H. J., ROTHAUG, J., KALKMAN, C. J. & MEISSNER, W. 2011. Determination of moderate-to-severe postoperative pain on the numeric rating scale: a cut-off point analysis applying four different methods. *Br J Anaesth,* 107**,** 619-26.

GERSTNER, G., ICHESCO, E., QUINTERO, A. & SCHMIDT-WILCKE, T. 2011. Changes in regional gray and white matter volume in patients with myofascial-type temporomandibular disorders: a voxel-based morphometry study. *J Orofac Pain,* 25**,** 99-106.

GIBBONS, C. H., FREEMAN, R. & VEVES, A. 2010. Diabetic neuropathy: a cross-sectional study of the relationships among tests of neurophysiology. *Diabetes Care,* 33**,** 2629-34.

GIORGIO, A. & DE STEFANO, N. 2013. Clinical use of brain volumetry. *J Magn Reson Imaging,* 37**,** 1-14.

GLOVER, G. H. 2011. Overview of functional magnetic resonance imaging. *Neurosurg Clin N Am,* 22**,** 133-9, vii.

GONCHAROV, N. V., POPOVA, P. I., AVDONIN, P. P., KUDRYAVTSEV, I. V., SEREBRYAKOVA, M. K., KORF, E. A. & AVDONIN, P. V. 2020. Markers of Endothelial Cells in Normal and Pathological Conditions. *Biochem (Mosc) Suppl Ser A Membr Cell Biol,* 14**,** 167-183.

GORE, M., BRANDENBURG, N. A., DUKES, E., HOFFMAN, D. L., TAI, K. S. & STACEY, B. 2005. Pain severity in diabetic peripheral neuropathy is associated with patient functioning, symptom levels of anxiety and depression, and sleep. *J Pain Symptom Manage,* 30**,** 374-85.

GOUDET, C., MAGNAGHI, V., LANDRY, M., NAGY, F., GEREAU, R. W. & PIN, J. P. 2009. Metabotropic receptors for glutamate and GABA in pain. *Brain Res Rev,* 60**,** 43-56.

GREIG, M., WILKINSON, I. D., SHILLO, P., SELVARAJAH, D., GANDHI, R. & TESFAYE, S. 2017. Impaired Hemodynamic Response to Thermal Pain in Patients with Painful Diabetic Neuropathy: A Dynamic Susceptibility Contrast MRI Study. NEURO DIAB 2017.

GROH, A., KRIEGER, P., MEASE, R. A. & HENDERSON, L. 2018. Acute and Chronic Pain Processing in the Thalamocortical System of Humans and Animal Models. *Neuroscience,* 387**,** 58-71.

GUO, C., FERREIRA, D., FINK, K., WESTMAN, E. & GRANBERG, T. 2019. Repeatability and reproducibility of FreeSurfer, FSL-SIENAX and SPM brain volumetric measurements and the effect of lesion filling in multiple sclerosis. *Eur Radiol,* 29**,** 1355-1364.

GYLFADOTTIR, S. S., CHRISTENSEN, D. H., NICOLAISEN, S. K., ANDERSEN, H., CALLAGHAN, B. C., ITANI, M., KHAN, K. S., KRISTENSEN, A. G., NIELSEN, J. S., SINDRUP, S. H., ANDERSEN, N. T., JENSEN, T. S., THOMSEN, R. W. & FINNERUP, N. B. 2020. Diabetic polyneuropathy and pain, prevalence, and patient characteristics: a cross-sectional questionnaire study of 5,514 patients with recently diagnosed type 2 diabetes. *Pain,* 161**,** 574-583.

HA, D. H., CHOI, S., OH, J. Y., YOON, S. K., KANG, M. J. & KIM, K. U. 2013. Application of 31P MR spectroscopy to the brain tumors. *Korean J Radiol,* 14**,** 477-86.

HAANPÄÄ, M., ATTAL, N., BACKONJA, M., BARON, R., BENNETT, M., BOUHASSIRA, D., CRUCCU, G., HANSSON, P., HAYTHORNTHWAITE, J. A., IANNETTI, G. D., JENSEN, T. S., KAUPPILA, T., NURMIKKO, T. J., RICE, A. S., ROWBOTHAM, M., SERRA, J., SOMMER, C., SMITH, B. H. & TREEDE, R. D. 2011. NeuPSIG guidelines on neuropathic pain assessment. *Pain,* 152**,** 14-27.

HALAWA, M. R., KARAWAGH, A., ZEIDAN, A., MAHMOUD, A. E., SAKR, M. & HEGAZY, A. 2010. Prevalence of painful diabetic peripheral neuropathy among patients suffering from diabetes mellitus in Saudi Arabia. *Curr Med Res Opin,* 26**,** 337-43.

HANSEN, C. S., JENSEN, T. M., JENSEN, J. S., NAWROTH, P., FLEMING, T., WITTE, D. R., LAURITZEN, T., SANDBAEK, A., CHARLES, M., FLEISCHER, J., VISTISEN, D. & JØRGENSEN, M. E. 2015. The role of serum methylglyoxal on diabetic peripheral and cardiovascular autonomic neuropathy: the ADDITION Denmark study. *Diabet Med,* 32**,** 778-85.

HANSEN, T. M., BROCK, B., JUHL, A., DREWES, A. M., VORUM, H., ANDERSEN, C. U., JAKOBSEN, P. E., KARMISHOLT, J., FRØKJÆR, J. B. & BROCK, C. 2019. Brain spectroscopy reveals that N-acetylaspartate is associated to peripheral sensorimotor neuropathy in type 1 diabetes. *J Diabetes Complications,* 33**,** 323-328.

HANSEN, T. M., FRØKJÆR, J. B., SELVARAJAH, D., MUTHULINGAM, J. A., TESFAYE, S., JUHL, A., DREWES, A. M., JAKOBSEN, P. E., KARMISHOLT, J., BROCK, B. & BROCK, C. 2021. Reduced Thalamic Volume and Metabolites in Type 1 Diabetes with Polyneuropathy. *Exp Clin Endocrinol Diabetes*, doi 10.1055/a-1347-2579.

HANSSON, P., BACKONJA, M. & BOUHASSIRA, D. 2007. Usefulness and limitations of quantitative sensory testing: clinical and research application in neuropathic pain states. *Pain,* 129**,** 256-9.

HAROUTOUNIAN, S., NIKOLAJSEN, L., BENDTSEN, T. F., FINNERUP, N. B., KRISTENSEN, A. D., HASSELSTRØM, J. B. & JENSEN, T. S. 2014. Primary afferent input critical for maintaining spontaneous pain in peripheral neuropathy. *Pain,* 155**,** 1272-9.

HARRIS, R. E. & CLAUW, D. J. 2012. Imaging central neurochemical alterations in chronic pain with proton magnetic resonance spectroscopy. *Neurosci Lett,* 520**,** 192-6.
HÉBERT, H. L., VELUCHAMY, A., TORRANCE, N. & SMITH, B. H. 2017. Risk factors for neuropathic pain in diabetes mellitus. *Pain,* 158**,** 560-568.
HENSSEN, D., DIJK, J., KNEPFLÉ, R., SIEFFERS, M., WINTER, A. & VISSERS, K. 2019. Alterations in grey matter density and functional connectivity in trigeminal neuropathic pain and trigeminal neuralgia: A systematic review and meta-analysis. *Neuroimage Clin,* 24**,** 102039.
HERDER, C., BONGAERTS, B. W., RATHMANN, W., HEIER, M., KOWALL, B., KOENIG, W., THORAND, B., RODEN, M., MEISINGER, C. & ZIEGLER, D. 2015. Differential association between biomarkers of subclinical inflammation and painful polyneuropathy: results from the KORA F4 study. *Diabetes Care,* 38**,** 91-6.
HERDMAN, M., GUDEX, C., LLOYD, A., JANSSEN, M., KIND, P., PARKIN, D., BONSEL, G. & BADIA, X. 2011. Development and preliminary testing of the new five-level version of EQ-5D (EQ-5D-5L). *Qual Life Res,* 20**,** 1727-36.
HOLLAND, N. R., STOCKS, A., HAUER, P., CORNBLATH, D. R., GRIFFIN, J. W. & MCARTHUR, J. C. 1997. Intraepidermal nerve fiber density in patients with painful sensory neuropathy. *Neurology,* 48**,** 708-11.
HUANG, J., HAN, C., ESTACION, M., VASYLYEV, D., HOEIJMAKERS, J. G., GERRITS, M. M., TYRRELL, L., LAURIA, G., FABER, C. G., DIB-HAJJ, S. D., MERKIES, I. S., WAXMAN, S. G. & GROUP, P. S. 2014. Gain-of-function mutations in sodium channel Na(v)1.9 in painful neuropathy. *Brain,* 137**,** 1627-42.
IASP. 2012. *IASP Taxonomy* [Online]. https://www.iasp-pain.org/Taxonomy?navItemNumber=576. [Accessed 17/7/17 2017].
ICHESCO, E., SCHMIDT-WILCKE, T., BHAVSAR, R., CLAUW, D. J., PELTIER, S. J., KIM, J., NAPADOW, V., HAMPSON, J. P., KAIRYS, A. E., WILLIAMS, D. A. & HARRIS, R. E. 2014. Altered resting state connectivity of the insular cortex in individuals with fibromyalgia. *J Pain,* 15**,** 815-826.e1.
ILYAS, Z., CHAIBAN, J. T. & KRIKORIAN, A. 2017. Novel insights into the pathophysiology and clinical aspects of diabetic nephropathy. *Rev Endocr Metab Disord,* 18**,** 21-28.
JA, L. & DM, M. 1992. *Laboratory Reference for Clinical Neurophysiology,* New York Oxford, Oxford University Press.
JAISWAL, M., DIVERS, J., DABELEA, D., ISOM, S., BELL, R. A., MARTIN, C. L., PETTITT, D. J., SAYDAH, S., PIHOKER, C., STANDIFORD, D. A., DOLAN, L. M., MARCOVINA, S., LINDER, B., LIESE, A. D., POP-BUSUI, R. & FELDMAN, E. L. 2017. Prevalence of and Risk Factors for Diabetic Peripheral Neuropathy in Youth With Type 1 and Type 2 Diabetes: SEARCH for Diabetes in Youth Study. *Diabetes Care,* 40**,** 1226-1232.
JAMBART, S., AMMACHE, Z., HADDAD, F., YOUNES, A., HASSOUN, A., ABDALLA, K., SELWAN, C. A., SUNNA, N., WAJSBROT, D. & YOUSEIF, E. 2011. Prevalence of painful diabetic peripheral neuropathy among patients with diabetes mellitus in the Middle East region. *J Int Med Res,* 39**,** 366-77.
JENSEN, T. S., BACKONJA, M. M., HERNÁNDEZ JIMÉNEZ, S., TESFAYE, S., VALENSI, P. & ZIEGLER, D. 2006. New perspectives on the management of diabetic peripheral neuropathic pain. *Diab Vasc Dis Res,* 3**,** 108-19.
JEYAM, A., MCGURNAGHAN, S. J., BLACKBOURN, L. A. K., MCKNIGHT, J. M., GREEN, F., COLLIER, A., MCKEIGUE, P. M., COLHOUN, H. M. & INVESTIGATORS, S. B. 2020. Diabetic Neuropathy Is a Substantial Burden in People With Type 1 Diabetes and Is Strongly Associated With Socioeconomic Disadvantage: A Population-Representative Study From Scotland. *Diabetes Care,* 43**,** 734-742.
JOHANSSON, O., WANG, L., HILLIGES, M. & LIANG, Y. 1999. Intraepidermal nerves in human skin: PGP 9.5 immunohistochemistry with special reference to the nerve density in skin from different body regions. *J Peripher Nerv Syst,* 4**,** 43-52.

JONGEN, C. & BIESSELS, G. J. 2008. Structural brain imaging in diabetes: a methodological perspective. *Eur J Pharmacol,* 585**,** 208-18.
KALTENIECE, A., FERDOUSI, M., AZMI, S., MUBITA, W. M., MARSHALL, A., LAURIA, G., FABER, C. G., SORAN, H. & MALIK, R. A. 2020. Corneal confocal microscopy detects small nerve fibre damage in patients with painful diabetic neuropathy. *Sci Rep,* 10**,** 3371.
KARSIDAG, S., MORALI, S., SARGIN, M., SALMAN, S., KARSIDAG, K. & US, O. 2005. The electrophysiological findings of subclinical neuropathy in patients with recently diagnosed type 1 diabetes mellitus. *Diabetes Res Clin Pract,* 67**,** 211-9.
KELLER, A. F., BEGGS, S., SALTER, M. W. & DE KONINCK, Y. 2007. Transformation of the output of spinal lamina I neurons after nerve injury and microglia stimulation underlying neuropathic pain. *Mol Pain,* 3**,** 27.
KEMP, G. J. 2000. Non-invasive methods for studying brain energy metabolism: what they show and what it means. *Dev Neurosci,* 22**,** 418-28.
KENNEDY, W. R. & WENDELSCHAFER-CRABB, G. 1993. The innervation of human epidermis. *J Neurol Sci,* 115**,** 184-90.
KENNEDY, W. R., WENDELSCHAFER-CRABB, G. & JOHNSON, T. 1996. Quantitation of epidermal nerves in diabetic neuropathy. *Neurology,* 47**,** 1042-8.
KIM, B. & FELDMAN, E. L. 2012. Insulin resistance in the nervous system. *Trends Endocrinol Metab,* 23**,** 133-41.
KIM, W., KIM, S. K. & NABEKURA, J. 2017. Functional and structural plasticity in the primary somatosensory cortex associated with chronic pain. *J Neurochem,* 141**,** 499-506.
KLOSE, U. 2008. Measurement sequences for single voxel proton MR spectroscopy. *Eur J Radiol,* 67**,** 194-201.
KREGEL, J., MEEUS, M., MALFLIET, A., DOLPHENS, M., DANNEELS, L., NIJS, J. & CAGNIE, B. 2015. Structural and functional brain abnormalities in chronic low back pain: A systematic review. *Semin Arthritis Rheum,* 45**,** 229-37.
KREIS, R. 2016. The trouble with quality filtering based on relative Cramér-Rao lower bounds. *Magn Reson Med,* 75**,** 15-8.
KUCERA, P., GOLDENBERG, Z., VARSIK, P., BURANOVA, D. & TRAUBNER, P. 2005. Spinal cord lesions in diabetes mellitus. Somatosensory and motor evoked potentials and spinal conduction time in diabetes mellitus. *Neuro Endocrinol Lett,* 26**,** 143-7.
LAURIA, G. 1999. Innervation of the human epidermis. A historical review. *Ital J Neurol Sci,* 20**,** 63-70.
LAURIA, G., BAKKERS, M., SCHMITZ, C., LOMBARDI, R., PENZA, P., DEVIGILI, G., SMITH, A. G., HSIEH, S. T., MELLGREN, S. I., UMAPATHI, T., ZIEGLER, D., FABER, C. G. & MERKIES, I. S. 2010a. Intraepidermal nerve fiber density at the distal leg: a worldwide normative reference study. *J Peripher Nerv Syst,* 15**,** 202-7.
LAURIA, G., HOLLAND, N., HAUER, P., CORNBLATH, D. R., GRIFFIN, J. W. & MCARTHUR, J. C. 1999. Epidermal innervation: changes with aging, topographic location, and in sensory neuropathy. *J Neurol Sci,* 164**,** 172-8.
LAURIA, G., HSIEH, S. T., JOHANSSON, O., KENNEDY, W. R., LEGER, J. M., MELLGREN, S. I., NOLANO, M., MERKIES, I. S., POLYDEFKIS, M., SMITH, A. G., SOMMER, C., VALLS-SOLÉ, J., SOCIETIES, E. F. O. N. & SOCIETY, P. N. 2010b. European Federation of Neurological Societies/Peripheral Nerve Society Guideline on the use of skin biopsy in the diagnosis of small fiber neuropathy. Report of a joint task force of the European Federation of Neurological Societies and the Peripheral Nerve Society. *Eur J Neurol,* 17**,** 903-12, e44-9.
LAURIA, G. & LOMBARDI, R. 2012. Small fiber neuropathy: is skin biopsy the holy grail? *Curr Diab Rep,* 12**,** 384-92.
LAURIA, G., MCARTHUR, J. C., HAUER, P. E., GRIFFIN, J. W. & CORNBLATH, D. R. 1998. Neuropathological alterations in diabetic truncal neuropathy: evaluation by skin biopsy. *J Neurol Neurosurg Psychiatry,* 65**,** 762-6.

LAURIA, G., MORBIN, M., LOMBARDI, R., CAPOBIANCO, R., CAMOZZI, F., PAREYSON, D., MANCONI, M. & GEPPETTI, P. 2006. Expression of capsaicin receptor immunoreactivity in human peripheral nervous system and in painful neuropathies. *J Peripher Nerv Syst,* 11**,** 262-71.

LEASHER, J. L., BOURNE, R. R., FLAXMAN, S. R., JONAS, J. B., KEEFFE, J., NAIDOO, K., PESUDOVS, K., PRICE, H., WHITE, R. A., WONG, T. Y., RESNIKOFF, S., TAYLOR, H. R. & STUDY, V. L. E. G. O. T. G. B. O. D. 2016. Global Estimates on the Number of People Blind or Visually Impaired by Diabetic Retinopathy: A Meta-analysis From 1990 to 2010. *Diabetes Care,* 39**,** 1643-9.

LIP, G. Y. & BLANN, A. 1997. von Willebrand factor: a marker of endothelial dysfunction in vascular disorders? *Cardiovasc Res,* 34**,** 255-65.

LITCHY, W. J., ALBERS, J. W., WOLFE, J., BOLTON, C. F., WALSH, N., KLEIN, C. J., ZAFFT, A. J., RUSSELL, J. W., ZWIRLEIN, M., OVERLAND, C. J., DAVIES, J. L., CARTER, R. E., DYCK, P. J. & INVESTIGATORS, C. N. T. 2014. Proficiency of nerve conduction using standard methods and reference values (Cl. NPhys Trial 4). *Muscle Nerve,* 50**,** 900-8.

LIU, J., HAO, Y., DU, M., WANG, X., ZHANG, J., MANOR, B., JIANG, X., FANG, W. & WANG, D. 2013. Quantitative cerebral blood flow mapping and functional connectivity of postherpetic neuralgia pain: a perfusion fMRI study. *Pain,* 154**,** 110-118.

LIU, Y., GU, Y. & YU, X. 2017. Assessing tissue metabolism by phosphorous-31 magnetic resonance spectroscopy and imaging: a methodology review. *Quant Imaging Med Surg,* 7**,** 707-726.

LØSETH, S., STÅLBERG, E., JORDE, R. & MELLGREN, S. I. 2008. Early diabetic neuropathy: thermal thresholds and intraepidermal nerve fibre density in patients with normal nerve conduction studies. *J Neurol,* 255**,** 1197-202.

LU, C., YANG, T., ZHAO, H., ZHANG, M., MENG, F., FU, H., XIE, Y. & XU, H. 2016. Insular Cortex is Critical for the Perception, Modulation, and Chronification of Pain. *Neurosci Bull,* 32**,** 191-201.

LUMPKIN, E. A. & CATERINA, M. J. 2007. Mechanisms of sensory transduction in the skin. *Nature,* 445**,** 858-65.

MAEDA, Y., KETTNER, N., KIM, J., KIM, H., CINA, S., MALATESTA, C., GERBER, J., MCMANUS, C., LIBBY, A., MEZZACAPPA, P., MAWLA, I., MORSE, L. R., AUDETTE, J. & NAPADOW, V. 2016. Primary somatosensory/motor cortical thickness distinguishes paresthesia-dominant from pain-dominant carpal tunnel syndrome. *Pain,* 157**,** 1085-1093.

MAGERL, W., KRUMOVA, E. K., BARON, R., TÖLLE, T., TREEDE, R. D. & MAIER, C. 2010. Reference data for quantitative sensory testing (QST): refined stratification for age and a novel method for statistical comparison of group data. *Pain,* 151**,** 598-605.

MALIK, R. A. 1997. The pathology of human diabetic neuropathy. *Diabetes,* 46 Suppl 2**,** S50-3.

MALIK, R. A., TESFAYE, S., THOMPSON, S. D., VEVES, A., SHARMA, A. K., BOULTON, A. J. & WARD, J. D. 1993. Endoneurial localisation of microvascular damage in human diabetic neuropathy. *Diabetologia,* 36**,** 454-9.

MANNUCCI, P. M. 1998. von Willebrand factor: a marker of endothelial damage? *Arterioscler Thromb Vasc Biol,* 18**,** 1359-62.

MANOR, B., NEWTON, E., ABDULJALIL, A. & NOVAK, V. 2012. The relationship between brain volume and walking outcomes in older adults with and without diabetic peripheral neuropathy. *Diabetes Care,* 35**,** 1907-12.

MARSHALL, A. G., LEE-KUBLI, C., AZMI, S., ZHANG, M., FERDOUSI, M., MIXCOATL-ZECUATL, T., PETROPOULOS, I. N., PONIRAKIS, G., FINEMAN, M. S., FADAVI, H., FRIZZI, K., TAVAKOLI, M., JEZIORSKA, M., JOLIVALT, C. G., BOULTON, A. J. M., EFRON, N., CALCUTT, N. A. & MALIK, R. A. 2017. Spinal Disinhibition in Experimental and Clinical Painful Diabetic Neuropathy. *Diabetes,* 66**,** 1380-1390.

MARTIN, C. L., ALBERS, J. W., POP-BUSUI, R. & GROUP, D. E. R. 2014. Neuropathy and related findings in the diabetes control and complications trial/epidemiology of diabetes interventions and complications study. *Diabetes Care,* 37**,** 31-8.

MARTIN, C. L., WABERSKI, B. H., POP-BUSUI, R., CLEARY, P. A., CATTON, S., ALBERS, J. W., FELDMAN, E. L., HERMAN, W. H. & GROUP, D. E. R. 2010. Vibration perception threshold as a measure of distal symmetrical peripheral neuropathy in type 1 diabetes: results from the DCCT/EDIC study. *Diabetes Care,* 33**,** 2635-41.

MASER, R. E., STEENKISTE, A. R., DORMAN, J. S., NIELSEN, V. K., BASS, E. B., MANJOO, Q., DRASH, A. L., BECKER, D. J., KULLER, L. H. & GREENE, D. A. 1989. Epidemiological correlates of diabetic neuropathy. Report from Pittsburgh Epidemiology of Diabetes Complications Study. *Diabetes,* 38**,** 1456-61.

MATSUSHITA, K., VAN DER VELDE, M., ASTOR, B. C., WOODWARD, M., LEVEY, A. S., DE JONG, P. E., CORESH, J., GANSEVOORT, R. T. & CONSORTIUM, C. K. D. P. 2010. Association of estimated glomerular filtration rate and albuminuria with all-cause and cardiovascular mortality in general population cohorts: a collaborative meta-analysis. *Lancet,* 375**,** 2073-81.

MAY, A. 2011. Structural brain imaging: a window into chronic pain. *Neuroscientist,* 17**,** 209-20.

MAYAUDON, H., MILOCHE, P. O. & BAUDUCEAU, B. 2010. A new simple method for assessing sudomotor function: relevance in type 2 diabetes. *Diabetes Metab,* 36**,** 450-4.

MCCARTHY, B. G., HSIEH, S. T., STOCKS, A., HAUER, P., MACKO, C., CORNBLATH, D. R., GRIFFIN, J. W. & MCARTHUR, J. C. 1995. Cutaneous innervation in sensory neuropathies: evaluation by skin biopsy. *Neurology,* 45**,** 1848-55.

MCCRIMMON, R. J., RYAN, C. M. & FRIER, B. M. 2012. Diabetes and cognitive dysfunction. *Lancet,* 379**,** 2291-9.

MENG, W., DESHMUKH, H. A., DONNELLY, L. A., TORRANCE, N., COLHOUN, H. M., PALMER, C. N., SMITH, B. H., (WTCCC2), W. T. C. C. C. & GROUP, S. M. F. M.-A. M.-V. H. E. F. I. D. T. S. S. 2015a. A Genome-wide Association Study Provides Evidence of Sex-specific Involvement of Chr1p35.1 (ZSCAN20-TLR12P) and Chr8p23.1 (HMGB1P46) With Diabetic Neuropathic Pain. *EBioMedicine,* 2**,** 1386-93.

MENG, W., DESHMUKH, H. A., VAN ZUYDAM, N. R., LIU, Y., DONNELLY, L. A., ZHOU, K., MORRIS, A. D., COLHOUN, H. M., PALMER, C. N., SMITH, B. H., (WTCCC2), W. T. C. C. C. & GROUP, S. M. F. M.-A. M.-V. H. E. F. I. D. T. S. S. 2015b. A genome-wide association study suggests an association of Chr8p21.3 (GFRA2) with diabetic neuropathic pain. *Eur J Pain,* 19**,** 392-9.

MEYERSPEER, M., BOESCH, C., CAMERON, D., DEZORTOVÁ, M., FORBES, S. C., HEERSCHAP, A., JENESON, J. A. L., KAN, H. E., KENT, J., LAYEC, G., PROMPERS, J. J., REYNGOUDT, H., SLEIGH, A., VALKOVIČ, L., KEMP, G. J. & MUSCLE, E. W. G. O. P. M. S. O. S. 2020. P magnetic resonance spectroscopy in skeletal muscle: Experts' consensus recommendations. *NMR Biomed***,** e4246.

MIKKELSEN, M., BARKER, P. B., BHATTACHARYYA, P. K., BRIX, M. K., BUUR, P. F., CECIL, K. M., CHAN, K. L., CHEN, D. Y., CRAVEN, A. R., CUYPERS, K., DACKO, M., DUNCAN, N. W., DYDAK, U., EDMONDSON, D. A., ENDE, G., ERSLAND, L., GAO, F., GREENHOUSE, I., HARRIS, A. D., HE, N., HEBA, S., HOGGARD, N., HSU, T. W., JANSEN, J. F. A., KANGARLU, A., LANGE, T., LEBEL, R. M., LI, Y., LIN, C. E., LIOU, J. K., LIRNG, J. F., LIU, F., MA, R., MAES, C., MORENO-ORTEGA, M., MURRAY, S. O., NOAH, S., NOESKE, R., NOSEWORTHY, M. D., OELTZSCHNER, G., PRISCIANDARO, J. J., PUTS, N. A. J., ROBERTS, T. P. L., SACK, M., SAILASUTA, N., SALEH, M. G., SCHALLMO, M. P., SIMARD, N., SWINNEN, S. P., TEGENTHOFF, M., TRUONG, P., WANG, G., WILKINSON, I. D., WITTSACK, H. J., XU, H., YAN, F., ZHANG, C., ZIPUNNIKOV, V., ZÖLLNER, H. J. & EDDEN, R. A. E. 2017. Big GABA: Edited MR spectroscopy at 24 research sites. *Neuroimage,* 159**,** 32-45.

MIZOKAMI-STOUT, K. R., LI, Z., FOSTER, N. C., SHAH, V., ALEPPO, G., MCGILL, J. B., PRATLEY, R., TOSCHI, E., ANG, L., POP-BUSUI, R., NETWORK, F. T. D. E. C. & K, T. D. E. C. N. 2020. The Contemporary Prevalence of Diabetic Neuropathy in Type 1 Diabetes: Findings From the T1D Exchange. *Diabetes Care,* 43**,** 806-812.

MOFFETT, J. R., ROSS, B., ARUN, P., MADHAVARAO, C. N. & NAMBOODIRI, A. M. 2007. N-Acetylaspartate in the CNS: from neurodiagnostics to neurobiology. *Prog Neurobiol,* 81**,** 89-131.

MOHAMMEDI, K., WOODWARD, M., MARRE, M., COLAGIURI, S., COOPER, M., HARRAP, S., MANCIA, G., POULTER, N., WILLIAMS, B., ZOUNGAS, S. & CHALMERS, J. 2017. Comparative effects of microvascular and macrovascular disease on the risk of major outcomes in patients with type 2 diabetes. *Cardiovasc Diabetol,* 16**,** 95.

MORIN, C. M., BELLEVILLE, G., BÉLANGER, L. & IVERS, H. 2011. The Insomnia Severity Index: psychometric indicators to detect insomnia cases and evaluate treatment response. *Sleep,* 34**,** 601-8.

MORTON, D. L., SANDHU, J. S. & JONES, A. K. 2016. Brain imaging of pain: state of the art. *J Pain Res,* 9**,** 613-24.

MOULTON, C. D., COSTAFREDA, S. G., HORTON, P., ISMAIL, K. & FU, C. H. 2015. Meta-analyses of structural regional cerebral effects in type 1 and type 2 diabetes. *Brain Imaging Behav,* 9**,** 651-62.

MULLINS, P. G., ROWLAND, L. M., JUNG, R. E. & SIBBITT, W. L. 2005. A novel technique to study the brain's response to pain: proton magnetic resonance spectroscopy. *Neuroimage,* 26**,** 642-6.

NAUDI, A., JOVE, M., AYALA, V., CASSANYE, A., SERRANO, J., GONZALO, H., BOADA, J., PRAT, J., PORTERO-OTIN, M. & PAMPLONA, R. 2012. Cellular dysfunction in diabetes as maladaptive response to mitochondrial oxidative stress. *Exp Diabetes Res,* 2012**,** 696215.

NEWRICK, P. G., WILSON, A. J., JAKUBOWSKI, J., BOULTON, A. J. & WARD, J. D. 1986. Sural nerve oxygen tension in diabetes. *Br Med J (Clin Res Ed),* 293**,** 1053-4.

NOLANO, M., BIASIOTTA, A., LOMBARDI, R., PROVITERA, V., STANCANELLI, A., CAPORASO, G., SANTORO, L., MERKIES, I. S., TRUINI, A., PORRETTA-SERAPIGLIA, C., CAZZATO, D., DACCI, P., VITALE, D. F. & LAURIA, G. 2015. Epidermal innervation morphometry by immunofluorescence and bright-field microscopy. *J Peripher Nerv Syst,* 20**,** 387-91.

NOVAK, J., WILSON, M., MACPHERSON, L., ARVANITIS, T. N., DAVIES, N. P. & PEET, A. C. 2014. Clinical protocols for ^{31}P MRS of the brain and their use in evaluating optic pathway gliomas in children. *Eur J Radiol,* 83**,** e106-12.

O'BRIEN, I. A., O'HARE, P. & CORRALL, R. J. 1986. Heart rate variability in healthy subjects: effect of age and the derivation of normal ranges for tests of autonomic function. *Br Heart J,* 55**,** 348-54.

OBERMANN, M., NEBEL, K., SCHUMANN, C., HOLLE, D., GIZEWSKI, E. R., MASCHKE, M., GOADSBY, P. J., DIENER, H. C. & KATSARAVA, Z. 2009. Gray matter changes related to chronic posttraumatic headache. *Neurology,* 73**,** 978-83.

OBROSOVA, I. G. 2009. Diabetic painful and insensate neuropathy: pathogenesis and potential treatments. *Neurotherapeutics,* 6**,** 638-47.

OCHOA, J. L., CAMPERO, M., SERRA, J. & BOSTOCK, H. 2005. Hyperexcitable polymodal and insensitive nociceptors in painful human neuropathy. *Muscle & Nerve,* 32**,** 459-472.

OCHS, A. L., ROSS, D. E., ZANNONI, M. D., ABILDSKOV, T. J., BIGLER, E. D. & INITIATIVE, A. S. D. N. 2015. Comparison of Automated Brain Volume Measures obtained with NeuroQuant and FreeSurfer. *J Neuroimaging,* 25**,** 721-7.

OGAWA, S., LEE, T. M., KAY, A. R. & TANK, D. W. 1990. Brain magnetic resonance imaging with contrast dependent on blood oxygenation. *Proc Natl Acad Sci U S A,* 87**,** 9868-72.

ORDIDGE, R. J., BOWLEY, R. M. & MCHALE, G. 1988. A general approach to selection of multiple cubic volume elements using the ISIS technique. *Magn Reson Med,* 8**,** 323-31.

ORGANIZATION, W. H. 2011. Waist circumference and waist-hip ratio: Report of a WHO expert consultation, Geneva, 8-11 December 2008. *In:* ORGANIZATION, W. H. (ed.). Geneva, Switzerland: World Health Organization.

ØSTERGAARD, L., FINNERUP, N. B., TERKELSEN, A. J., OLESEN, R. A., DRASBEK, K. R., KNUDSEN, L., JESPERSEN, S. N., FRYSTYK, J., CHARLES, M., THOMSEN, R. W., CHRISTIANSEN, J. S., BECK-

NIELSEN, H., JENSEN, T. S. & ANDERSEN, H. 2015. The effects of capillary dysfunction on oxygen and glucose extraction in diabetic neuropathy. *Diabetologia,* 58**,** 666-77.
OYIBO, S. O., PRASAD, Y. D., JACKSON, N. J., JUDE, E. B. & BOULTON, A. J. 2002. The relationship between blood glucose excursions and painful diabetic peripheral neuropathy: a pilot study. *Diabet Med,* 19**,** 870-3.
PABBIDI, R. M., YU, S. Q., PENG, S., KHARDORI, R., PAUZA, M. E. & PREMKUMAR, L. S. 2008. Influence of TRPV1 on diabetes-induced alterations in thermal pain sensitivity. *Mol Pain,* 4**,** 9.
PARTANEN, J., NISKANEN, L., LEHTINEN, J., MERVAALA, E., SIITONEN, O. & UUSITUPA, M. 1995. Natural history of peripheral neuropathy in patients with non-insulin-dependent diabetes mellitus. *N Engl J Med,* 333**,** 89-94.
PEEK, A. L., REBBECK, T., PUTS, N. A., WATSON, J., AGUILA, M. R. & LEAVER, A. M. 2020. Brain GABA and glutamate levels across pain conditions: A systematic literature review and meta-analysis of 1H-MRS studies using the MRS-Q quality assessment tool. *Neuroimage,* 210**,** 116532.
PERKINS, B. A., OLALEYE, D., ZINMAN, B. & BRIL, V. 2001. Simple screening tests for peripheral neuropathy in the diabetes clinic. *Diabetes Care,* 24**,** 250-6.
PETROU, M., POP-BUSUI, R., FOERSTER, B. R., EDDEN, R. A., CALLAGHAN, B. C., HARTE, S. E., HARRIS, R. E., CLAUW, D. J. & FELDMAN, E. L. 2012. Altered excitation-inhibition balance in the brain of patients with diabetic neuropathy. *Acad Radiol,* 19**,** 607-12.
PITTENGER, G. L., RAY, M., BURCUS, N. I., MCNULTY, P., BASTA, B. & VINIK, A. I. 2004. Intraepidermal nerve fibers are indicators of small-fiber neuropathy in both diabetic and nondiabetic patients. *Diabetes Care,* 27**,** 1974-9.
PONIRAKIS, G., ELHADD, T., CHINNAIYAN, S., DABBOUS, Z., SIDDIQUI, M., AL-MUHANNADI, H., PETROPOULOS, I., KHAN, A., ASHAWESH, K. A., DUKHAN, K. M., MAHFOUD, Z. R., MURGATROYD, C., SLEVIN, M. & MALIK, R. A. 2019. Prevalence and risk factors for painful diabetic neuropathy in secondary healthcare in Qatar. *J Diabetes Investig,* 10**,** 1558-1564.
POOLEY, R. A. 2005. AAPM/RSNA physics tutorial for residents: fundamental physics of MR imaging. *Radiographics,* 25**,** 1087-99.
POP-BUSUI, R., BOULTON, A. J., FELDMAN, E. L., BRIL, V., FREEMAN, R., MALIK, R. A., SOSENKO, J. M. & ZIEGLER, D. 2017. Diabetic Neuropathy: A Position Statement by the American Diabetes Association. *Diabetes Care,* 40**,** 136-154.
POWELL, H. C., ROSOFF, J. & MYERS, R. R. 1985. Microangiopathy in human diabetic neuropathy. *Acta Neuropathol,* 68**,** 295-305.
PRISCIANDARO, J. J., MIKKELSEN, M., SALEH, M. G. & EDDEN, R. A. E. 2020. An evaluation of the reproducibility of. *Magn Reson Imaging,* 65**,** 109-113.
PROVITERA, V., GIBBONS, C. H., WENDELSCHAFER-CRABB, G., DONADIO, V., VITALE, D. F., STANCANELLI, A., CAPORASO, G., LIGUORI, R., WANG, N., SANTORO, L., KENNEDY, W. R. & NOLANO, M. 2016. A multi-center, multinational age- and gender-adjusted normative dataset for immunofluorescent intraepidermal nerve fiber density at the distal leg. *Eur J Neurol,* 23**,** 333-8.
PURWATA, T. E. 2011. High TNF-alpha plasma levels and macrophages iNOS and TNF-alpha expression as risk factors for painful diabetic neuropathy. *J Pain Res,* 4**,** 169-75.
PUSZTASZERI, M. P., SEELENTAG, W. & BOSMAN, F. T. 2006. Immunohistochemical expression of endothelial markers CD31, CD34, von Willebrand factor, and Fli-1 in normal human tissues. *J Histochem Cytochem,* 54**,** 385-95.
PUTS, N. A. & EDDEN, R. A. 2012. In vivo magnetic resonance spectroscopy of GABA: a methodological review. *Prog Nucl Magn Reson Spectrosc,* 60**,** 29-41.
QUATTRINI, C., HARRIS, N. D., MALIK, R. A. & TESFAYE, S. 2007a. Impaired skin microvascular reactivity in painful diabetic neuropathy. *Diabetes Care,* 30**,** 655-9.

QUATTRINI, C., JEZIORSKA, M., BOULTON, A. J. & MALIK, R. A. 2008. Reduced vascular endothelial growth factor expression and intra-epidermal nerve fiber loss in human diabetic neuropathy. *Diabetes Care,* 31**,** 140-5.

QUATTRINI, C., TAVAKOLI, M., JEZIORSKA, M., KALLINIKOS, P., TESFAYE, S., FINNIGAN, J., MARSHALL, A., BOULTON, A. J., EFRON, N. & MALIK, R. A. 2007b. Surrogate markers of small fiber damage in human diabetic neuropathy. *Diabetes,* 56**,** 2148-54.

QUINTERO, G. C. 2013. Advances in cortical modulation of pain. *J Pain Res,* 6**,** 713-25.

RAE, C. D. 2014. A guide to the metabolic pathways and function of metabolites observed in human brain 1H magnetic resonance spectra. *Neurochem Res,* 39**,** 1-36.

RAGÉ, M., VAN ACKER, N., KNAAPEN, M. W., TIMMERS, M., STREFFER, J., HERMANS, M. P., SINDIC, C., MEERT, T. & PLAGHKI, L. 2011. Asymptomatic small fiber neuropathy in diabetes mellitus: investigations with intraepidermal nerve fiber density, quantitative sensory testing and laser-evoked potentials. *J Neurol,* 258**,** 1852-64.

RANDI, A. M. & LAFFAN, M. A. 2017. Von Willebrand factor and angiogenesis: basic and applied issues. *J Thromb Haemost,* 15**,** 13-20.

RANGO, M., BONIFATI, C. & BRESOLIN, N. 2006. Parkinson's disease and brain mitochondrial dysfunction: a functional phosphorus magnetic resonance spectroscopy study. *J Cereb Blood Flow Metab,* 26**,** 283-90.

RAPUTOVA, J., SROTOVA, I., VLCKOVA, E., SOMMER, C., ÜÇEYLER, N., BIRKLEIN, F., RITTNER, H. L., REBHORN, C., ADAMOVA, B., KOVALOVA, I., KRALICKOVA NEKVAPILOVA, E., FORER, L., BELOBRADKOVA, J., OLSOVSKY, J., WEBER, P., DUSEK, L., JARKOVSKY, J. & BEDNARIK, J. 2017. Sensory phenotype and risk factors for painful diabetic neuropathy: a cross-sectional observational study. *Pain,* 158**,** 2340-2353.

REIBER, G. E., VILEIKYTE, L., BOYKO, E. J., DEL AGUILA, M., SMITH, D. G., LAVERY, L. A. & BOULTON, A. J. 1999. Causal pathways for incident lower-extremity ulcers in patients with diabetes from two settings. *Diabetes Care,* 22**,** 157-62.

RESKE-NIELSEN, E. & LUNDBAEK, K. 1968. Pathological changes in the central and peripheral nervous system of young long-term diabetics. II. The spinal cord and peripheral nerves. *Diabetologia,* 4**,** 34-43.

RESKE-NIELSEN, E., LUNDBÆK, K. & RAFAELSEN, O. J. 1966. Pathological changes in the central and peripheral nervous system of young long-term diabetics : I. Diabetic encephalopathy. *Diabetologia,* 1**,** 233-41.

REUTER, M., ROSAS, H. D. & FISCHL, B. 2010. Highly accurate inverse consistent registration: a robust approach. *Neuroimage,* 53**,** 1181-96.

ROBINSON, M. E., CRAGGS, J. G., PRICE, D. D., PERLSTEIN, W. M. & STAUD, R. 2011. Gray matter volumes of pain-related brain areas are decreased in fibromyalgia syndrome. *J Pain,* 12**,** 436-43.

RODE, J., DHILLON, A. P., DORAN, J. F., JACKSON, P. & THOMPSON, R. J. 1985. PGP 9.5, a new marker for human neuroendocrine tumours. *Histopathology,* 9**,** 147-58.

ROLKE, R., BARON, R., MAIER, C., TÖLLE, T. R., TREEDE, R. D., BEYER, A., BINDER, A., BIRBAUMER, N., BIRKLEIN, F., BÖTEFÜR, I. C., BRAUNE, S., FLOR, H., HUGE, V., KLUG, R., LANDWEHRMEYER, G. B., MAGERL, W., MAIHÖFNER, C., ROLKO, C., SCHAUB, C., SCHERENS, A., SPRENGER, T., VALET, M. & WASSERKA, B. 2006. Quantitative sensory testing in the German Research Network on Neuropathic Pain (DFNS): standardized protocol and reference values. *Pain,* 123**,** 231-43.

ROSENBERGER, D. C., BLECHSCHMIDT, V., TIMMERMAN, H., WOLFF, A. & TREEDE, R. D. 2020. Challenges of neuropathic pain: focus on diabetic neuropathy. *J Neural Transm (Vienna),* 127**,** 589-624.

SADOSKY, A., MARDEKIAN, J., PARSONS, B., HOPPS, M., BIENEN, E. J. & MARKMAN, J. 2015. Healthcare utilization and costs in diabetes relative to the clinical spectrum of painful diabetic peripheral neuropathy. *J Diabetes Complications,* 29**,** 212-7.

SAEEDI, P., PETERSOHN, I., SALPEA, P., MALANDA, B., KARURANGA, S., UNWIN, N., COLAGIURI, S., GUARIGUATA, L., MOTALA, A. A., OGURTSOVA, K., SHAW, J. E., BRIGHT, D., WILLIAMS, R. & COMMITTEE, I. D. A. 2019. Global and regional diabetes prevalence estimates for 2019 and projections for 2030 and 2045: Results from the International Diabetes Federation Diabetes Atlas, 9. *Diabetes Res Clin Pract,* 157**,** 107843.

SAEGUSA, H., KURIHARA, T., ZONG, S., KAZUNO , A., MATSUDA, Y., NONAKA, T., HAN, W., TORIYAMA, H. & TANABE, T. 2001. Suppression of inflammatory and neuropathic pain symptoms in mice lacking the N-type Ca2+ channel. *EMBO J,* 20**,** 2349-56.

SAHIN, I., ALKAN, A., KESKIN, L., CIKIM, A., KARAKAS, H. M., FIRAT, A. K. & SIGIRCI, A. 2008. Evaluation of in vivo cerebral metabolism on proton magnetic resonance spectroscopy in patients with impaired glucose tolerance and type 2 diabetes mellitus. *J Diabetes Complications,* 22**,** 254-60.

SALEH, M. G., NEAR, J., ALHAMUD, A., ROBERTSON, F., VAN DER KOUWE, A. J. & MEINTJES, E. M. 2016a. Reproducibility of macromolecule suppressed GABA measurement using motion and shim navigated MEGA-SPECIAL with LCModel, jMRUI and GANNET. *MAGMA,* 29**,** 863-874.

SALEH, M. G., OELTZSCHNER, G., CHAN, K. L., PUTS, N. A. J., MIKKELSEN, M., SCHÄR, M., HARRIS, A. D. & EDDEN, R. A. E. 2016b. Simultaneous edited MRS of GABA and glutathione. *Neuroimage,* 142**,** 576-582.

SCHERENS, A., MAIER, C., HAUSSLEITER, I. S., SCHWENKREIS, P., VLCKOVA-MORAVCOVA, E., BARON, R. & SOMMER, C. 2009. Painful or painless lower limb dysesthesias are highly predictive of peripheral neuropathy: comparison of different diagnostic modalities. *Eur J Pain,* 13**,** 711-8.

SCHMAHMANN, J. D. 2003. Vascular syndromes of the thalamus. *Stroke,* 34**,** 2264-78.

SCHMIDT-WILCKE, T., LEINISCH, E., GÄNSSBAUER, S., DRAGANSKI, B., BOGDAHN, U., ALTMEPPEN, J. & MAY, A. 2006. Affective components and intensity of pain correlate with structural differences in gray matter in chronic back pain patients. *Pain,* 125**,** 89-97.

SEGERDAHL, A. R., THEMISTOCLEOUS, A. C., FIDO, D., BENNETT, D. L. & TRACEY, I. 2018. A brain-based pain facilitation mechanism contributes to painful diabetic polyneuropathy. *Brain,* 141**,** 357-364.

SÉGONNE, F., DALE, A. M., BUSA, E., GLESSNER, M., SALAT, D., HAHN, H. K. & FISCHL, B. 2004. A hybrid approach to the skull stripping problem in MRI. *Neuroimage,* 22**,** 1060-75.

SÉGONNE, F., PACHECO, J. & FISCHL, B. 2007. Geometrically accurate topology-correction of cortical surfaces using nonseparating loops. *IEEE Trans Med Imaging,* 26**,** 518-29.

SELVARAJAH, D., CASH, T., SANKAR, A., THOMAS, L., DAVIES, J., CACHIA, E., GANDHI, R., WILKINSON, I. D., WILKINSON, N., EMERY, C. J. & TESFAYE, S. 2014a. The contributors of emotional distress in painful diabetic neuropathy. *Diab Vasc Dis Res,* 11**,** 218-225.

SELVARAJAH, D., PETRIE, J., WHITE, D., JULIOUS, S., BORTOLAMI, O., COOPER, C., BRADBURN, M., LOBAN, A., BOWLER, H., SWABY, L., SUTHERLAND, K., TESFAYE, S. & GROUP, O.-D. 2018. Multicentre, double-blind, crossover trial to identify the Optimal Pathway for TreatIng neurOpathic paiN in Diabetes Mellitus (OPTION-DM): study protocol for a randomised controlled trial. *Trials,* 19**,** 578.

SELVARAJAH, D., WILKINSON, I. D., EMERY, C. J., HARRIS, N. D., SHAW, P. J., WITTE, D. R., GRIFFITHS, P. D. & TESFAYE, S. 2006. Early involvement of the spinal cord in diabetic peripheral neuropathy. *Diabetes Care,* 29**,** 2664-9.

SELVARAJAH, D., WILKINSON, I. D., EMERY, C. J., SHAW, P. J., GRIFFITHS, P. D., GANDHI, R. & TESFAYE, S. 2008. Thalamic neuronal dysfunction and chronic sensorimotor distal symmetrical polyneuropathy in patients with type 1 diabetes mellitus. *Diabetologia,* 51**,** 2088-92.

SELVARAJAH, D., WILKINSON, I. D., FANG, F., SANKAR, A., DAVIES, J., BOLAND, E., HARDING, J., RAO, G., GANDHI, R., TRACEY, I. & TESFAYE, S. 2019. Structural and Functional Abnormalities of the Primary Somatosensory Cortex in Diabetic Peripheral Neuropathy: A Multimodal MRI Study. *Diabetes,* 68**,** 796-806.

SELVARAJAH, D., WILKINSON, I. D., GANDHI, R., GRIFFITHS, P. D. & TESFAYE, S. 2011. Microvascular perfusion abnormalities of the Thalamus in painful but not painless diabetic polyneuropathy: a clue to the pathogenesis of pain in type 1 diabetes. *Diabetes Care,* 34**,** 718-20.

SELVARAJAH, D., WILKINSON, I. D., MAXWELL, M., DAVIES, J., SANKAR, A., BOLAND, E., GANDHI, R., TRACEY, I. & TESFAYE, S. 2014b. Magnetic resonance neuroimaging study of brain structural differences in diabetic peripheral neuropathy. *Diabetes Care,* 37**,** 1681-8.

SEMINOWICZ, D. A., WIDEMAN, T. H., NASO, L., HATAMI-KHOROUSHAHI, Z., FALLATAH, S., WARE, M. A., JARZEM, P., BUSHNELL, M. C., SHIR, Y., OUELLET, J. A. & STONE, L. S. 2011. Effective treatment of chronic low back pain in humans reverses abnormal brain anatomy and function. *J Neurosci,* 31**,** 7540-50.

SERRA, J., BOSTOCK, H., SOLA, R., ALEU, J., GARCIA, E., COKIC, B., NAVARRO, X. & QUILES, C. 2012. Microneurographic identification of spontaneous activity in C-nociceptors in neuropathic pain states in humans and rats. *Pain,* 153**,** 42-55.

SHI, X. F., CARLSON, P. J., SUNG, Y. H., FIEDLER, K. K., FORREST, L. N., HELLEM, T. L., HUBER, R. S., KIM, S. E., ZUO, C., JEONG, E. K., RENSHAW, P. F. & KONDO, D. G. 2015. Decreased brain PME/PDE ratio in bipolar disorder: a preliminary (31) P magnetic resonance spectroscopy study. *Bipolar Disord,* 17**,** 743-52.

SHILLO, P. 2019. *Peripheral and Central Biomarkers in Painful Diabetic Peripheral Neuropathy.* MD, The University of Sheffield.

SHILLO, P., SELVARAJAH, D., GREIG, M., GANDHI, R., RAO, G., WILKINSON, I. D., ANAND, P. & TESFAYE, S. 2019a. Reduced vitamin D levels in painful diabetic peripheral neuropathy. *Diabet Med,* 36**,** 44-51.

SHILLO, P., SELVARAJAH, D., GREIG, M., RAO, D., EDDEN, R., WILKINSON, I. & TESFAYE, S. 2016. Painless diabetic peripheral neuropathy is characterised by reduced thalamic gamma-aminobutyric acid (GABA). Diabetic Medicine.

SHILLO, P., SELVARAJAH, D., GREIG, M., WILKINSON, I., YIANGOU, Y., DONATIEN, P., ANAND, P. & TESFAYE, S. 2017. Nerve and vascular biomarkers in skin biopsies differentiate painful from painless advanced diabetic peripheral neuropathy. Diabetic Medicine.

SHILLO, P., SLOAN, G., GREIG, M., HUNT, L., SELVARAJAH, D., ELLIOTT, J., GANDHI, R., WILKINSON, I. D. & TESFAYE, S. 2019b. Painful and Painless Diabetic Neuropathies: What Is the Difference? *Curr Diab Rep,* 19**,** 32, doi 10.1007/s11892-019-1150-5.

SHUN, C. T., CHANG, Y. C., WU, H. P., HSIEH, S. C., LIN, W. M., LIN, Y. H., TAI, T. Y. & HSIEH, S. T. 2004. Skin denervation in type 2 diabetes: correlations with diabetic duration and functional impairments. *Brain,* 127**,** 1593-605.

SIMONS, L. E., PIELECH, M., ERPELDING, N., LINNMAN, C., MOULTON, E., SAVA, S., LEBEL, A., SERRANO, P., SETHNA, N., BERDE, C., BECERRA, L. & BORSOOK, D. 2014. The responsive amygdala: treatment-induced alterations in functional connectivity in pediatric complex regional pain syndrome. *Pain,* 155**,** 1727-1742.

SLOAN, G., SELVARAJAH, D. & TESFAYE, S. 2021. Pathogenesis, diagnosis and clinical management of diabetic sensorimotor peripheral neuropathy. *Nat Rev Endocrinol*.

SLOAN, G., SHILLO, P., SELVARAJAH, D., WU, J., WILKINSON, I. D., TRACEY, I., ANAND, P. & TESFAYE, S. 2018. A new look at painful diabetic neuropathy. *Diabetes Res Clin Pract,* 144**,** 177-191.

SMALLWOOD, R. F., LAIRD, A. R., RAMAGE, A. E., PARKINSON, A. L., LEWIS, J., CLAUW, D. J., WILLIAMS, D. A., SCHMIDT-WILCKE, T., FARRELL, M. J., EICKHOFF, S. B. & ROBIN, D. A. 2013. Structural brain anomalies and chronic pain: a quantitative meta-analysis of gray matter volume. *J Pain,* 14**,** 663-75.

SMITH, A. G., RUSSELL, J., FELDMAN, E. L., GOLDSTEIN, J., PELTIER, A., SMITH, S., HAMWI, J., POLLARI, D., BIXBY, B., HOWARD, J. & SINGLETON, J. R. 2006. Lifestyle intervention for pre-diabetic neuropathy. *Diabetes Care,* 29**,** 1294-9.

SMITH, S. M., DWORKIN, R. H., TURK, D. C., BARON, R., POLYDEFKIS, M., TRACEY, I., BORSOOK, D., EDWARDS, R. R., HARRIS, R. E., WAGER, T. D., ARENDT-NIELSEN, L., BURKE, L. B., CARR, D. B.,

CHAPPELL, A., FARRAR, J. T., FREEMAN, R., GILRON, I., GOLI, V., HAEUSSLER, J., JENSEN, T., KATZ, N. P., KENT, J., KOPECKY, E. A., LEE, D. A., MAIXNER, W., MARKMAN, J. D., MCARTHUR, J. C., MCDERMOTT, M. P., PARVATHENANI, L., RAJA, S. N., RAPPAPORT, B. A., RICE, A. S. C., ROWBOTHAM, M. C., TOBIAS, J. K., WASAN, A. D. & WITTER, J. 2017. The Potential Role of Sensory Testing, Skin Biopsy, and Functional Brain Imaging as Biomarkers in Chronic Pain Clinical Trials: IMMPACT Considerations. *J Pain,* 18**,** 757-777.

SMITHA, K. A., AKHIL RAJA, K., ARUN, K. M., RAJESH, P. G., THOMAS, B., KAPILAMOORTHY, T. R. & KESAVADAS, C. 2017. Resting state fMRI: A review on methods in resting state connectivity analysis and resting state networks. *Neuroradiol J,* 30**,** 305-317.

SORENSEN, L., MOLYNEAUX, L. & YUE, D. K. 2006. The relationship among pain, sensory loss, and small nerve fibers in diabetes. *Diabetes Care,* 29**,** 883-7.

SORENSEN, L., SIDDALL, P. J., TRENELL, M. I. & YUE, D. K. 2008. Differences in metabolites in pain-processing brain regions in patients with diabetes and painful neuropathy. *Diabetes Care,* 31**,** 980-1.

SPALLONE, V. & GRECO, C. 2013. Painful and painless diabetic neuropathy: one disease or two? *Curr Diab Rep,* 13**,** 533-49.

SPALLONE, V., MORGANTI, R., D'AMATO, C., GRECO, C., CACCIOTTI, L. & MARFIA, G. A. 2012. Validation of DN4 as a screening tool for neuropathic pain in painful diabetic polyneuropathy. *Diabet Med,* 29**,** 578-85.

STEFAN, D., CESARE, F.D., ANDRASESCU, A., POPA, E., LAZARIEV, A., VESCOVO, E., STRBAK, O., WILLIAMS, S., STARCUK, Z. & CABANAS, M. 2009. Quantitation of magnetic resonance spectroscopy signals: jMRUI software package. *Measurement Science and Technology,* 20.

SULLIVAN, M. J. L., BISHOP, S. R. & PIVIK, J. 1995. <h2 _ngcontent-c21="" class="title" style="box-sizing: border-box; font-family: sans-serif; font-weight: 500; line-height: 1.1; color: rgb(0, 119, 191); margin-top: 20px; margin-bottom: 10px; background-color: rgb(255, 255, 255);">The Pain Catastrophizing Scale: Development and validation. Psychological Assessment.

SUZUKI, C., OZAKI, I., TANOSAKI, M., SUDA, T., BABA, M. & MATSUNAGA, M. 2000. Peripheral and central conduction abnormalities in diabetes mellitus. *Neurology,* 54**,** 1932-7.

TACK, C. J., VAN GURP, P. J., HOLMES, C. & GOLDSTEIN, D. S. 2002. Local sympathetic denervation in painful diabetic neuropathy. *Diabetes,* 51**,** 3545-53.

TANG, Y., LENZINI, P. A., POP-BUSUI, R., RAY, P. R., CAMPBELL, H., PERKINS, B. A., CALLAGHAN, B., WAGNER, M. J., MOTSINGER-REIF, A. A., BUSE, J. B., PRICE, T. J., MYCHALECKYJ, J. C., CRESCI, S., SHAH, H. & DORIA, A. 2019. A Genetic Locus on Chromosome 2q24 Predicting Peripheral Neuropathy Risk in Type 2 Diabetes: Results From the ACCORD and BARI 2D Studies. *Diabetes,* 68**,** 1649-1662.

TAYLOR-STOKES, G., PIKE, J., SADOSKY, A., CHANDRAN, A. & TOELLE, T. 2011. Association of patient-rated severity with other outcomes in patients with painful diabetic peripheral neuropathy. *Diabetes Metab Syndr Obes,* 4**,** 401-8.

TAYLOR, A. M., MEHRABANI, S., LIU, S., TAYLOR, A. J. & CAHILL, C. M. 2017. Topography of microglial activation in sensory- and affect-related brain regions in chronic pain. *J Neurosci Res,* 95**,** 1330-1335.

TEH, K., WILKINSON, I. D., HEIBERG-GIBBONS, F., AWADH, M., KELSALL, A., SHILLO, P., SLOAN, G., TESFAYE, S. & SELVARAJAH, D. 2021. Somatosensory network functional connectivity differentiates clinical pain phenotypes in diabetic neuropathy. *Diabetologia,* 64**,** 1412-1421.

TESFAYE, S. 2011. Recent advances in the management of diabetic distal symmetrical polyneuropathy. *J Diabetes Investig,* 2**,** 33-42.

TESFAYE, S., BOULTON, A. J. & DICKENSON, A. H. 2013. Mechanisms and management of diabetic painful distal symmetrical polyneuropathy. *Diabetes Care,* 36**,** 2456-65.

TESFAYE, S., BOULTON, A. J., DYCK, P. J., FREEMAN, R., HOROWITZ, M., KEMPLER, P., LAURIA, G., MALIK, R. A., SPALLONE, V., VINIK, A., BERNARDI, L., VALENSI, P. & the Toronto Diabetic

Neuropathy Expert Group. 2010. Diabetic neuropathies: update on definitions, diagnostic criteria, estimation of severity, and treatments. *Diabetes Care,* 33**,** 2285-93.
TESFAYE, S., CHATURVEDI, N., EATON, S. E., WARD, J. D., MANES, C., IONESCU-TIRGOVISTE, C., WITTE, D. R., FULLER, J. H. & the EURODIAB Prospective Complications Study Group. 2005. Vascular risk factors and diabetic neuropathy. *N Engl J Med,* 352**,** 341-50.
TESFAYE, S., HARRIS, N., JAKUBOWSKI, J. J., MODY, C., WILSON, R. M., RENNIE, I. G. & WARD, J. D. 1993. Impaired blood flow and arterio-venous shunting in human diabetic neuropathy: a novel technique of nerve photography and fluorescein angiography. *Diabetologia,* 36**,** 1266-74.
TESFAYE, S., HARRIS, N. D., WILSON, R. M. & WARD, J. D. 1992. Exercise-induced conduction velocity increment: a marker of impaired peripheral nerve blood flow in diabetic neuropathy. *Diabetologia,* 35**,** 155-9.
TESFAYE, S., SELVARAJAH, D., GANDHI, R., GREIG, M., SHILLO, P., FANG, F. & WILKINSON, I. D. 2016. Diabetic peripheral neuropathy may not be as its name suggests: evidence from magnetic resonance imaging. *Pain,* 157 Suppl 1**,** S72-80.
TESFAYE, S., STEVENS, L. K., STEPHENSON, J. M., FULLER, J. H., PLATER, M., IONESCU-TIRGOVISTE, C., NUBER, A., POZZA, G. & WARD, J. D. 1996. Prevalence of diabetic peripheral neuropathy and its relation to glycaemic control and potential risk factors: the EURODIAB IDDM Complications Study. *Diabetologia,* 39**,** 1377-84.
THEMISTOCLEOUS, A. C., RAMIREZ, J. D., SHILLO, P. R., LEES, J. G., SELVARAJAH, D., ORENGO, C., TESFAYE, S., RICE, A. S. & BENNETT, D. L. 2016. The Pain in Neuropathy Study (PiNS): a cross-sectional observational study determining the somatosensory phenotype of painful and painless diabetic neuropathy. *Pain,* 157**,** 1132-45.
THOMPSON, R. J., DORAN, J. F., JACKSON, P., DHILLON, A. P. & RODE, J. 1983. PGP 9.5--a new marker for vertebrate neurons and neuroendocrine cells. *Brain Res,* 278**,** 224-8.
TIMAR, B., POPESCU, S., TIMAR, R., BADERCA, F., DUICA, B., VLAD, M., LEVAI, C., BALINISTEANU, B. & SIMU, M. 2016. The usefulness of quantifying intraepidermal nerve fibers density in the diagnostic of diabetic peripheral neuropathy: a cross-sectional study. *Diabetol Metab Syndr,* 8**,** 31.
TKÁC, I., STARCUK, Z., CHOI, I. Y. & GRUETTER, R. 1999. In vivo 1H NMR spectroscopy of rat brain at 1 ms echo time. *Magn Reson Med,* 41**,** 649-56.
TÖLLE, T., XU, X. & SADOSKY, A. B. 2006. Painful diabetic neuropathy: a cross-sectional survey of health state impairment and treatment patterns. *J Diabetes Complications,* 20**,** 26-33.
TOMLINSON, D. R. & GARDINER, N. J. 2008. Glucose neurotoxicity. *Nat Rev Neurosci,* 9**,** 36-45.
TRACEY, I. & MANTYH, P. W. 2007. The cerebral signature and its modulation for pain perception. *Neuron,* 55**,** 377-391.
TRACEY, I., WOOLF, C. J. & ANDREWS, N. A. 2019. Composite Pain Biomarker Signatures for Objective Assessment and Effective Treatment. *Neuron,* 101**,** 783-800.
TREEDE, R. D., JENSEN, T. S., CAMPBELL, J. N., CRUCCU, G., DOSTROVSKY, J. O., GRIFFIN, J. W., HANSSON, P., HUGHES, R., NURMIKKO, T. & SERRA, J. 2008. Neuropathic pain: redefinition and a grading system for clinical and research purposes. *Neurology,* 70**,** 1630-5.
TRUINI, A., BIASIOTTA, A., DI STEFANO, G., LEONE, C., LA CESA, S., GALOSI, E., PIROSO, S., PEPE, A., GIORDANO, C. & CRUCCU, G. 2014. Does the epidermal nerve fibre density measured by skin biopsy in patients with peripheral neuropathies correlate with neuropathic pain? *Pain,* 155**,** 828-832.
TRUINI, A., SPALLONE, V., MORGANTI, R., TAMBURIN, S., ZANETTE, G., SCHENONE, A., DE MICHELIS, C., TUGNOLI, V., SIMIONI, V., MANGANELLI, F., DUBBIOSO, R., LAURIA, G., LOMBARDI, R., JANN, S., DE TONI FRANCESCHINI, L., TESFAYE, S., FIORELLI, M., SPAGNOLI, A. & CRUCCU, G. 2018. A cross-sectional study investigating frequency and features of definitely diagnosed diabetic painful polyneuropathy. *Pain,* 159**,** 2658-2666.

TSENG, M. T., CHIANG, M. C., CHAO, C. C., TSENG, W. Y. & HSIEH, S. T. 2013. fMRI evidence of degeneration-induced neuropathic pain in diabetes: enhanced limbic and striatal activations. *Hum Brain Mapp,* 34**,** 2733-46.

TSIGOS, C., WHITE, A. & YOUNG, R. J. 1992. Discrimination between painful and painless diabetic neuropathy based on testing of large somatic nerve and sympathetic nerve function. *Diabet Med,* 9**,** 359-65.

TU, Y., FU, Z., MAO, C., FALAHPOUR, M., GOLLUB, R. L., PARK, J., WILSON, G., NAPADOW, V., GERBER, J., CHAN, S. T., EDWARDS, R. R., KAPTCHUK, T. J., LIU, T., CALHOUN, V., ROSEN, B. & KONG, J. 2020. Distinct thalamocortical network dynamics are associated with the pathophysiology of chronic low back pain. *Nat Commun,* 11**,** 3948.

UMAPATHI, T., TAN, W. L., LOKE, S. C., SOON, P. C., TAVINTHARAN, S. & CHAN, Y. H. 2007. Intraepidermal nerve fiber density as a marker of early diabetic neuropathy. *Muscle Nerve,* 35**,** 591-8.

VALKOVIČ, L., CHMELÍK, M. & KRŠŠÁK, M. 2017. In-vivo. *Anal Biochem,* 529**,** 193-215.

VAN ACKER, K., BOUHASSIRA, D., DE BACQUER, D., WEISS, S., MATTHYS, K., RAEMEN, H., MATHIEU, C. & COLIN, I. M. 2009. Prevalence and impact on quality of life of peripheral neuropathy with or without neuropathic pain in type 1 and type 2 diabetic patients attending hospital outpatients clinics. *Diabetes Metab,* 35**,** 206-13.

VAN DEN HEUVEL, M. P. & HULSHOFF POL, H. E. 2010. Exploring the brain network: a review on resting-state fMRI functional connectivity. *Eur Neuropsychopharmacol,* 20**,** 519-34.

VANHAMME, L., VAN DEN BOOGAART A & VAN HUFFEL S 1997. Improved method for accurate and efficient quantification of MRS data with use of prior knowledge. *J Magn Reson,* 129**,** 35-43.

VAS, P. R., SHARMA, S. & RAYMAN, G. 2015. Distal Sensorimotor Neuropathy: Improvements in Diagnosis. *Rev Diabet Stud,* 12**,** 29-47.

VEVES, A., AKBARI, C. M., PRIMAVERA, J., DONAGHUE, V. M., ZACHAROULIS, D., CHRZAN, J. S., DEGIROLAMI, U., LOGERFO, F. W. & FREEMAN, R. 1998. Endothelial dysfunction and the expression of endothelial nitric oxide synthetase in diabetic neuropathy, vascular disease, and foot ulceration. *Diabetes,* 47**,** 457-63.

VEVES, A., BACKONJA, M. & MALIK, R. A. 2008. Painful diabetic neuropathy: epidemiology, natural history, early diagnosis, and treatment options. *Pain Med,* 9**,** 660-74.

VINCENT, A. M., CALLAGHAN, B. C., SMITH, A. L. & FELDMAN, E. L. 2011. Diabetic neuropathy: cellular mechanisms as therapeutic targets. *Nat Rev Neurol,* 7**,** 573-83.

VINCENT, A. M., EDWARDS, J. L., MCLEAN, L. L., HONG, Y., CERRI, F., LOPEZ, I., QUATTRINI, A. & FELDMAN, E. L. 2010. Mitochondrial biogenesis and fission in axons in cell culture and animal models of diabetic neuropathy. *Acta Neuropathol,* 120**,** 477-89.

VLCKOVÁ-MORAVCOVÁ, E., BEDNARÍK, J., DUSEK, L., TOYKA, K. V. & SOMMER, C. 2008. Diagnostic validity of epidermal nerve fiber densities in painful sensory neuropathies. *Muscle Nerve,* 37**,** 50-60.

VOLLERT, J., ATTAL, N., BARON, R., FREYNHAGEN, R., HAANPÄÄ, M., HANSSON, P., JENSEN, T. S., RICE, A. S., SEGERDAHL, M., SERRA, J., SINDRUP, S. H., TÖLLE, T. R., TREEDE, R. D. & MAIER, C. 2016. Quantitative sensory testing using DFNS protocol in Europe: an evaluation of heterogeneity across multiple centers in patients with peripheral neuropathic pain and healthy subjects. *Pain,* 157**,** 750-8.

WAGER, T. D., ATLAS, L. Y., LINDQUIST, M. A., ROY, M., WOO, C. W. & KROSS, E. 2013. An fMRI-based neurologic signature of physical pain. *N Engl J Med,* 368**,** 1388-97.

WALCHHOFER, L. M., STEIGER, R., RIETZLER, A., KERSCHBAUMER, J., FREYSCHLAG, C. F., STOCKHAMMER, G., GIZEWSKI, E. R. & GRAMS, A. E. 2021. Phosphorous Magnetic Resonance Spectroscopy to Detect Regional Differences of Energy and Membrane Metabolism in Naïve Glioblastoma Multiforme. *Cancers (Basel),* 13.

WALSH, J. W., HOFFSTAD, O. J., SULLIVAN, M. O. & MARGOLIS, D. J. 2016. Association of diabetic foot ulcer and death in a population-based cohort from the United Kingdom. *Diabet Med,* 33**,** 1493-1498.

WANG, L., HILLIGES, M., JERNBERG, T., WIEGLEB-EDSTRÖM, D. & JOHANSSON, O. 1990. Protein gene product 9.5-immunoreactive nerve fibres and cells in human skin. *Cell Tissue Res,* 261**,** 25-33.

WARD, J. D. 1982. The diabetic leg. *Diabetologia,* 22**,** 141-7.

WATANABE, K., HIRANO, S., KOJIMA, K., NAGASHIMA, K., MUKAI, H., SATO, T., TAKEMOTO, M., MATSUMOTO, K., IIMORI, T., ISOSE, S., OMORI, S., SHIBUYA, K., SEKIGUCHI, Y., BEPPU, M., AMINO, H., SUICHI, T., YOKOTE, K., UNO, T., KUWABARA, S. & MISAWA, S. 2018. Altered cerebral blood flow in the anterior cingulate cortex is associated with neuropathic pain. *J Neurol Neurosurg Psychiatry,* 89, 1082-1087.

WEISMAN, A., BRIL, V., NGO, M., LOVBLOM, L. E., HALPERN, E. M., ORSZAG, A. & PERKINS, B. A. 2013. Identification and prediction of diabetic sensorimotor polyneuropathy using individual and simple combinations of nerve conduction study parameters. *PLoS One,* 8**,** e58783.

WHITFIELD-GABRIELI, S. & NIETO-CASTANON, A. 2012. Conn: a functional connectivity toolbox for correlated and anticorrelated brain networks. *Brain Connect,* 2**,** 125-41.

WILKINSON, I. D. & PALEY, M. N. J. 2008. Magnetic Resonance Imaging: Basic Principles. *In:* ADAM, A., DIXON, A. K., GRAINGER, R. G. & ALLISON, D. J. (eds.) *Diagnostic Radiology.* 5th ed.: Elsevier.

WILKINSON, I. D., TEH, K., HEIBERG-GIBBONS, F., AWADH, M., KELSALL, A., SHILLO, P., SLOAN, G., TESFAYE, S. & SELVARAJAH, D. 2020. Determinants of Treatment Response in Painful Diabetic Peripheral Neuropathy. A Combined Deep Sensory Phenotyping and Multi-modal Brain Magnetic Resonance Imaging Study. *Diabetes*.

WILKINSON, K. D., LEE, K. M., DESHPANDE, S., DUERKSEN-HUGHES, P., BOSS, J. M. & POHL, J. 1989. The neuron-specific protein PGP 9.5 is a ubiquitin carboxyl-terminal hydrolase. *Science,* 246**,** 670-3.

WILLIAMS, R., KARURANGA, S., MALANDA, B., SAEEDI, P., BASIT, A., BESANÇON, S., BOMMER, C., ESTEGHAMATI, A., OGURTSOVA, K., ZHANG, P. & COLAGIURI, S. 2020. Global and regional estimates and projections of diabetes-related health expenditure: Results from the International Diabetes Federation Diabetes Atlas, 9th edition. *Diabetes Res Clin Pract,* 162**,** doi 10.1016/j.diabres.2020.108072.

WILSON, M., ANDRONESI, O., BARKER, P. B., BARTHA, R., BIZZI, A., BOLAN, P. J., BRINDLE, K. M., CHOI, I. Y., CUDALBU, C., DYDAK, U., EMIR, U. E., GONZALEZ, R. G., GRUBER, S., GRUETTER, R., GUPTA, R. K., HEERSCHAP, A., HENNING, A., HETHERINGTON, H. P., HUPPI, P. S., HURD, R. E., KANTARCI, K., KAUPPINEN, R. A., KLOMP, D. W. J., KREIS, R., KRUISKAMP, M. J., LEACH, M. O., LIN, A. P., LUIJTEN, P. R., MARJAŃSKA, M., MAUDSLEY, A. A., MEYERHOFF, D. J., MOUNTFORD, C. E., MULLINS, P. G., MURDOCH, J. B., NELSON, S. J., NOESKE, R., ÖZ, G., PAN, J. W., PEET, A. C., POPTANI, H., POSSE, S., RATAI, E. M., SALIBI, N., SCHEENEN, T. W. J., SMITH, I. C. P., SOHER, B. J., TKÁČ, I., VIGNERON, D. B. & HOWE, F. A. 2019. Methodological consensus on clinical proton MRS of the brain: Review and recommendations. *Magn Reson Med,* 82**,** 527-550.

WILSON, P. O., BARBER, P. C., HAMID, Q. A., POWER, B. F., DHILLON, A. P., RODE, J., DAY, I. N., THOMPSON, R. J. & POLAK, J. M. 1988. The immunolocalization of protein gene product 9.5 using rabbit polyclonal and mouse monoclonal antibodies. *Br J Exp Pathol,* 69**,** 91-104.

WITZEL, I. I., JELINEK, H. F., KHALAF, K., LEE, S., KHANDOKER, A. H. & ALSAFAR, H. 2015. Identifying Common Genetic Risk Factors of Diabetic Neuropathies. *Front Endocrinol (Lausanne),* 6**,** 88.

WOODWORTH, D. C., HOLLY, L. T., MAYER, E. A., SALAMON, N. & ELLINGSON, B. M. 2019. Alterations in Cortical Thickness and Subcortical Volume are Associated With Neurological Symptoms and Neck Pain in Patients With Cervical Spondylosis. *Neurosurgery,* 84**,** 588-598.

WOOTTON-GORGES, S. L., BUONOCORE, M. H., KUPPERMANN, N., MARCIN, J. P., BARNES, P. D., NEELY, E. K., DICARLO, J., MCCARTHY, T. & GLASER, N. S. 2007. Cerebral proton magnetic

resonance spectroscopy in children with diabetic ketoacidosis. *AJNR Am J Neuroradiol,* 28**,** 895-9.
WU, G., LIN, L., ZHANG, Q. & WU, J. 2017. Brain gray matter changes in type 2 diabetes mellitus: A meta-analysis of whole-brain voxel-based morphometry study. *J Diabetes Complications,* 31**,** 1698-1703.
XIE, Y. F., HUO, F. Q. & TANG, J. S. 2009. Cerebral cortex modulation of pain. *Acta Pharmacol Sin,* 30**,** 31-41.
YANG, H., SLOAN, G., YE, Y., WANG, S., DUAN, B., TESFAYE, S. & GAO, L. 2019. New Perspective in Diabetic Neuropathy: From the Periphery to the Brain, a Call for Early Detection, and Precision Medicine. *Front Endocrinol (Lausanne),* 10**,** 929.
YAO, L., YANG, C., ZHANG, W., LI, S., LI, Q., CHEN, L., LUI, S., KEMP, G. J., BISWAL, B. B., SHAH, N. J., LI, F. & GONG, Q. 2021. A multimodal meta-analysis of regional structural and functional brain alterations in type 2 diabetes. *Front Neuroendocrinol,* 62**,** 100915.
YASEN, A. L., SMITH, J. & CHRISTIE, A. D. 2017. Reliability of glutamate and GABA quantification using proton magnetic resonance spectroscopy. *Neurosci Lett,* 643**,** 121-124.
YIM, Y., LEE, J. Y., OH, S. W., CHUNG, M. S., PARK, J. E., MOON, Y., JEON, H. J. & MOON, W. J. 2021. Comparison of Automated Brain Volume Measures by NeuroQuant vs. Freesurfer in Patients with Mild Cognitive Impairment: Effect of Slice Thickness. *Yonsei Med J,* 62**,** 255-261.
YOREK, M. A. 2016. Alternatives to the Streptozotocin-Diabetic Rodent. *Int Rev Neurobiol,* 127**,** 89-112.
YOUNG, M. J., BOULTON, A. J., MACLEOD, A. F., WILLIAMS, D. R. & SONKSEN, P. H. 1993. A multicentre study of the prevalence of diabetic peripheral neuropathy in the United Kingdom hospital clinic population. *Diabetologia,* 36**,** 150-4.
ZAMPONI, G. W., LEWIS, R. J., TODOROVIC, S. M., ARNERIC, S. P. & SNUTCH, T. P. 2009. Role of voltage-gated calcium channels in ascending pain pathways. *Brain Res Rev,* 60**,** 84-9.
ZANETTA, L., MARCUS, S. G., VASILE, J., DOBRYANSKY, M., COHEN, H., ENG, K., SHAMAMIAN, P. & MIGNATTI, P. 2000. Expression of Von Willebrand factor, an endothelial cell marker, is up-regulated by angiogenesis factors: a potential method for objective assessment of tumor angiogenesis. *Int J Cancer,* 85**,** 281-8.
ZHANG, Y., QU, M., YI, X., ZHUO, P., TANG, J., CHEN, X., ZHOU, G., HU, P., QIU, T., XING, W., MAO, Y., CHEN, B. T., WU, J. & LIAO, W. 2019. Sensorimotor and pain-related alterations of the gray matter and white matter in Type 2 diabetic patients with peripheral neuropathy. *Hum Brain Mapp*.
ZHAO, X., HAN, Q., GANG, X. & WANG, G. 2018. Altered brain metabolites in patients with diabetes mellitus and related complications - evidence from. *Biosci Rep,* 38.
ZIEGLER, D., PAPANAS, N., VINIK, A. I. & SHAW, J. E. 2014. Epidemiology of polyneuropathy in diabetes and prediabetes. *Handb Clin Neurol,* 126**,** 3-22.
ZIEGLER, D., RATHMANN, W., DICKHAUS, T., MEISINGER, C., MIELCK, A. & GROUP, K. S. 2009. Neuropathic pain in diabetes, prediabetes and normal glucose tolerance: the MONICA/KORA Augsburg Surveys S2 and S3. *Pain Med,* 10**,** 393-400.
ZIGMOND, A. S. & SNAITH, R. P. 1983. The hospital anxiety and depression scale. *Acta Psychiatr Scand,* 67**,** 361-70.
ZILLIOX, L. A., RUBY, S. K., SINGH, S., ZHAN, M. & RUSSELL, J. W. 2015. Clinical neuropathy scales in neuropathy associated with impaired glucose tolerance. *J Diabetes Complications,* 29**,** 372-7.